Ad Proc Add

Project no. 486

Advanced Processing of Additively Manufactured Parts

Final report

Abstract:

The Ad-Proc-Add project aims in the systematic and comprehensive investigation of additive-subtractive manufacturing (ASM) process chains in order to achieve a detailed understanding of influences and interdependencies of parameters, strategies and boundary conditions with respect to the material and workpiece properties of additively manufactured (AM) and post-processed parts in various applications. The visionary goal is to achieve the capability to adjust the workpiece properties regarding geometric, surface, and subsurface characteristics throughout ASM process chains so that pre-defined requirements can be fulfilled. This enables a targeted layout and implementation of ASM process chains in various industrial sectors. For this, an international approach of re- search associations and institutes is chosen, which combines the necessary expertise in the areas of additive manufacturing, material removal processes, process monitoring and control, machinery and equipment, simulation, and optimization as well as energy efficiency analysis. Comprehensive experimental studies regarding interrelationships be- tween parameter settings and influences on the workpiece proper-ties in additive and subtractive process steps, correlation analysis, the detailed investigation of physical effects as well as methods for process monitoring and quality inspection are planned within a distributed and interconnected research approach that exploits synergies and capacities of the in-volved partners in an optimal way. New tool concepts, strategies for 3D-printing of metal parts, methods for the sophisticated layout of post-machining processes, system prototypes for monitoring devices and fixtures, as well as new services will be derived from the insights of this project. Furthermore, the new knowledge enables part manufacturers, system, and service providers to develop new products with enhanced functionality and allows end-users to implement ASM process chains with higher productivity and economic as well as ecologic efficiency. The project results will lead to a digital compendium, based on a new performance measurement system, usable for design and pro-duction engineers and service staff. The project will be accompanied by a user committee of SMEs from all relevant market sectors: tool manufacturing, 3D-Printing equipment, machine tool builders, software, and service providers as well as end-users. The intensive communication with the industrial partners ensures the elaboration of industrially relevant and usable results. The findings, insights, prototypes, and experimental results will be presented towards the international public by workshops, practical seminars, publications, website and exhibition at fairs.
The goal of the research project was achieved. The AdProcAdd project was implemented by nine research institutions from Germany, Austria, Belgium and Switzerland. It was supported by a high number of industrial companies. The coordination of the project was carried out by the Forschungskuratorium Maschinenbau e.V. (FKM). The technical management was conducted by the Institute for Machine Tools (IfW), University of Stuttgart.

The objective of the research project was achieved.

Duration:	01.09.2019 – 30.11.2021
Funding organisation(s):	Federal Ministry for Economic Affairs and Climate Action / German Federation of Industrial Research Associations eV / Collective Research Networking (BMWK/AiF-CORNET) Flanders Agency for Innovation & Entrepreneurship (VLAIO) Austrian Research Promotion Agency (FFG) Eidgenössisches Departement für Umwelt, Verkehr, Energie und Kommunikation UVEK / Bundesamt für Energie BFE, Sektion Energieforschung und Cleantech
Funding number(s):	IGF 255 EBG

RTD performers:

Institute for Machine Tools (IfW), University of Stuttgart
Head: Prof. Dr.-Ing. Hans-Christian Möhring

Institute of Machining Technology (ISF), TU Dortmund University
Head: Prof. Dr.-Ing. Prof. h.c. Dirk Biermann

GFE - Gesellschaft für Fertigungstechnik und Entwicklung e.V. (GFE), Schmalkalden
Head: Prof. Dr.-Ing. Frank Barthelmä

ecoplus (ecoplus), Austria
Head: Helmut Miernicki

Institut für Fertigungstechnik u. Hochleistungslasertechnik (IFT), Technische Universität Wien
Head: Univ.-Prof. Dr. Friedrich Bleicher

FOTEC Forschungs- und Technologietransfer GmbH (FOTEC), Austria
Head: Dipl.-Ing. Helmut Loibl, M.Sc.

KU Leuven (KUL), Belgium
Head: Prof. Bert Lauwers

Thomas More University (TM), Belgium
Head: Machteld Verbruggen

Sirris (Sirris), Belgium
Head: Herman Derache

Belgian Welding Institute npo (BWI npo), Belgium
Head: Fleur Maas

Institut für Werkzeugmaschinen und Fertigung (IWF) Eidgenössische Technische Hochschule Zürich
Head: Prof. Dr. Konrad Wegener

inspire AG (inspire), Switzerland
Head: Martin Stöckli

Research associate(s) / author(s):

Clemens Maucher, M.Sc. (IfW)
Dr. Thomas Stehle (IfW)
Prof. Dr.-Ing. Prof. h.c. Dirk Biermann (ISF)
Dipl.-Ing. Meik Tilger (ISF)
Steffen Lutze (GFE)
Dr. Heiko Frank (GFE)
Martin Ambos (GFE)
Markus Uhl (GFE)
Dipl.-Ing. Dimitrii Nikolaev (IFT)
Dipl.-Ing. Ismail Yavuz (IFT)
Thomas Schlauf (FOTEC)
Ing. Nathaliia Chernovol (KUL)
Dries Van Camp (KUL)
Prof. Dr. Bert Lauwers (KUL)
Dr. Patrick Van Rymenant (KUL)
Frederik Vogeler (TM)
Wim Verlinde (BIL)
Dipl. Ing. Lukas Weiss (inspire / ETH)
Elif Öztürk, M.Eng. (inspire / ETH)
Uroš Hudomalj, M.Sc. (inspire / ETH)

Project coordination / user committee:	Dr.-Ing. Matthias Luik (Hartmetall-Werkzeugfabrik Paul Horn GmbH)
President FKM:	Dipl.-Ing. Hartmut Rauen (VDMA)

Acknowledgement

This report is the scientific result of a research project undertaken by the FKM (The Research Association for Mechanical Engineering eV) and performed by the Institut for Machine Tools (IfW) at the University of Stuttgart under the direction of Prof. Dr. Hans-Christian Möhring, the Institute of Machining Technology (ISF) at Technische Universität Dortmund under the direction of Prof. Dr.-Ing. Prof. h.c. Dirk Biermann, the Gesellschaft für Fertigungstechnik und Entwicklung Schmalkalden e.V. (GFE) under the direction of Dr. Welzel, the Institut für Fertigungstechnik und Hochleisungslasertechnik (IFT) at the Technische Universität Wien under the direction of Univ.-Prof. Dr. Friedrich Bleicher, the Forschungs- und Technologietransfer GmbH (FOTEC) under the direction of Dipl.-Ing. Helmut Loibl, M.Sc., the ecoplus (ecoplus) under the direction of Helmut Miernicki, the KU Leuven (KUL), Belgium under the direction of Prof. Bert Lauwers, the Thomas More University (TM) under the direction of Machteld Verbruggen, the Sirris (Sirris) under the direction of Herman Derache, the Belgian Welding Institute npo (BWI npo) under the direction of Fleur Maas, the Institut für Werkzeugmaschinen und Fertigung (IWF) at the Eidgenössiche Technische Hochschule Zürich under the direction of Prof. Dr. Konrad Wegener and the inspire AG (inspire) under the direction of Martin Stöckli.

The FKM would like to thank the professors Möhring (IfW), Biermann (ISF), Bleicher (IFT), Lauwers (KUL) and Wegener (IWF) and their scientific research assistants for the implementation of the project. Special thanks are due to the AiF (German Federation of Industrial Research Associations eV) for funding the project within the framework of the collective research networking (CORNET) program. The project was conducted by an expert group led by Dr.-Ing. Matthias Luik (Hartmetall-Werkzeugfabrik Paul Horn GmbH). We gratefully acknowledge the support received from the project coordination and from all members of the project user committee.

The research project was carried out in the framework of the industrial collective research program (IGF-CORNET no. 255 EBG). It was supported by the Federal Ministry for Economic Affairs and Climate Action (BMWK) through the AiF (German Federation of Industrial Research Associations eV) based on a decision taken by the German Bundestag. In Austria this project was funded by the Austrian Research Promotion Agency. In Belgium the research is supported by Flanders Agency for Innovation & Entrepreneurship (VLAIO) within the Tetra-Cornet framework. In Switzerland this project is funded by Swiss Federal Office of Energy and supervised by the "Inspire AG für mechatronische Produktionssysteme und Fertigungstechnik".

Table of contents

1 Executive Summary

1.1 Executive summary (EN)

The Ad-Proc-Add project involves the following research partners and industrial associations:

- Forschungskuratorium Maschinenbau e.V. (FKM), Germany
- Ecoplus. Niederösterreichs Wirtschaftsagentur GmbH, Austria
- KU Leuven, Belgium
- Inspire AG, Switzerland
- Institute for Machine Tools, IfW, University of Stuttgart
- Institute of Machining Technology (ISF), TU Dortmund University, Germany
- GFE - Gesellschaft für Fertigungstechnik und Entwicklung Schmalkalden e.V., Germany
- Institute for Production Engineering and Laser Technology (IFT), Technical University of Vienna, Austria
- Forschungs- und Technologietransfer GmbH, FOTEC, Österreich
- Thomas More University College, TM, Belgien
- Sirris, Belgien
- Belgian Welding Institute npo, BIL Belgien
- SIRRIS, Belgium
- Institut für Werkzeugmaschinen und Fertigung, IWF, ETH Zürich

A total budget of 2,390,085.89 EUR (project costs) and 1,975,512.29 EUR funding were provided in order to conduct this highly innovative and comprehensive project.

The following major results are available as an output of the Ad-Proc-Add project and will be further developed with respect to a transfer into industrial products and applications:

Project results of partners (and related chapters)	**Type**	**Transfer to industry** (especially SMEs)
In-Situ defect detection and monitoring for laser powder bed fusion using a multi-sensor build platform	New technology, prototype of possible new products	New technology is available for transfer developments with respect to industrial applications.
Interactions between AM and subtractive machining (chapter 3) and fine machining (chapter 4)	Technological knowledge	By presentations and publications in trade magazines
Final surface quality is highly influenced by the AM process result with respect to oxidations or pores in the material structure (chapter 4)	Technological knowledge	By presentations and publications in trade magazines
Suitability of different microfinishing tools for AM parts (chapter 4)	Technological knowledge	By presentations and publications in trade magazines

The Ad-Proc-Add project was characterized by an intensive collaboration among the research partners as well as between the research institutes, the industrial associations, and the industrial companies. In total, 7 official general project meetings with all research partners and participation of associated companies were carried out.

The project was presented to the public at the 8. Dortmunder Schleifseminar 2019, Hanser Schleiftagung2021, MAMC 2020, TAE Additive Manufacturing Conference 2019, MIC 2020, Conference on Supervising and Diagnostics of Machining Systems 2020, 7. And 8. Austrian 3D-Printing Forum 2020 and 2021, GrindTec 2022, 22. Werkstofftechnisches Kolloquium Chemnitz 2021. In addition, the project results were introduced at the VDMA Forschungstag Präzisionswerkzeuge 2020 and 2021.

Following the duration of the Ad-Proc-Add project, intensive dissemination and exploitation activities will be conducted in terms of workshops, seminars, scientific publication, presentation at international fairs, courses and education, websites, etc.

The results and experiences of the Ad-Proc-Add project also revealed new aspects for future research and development which will be investigated in subsequent Cornet project “AdProcAdd II”.

1.2 Executive Summary (DE)

Am Projekt Ad-Proc-Add sind folgende Forschungspartner und Industrieverbände beteiligt:

- Forschungsausschuss Maschinenbau (FKM), Deutschland
- Ecoplus. Niederösterreichische Wirtschaftsagentur GmbH, Österreich
- KU Leuven, Belgien
- Inspire AG, Schweiz
- Institut für Werkzeugmaschinen, IfW, Universität Stuttgart
- Institut für Fertigungstechnik (ISF), TU Dortmund, Deutschland
- GFE – Gesellschaft für Fertigungstechnik und Entwicklung Schmalkalden e.V., Deutschland
- Institut für Produktionstechnik und Lasertechnik (IFT), Technische Universität Wien, Österreich
- Forschung und Technologietransfer GmbH, FOTEC, Österreich
- Thomas More University College, TM, Belgien
- Sirris, Belgien
- Belgisches Schweißinstitut npo, BIL Belgien
- SIRRIS, Belgien
- Institut für Werkzeugmaschinen und Fertigung, IWF, ETH Zürich

Ein Gesamtbudget von 2.390.085,89 EUR (Projektkosten) und 1.975.512,29 EUR Fördermittel wurden bereitgestellt, um dieses hochinnovative und umfassende Projekt durchzuführen.

Folgende wesentliche Ergebnisse liegen als Output des Ad-Proc-Add-Projekts vor und werden im Hinblick auf einen Transfer in industrielle Produkte und Anwendungen weiterentwickelt:

Projektergebnisse der Partner (und verwandte Kapitel)	**Typ**	**Übertragung an die Industrie** (insbesondere KMU)
In-Situ-Defekterkennung und -überwachung für das Laser-Pulverbettschmelzen mit einer Multisensor-Bauplattform	Neue Technologie, Prototyp möglicher neuer Produkte	Neue Technologie steht für Transferentwicklungen in Bezug auf industrielle Anwendungen zur Verfügung.
Wechselwirkungen zwischen AM und subtraktiver Bearbeitung (Kapitel 3) und Feinbearbeitung (Kapitel 4)	Technologiewissen	Durch Präsentationen und Veröffentlichungen in Fachzeitschriften
Die endgültige Oberflächenqualität wird stark vom Ergebnis des AM-Prozesses in Bezug auf	Technologiewissen	Durch Präsentationen und Veröffentlichungen in Fachzeitschriften

Oxidationen oder Poren in der Materialstruktur beeinflusst (Kapitel 4).		
Eignung verschiedener Mikrofinish-Werkzeuge für AM-Teile (Kapitel 4)	Technologiewissen	Durch Präsentationen und Veröffentlichungen in Fachzeitschriften

Das Ad-Proc-Add-Projekt zeichnete sich durch eine intensive Zusammenarbeit zwischen den Forschungspartnern sowie zwischen den Forschungsinstituten, den Industrieverbänden und den Industrieunternehmen aus. Insgesamt wurden 7 offizielle Hauptversammlungen mit allen Forschungspartnern und beteiligten assoziierter Unternehmen durchgeführt.

Das Projekt wurde auf dem 8. Dortmunder Schleifseminar 2019, Hanser Grinding Conference 2021, MAMC 2020, TAE Additive Manufacturing Conference 2019, MIC 2020, Conference on Supervising and Diagnostics of Machining Systems 2020, 7. und 8. Austrian 3D-Printing Forum 2020 und 2021, GrindTec 2022 und auf dem 22. Werkstofftechnisches Kolloquium in Chemnitz 2021 der Öffentlichkeit vorgestellt. Darüber hinaus wurden die Projektergebnisse auf dem VDMA-Forschungstag Präzisionswerkzeuge 2020 und 2021 vorgestellt.

Nach der Laufzeit des Ad-Proc-Add-Projekts werden intensive Verbreitungs- und Verwertungsaktivitäten in Form von Workshops, Seminaren, wissenschaftlichen Veröffentlichungen, Präsentationen auf internationalen Messen, Kursen und Schulungen, Websites usw. durchgeführt.

Die Ergebnisse und Erfahrungen des Ad-Proc-Add-Projekts haben auch neue Aspekte für zukünftige Forschung und Entwicklung aufgezeigt, die im nachfolgenden Cornet-Projekt „AdProcAdd II“ untersucht werden.

2 Introduction

The Ad-Proc-Add project aims at the development and investigation of innovative technologies for a targeted implementation of controlled additive-subtractive manufacturing (ASM) process chains for metal parts in various applications (Fig. 2-1). The goal is to achieve the technological capability to set up, parameterize, monitor and control ASM process chains so that pre-defined workpiece characteristics and quality criteria (geometry, surface, subsurface) can be accomplished directly. Almost always, additively manufactured (AM) parts have to be post-treated and machined in order to fulfil functional demands or to enable their assembly. The final properties of the parts result from the interactions of the various consecutive processes and their influence on the workpiece. The Ad-Proc-Add project involves several market sectors and fields of applications of ASM parts and products. Industrial partners of various branches are associated.

Figure 2-1: Targeted market sectors and fields of application of Ad-Proc-Add results.

Due to an increasing demand for industrial AM, the market of powder materials for 3D- Printing (3DP) is expected to grow by 24.4 %/year up to 637 Mio. USD until 2020 [Markets&Markets, 2015]. For 3DP machines, a market growth of 30 – 45 % is forecasted by different institutions. The WOHLERS report 2017 denotes a growth of 17.4 % of the global 3DP industry. In a study of IDTechEx, a growth of 23 %/year and a turnover of 12 bn USD is predicted for metal-3DP in 2018 – 2028. The market research company IDC expects an invest of 2.9 bn EUR for 3DP in the Asian-Pacific region until 2021 and a growth of 22.4 %/year. Most important are the automotive, aerospace and medical industry (prosthesis, implants, medical instruments). A global invest of 31.54 bn EUR until 2020 and an annual growth of 24.1 % in 2015 - 2020 is anticipated. The turnover (14.17 bn EUR in 2016) mainly consists of 3DP machines and materials. Software and services grow by a factor of 3. The direct metal laser sintering technology (DMLS) has a market share of 84 %. Approx. 3.56 bn EUR of turnover is produced by the automotive industry and 2.14 bn EUR by the aerospace sector. The manufacturing industry shares 56 % of the turnover, followed by health and medical applications as well as professional service providers. In

a survey of KPMG (2016), 25 % of the considered manufacturing companies already incorporated 3DP and 31 % planned further investments until 2018. Ernst&Young identified a leading role of German companies in Europe regarding the application of 3DP (37 %). In the US 16 % of companies work with 3DP and 24 % in China. Over 20% of automotive, aerospace and mechanical engineering companies with 3DP experience apply the technology to make tools. The annual turnover of 3DP in Germany is estimated to 1 bn EUR. More than 75 % of manufacturing companies will use 3DP in production until 2020. However, a severe challenge is the necessary knowhow for the successful implementation of additive production. Major objectives are an acceleration of product development and prototyping as well as customized products and production flexibility. 23 % of 3DP materials are metal materials. The Selective Laser Sintering (SLS) process is predominantly used (38 %). Roland Berger points out that powder bed additive manufacturing technology is “production-ready” and direct powder/wire deposition by melting is in a late development stage.

Economic Impact

The mechanical engineering sector, with a turnover of 220 bn EUR, is the largest industrial employer in Germany [VDMA2017]. In 2016, approx. 1,018,000 employees worked in 6,780 companies with an average size of 168 employees. The export share is about 77 %. Europe, Asia and North America are the most important export markets. For re- search and development (R&D), an internal investment of 5.8 bn EUR took place in 2016. The number of employees in R&D is increasing and amounts to approx. 44,500. The in- vestment in external R&D increased by 19.3 % to 655 million EUR. This means, that the mechanical engineering sector is an extremely innovative one, dominated by SMEs. In 2017, the producing sector employed 909,034 people in Austria. The mechanical engineering industry has had a turnover of 21.4 bn EUR and employed 82,801 people. The metal working industry provides a turnover of 16.9 bn EUR, the manufacturing of auto- motive products 15.9 bn EUR and the production of metal parts 15.8 bn EUR with 74,952 employees [statistik-austria.at]. About half of the imports in Austria are provided by Ger- many. In 2018 an export growth of 3,5% is expected [WIFO]. In 2016, 82% of total invest was spend for new equipment in the manufacturing industry. Manufacturing is also vital for the Flanders region. The manufacturing industry report made by MT.be stated that the Belgium manufacturing industry consists of over 5,700 high-tech companies. This sector is responsible for 20% of the employment in Belgium, with 200,000 direct jobs. The tool making, machinery and manufacturing industry in the here involved regions possess a significant relevance for employment and prosperity. Considering the expected market development, influence and pervasion of the 3DP technology in industry, these sectors are intensively affected by the ongoing innovations in this field. The Ad- Proc-Add project provides fundamental insights, detailed understanding and the technological background for a knowledge based and effective implementation of innovative 3DP systems and ASM process chains in various applications. This enables an economic and technically advantageous realization of new products with improved functionalities. The machinery and tool suppliers, software and service companies can offer sophisticated systems and support that contribute optimally to innovative ASM chains. Consequently, the Ad-Proc-Add project has a significant technical but also socio-economic impact on the mentioned sectors.

The Need

The implementation of ASM process chains is more and more requested by SMEs in various industrial sectors. Producers of components and subsystems are involved in increasingly flexible and fast reacting supply chains based on the principle availability of AM technologies. Even more complex parts have to be produced as a consequence of the growing awareness, knowledge and experience of design engineers with respect to the technical possibilities offered by AM. Raising quality demands regarding geometric ac- curacy and surface configuration, but also strength, safety and reliability of AM parts have to be fulfilled. The variety of materials for AM increases and application oriented functional integrated parts have to be realized in short time. Besides small OEMs and OEM suppliers, also tool manufacturers, producers of auxiliaries and technical equipment as well as service provider have to tackle these challenges.

So far, the successful implementation of pure additive processes with respect to the technical requirements of the parts constitutes the main focus of research and development activities in industry and academia. The necessity of post-treatment and machining of the AM parts in order to achieve the required geometric accuracy and functional features is often neglected. Since both the additive manufacturing as well as the subtractive machining process step significantly influence the final properties of the parts, a com- prehensive layout, adjustment and control of the entire ASM process chain is desirable (Fig. 2-2). However, especially in SMEs, the necessary knowhow cannot be achieved, and technologies cannot be implemented within the requested market driven time frame. Consequently, there is a serious need in systematic investigations on (a) how the inter- actions of additive and subtractive processes influence the properties of produced and post-treated parts, (b) how quality criteria can be assessed throughout the ASM process chain, (c) how process steps can be adjusted in order to achieve targeted workpiece properties without multiple empirical iterations, (d) how the layout of ASM process chains can be optimized efficiently, (e) how costs and resource efficiency of ASM process chains can be assessed.

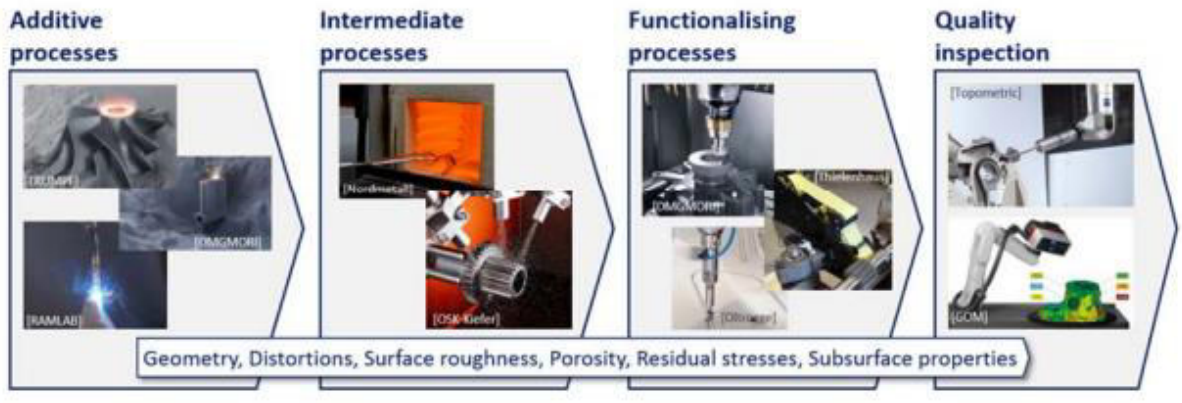

Figure 2-2: General approach of the Ad-Proc-Add project.

3 Analysis of additive and functionalizing process technology – Results of the IfW

C. Maucher https://orcid.org/0000-0002-2988-2321
(Institute for Machine Tools, IfW, University of Stuttgart)

3.1 Introduction

In the course of this project, several aspects of the ASM process chain have been investigated, to identify an optimal process chain layout. During this project, the impact of the different processes withing the ASM process chain on the quality of the final part were investigated for the components produced by the LPBF process. The following sections summarizes the results regarding investigations on the additive and subtractive manufacturing processes. The Institute for Machine Tools (IfW) of the University of Stuttgart focused in this project on the following topics:

- Parameter development for the laser-powder-bed-fusion process (Chapter 3.2)
- Analysis of intermediate workpiece treatment in terms of blasting (Chapter 3.3)
- Analysis of functionalizing process technology in terms of orthogonal cutting (Chapter 3.4)
- Influence of LPBF Parameters and strategies on fine machining of pre-built bores (Chapter 3.5)
- Analysis of functionalizing process technology in terms of milling (Chapter 3.6)
- In-Situ defect detection and monitoring for laser powder bed fusion using a multi-sensor build platform (Chapter 3.7)
- Geometric simulation of the ASM process chain (Chapter 3.8)

3.2 WP2 Analysis of powder-bed-based process technologies

The LPBF process, is a thermal process which utilizes lasers to selectively heat and melt powder to build up fine layers of metal powder. The heat balance is determined by a large number of process-specific parameters and in addition to the composition of the melt pool, the heat balance is characterized by local temperatures, dwell times and local cooling gradients, determining properties for the later material phases [3]. In the course of this project the influence of these process parameters in the LPBF process was examined. The aim here was to develop a procedure for how these parameters can be worked out efficiently with the support of simulative methods.

The following parameters were considered:

- Laser power
- Laser speed
- Lane spacing (hatch distance)

The Trumpf TruPrint1000 system and titanium (Ti64) as the starting material were used to develop the method. For this purpose, individual melting tracks were first built up additively on a specially developed test component in order to evaluate them with regard to process stability. The system manufacturer's parameters were used as the initial value for the process parameters. The test part is shown in Fig.3-1.

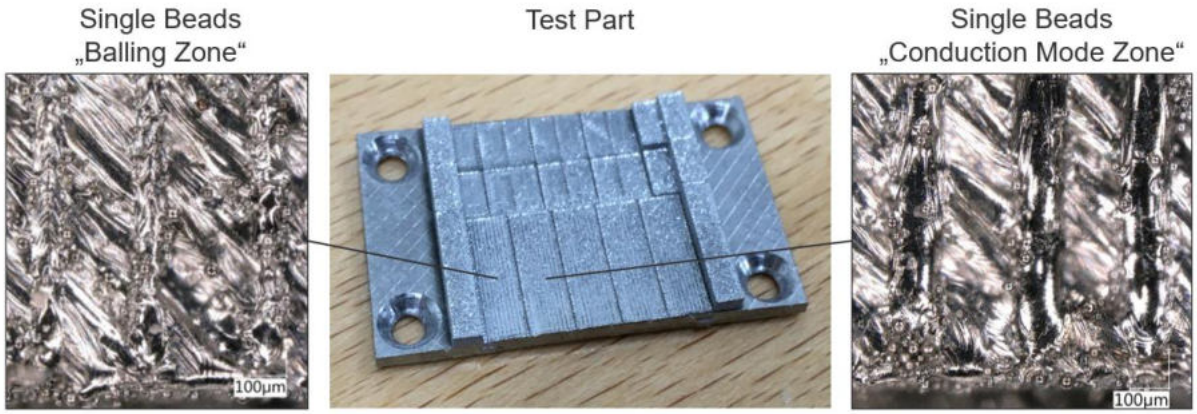

Figure 3-1: Developed test part with a magnified view of two different parameter sets and the corresponding single beads.

The width and depth of the melt pool were measured by cutting through the melt tracks and then grinding them in order to calibrate the simulation software. The micrographs also enabled the now visible melt tracks to be examined for characteristic pores, such as keyhole pores, lack of fusion pores, gas pores, oxide pores and other defects. These in turn provided information about the printing process. From these findings, simulations could be carried out in the ANSYS Additive Science software in order to be able to define the process window between laser power and laser speed. The result of these simulations was the so-called length to width ratio, this makes it possible to evaluate the resulting melting line and classify it into four areas. This was done by defined conditions which are listed in table 3-1.

Condition to exclude the P,v combination:	**Note on:**
Median Melt Pool Reference Depth < 2,5 Layer thickness = 0,03 mm	lack of fusion (melt pool not deep enough)
Depth-to-width ratio > 0,95	keyhole formation (melt pool too deep)
Length-to-width ratio > 4,0	Balling (melt pool too long)

Table 3-1: Evaluation basis of the simulation results.

The targeted field is the so-called "conduction mode zone", this creates a stable melting path. Apart from that, there are three fields known as "lack of fusion", "balling" and "keyhole" areas and are usually not desirable. These areas could be defined by the simulation and the length to width ratio. The simulations and the identification of which area is involved are shown in Fig.3-2.

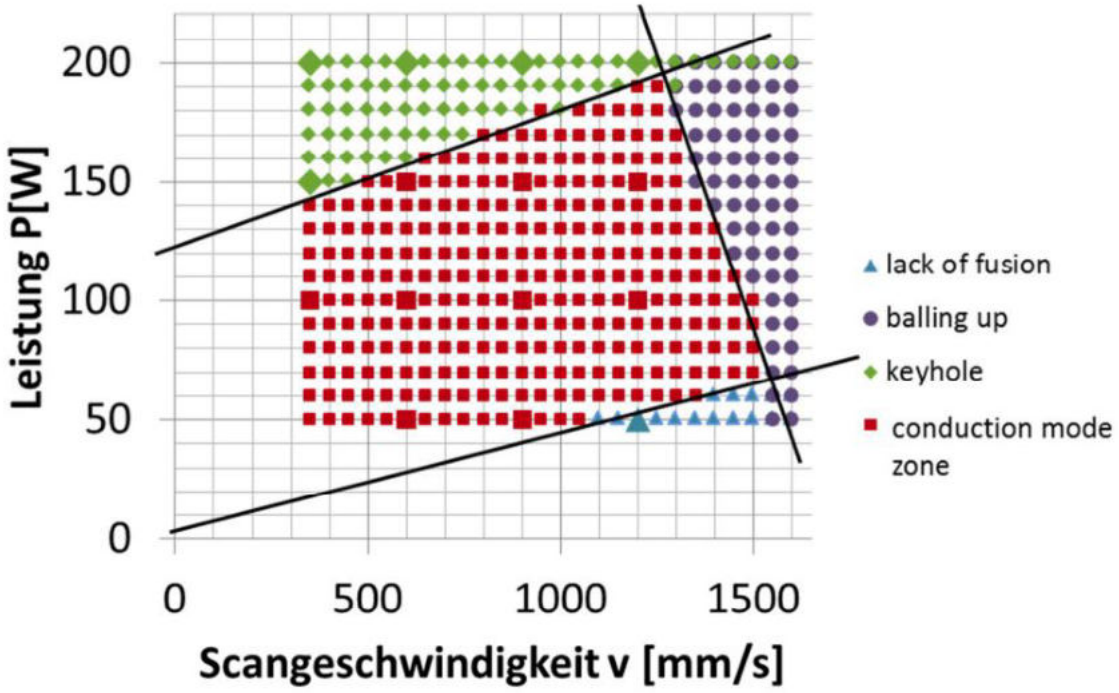

Figure 3-2: Evaluated simulation results shown in the P,v diagram.

The following findings emerged from the consideration of the melting tracks: The hatching distance can be adjusted so that there are no gaps between the tracks, and they are sufficiently well fused with each other. Since the melt path and the melt pool are not significantly influenced by the hatching spacing, this size is set at the end. The melting line width serves as a guide for the hatching spacing. The hatch spacing should be at least the melt track width so that the traces are connected. The melt path width depends on the layer thickness, the substrate temperature and the energy introduced. The melt path width can be specified with so called "Single Bead" simulations in ANSYS Additive can be determined. The "lack of fusion" area can be checked with printed fusion tracks. It can be assumed that strong "balling" is also visible in the melt tracks. At the beginning of the parameter determination, research can be carried out in order to narrow down the parameters and reduce the number of simulations. The laser spot diameter is often specified by the machine. At the beginning, the substrate temperature should be set to 20°C in the “single bead” simulation. The substrate temperature causes longer weld pools, which results in a higher length-to-width ratio and thus a reduced conduction mode range and an increase in the balling range. The choice of the layer thickness correlates strongly with the energy input into the powder and thus with the laser power, scanning speed and laser spot diameter. The layer thickness determines the resolution of the component and the build rate. Several aspects are therefore relevant for the selection of the layer thickness. The following methodology was developed from this:

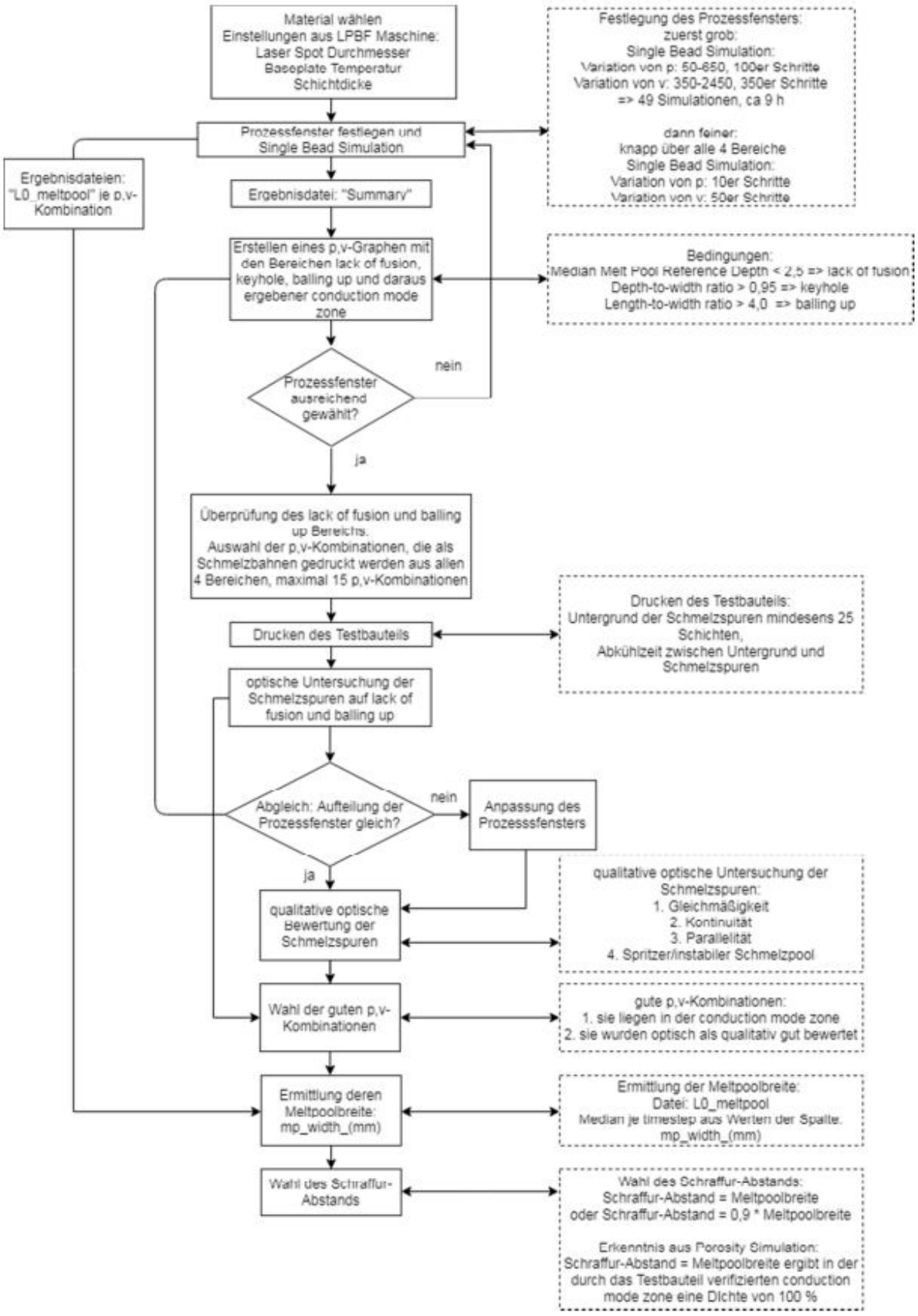

Figure 3-3: Methodology for LPBF process parameter development.

For the evaluation of the process parameters from the "single bead" investigation, cubes were produced with the corresponding parameters and their density was examined. For this purpose, the density determination method was implemented according to the Archimedean principle. The procedure for determining density according to Archimedes was recorded in a guide. The accuracy of the density determination was examined. Density differences of around 0.1% can be easily determined, but if the density differences are small, further investigations must be carried out in order to rule out any influence on the density fluctuations.

3.3 WP2 Analysis of intermediate workpiece treatment in terms of blasting 1

The LPBF process creates relatively rough surfaces with residues from the powder material which adhere to the surface that has to be cleaned. In industrial applications, blasting processes are used for smoothing and cleaning but also to introduce compressive residual stresses.

In the course of this project blasting of AM surfaces is examined on varying materials with regard to the material removal rate and the resulting smoothing of the staircase effect. In addition, a more detailed examination on the influence of blasting material, time and pressure on the surface topography and subsurface properties is carried out on maraging steel.

The intense heat in the LPBF process generated by the laser beam to melt the material must be dissipated quickly enough so as not to affect the adjacent loose powder or cause local overheating of the part. This inevitably leads to the powder being partially melted and adhering to the solidified melt path. This represents a deficit of the AM processes, as the resulting surface quality and dimensional accuracy are negatively affected.

Another negative influence associated with the layered structure is the so-called staircase effect. The layers in the LPBF process are usually 20 - 100 µm thick and cause steps on inclined surfaces due to their geometry. This effect has already been largely described in the literature [1,2]. Since the individual melt tracks are not rectangular, a wavy shape is created over the profile. According to Yasa et al [3], this waviness, as well as the derived roughness, can be determined analytically.

Because of these deficits, functional surfaces must be machined so that they are within the desired tolerances [4]. In addition, loosening adhesions can lead to contamination along the process chain. In order to remove these powder particles and improve the surface quality, blasting processes are preferred in industrial applications [5,6]. According to DIN 8200, blasting is understood to be a manufacturing process in which a blasting agent is accelerated and made to impact the surface of a workpiece to be processed. When the blasting agent hits the workpiece, the kinetic energy is converted, in particular, into elastic-plastic deformation work.

The following process parameters influence the blasting result and thus the condition of the surface as well as the subsurface properties: the blasting media, determined by its shape and hardness, the blasting abrasive speed, determined by the pressure, the distance between the blasting, the blasting angle and the duration of the blasting action.

[1] This chapter is adopted from the paper: Maucher, C.; Cera, P.; Möhring, H.-C.: Quantification and Surface Analysis on Blasting of Additively Manufactured Components; 6th CIRP Conference on Surface Integrity (2022)

Different abrasives can be used for blasting. Corundum is used to clean contaminated components. In contrast, fine blasting with glass balls is an effective method of releasing tensile stress and strengthening surfaces. Depending on the objective, blasting can be divided into cleaning blasting and solidifying blasting [7,8]. The task of blast cleaning is to remove particles, layers or adhesions which can have a disruptive effect during subsequent further processing. The adhesions that occur in the LPBF process are partially melted metal particles which are very fine (15 - 45 µm in diameter). Edged blasting media are very suitable for blast cleaning due to their abrasive effect.

In the case of solidification blasting, a relatively heavy and rather spherical blasting agent is used with the aim of maximizing the kinetic energy and the resulting plastic deformation and minimizing the abrasive removal. Surface roughness and subsurface properties are of particular interest in this combined application. The influence of blasting on the staircase effect is also relevant. The removal rate and the resulting roughness are of particular importance.

In this study the application of blasting of additively manufactured components is examined, in order to improve the overall post treatment process of AM parts. For this purpose, multiple specimens were produced and processed. The goal was to provide practical recommendations for abrasive selection and processing time, as well as empirical values regarding the achievable roughness and subsurface properties of AM components in industrial applications.

3.3.1 Experimental Setup

The investigations were carried out in several stages. First, it was evaluated which blasting material meets the purpose of blast cleaning vertical surfaces of AM produced maraging steel (1.2709) specimen. The cleaning performance of the previously selected blasting material was then examined on various specimen produced with varying AM machines, material, and build-up direction. A total of four materials (1.2709; 1.4404; AlSi10Mg; Ti6Al4V) each in seven build-up directions (0°; 30°; 15°; 45°; 60°; 75°; 90°) were examined.

The influence of the abrasiveness of the blasting on the staircase effect of the test specimens was examined depending on the orientation and blasting duration. Finally, the compressive effect which leads to a hardening of the subsurface region of blasted maraging steel samples was examined.

Additive manufacturing

The four selected materials are preferred for use in industrial environments. For production, various AM systems from the partners in the consortium were used. These and the process parameters utilized can be found in Table 3-2.

Material	Machine	Spotsize	Layer height	Institut
1.2709	Renishaw - RenAM500Q	80 µm	50 µm	IfW
1.4404	SLM Solutions - SLM 280 HL	90 µm	30 µm	ISF
AlSi10Mg	DMG - Lasertec 30 SLM 2nd Gen.	70 µm	50 µm	IFT
Ti6Al4V	Trumpf - TruPrint 1000	30 µm	20 µm	IfW

Table 3-2: Process parameters and utilized machine for 1.2709, 1.4404, AlSi10Mg and Ti6Al4V.

Specimen design

Two types of components were used to consider the effects to be investigated. For the investigation of the cleaning blasting as well as the influence of the blasting on the subsurface properties, cuboids with an edge length of 5 x 20 x 20 mm were additively manufactured upright. The investigation regarding the abrasive smoothing of the staircase effect by blasting was carried out with the geometry defined in the ISO / ASTM DIS 52902: 2018 standard (see Fig. 3-4) on the upper surface of the specimen (Fig. 3-4 marker 1). The individual bars were separated at the connection point (Fig. 3-4 marker 2) after the additive process and examined individually.

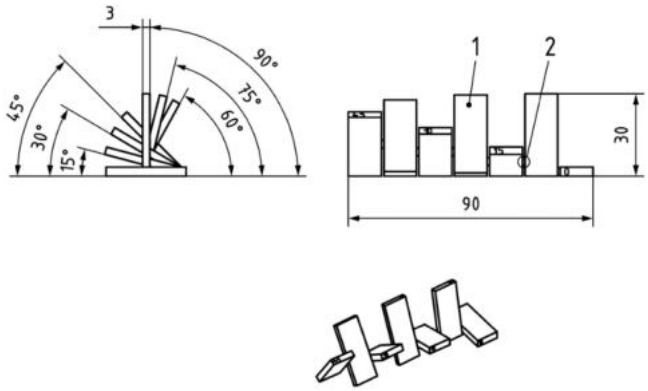

Figure 3-4: Surface texture specimen according to ISO/ASTM DIS 52902:2018 (all dimensions in mm).

Blasting

The samples were blasted in a blasting cabin from MHG Strahlanlagen GmbH. Corundum and glass balls with a particle size distribution of 106-150 µm and 100-200 µm, respectively, were used as the blasting medium. The blasting pressure was set to 6 bar. The distance between the jet nozzle and the surface to be treated was kept constant at 20 mm in all tests. For blast cleaning, the angle was set to 45°. In the case of solidification blasting, the samples are blasted vertically (90 °). The processing time in all experiments was varied in four stages (one, three, five and seven seconds).

After each blasting process, the samples were weighed with a fine balance to determine the removal rate and the roughness achieved was measured geometrically by means of a focus variation. Rz was measured on three parallel lines with a length of 1,6 mm each. Sa was measured on an area of about 2,5 mm^2 also three times. For both characteristics the mean values of the three measured values were determined.

3.3.2 Results on blasting medium and cleaning

In industrial applications, corundum is often used as a blasting medium for cleaning AM components. In comparison with glass balls as a blasting material, however, a very similar cleaning effect can be achieved after a short blasting time of one second. In addition, corundum grains were found on the surface after the first blasting stage. It can be observed that the angular corundum grains tilt in the rough AM surfaces, in particular in the valleys between the melt tracks, and remain there. Such a canted corundum grain can be seen in Fig. 3-5. These grains represent a danger for subsequent fine machining processes such as reaming, as the grains affect the cutting edge of the tool. When AM surfaces are

blasted with glass balls, no residues of the blasting medium can be found on the surface. It was therefore decided to carry out the further experiments with glass balls.

To determine the blasting duration, samples with a varied blasting time were treated and examined for the number of remaining adhesions from the AM process. For this purpose, the remaining adhesions were counted visually and the change in weight was measured with a micro-balance. For this purpose, the samples were examined accordingly after each blasting cycle. In Fig. 3-5, the removal rates are

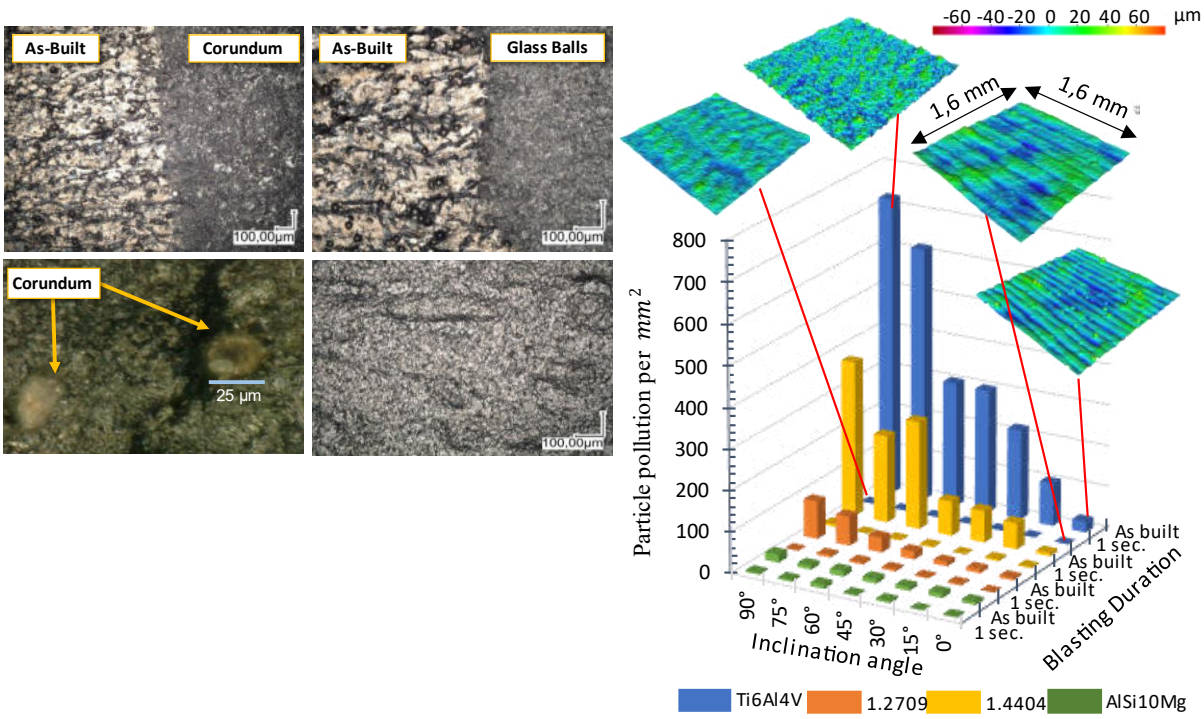

Figure 3-5: Microscope images of blasted vs. as built surface for corundum and glass balls as blasting medium (left). Particle pollution per mm² for investigated materials before blasting and after 1 second blasting over investigated inclination angles between 0° and 90° (right).

plotted in relation to the blasting time. It can be seen that even after the shortest blasting times (one second) there are hardly any adhesions left on the AM surface. Correlated to this, the weight reduction decreases sharply after the start (see Chapter 3.3.3, Fig. 3-6). With longer blasting times, between five and seven seconds, there are no longer any discernible adhesions on the surface and only a small amount of material is removed by the blasting in the further curse of treatment time. Regarding the orientations of the materials in each case, it is striking that the number of adhesions is greatest in the case of the samples in a 90° orientation. This can be explained that the melt pool during the AM process solidifies on adjacent powder, and this partially melts and thus bonds with the surface. As orientations become flatter, the number of adhesions is decreasing with a minimum at an orientation of 0°.

When comparing the samples made from the different materials, it is evident that the samples made from titanium and stainless steel have by far the greatest number of adhesions. Both materials were produced in this study with relatively thin layers of 20 µm for titanium and 30 µm for stainless steel. The smallest number of adhesions can be found on the samples made of aluminum. The aluminum samples, however, show most of adhesions after 1 second of blasting. Overall, no adhesions can be observed in any of the samples after the blasting duration of 3, 5 and 7 seconds.

3.3.3 Results on surface smoothing of staircase effect

To consider the influence of the abrasiveness of the blasting on the staircase effect of the test specimens, the roughness with Sa and Rz, as well as the relative weight reduction depending on the orientation and blasting duration were examined. The results of the individual materials are shown in Fig. 3-6.

Overall, it can be seen in all samples that the direction of build-up and thus the staircase effect significantly influence the roughness of the components. A similar course of roughness can be observed in all samples, as was predicted in the analytical formula according to Yasa [3]. This formula describes the surface roughness as a function of the layer thickness and the inclination angle of the surface. It is made up of the sum of the maximum valley and the maximum peak of each layer. The resulting parameter can be compared with the measured roughness parameter Rz since this also indicates the difference between the maximum and minimum value on a measuring section [3]. All samples have the highest roughness at an orientation of 15°, following a decrease till 90°. The roughness of the samples in 0° orientation must be considered separately. The examined levels are horizontal and thus represent a single layer from the AM process. Effects such as the staircase effect or the characteristics of the layers are not present. The roughness is largely driven by the selected scan strategy. Due to the material and system-specific scanning strategies, there are large fluctuations in these samples, which makes a comparison impossible. In comparison between the single material specimen Ti6Al4V and 1.4404 exhibit the lowest roughness Sa and Rz. This can be explained by the lower layer thickness, and therefore smaller staircase effect. The analytical prediction of the roughness also has the best fit on these samples. For the other samples (1.2709 and AlSi10Mg) an overall better surface roughness than predicted could be achieved except for the Specimen made of titanium.

Furthermore, it can be seen that irrespective of the orientation, the blasting reduces the roughness. As the blasting time progresses, the reduction in roughness decreases. Likewise, the weight change is initially high for all samples and then falls off as the process progresses.

In comparison of the samples with different orientations, trends in the change in weight can also be identified. This is the most pronounced for all materials for the orientations 0° to 30°. The change in weight is smallest for samples in the range of 60° to 90°. From this it can be deduced that the reduction in roughness due to the staircase effect removes more material than is removed by the increased number of adhesions. However, this effect cannot be seen in the roughness values. One reason for this could be the choice of the roughness parameters Sa and Rz. These roughness parameters deliver the short wavelength components of the surface roughness. However, the effects of the staircase effect are more likely to be characterized as texture properties of larger wave lengths and are therefore not sufficiently recognized by these roughness parameters [9].

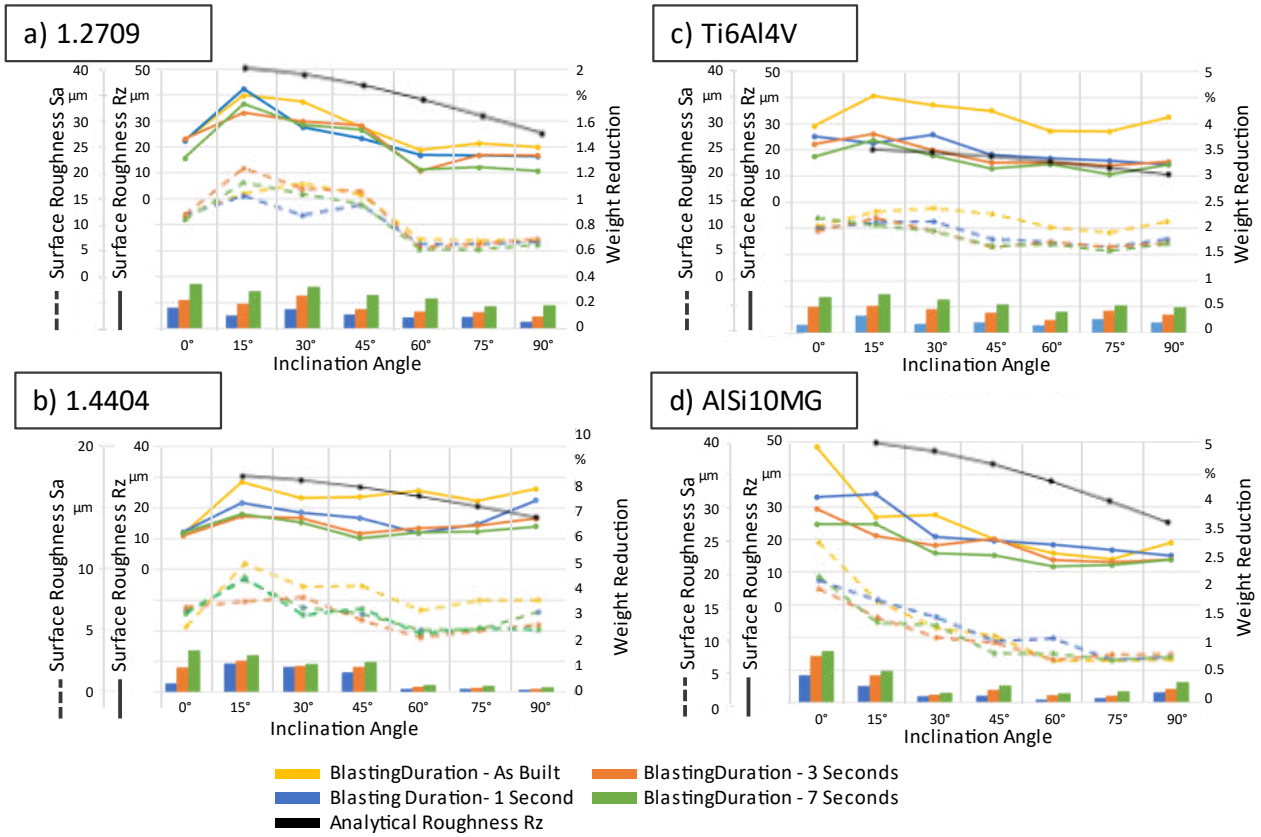

Figure 3-6: Roughness characteristics Rz and Sa as well as weight reduction for examined materials with analytical course of roughness as a function of inclination angle and blasting duration.

3.3.4 Results on subsurface manipulation

Even though blasting with glass balls is not genuinely used to manipulate subsurface properties it can be used to slightly change it. Figure 3-7 shows the microhardness curve of a sample from 1.2709 near the surface, after blasting (a) and before (b). The sample was blasted for 15 seconds. The micro hardness was measured with 5 parallel lines, starting below the surface, and ending 2,5 mm deep in the material. Each line consists of 90 measuring points. The test force for this investigation was 490,3 mN.

It took 7 seconds until this force was reached and it was held another 14 seconds before relief. In the data of the untreated specimen, it can be seen that the hardness varies between 350 and 390 hardness

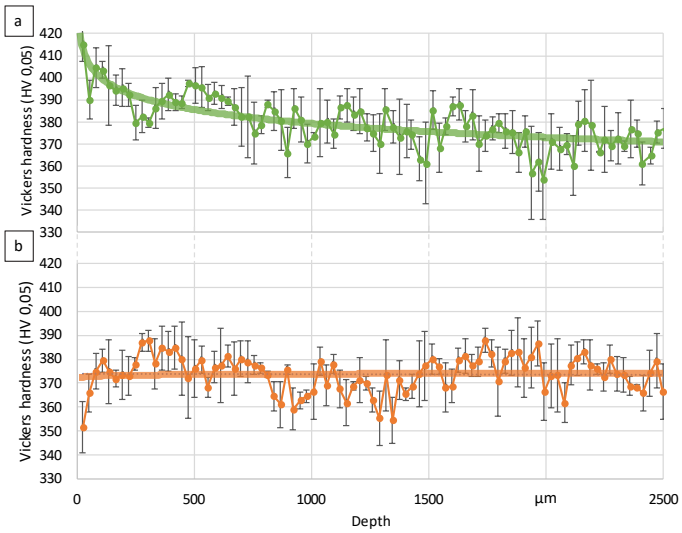

Figure 3-7: Vickers hardness as a function of the component depth for a) blasted and b) as built surface.

Vickers. However, along the measuring points the hardness remains relatively constant. In comparison, the blasted specimen shows an increased hardness near the surface, which decreases along the depth. This clear increase in hardness can be seen down to a depth of approx. 1000 µm.

3.3.5 Conclusion

In the presented investigation postprocessing of surfaces produced in the LPBF process was examined. Especially with regard to smoothing and cleaning but also to introduce compressive residual stresses. This was done with varying materials with regard to the material removal rate and the resulting smoothing of the staircase effect. It could be shown that blasting indeed smooths the AM surfaces. The examination on the influence of blasting medium and time on the surface topography and subsurface properties of maraging steel have shown that corundum is not suitable for blasting in terms of adhesions of the blasting medium on the surface. However, glass balls have shown to be suitable for blasting AM surfaces. In addition, this blasting medium was able to not only clean sufficiently the surface but also to introduce residual stresses into the subsurface, resulting in a higher hardness.

In summary it can be said:

- Particle pollution on AM surfaces is inclination and material dependent. On steeper surfaces more particles adhere.
- Short blasting times between one and three seconds are sufficient for cleaning purposes. Glass balls are more suitable better for this purpose.
- Blasting with glass balls can improve subsurface properties.

3.4 WP3 Analysis of functionalizing process technology in terms of orthogonal cutting 2

3.4.1 3.4.1 Introduction

In the LPBF process, the locally concentrated melting and fast solidification leads to a fine dendritic microstructure depending on the melt pool size. In this dendritic structure the layer wise build-up is still visible. It is well known that this leads to an anisotropic material behavior. The layer wise melting of material in the AM process, results in different material properties compared to parts made from the same material in a conventional way [6, 7].

During this project, the influence of the build-up orientation relative to the cutting vector on the cutting process was studied. For this objective, specimens out of maraging steel with different build-up di-rections were build and subsequently examined utilizing an orthogonal cut.

The aim of this study was to investigate a possible interrelation between not only the build-up direc-tion but also the orientation of the dendritic structure. For this purpose, two angles are introduced which describe the orientation of the dendritic structure relative to the cutting vector. For this purpose, different specimens were manufactured and machined. These experiments were then analyzed regard-ing cutting forces, vibrations, chip geometries and surface finish. Samples of the resulting chips were examined microscopically, and the chip thickness t, the lamella distance d, and the lamella height were determined. The results are statistically validated by test repetitions and a regression model was formulated.

The additively manufactured specimens are made of tool steel 1.2709. To produce the specimens, a LPBF Machine RenAM 500Q from the company Renishaw was used. Renishaw provided settings were used as process parameters for all parts and support structures. The specimens were produced with the inert gas nitrogen at a flow rate of 190 m3/h. The base plate was heated to 60 °C to reduce thermal influences on the support structures by gradually heating the build plate during the built-up. The layer height was set to 50 µm. An excerpt of the process parameters is listed in Table 3-3.

Process parameter value	Process parameter value
Layer thickness	50 µm
Laser power border	150 W
Laser scan speed border	300 mm/s
Laser power hatch	250 W
Laser scan speed hatch	1000 mm/s
Atmosphere	Nitrogen

Table 3-3: LPBF process parameters used for material 1.2709.

Specimen design

The workpiece geometry for the orthogonal cutting investigations is made of a beam of maraging steel with a length of 180 mm, width of 4 mm and height of 50 mm. Residual stresses exist in AM components. However, utilization of build plate heating and adapted process parameters, reduces thermally induced stress [15]. In addition, the specimens were prepared by removing the layer in which the tensions occur.

[2] This chapter is adopted from the paper: Maucher, C.; Gutsche, D.; Möhring, H.-C.: Investigation on anisotropic behavior of additively manufactured maraging steel during orthogonal cutting; 21st CIRP Conference on Electro Physical and Chemical Machining (2022)

This releases the residual stress in resulting deformations which are again equalized by surface grinding. For this the specimens were additively produced with a width of 5 mm, then milled to remove the support structures and then ground to ensure a constant specimen thickness of 4 mm. For each orientation, two specimens were produced, and seven orthogonal cuts are performed on one sample.

For the definition of the orientation of the dendritic grains, two angles are defined. Alpha is the angle between the cutting vector and the build-up direction. Beta defines the angle between the vector perpendicular to the cutting vector and the build-up direction. With this definition, alpha and beta can be varied between 0° and 90°. Based on this definition the design of experiment can be seen in Fig. 3-8.

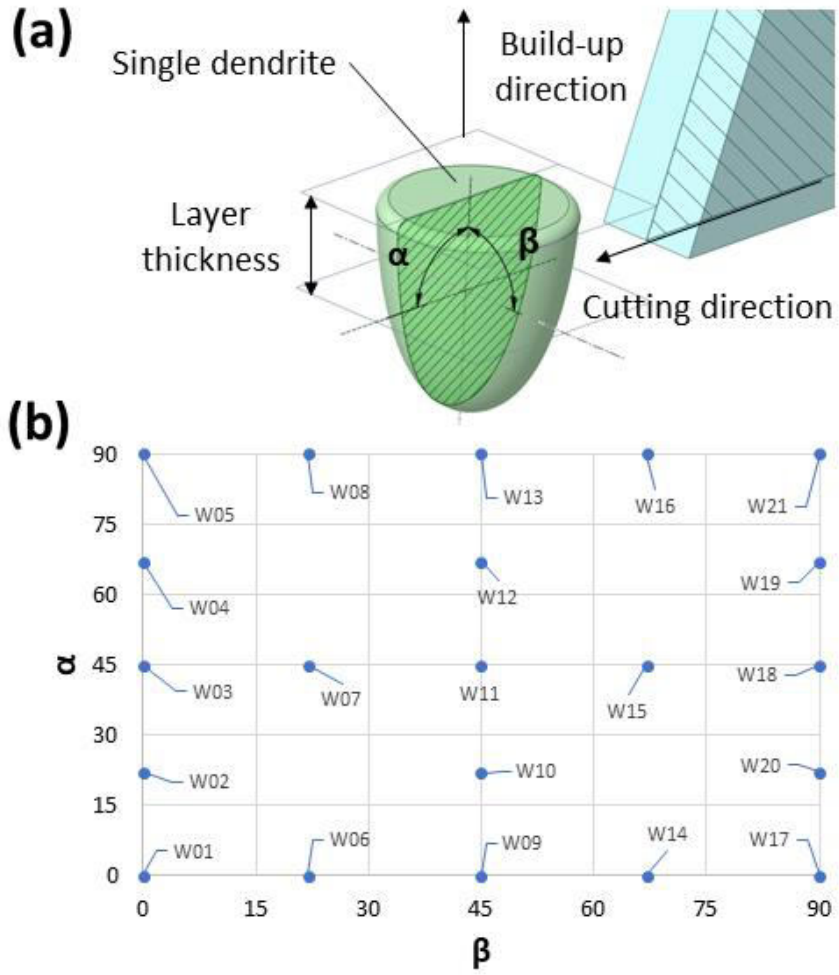

Figure 3-8: Schematic representation of the angle definition in relation to the build-up and cutting direction (a) with the resulting design of experiment (b).

Machining

The relative linear movement during orthogonal cutting is performed on a special test stand. The workpiece holder is driven by a linear motor. The stationary tool holder can be adjusted in height to set the depth of cut. Samples are clamped on a piezo-electrical dynamometer to measure the resultant cutting force F_c and thrust force F_t. The used tool insert is a parting and grooving tool by Paul Horn GmbH, made from a proprietary tungsten carbide compound called Ti 25. Table 3-4 lists essential tool characteristics and the chosen cutting parameters.

Tool feature	Value
Rake angle γ	15°
Wedge angle β	63°
Clearance angle α	12°
Cutting edge radius r_e	47.6 µm
Cutting parameters	
Feed rate f	0.1 mm
Cutting speed of v_c	80 m/min

Table 3-4: Tool characteristics and the chosen cutting parameters.

In addition, a structure-borne noise sensor using High Frequency Impulse Measuring (HFIM) and a 50g accelerometer is placed on the tool holder to analyze impact of the layer-wise microstructure of the material. To evaluate the chip formation a high-speed camera is placed perpendicular to the cutting direction. After machining, the resulting surface was examined regarding the roughness.

3.4.2 Tool wear and cutting speed determination

Cutting speed determination

An analysis of dependency of cutting speed on cutting forces was conducted to define the optimal cutting speed for further experiments. As commonly agreed, on in literature an increase in cutting speed leads to a decrease in cutting forces. As the machined samples were made by means of additive manufacturing and therefore don't show an isotropic structure it was decided to verify the validity of this axiom for parts made from additive manufacturing.

In Fig. 3-9 an effect of anisotropy is already clearly visible as the curve for α = 90° is lower than the curve for α = 0°. The maximum difference between forces recorded for α = 0° and α = 90° is 5.25 % at a cutting speed of 100 m/min.

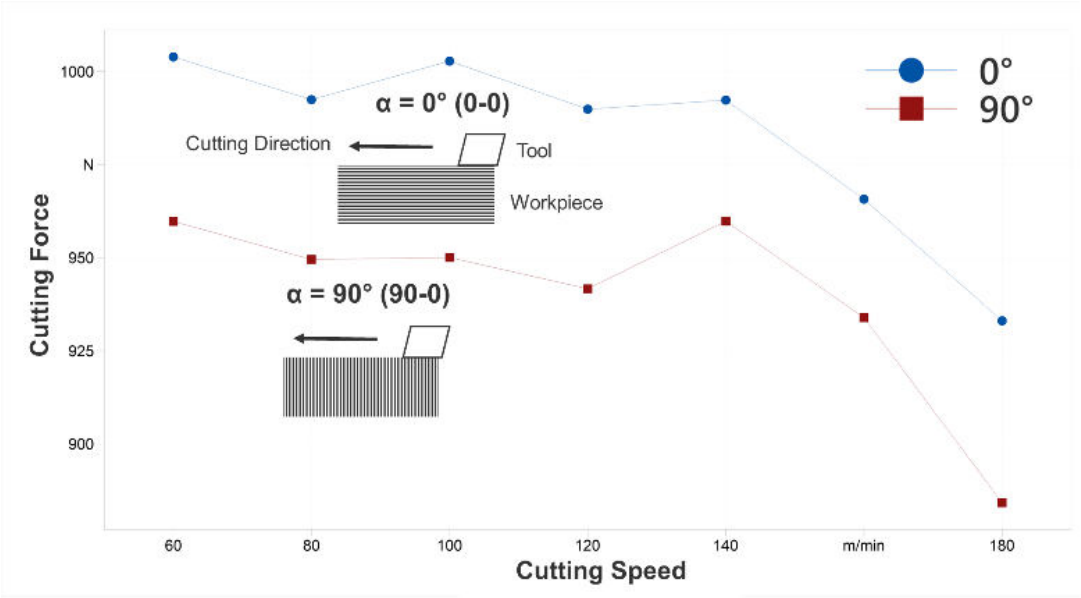

Figure 3-9: Influence of cutting speed on cutting force.

Tool wear

To examine the tool wear characteristics of the used tools a test series of a total of 50 cuts was conducted. The results of the experiment are shown in Fig. 3-10. In the beginning an increase of both cutting force and thrust force is noticeable. However, when considering the forces from cut number 6 onwards no relevant trend is distinguishable.

3.4.3 Orthogonal cutting results

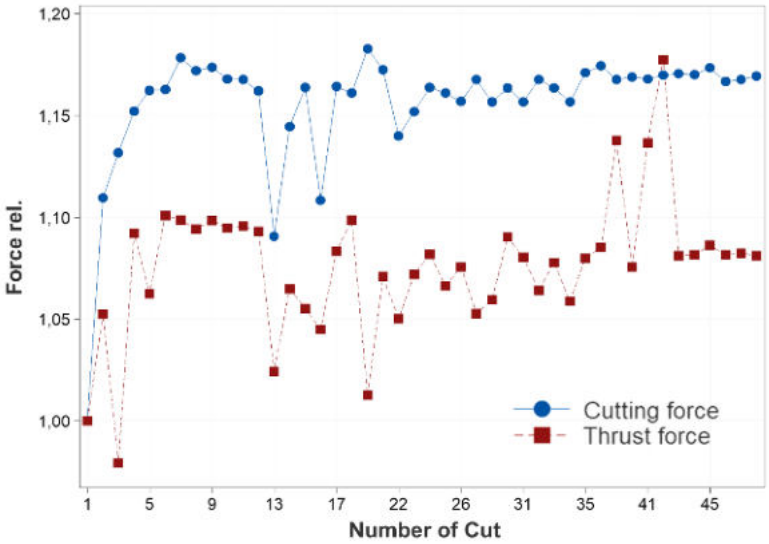

Figure 3-10: Cutting forces measured during wear analysis.

Cutting forces

Figure 3-11 presents the cutting force F_c and the thrust force F_t over time (sampling rate f = 10 kHz). As shown in section 3.4.2 there clearly is a measurable anisotropy regarding cutting forces when varying the angle α. As shown in Fig. 3.11 the cutting force decreases by ΔFc_rel = 8 %. The curve shows a non-linear behavior of the cutting force in relationship to the angle α. To further understand the relationship of angles with both cutting force and thrust force a larger series of experiments was conducted.

To obtain useful information from the gathered data a polynomial regression analysis was performed. The chosen polynomial regression is of second degree for both variables α and β. Therefore, the polynomial regression yields a model consisting of linear, square, and composite terms. A model fit of R^2_{Fc} = 63.47 % and R^2_{Ft} = 92.89 % was achieved. For both forces the model includes the same terms. The general form of the regression model is listed in Formula (1). For both F_c and F_t, all terms including α show statistical significance assuming a confidence level of 0.05. Terms containing β don't show statistical significance.

As the interest of this analysis is the relative change of cutting forces due to the change of parameters, the absolute cutting forces are normalized relative to the orientation α = β = 0°.

$$F(\alpha,\beta) = k_1 + k_2 * \alpha + k_3 * \alpha^2 + k_4 * \beta + k_5 * \beta^2 + k_6 * \alpha\beta \quad (1)$$

Again, the suspected anisotropy is confirmed. A statistically significant difference between both the orientations angle α as well as angle β are evident following the regression model.

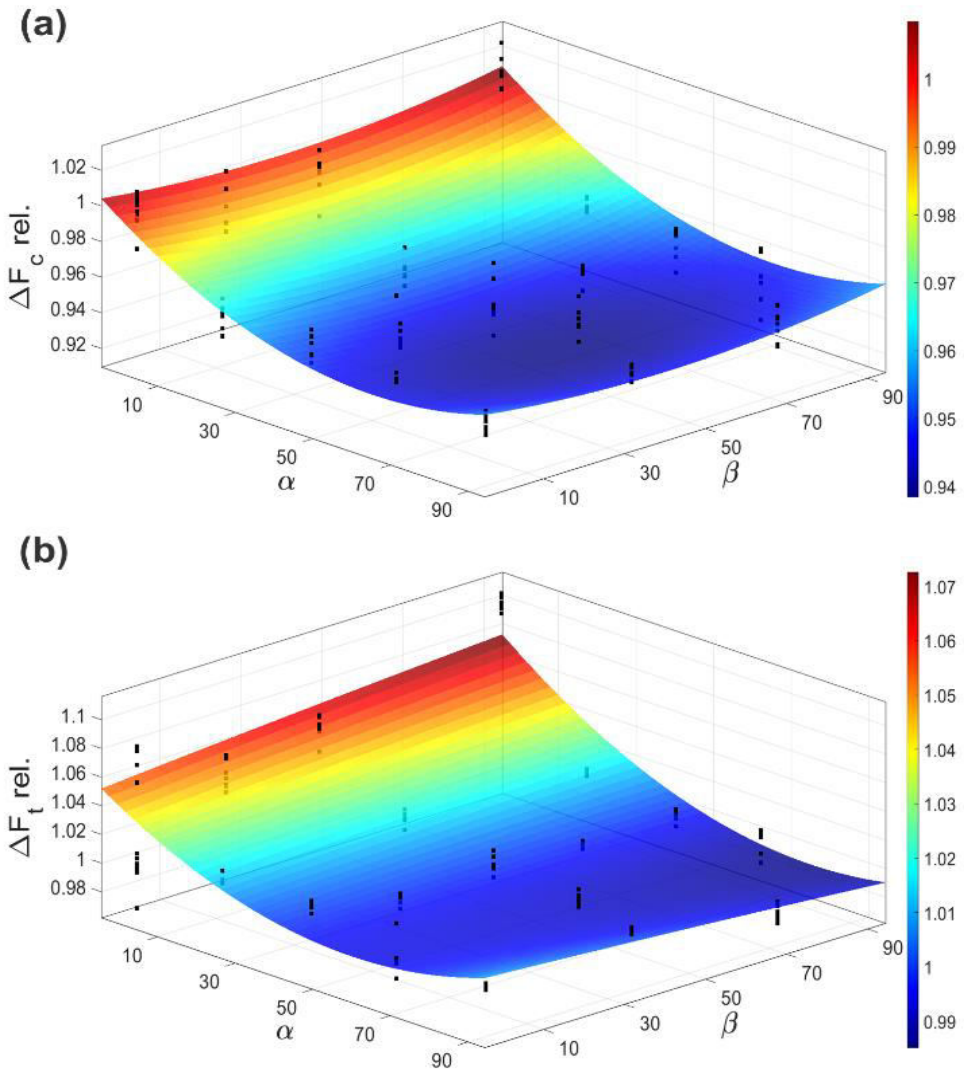

Figure 3-11: Surface plot of regression model for cutting force F_c (a) and thrust force F_t (b).

Vibrations and acoustic emissions

With the assumption that a single dendritic grain has the approximate size of the melt pool, it was expected that a signal should be detectable in a multiple of the penetration frequency of the cutting edge through the grains. In the measurements, however, no differences were found in the acceleration measurements or in the HFIM signals. In the qualitative assessment of the results, only very small differences could be determined, which, however, cannot be represented statically. Figure 3-12 shows the fast fourier transformation (FFT) of the structure-borne noise signal recorded with a sampling rate of f = 800 kHz during the cutting process.

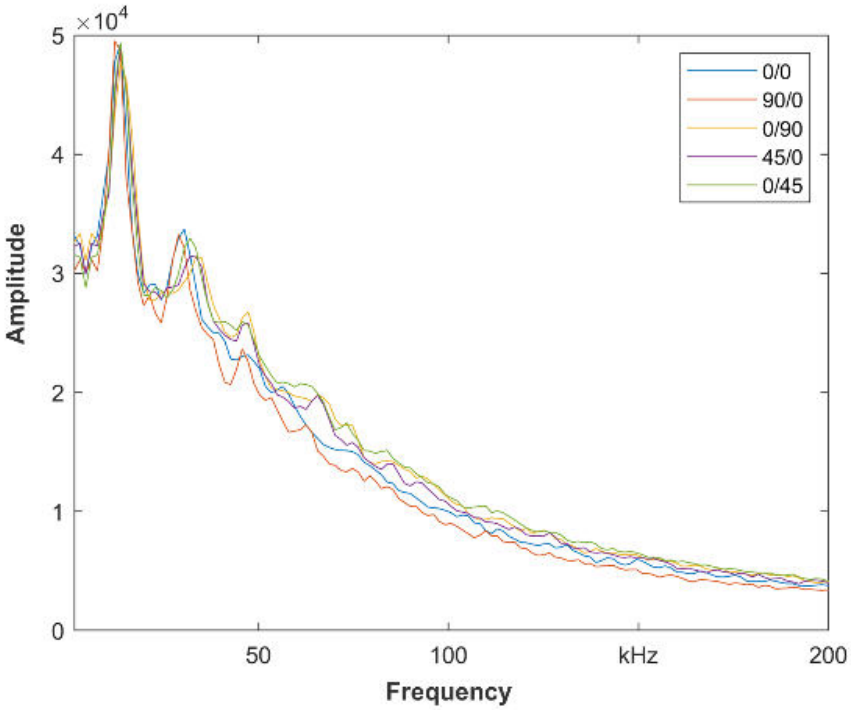

Figure 3-12: FFT of the structure-borne noise signal during cutting.

Chip formation

The different orientations can also be distinguished in the chip formation. The chips produced by orthogonal cutting have been collected and analyzed. For this purpose, three chips of each specimen were embedded, ground and polished. The chips show the formation of lamellas but not a segmentation. The geometric measurement of the thickness and lamella distances was carried out using a microscope. The thickness was measured from the lowest point between the chip lamellas to the back of the chip. In addition, the surface topography on the chip back was examined.

Comparing the chip thickness and surface topography of the chip backs between the different chips, an influence of the build-up direction can be determined. For this purpose, microscopic images of the chips from samples 0-0, 0-90, 45-45, 90-0 are shown in Fig. 3-13. The average thickness for the $\alpha = 0°$ is 112.9 µm and for $\alpha = 90°$ 96.4 µm. The effect is statistically significant.

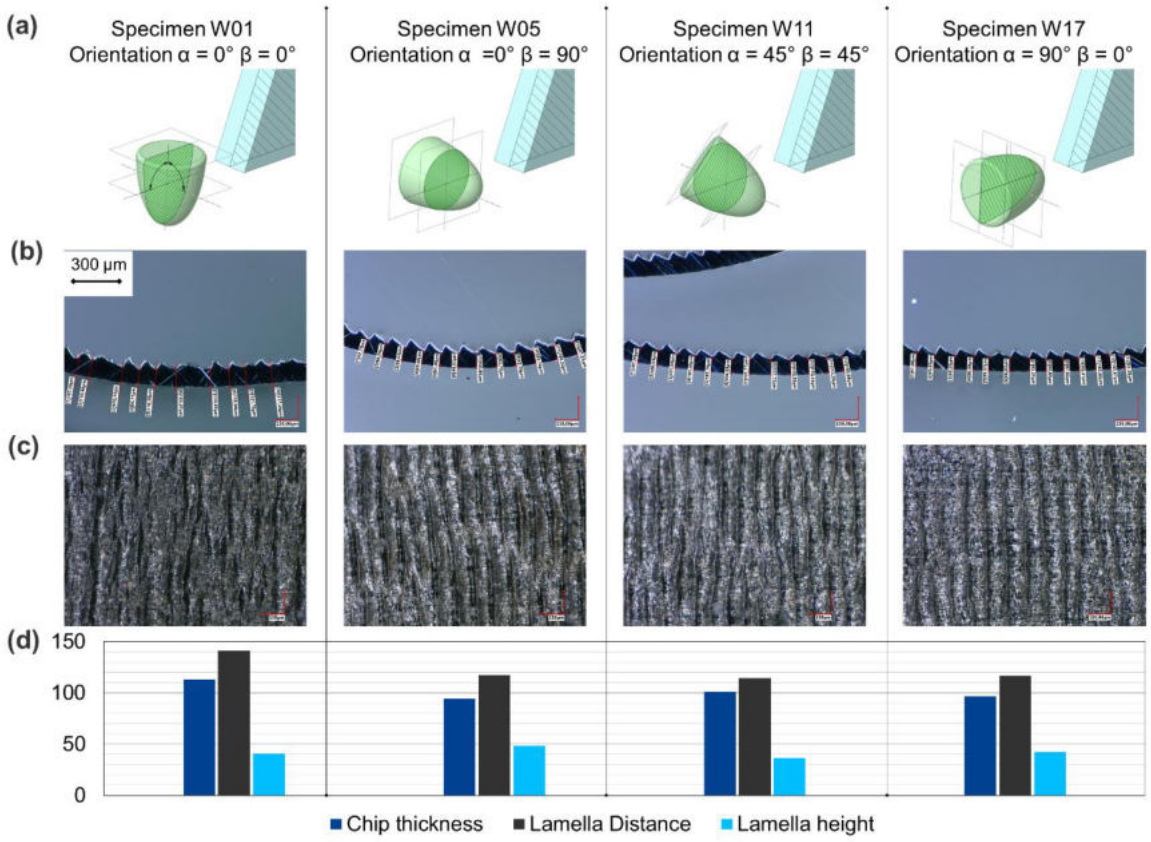

Figure 3-133: Exemplary excerpt of different specimen orientations with a representation of the schematic penetration of the dendritic structure (a), images of the chip cross-section (b), the back of the chips (c) and the results of the chip analysis (d).

Surface finish

The resulting surface has been measured regarding the resulting roughness after the cutting process. As shown in Fig. 3-14 the effect size of both angel α and angel β the differences are between values of Ra 0.05 µm and 0.25 µm. Since this difference is small, no implications for a practical guideline can be drawn in terms of orienting parts differently to attain a certain surface finish. Nevertheless, a certain effect of microstructure orientation on the surface finish can be seen.

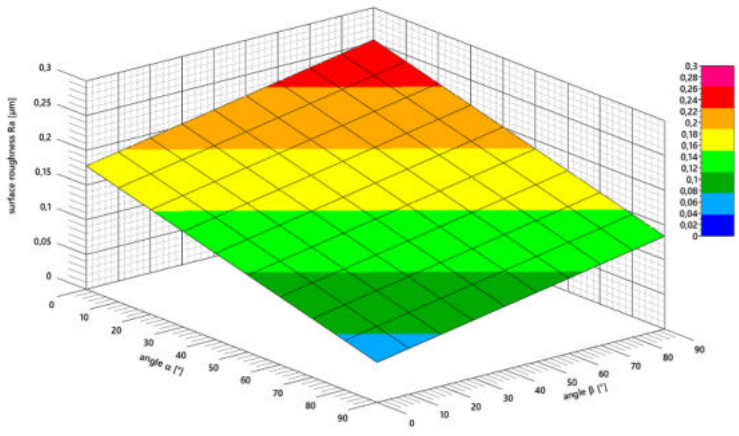

Figure 3-14: Surface plot of the regression model for mean surface roughness Ra.

3.4.4 Discussion and Conclusion

All the performed investigations show that both researched parameters, angle α and β contribute to an anisotropic behavior of AM parts during machining. Therefore, it is proven that there are anisotropic effects, especially regarding the effect of build-up angles on cutting forces.

However, the cause of these effects remains unclear. In the following, it is tried to give an overview of some possible explanations for these effects. Due to the layer-wise nature of the AM process the microstructure of the AM parts is anisotropic. The cutting of material is based on plastic deformation. Therefore, the orientation of grains and grain boundaries play an important role in the cutting process itself.

When changing the build-up angle α, the amount of grain boundaries that are encountered by the cutting-edge increases, too. In literature a higher ductility of fine-grained materials is reported due to more possible dislocation movements between grains. An explanation for the decrease in cutting forces with an increasing angle α may be that the higher number of grain boundaries has a similar effect as a fine-grained material and therefore allows easier deforming of the material and results in lower cutting forces. Additionally, it is reported, that the melt pool boundaries are the most common source of cracking for AM parts. The different amounts of grain and melt pool boundaries that are encountered are visible in Fig. 3-15. When following this explanation, the chip produced by machining of the α = 90° specimen should be buckled up more than that of the α = 0° specimen. More buckling would result in a lower chip

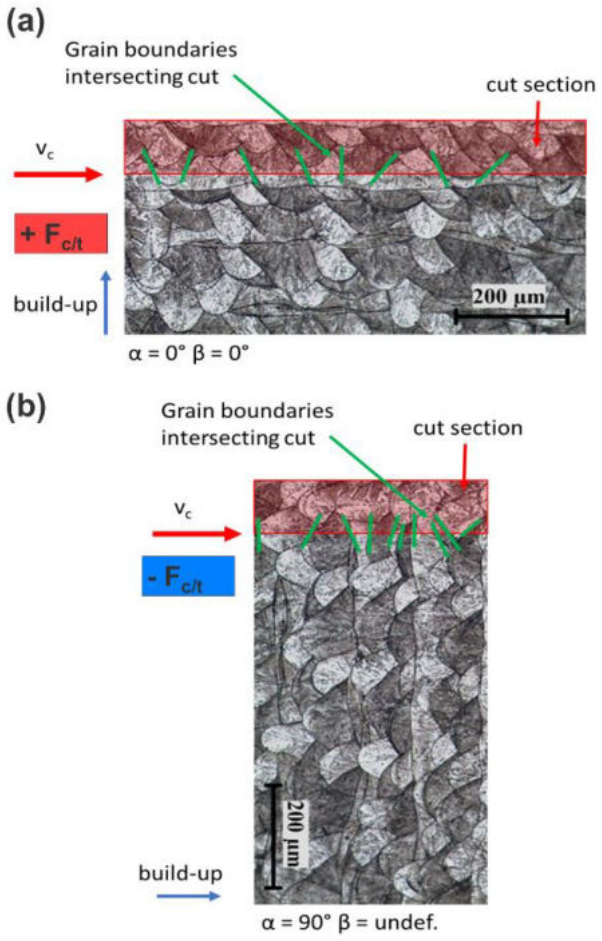

Figure 3-15: Grain boundaries in relation to the cut, base images from [8].

ration and in a stronger segmentation. When looking at the chip analysis performed in this work, a higher chip ratio is evident. The distance of chip lamellas shows an even bigger influence between build-up orientation α = 0° and the other examined chips.

Regarding the build-up angle β a different trajectory of the force plot for varying β-values can be seen. Considering the extreme points β = 0° and β = 90° there is almost no difference in terms of cutting forces. For the β = 0° angle, the dendritic grains are aligned orthogonal to the cutting plane, the layer boundaries are parallel to the cutting plane. For the 90° orientation, layer boundaries are perpendicular to the cutting plane. When the angle β increases the number of different layers also increases. However, in the presented data, no major influence of the β angle can be identified. In general, grain boundaries as well as layer boundaries could play a role in these phenomena.

Based on the findings, a model is developed which maps the specific material properties. This makes it possible to predict resulting cutting forces and chip volume, based on the layer penetration count and angle. The main findings can be summarized as follows:

- AM parts exhibit anisotropic behavior when machined using orthogonal cutting. The angle α influences the cutting forces generated by the orthogonal cut.
- The anisotropic behavior is visible both in cutting forces as well as in the chip thickness.
- Cutting force varies by up to 6 % and thrust force by up to 8 % when the orientation of specimens in the build volume is changed.
- A regression model was fitted to the data gathered by the experiments. A good model fit was achieved.

3.5 WP3 Influence of LPBF Parameters and strategies on fine machining of pre-built bores 3

3.5.1 Introduction

During the project Ad-Proc-Add, the influence and the interaction of the LPBF process parameters on the subtractive post-processing were investigated. The effects of the parameters on the geometry of bores are examined and subsequently the precision machinability was analyzed using reaming. In addition, a process simulation of the LPBF process was carried out to correlate the simulated defor-mation to the required machining allowance for subsequent reaming (see Chapter 3.8). The aim of this investigation was to examine the capabilities of the LPBF process to produce bores at angles of 90° (vertical), 60° and 45° that can be machined directly with a reaming tool without the need for drilling.

3.5.2 Experimental Setup

AM manufactured parts cannot always be freely oriented, and bores can be in different orientations on the build plate. It is therefore important to know the influence of bores in various orientations when

[3] This chapter is adopted from the paper: Maucher, C.; Teich, H; Möhring, H.-C.: Influence of LPBF Parameters and Strategies on Fine Machining of Pre-Built Bores. Journal of Machine Engineering (2021) 21(2):91-101. doi:10.36897/jme/133344 (peer reviewed)

building parts with the LPBF process. Inclinations of 90° (vertical), 60°, 45° and 0° (horizontal) with respect to the baseplate are investigated to determine the influence of the build orientation. Speci-mens are designed as simple cylinders without complex geometry, to exclude as many influences of the LPBF process as possible. The outer diameter is set to 30 mm and specimens are either built completely solid (all angles) or with a prebuilt bore (excluding 0° angle) with a diameter of 14 mm (see Fig. 3-16 and 3 17). The samples with the IDs 3,6 and 9 have been tested with a double scan ap-proach to examine its influence, which was adapted from Černašėjus et al. [23]. Double scan means all border paths are scanned twice for each layer. Three samples are built for each variation to im-prove statistical confi-dence.

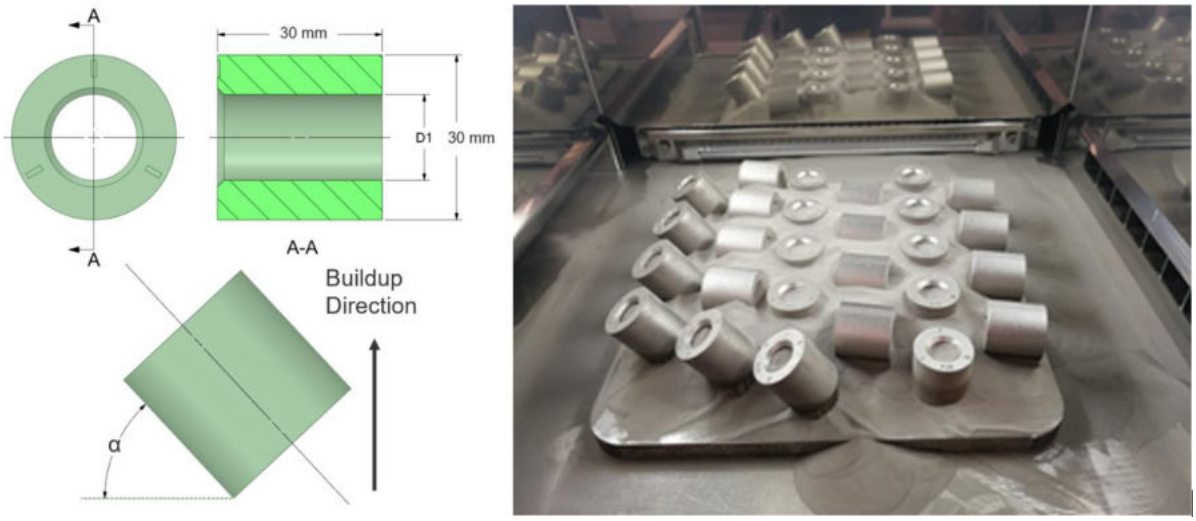

Figure 3-16: Sample dimensions design features (left). Samples after printing (right).

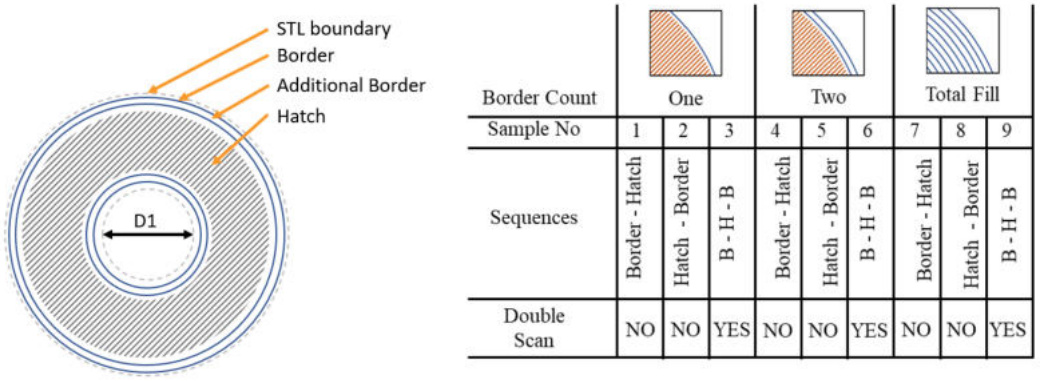

Border Count	One			Two			Total Fill		
Sample No	1	2	3	4	5	6	7	8	9
Sequences	Border - Hatch	Hatch - Border	B - H - B	Border - Hatch	Hatch - Border	B - H - B	Border - Hatch	Hatch - Border	B - H - B
Double Scan	NO	NO	YES	NO	NO	YES	NO	NO	YES

Figure 3-17: Overview of the varied parameters used to inspect as-built surface quality.

3.5.3 Results on Border Influence on Surface Quality

The first experiments have been performed to understand the effects of build parameters "border count", "hatch / border sequence" and "double scan border exposure" on the samples in as-built condition. Figure 3-18 shows the roughness comparison between the samples. Within those groups the hatch and border sequence has changed (see Fig. 3-17). It is evident from the results, that a count of two borders (ID 4 / 5 / 6) is superior to just one border. Furthermore, the results show an indication that the sequence in which the border and hatch are scanned also matter. Sample IDs 1 and 4 respectively are scanned

border first, hatch second and Sample IDs 2 / 5 the other way around, which the data suggests would be preferable. Furthermore, while preliminary experiments suggested that the double scan border exposure can be beneficial for the surface roughness, the main inspection does not show a significant advantage. Finally, the total fill samples have a wider spread in measured roughness, show defects when inspecting them visually and are therefore discarded from further consideration.

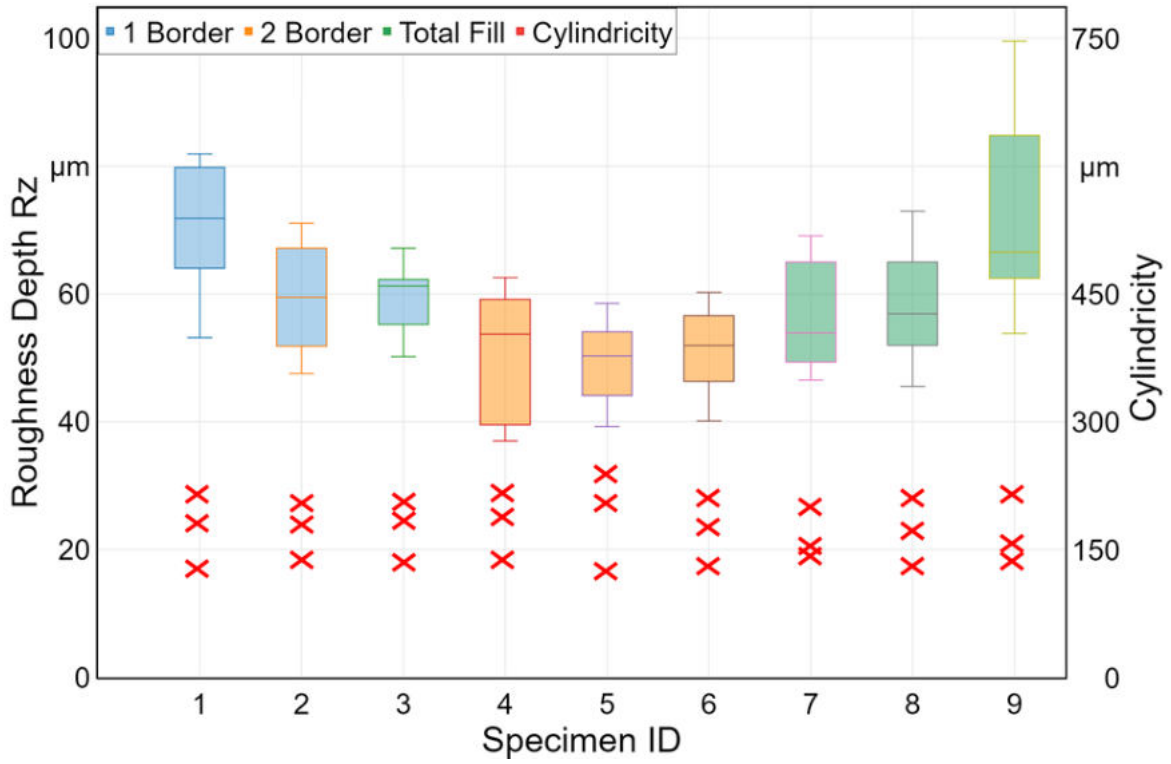

Figure 3-18: Roughness and cylindricity comparison for different build parameters.

The cylindricity in the as-built condition of vertical samples does not seem to be affected by the double scan border exposure or other border settings. Both double and single border scan exposure results in a cylindricity in as-built condition between 130 – 170 µm for vertical samples.

To examine the impact of the double border scan exposure on the machining process, the force and moment during drilling are plotted in Fig. 3-19. Both graphs show the traces of six samples: three with single border (Blue) and three with double border (Orange). The data shows no difference in the force measurements with all six samples experiencing the same force Fz during drilling. The moment on the other hand shows a significant difference: While the single border samples have their median moment Mz at 440 Ncm, the double border samples are subjected to a median Mz of 490, 580 and 810 Ncm for the three samples respectively. A reason for this might be the change in microstructure due to the different thermal profile of the double scan strategy.

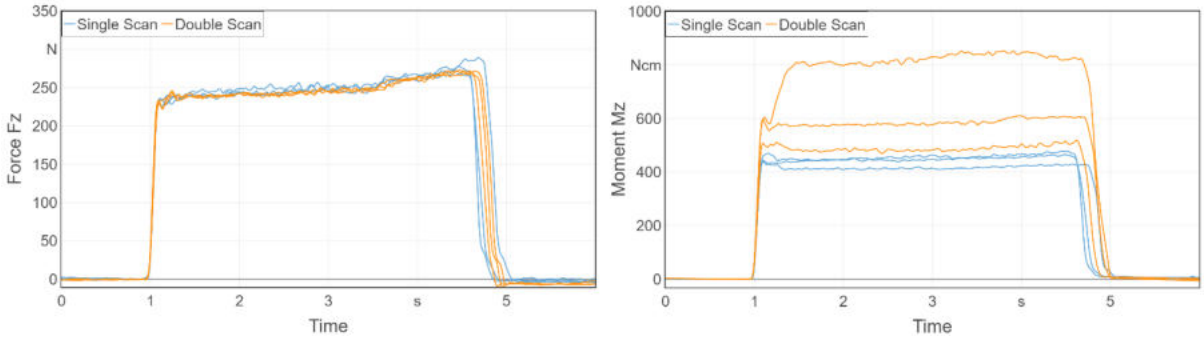

Figure 3-19: Force and moment measurements for single and double scan samples during drilling.

3.5.4 Results on Bore Orientation As-Built

Figure 3-20 shows the roughness for bores in different orientations measured in the as-built condition, meaning no post-processing has been performed yet. The vertical axis shows the roughness depth Rz in µm. The horizontal axis splits the measurements into three groups: measurements on bores in 45°, 60° and 90° (vertical) orientation. Each orientation uses measurements from three samples and outliers are removed. The outliers are measured on the overhanging surfaces, also called down-skin, of the 45° and 60° samples. Their Rz values are in the range of 150 to 250 µm for the 45° samples and 100 to 120 µm for the 60° samples. Figure 3-20 shows that the bore orientation has an influence on the resulting surface quality, even with down-skin measurements removed. While the median and lowest achieved Rz values are comparable between the sample orientations, the maximum differs significant-ly, from 64 µm for vertical up to 90 µm for 45° samples. This can be attributed to the staircase-effect [5].

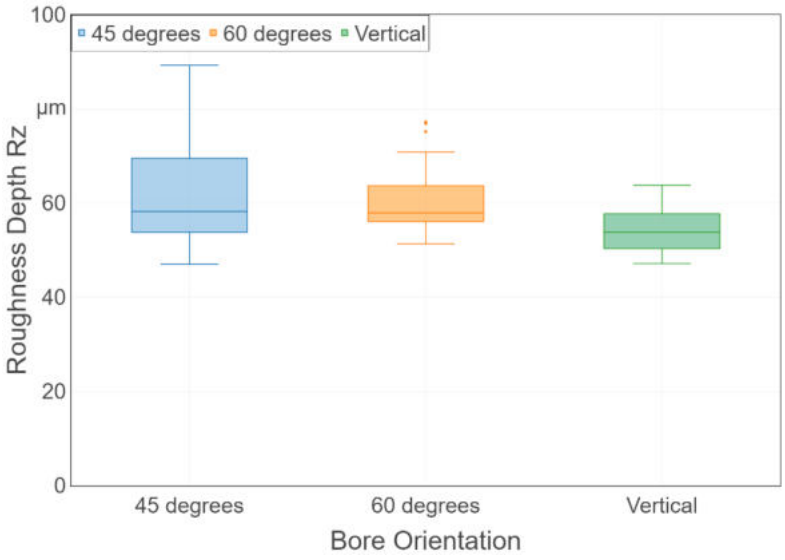

Figure 3-20: Roughness depth in as-built condition for different bore orientations.

The surface quality is also affected by shape deformations resulting from residual stresses. Figure 3-21 visualizes the deviation in shape of the inner bore for 45°, 60° and 90° samples in their as-built condition. The downskin effects can be seen on the 45° and 60° samples (marker 1), resulting from the laser penetrating several layers instead of just one on each scan pass. Although the influence of the downskin effect on the steeper 60° sample is smaller the influence of thermal distortion on the local deformation is higher (marker 2). Finally, Fig. 3-21 c displays the results in vertical orientation. The expected trend of better shape accuracy for vertical samples is clearly visible across the range of measurements.

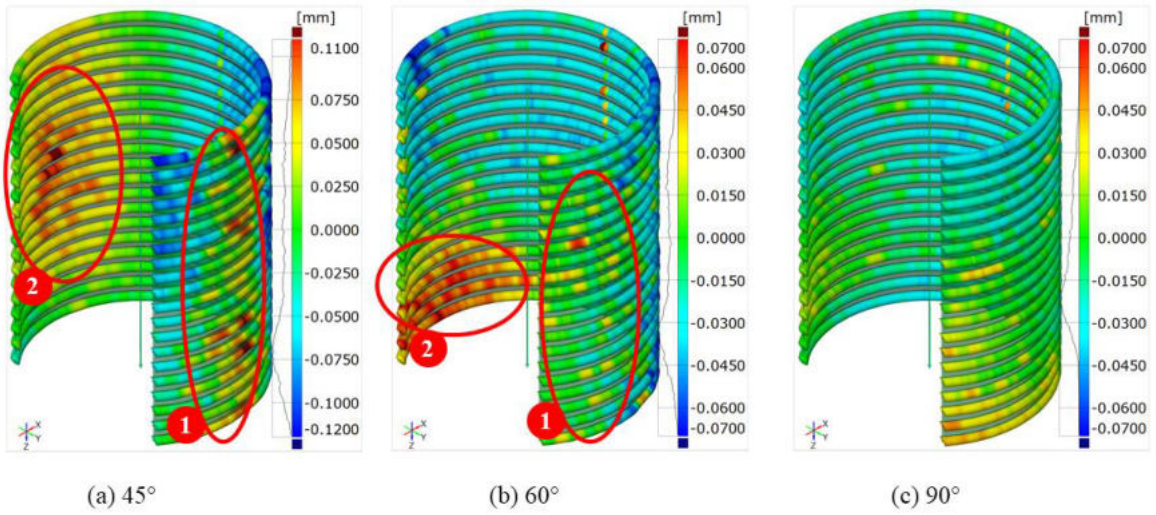

Figure 3-21: Measurement results (as-built condition) of 45°, 60° and 90° inclination angle samples.

3.5.5 Results on Bore Orientation and Drilling

The results so far show that building bores vertically results in a better surface roughness in the as-built condition. Roughness measurements are taken after drilling, to determine if this influence is still present (Fig. 3-22). The vertical axis shows the roughness depth Rz and the horizontal axis the build angle. The data is color-coded between “Prebuilt Bore” and “Solid” samples. No measurements are available for the horizontal prebuilt bore samples as they cannot be built without support structures.

Each box in Fig. 3-22 represents 12 measurements from 3 samples. The data shows that drilling out prebuilt bores results in a roughness depth Rz of around 4.1 to 5.8 µm (median). In contrast to that, the median Rz value after drilling for the solid samples is between 9.3 and 11.1 µm, around two times as high. Samples with prebuilt bores possess a better surface quality than solid specimen. While the distinction between prebuilt bore and solid samples is very clear, the built orientation does not seem to influence the surface roughness after drilling.

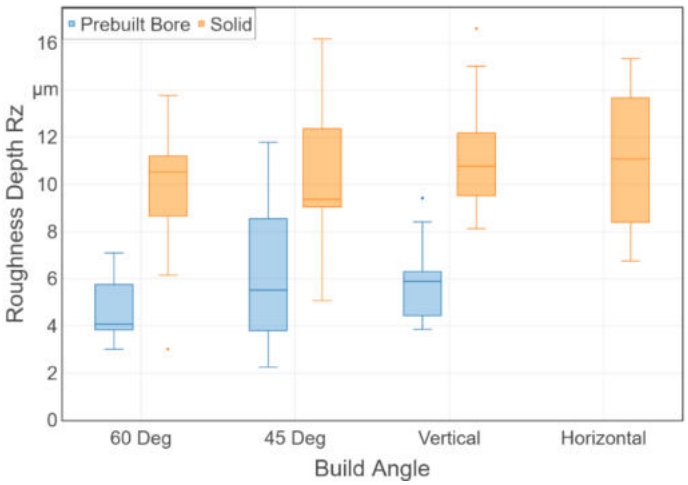

Figure 3-22: Roughness comparison of prebuilt and solid samples for different bore orientations.

After measuring the “as-built” condition and centering the samples in the machine, reaming of the prebuilt bore is carried out. Based on the process simulation, a machining window for reaming can be

defined based on the deformation rate. This is achieved by defining the maximum deformation as the minimum allowance, taking into account the process-related basic deviation of the surface quality [13]. Samples build in vertical direction (90°) have the best cylindricity and reaming those samples with a prebuild diameter of D1 = 15.8 mm results in a high-quality surface in most areas. Therefore, the roughness and CMM measurements produce acceptable characteristic values. The visual inspection however, shows that there are still areas with remaining surface porosity of the as-built surface present. This can be seen in Fig. 3-23 (center) with the corresponding measurements. The as-built condition can be seen on the left in Fig. 3-23. Reaming with a prebuild bore diameter of D1 = 15.7 mm (machining allowance of 0.3 mm) provides good results and can be seen on the right in Fig. 3-23.

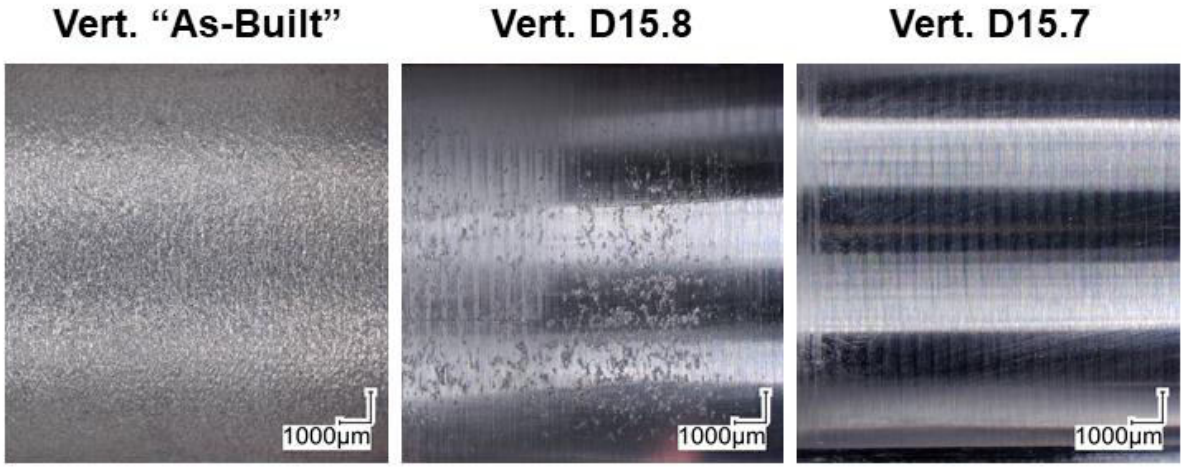

Roughness

R_a = 6,49 µm	R_a = 0,75 µm	R_a = 0,30 µm
R_z = 53,97 µm	R_z = 9,80 µm	R_z = 1,66 µm

Cylindricity

0,148 mm	0,046 mm	0,034 mm

Figure 3-23: Surface quality of the specimens.

Due to increasing deformation effects with decreasing inclination, a machining allowance of 0.3 mm is not sufficient for 60° samples. Increasing the machining allowance to 0.35 mm, with a prebuild diameter of D1 = 15.65 mm, results in a good surface quality after as-built reaming.

The same effect is present with the 45° samples, which exhibit an even higher deformation in addition to surface deterioration at down-skin surfaces, due to meltpool layer penetration. Therefore, reaming needs more allowance to provide a constant cut through the material. An allowance of 0.4 mm (D1 = 15.60 mm) proved sufficient to achieve a good surface finish after reaming. It is still possible to machine the samples with this higher machining allowance, although the recommended value is in the range between 0.2 to 0.3 mm for the utilized tool with a diameter of 16 mm. It should be noted, however, that this recommendation is based on the conventional drilling – reaming process chain, and not the as-built reaming process as investigated in this investigation.

The as-built condition shows a cylindricity range between 140–370 µm, and a straightness range between 22–48 µm. The reaming operation improves those values for all samples and narrows the range. After as-built reaming the cylindricity is between 15–47 µm with the median at 30 µm, and the straightness is between 2–7 µm with the median at 4 µm (see Fig. 3-24).

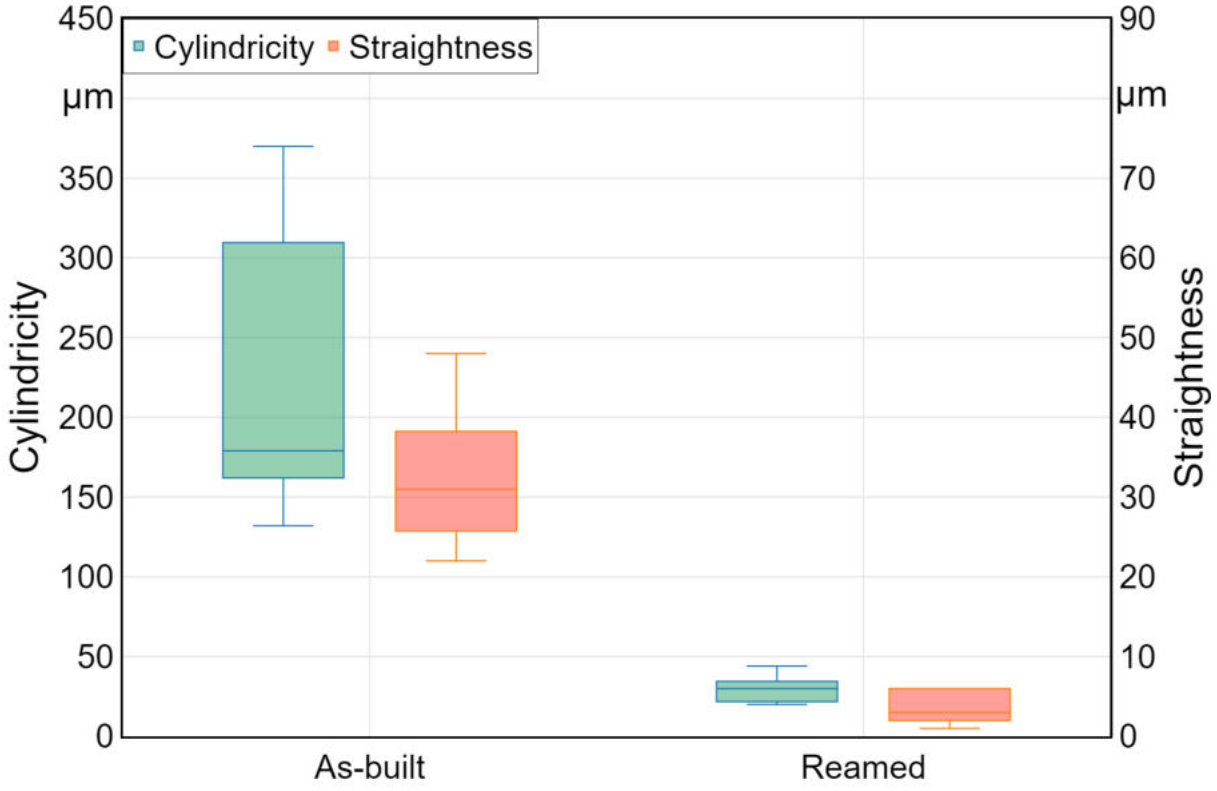

Figure 3-24: Cylindricity and straightness of the as-built and reamed bores.

Figure 3-25 shows the roughness depth Rz comparison for samples after reaming. In addition, for comparison reasons samples without a prebuild bore are manufactured, drilled and then reamed. The roughness after as-built reaming is measured to be between 1.3–2.8 µm, compared to 1.3–2.5 µm for the solid reference samples after drilling and reaming. CMM measurements give diameter results between 16.007 mm and 16.018 mm for all samples, with no discernible trend for specific parameters within the dataset. Therefore, all samples are within the desired 16H7 tolerance after machining.

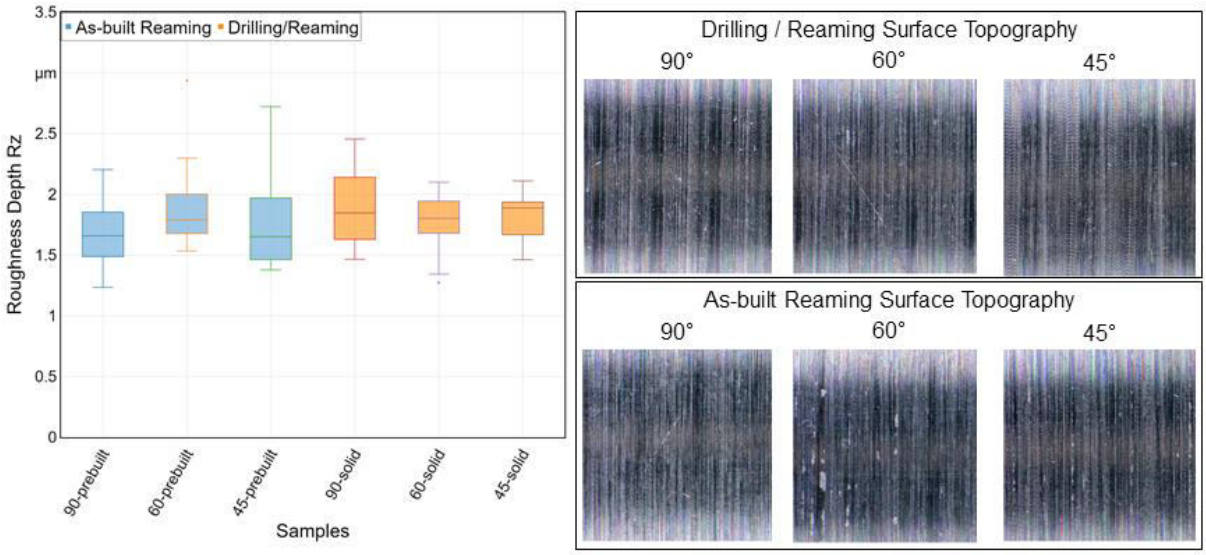

Figure 3-25: Roughness depth Rz comparison for samples after reaming.

3.5.6 Conclusion

The interactions in the subtractive processing of additively produced samples are examined. It is achieved to design bores in additive manufacturing in such a way that as-built reaming of the pre-built bore is made possible. The drilling process step can thus be omitted. In addition, an LPBF process simulation can be used to assess whether as-built reaming is possible and which machining allowance should be provided. The most important conclusions of this investigation are:

- Reaming without previous drilling is possible and can produce good results regarding surface finish and dimensional accuracy if proper care is taken in choosing the right tool and machining allowance.
- A diameter of 15.8 mm results in surface defects after reaming of vertical and 60° samples. 0.2 mm is therefore not enough machining allowance for as-built reaming.
- A diameter of 15.7 mm with vertical samples produces very good results after as-built reaming. Roughness, cylindricity and straightness are similar to samples that are drilled before reaming.
- Bore orientation matters and requires a slightly higher machining allowance as can be seen with 60° and 45° samples.

Additional analysis must be conducted in order to create an analytical model for as-built reaming of additively pre-built bores with different bore sizes and orientations, based on further measurements, simulations and statistical surface models

3.6 WP3 Analysis of functionalizing process technology in terms of milling

3.6.1 Introduction

Based on the results of chapter 3.4 further investigations regarding the influence of the build up direction on the milling process were conducted. In addition, the influence of two different heat treatment strategies was examined. The milling investigations were conducted on a DMG 65 3D Hybrid. As tool a carbide mill was used with end face milling strategy with varying parameters. The parameters can be seen in table 3-5. For the two parameters we choose a full factorial design of experiment with four stages resulting. The setup can be seen in Fig. 3-26. To measure the forces a three axis dyna-moter was used and vibrations were measured with an accelerometer. The specimens were printed as cubes with an edge length of 30 mm. The additively manufactured specimens are made of tool steel 1.2709. To produce the specimens, a LPBF Machine RenAM 500Q from the company Renishaw was used.

Carbide Mill with Internal Cooling	
Cutting Speed	vc = 130 – 160 m/min
Tooth Feed	fz= 0,06 – 0,09 mm/tooth
Depth of Cut	ap = 10 mm
	ae = 1 mm
Coating: AlCrN,	dc =10mm

Table 3-5: Utilized tool and parameters.

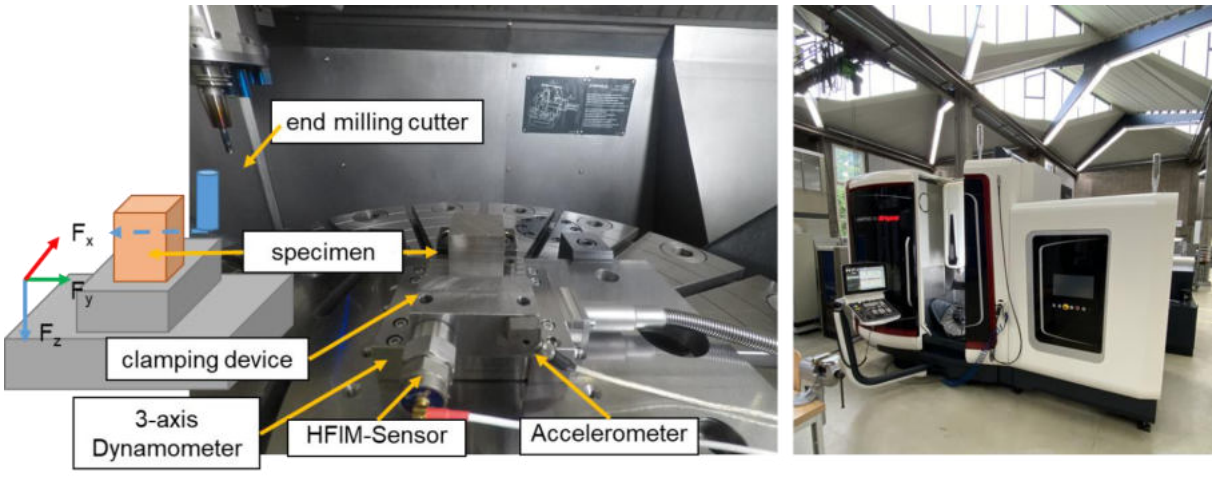

Figure 3-26: Experimental setup.

To determine the minimum allowance, the samples were first machined with varying depth infeed. The depth was varied in the following steps: 0; -50um; -100um; -200um and -300um.

In the case of a cube that was built up additively at an angle of 45°, the machined surface is shown in Fig. 3-27. There are surface defects caused by the so-called Staircase effect visible at a depth of -50um. From a depth of 100 µm machining allowance, surface defects are no longer visible.

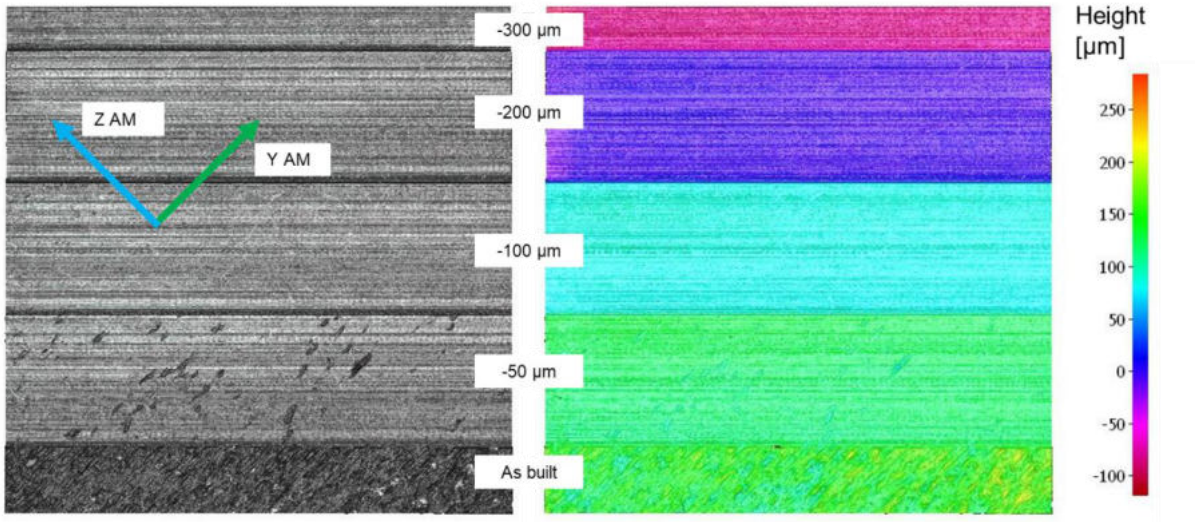

Figure 3-27: Surface topography of milled skin surface.

The same was considered when processing vertical surfaces. When processing horizontally built surfaces, more surface defects resulting from the scan pattern were monitored. Low spots in the upper skin surface derive from meeting points of the "stripe" fill pattern used. These low points have depths of about −100 to −200 µm when measured from the surface peaks on the as-built surface. As can be seen in the figure, an increased allowance of at least 300 µm is therefore required on horizontal surfaces.

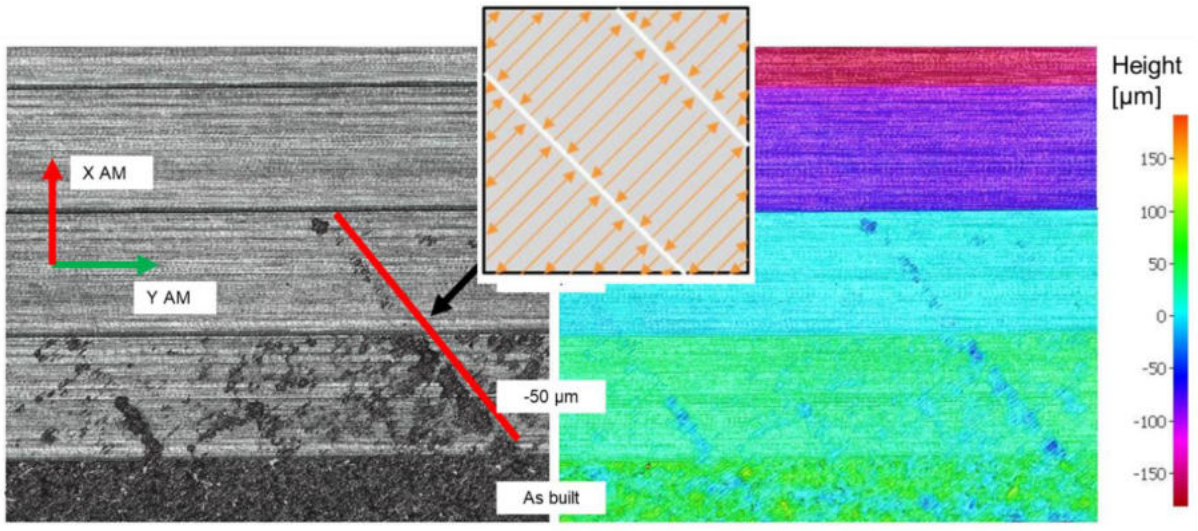

Figure 3-28: Surface topography of milled up-skin surface.

The Results are summarized in the table 3-6.

allowance	Vertical skin	Inclined skin	Upfacing skin
50 µm	Minor defects	Visible low spots from staircase-effect	Visible low-spots from intersections of hatch pattern
100 µm	No defects	Rare defects, mainly pores	Visible low spots from intersection
200 µm	No defects	No defects	Visible changes in surface, not measurable
300 µm	No defects	No defects	No defects

Table 3-6: Surface quality.

3.6.2 Influence of heat treatment

In order to investigate the influence of the heat treatment on the milling finish, a number of samples were heat treated. In this comparison differences in build-up direction are excluded. In total 69 singular data points, 37 of which have been tested in the as-built condition, and 16 for the solution annealed as well as the age hardened state.

Two strategies were used for this: Solution annealing and age hardening. Solution annealing was done for 2h at 860°C with rapid cooling in standing room air. The goal of solution annealing is commonly the reduction of residual stress. In Literature it is stated that the as-built condition nearly equals the solution annealed condition. When looking at the microstructure, which can be seen in Fig. 3-29, however differences can be distinguished. Age hardening was done for 6hours at 460°C with slow cooling in the oven. The goal of hardening is commonly Increasing hardness and reduction of residual stress. The target hardness with this material can be 55 Rockwell.

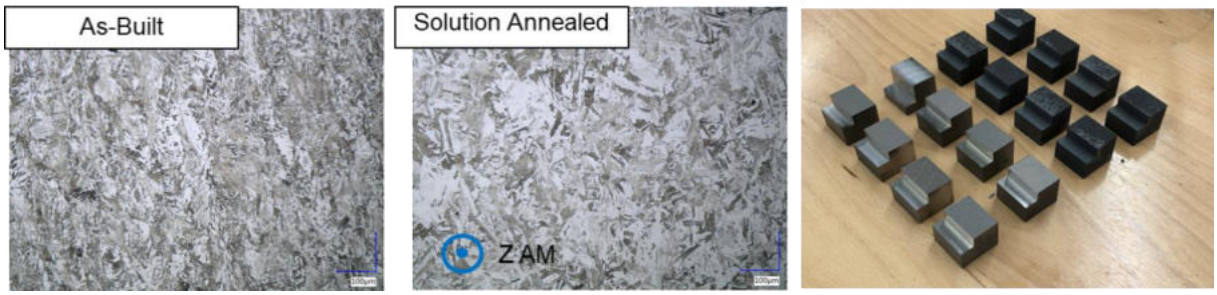

Figure 3-29: Microstructure of the as-built and solutions annealed specimens.

Figure 3-30 visualize the acquired force data in boxplots. The blue box shows the range between first and fourth quartile, the whiskers show the range between maximum and minimum value.

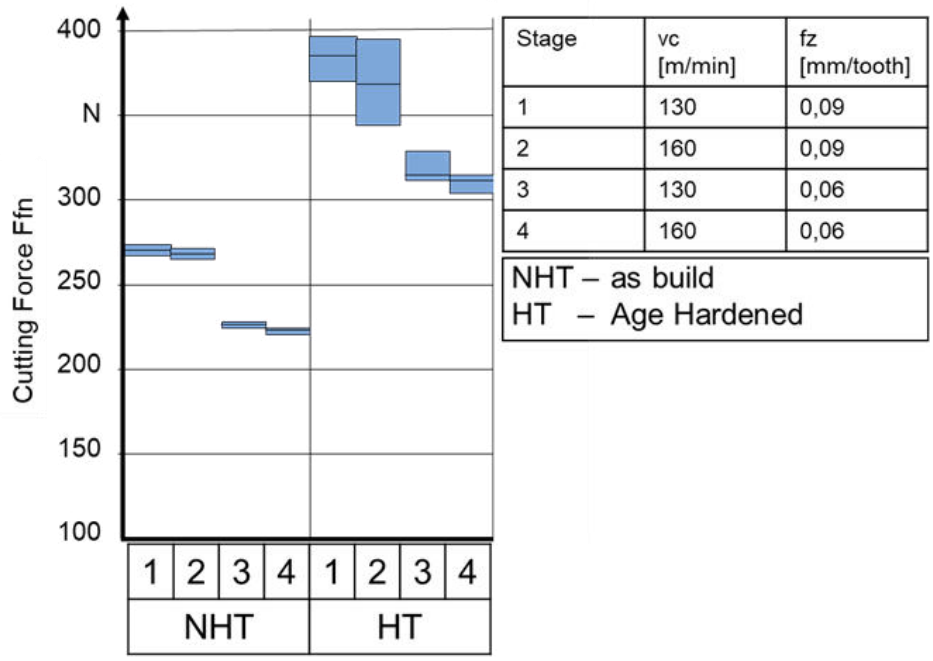

Figure 3-30: Cutting force during milling with different heat treatment strategies and varying process parameters.

It is evident, that the age hardened samples create much higher active forces than those of the solution annealed or as built samples. The increase in thrust force is of approximately the same relative magnitude as that of the active force, so it can be assumed that there are no additional effects here. The influence of different heat treatments on the cutting forces can be clearly confirmed. Solution annealing leads to slightly lower forces compared to an as-built condition. Overall, solution annealing reduces the range of measurement results. Several factors could underlie this behavior:

Solution annealing and the associated reorganization of the microstructure leads to a reduction in the residual stress states bracketed by the LPBF process and thus to a correspondingly smaller variation in the cutting forces. Solution annealing allows for a reorganization of the microstructure of the part. Due to local differences in heat flow and heat distribution during the LPBF process the microstructure of the part isn't uniform. Different grain structures are known to influence the mechanical properties of material and in turn have effects on cutting forces.

3.6.3 interaction between the build-up direction and the cutting forces during milling

Subject of the investigation was the influences of different build-up orientations as well as heat treatment processes on the cutting forces required to machine the material produced by the LPBF-process. For defining build-up orientations two different angles are used. These angles have been designated α and β. Angle α describes the tilt of the part around the x-axis, angle β around the y-axis. The coordinate system refers to this can be seen in Fig. 3-31. A better explanation of the mentioned angles α and β is also given there.: The red arrow indicates the vector of the feed motion, the blue arrow indicates the build up-direction (respective the z-axis) of the LPBF-machine.

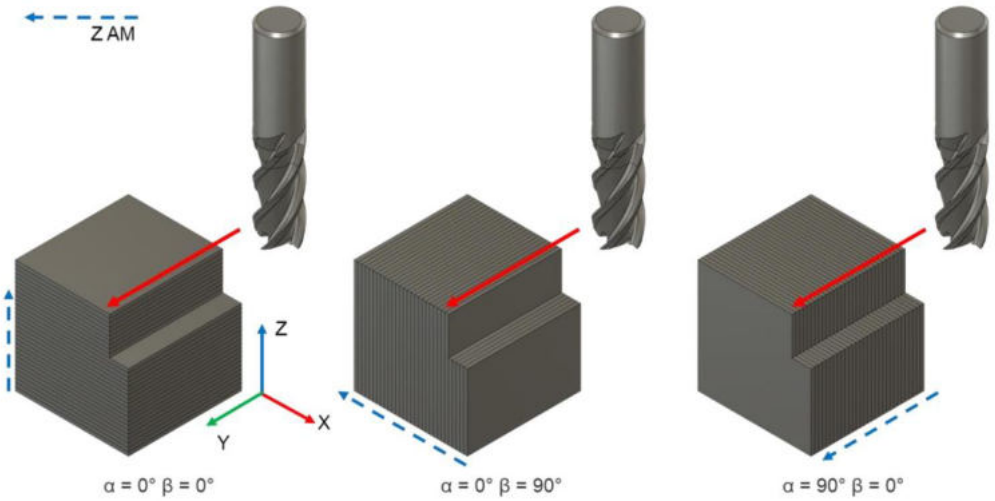

Figure 3-31: Build-up direction relative to feed direction.

As described, a main motivation of this work is to determine whether the influences of varying orientation of layers relative to the cutting direction that have been shown for orthogonal cutting are also present in milling machining. The experiments and the data processing steps described above result in a total of 276 data sets which are included in the following evaluations. The variables build-up angle alpha and beta as well as the variable heat treatment were examined in a mixed manner. To evaluate the actual influence of a variable, a multilevel procedure based on different statistical measures is applied. First, a regression analysis is performed with the aim of describing the recorded measurement data with a mathematical model of the influence variables alpha and beta. Based on the significance levels reached by each term and the model fit of the whole regression model, a first statement about the influence of a variable can be made. Subsequently, based on the actual differences of the measured values, a further evaluation of the results is made. It must be evaluated whether the shown effect does not originate from a coincidental circumstance. A further indication for the evaluation is provided by the size of the respective data set examined and the corresponding partial data sets of the respective parameter level, the larger the dataset is, the more trustworthy the results are.

An influence of different orientations of the layers from the LPBF process on the components can neither be confirmed nor ruled out from the investigations carried out. The data on which this evaluation is based show relatively large fluctuations, especially between different test runs, which indicates a high sensitivity of the investigations to boundary conditions. The inconsistent occurrence of statistically significant influences on the cutting forces in this study may be a peculiarity of the test program. On the one hand, no cutting parameters were varied for the purpose of comparability of all tests. It is possible that the chosen cutting data is an unfortunate coincidence that does not reveal the desired effect. On the other hand, it is conceivable that any results obtained during corner milling do not stand out, since the angle between the cutting edge and the cut structure is subject to constant change. For specimens in an α=0° β=0° orientation, the cutting edges of the cutter move exclusively in the build-up plane, so the microstructure to be cut should not change much. If, on the other hand, specimens are viewed in a different build-up direction, the angle between the cutting edge and the microstructure or layer structure of the

specimen is constantly variable. Due to the helical design of the cutting edge, there is also no constant angle between the cutting edge and the layer structure.

3.7 WP4 In-Situ defect monitoring for LPBF using a multi-sensor build platform

3.7.1 Introduction

Process monitoring of the LPBF process can be difficult. Due to the high energy input and the resulting residual stresses, the structural integrity of the built component is at risk during production. However, these areas lie within the powder bed and are difficult to monitor. During the project a new method was developed to monitor the process by measuring the heat flow inside of the build plate to detect possible process interruptions. This is achieved by a multi-sensor build platform which measures the temperature below the build plate. Furthermore, the method offers insights about the discrete temperature history based on the heat balance.

The LPBF process, is a thermal process which utilizes lasers to selectively heat and melt powder to build up these layers. The heat balance is determined by a large number of process-specific influences and in addition to the composition of the melt pool, the heat balance is characterized by local temperatures, dwell times and local cooling gradients, determining properties for the later material phases [14]. The heat balance of a layer or the solidified volume is in turn dependent on the temperature of the build volume, the energy input and the local heat dissipation. In addition, the layer times in the LPBF process with a constant build rate are determined by the number and size of the components in the build volume. However, since the cross-sectional areas in the individual layers vary, there are also variable layer or cooling times and thus variable temperatures at the start of subsequent layers. The heat balance of a layer is further characterized by the chronological sequence of the individual scan vectors and the above-mentioned process parameters. They determine the internal stresses and deformations during the build-up process [15] and, according to Branner, are directly related to the component structure behavior [16]. To dissipate heat and avoid thermally induced deformations, the to be printed part needs to be attached to the build plate and support structures are needed on overhanging surfaces [17]. The powder material has a thermal diffusivity that is orders of magnitude lower than the solid material, so that it effectively acts as an insulator [18]. This means that most of the heat is dissipated via the build plate. Because of the rapid melting and solidification of the material, caused by the heat sink, created by the underlying metal build plate and the already built layers of the geometry, lead to a rapid cooling of the melt pool resulting in a high temperature gradient [19] leading to thermally induced residual stresses [1].

In this study, titanium (Ti-6Al-4V) is utilized as powder material for the LPBF process. Particular attention should be paid to the heat flows that occur during the process. Since the used titanium alloy has a high melting temperature of 1675 °C and a low thermal conductivity, large temperature gradients occur within the component during the process. These can severely impair the mechanical properties and cause internal stresses [20]. If an induced residual stress exceeds the tensile strength of the material, the component can partially or completely detach from the build plate. Because of the possible occurrence of such failure inside of the part, it is not sufficient to only monitor melt pool quality [21].

There are numerous research efforts that address the monitoring and control of the melt pool to improve part quality. Most of the studies within the monitoring of temperatures are centered on pyrometry, which is defined as the noncontact measurement of temperature of a body based upon its emitted thermal radiation [22]. However, with the complexity of geometries and the location of possible failures inside of the powder bed in the LPBF processes, this approach is not sufficient to ensure process stability.

In this experiment, thermocouples attached underneath the build plate were used to monitor the heat flow. To integrate this method in an AM production machine a self-sufficient measuring platform is successfully developed, built and tested. With the help of a sensor field, which measures the temperature distribution below the build plate on which the printing is being carried out, a statement can be made about the thermal behavior of the layer structure.

3.7.2 System Design

In order to be able to estimate the temperatures to which the sensors and measuring electronics are exposed, the complex thermal relationships of the system must be considered, shown schematically in Fig. 3-32. Since optical investigation methods can only provide insight into the thermodynamic events of the youngest layers, a measuring system is developed which primarily records the temperature distribution within the build platform in detail. As already explained, this is an indication of the temperature differences within the component and it makes it possible to identify relationships between these and the structural integrity of the build component.

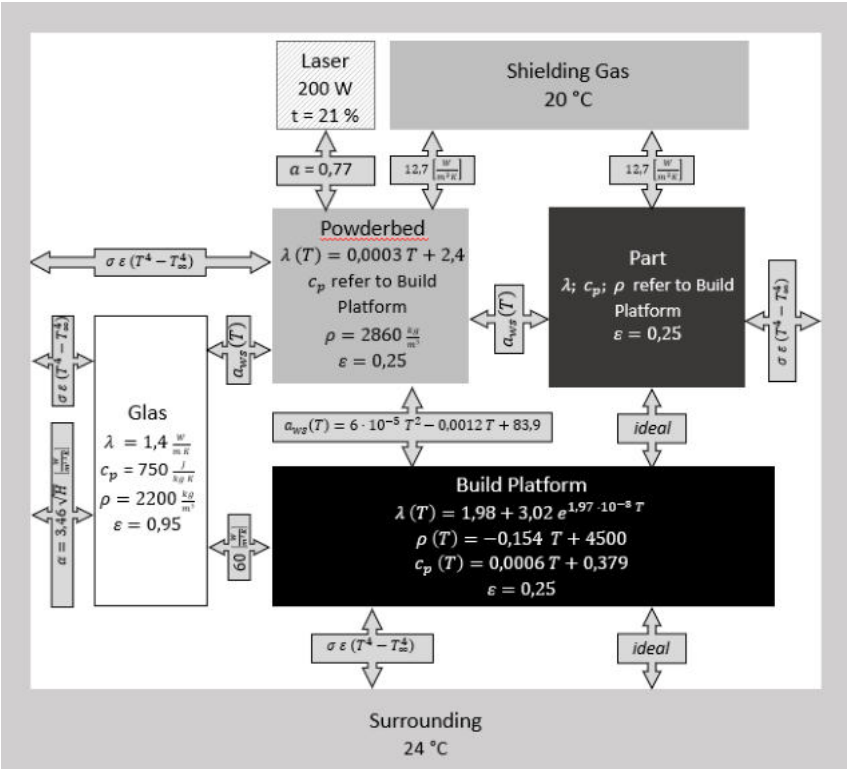

Figure 3-32: Temperature transition coefficients in PLBF process.

3.7.3 Numerical Process Simulation for System Setup

In order to ensure that phenomena such as delamination can be measured with the sensor concept, a multi-stage simulation is carried out. The aim of these simulations is to compare the temperature distribution of a printing process with delamination with the temperature distribution of a printing process without delamination. A component that is 8 mm high and 60 mm long is to be printed. This corresponds to 400 layers with a layer thickness of 20 µm.

After 200 layers have been applied, i.e. after about 4500 s, in the case of delamination, a crack is inserted over half the length (30 mm), which is 1 mm thick, as can be seen in Fig. 3-33.

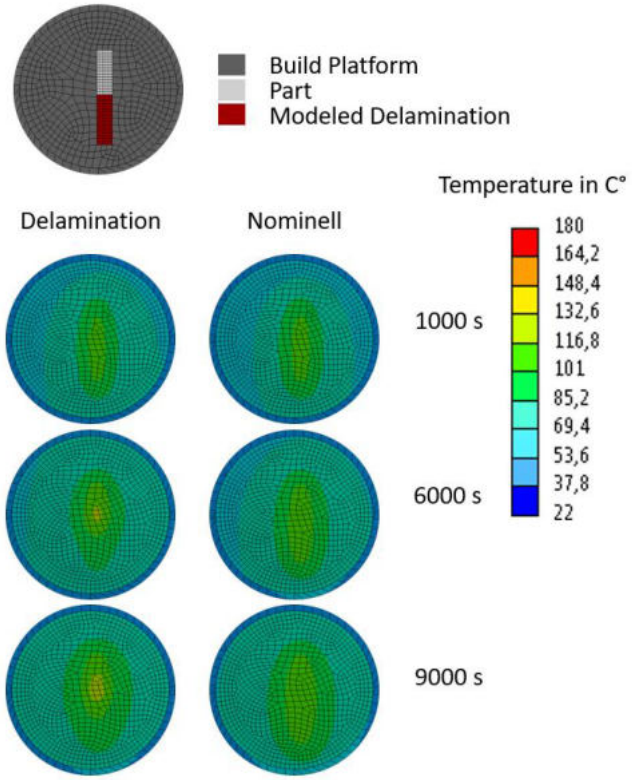

Figure 3-33: Thermal process simulation of delamination.

To obtain the corresponding temperature curves, the entire printed body (one with and one without a crack) is simulated in the fully built-up powder bed in both cases utilizing the values given in Figure 3-33. The laser beams homogeneously over the entire top of the component. First of all, it must be validated whether the temperature profile after 200 shifts corresponds to the one that would be seen if only 200 layers are built up and not all 400. It can be seen that the basic temperature profile is corresponding over the entire period, even after the 200 shifts (4500 s), as can be seen in Figure 3-33. The further procedure for investigating the impact of a crack on the temperature distribution during the printing process is therefore considered to be sufficiently representative. In the next step, the temperature distributions with and without delamination are shown after the delamination occurred at 4500 seconds.

After the delamination, as expected, a concentration of the heat flow can be observed in the area in which no delamination has taken place, whereas a decrease in heat can be seen in the area of the

delamination in the printing plate. This has proven the principle that a phenomenon such as delamination can be seen during the printing process from the temperature in the building platform.

During the printing process, heat is repeatedly introduced into the build platform at various points by the laser. At the beginning the building platform has a homogeneous heat distribution, the heat spreads unhindered and evenly. However, this condition only persists for a short time. The component heats up in different places, it becomes difficult to differentiate between the laser spot heat source location. The sideways spread of the heat is particularly disruptive and hardly allows conclusions to be drawn about the position of the active source. To achieve clearer measurements and to control the heat propagation elements that make it very difficult for heat to spread in the undesired directions are used. This can be achieved by a design from pins, since the highly heat-insulating gaseous argon is between the pins during the printing process, heat exchange between the pins is hardly possible and improves the precision of the measurements with regard to the localization of the heat source, as can be seen in Figure 3-34.

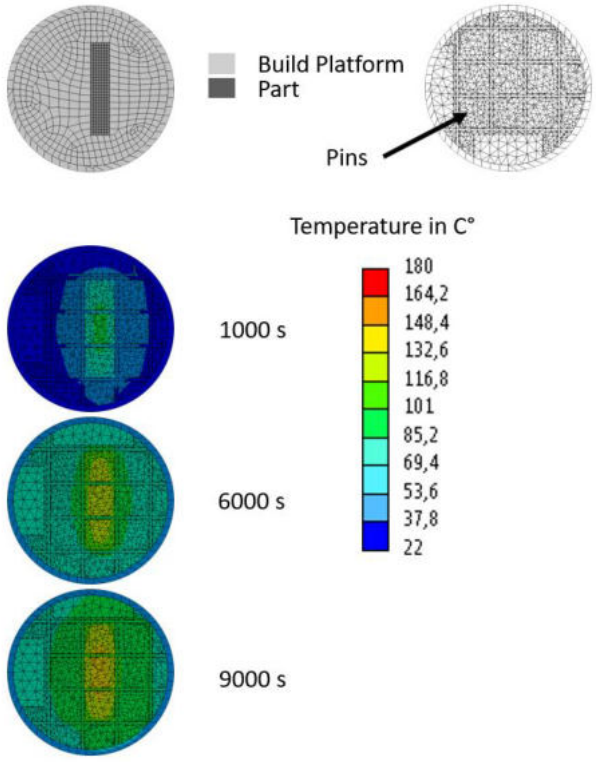

Figure 3-34: Pin-Design validation with thermal process simulation.

3.7.4 Sensor Platform & Data-Recording

The principle of the intended temperature measurement is based on the principle of heat transfer. Quickly reacting and unadulterated measured values are achieved if the sensors are attached as directly as possible to the heat source to be observed. This means that there is as little material as possible between the sensor and the source. In this case, this means that the build platform should be designed to be as thin as possible and the sensors should be attached to it directly from below, if possible. For further considerations, the thickness of the building platform is assumed to be 10 mm, since this corresponds approximately to the thickness required for mechanical integrity.

The distance between the pins should be kept as small as possible in order to prevent heat build-up by reducing the heat-conducting cross-sectional area even further. With a measured cable thickness of 1.2 mm, a distance between the pins of 1.3 mm is provided. With an available length of 5.08 mm for 5 pins with the respective distances in between, a side length of 8 mm is chosen for each pin. This corresponds to a length of 45.2 mm and thus leaves space for any cable routing around the pins to the microcontroller. The height of the pins is set to 10 mm, as this corresponds to the height from the simulation and thus provides good, comparable measured values (Figure 3-35).

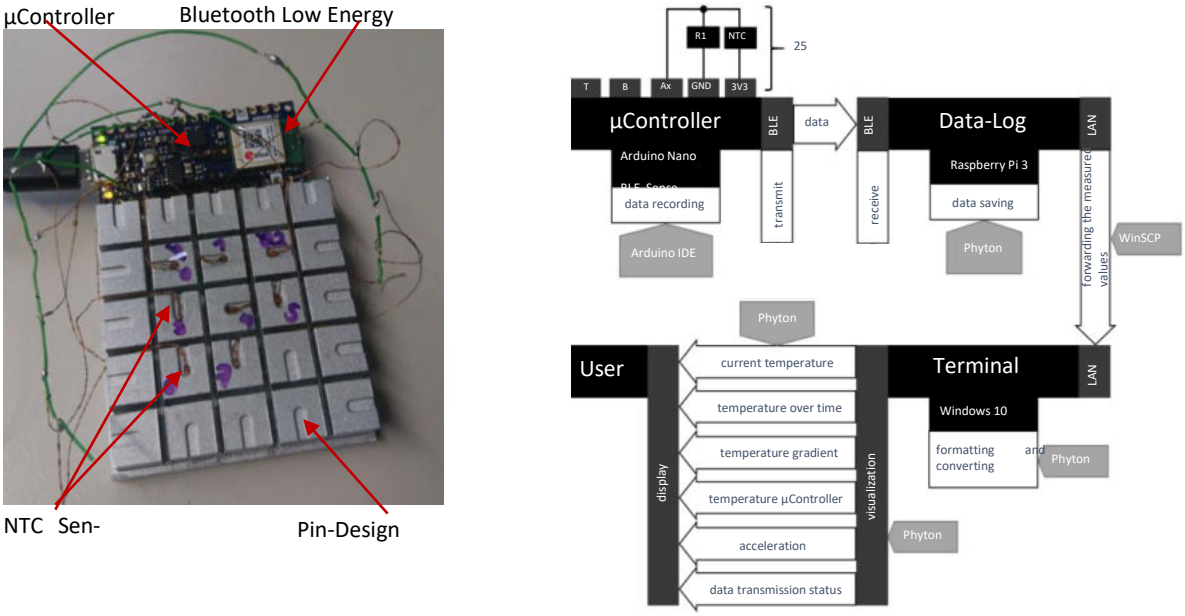

Figure 3-35: First test of 8 NTC-sensors with an Arduino Nano 33 (left). Communication diagramm (right).

The measurement takes place via 25 EPCOS NTC sensors (EPC B57540G1103 NTC). These sensors are measured using an Arduino Nano 33 BLE Sense and sent to a Raspberry Pi via Bluetooth Low Energy. In order to gain insight into what is happening inside the AM machine during the printing process, it is necessary to be able to read out the measurement data in near real time. Therefore a program is written in Python which converts the measurement data and visualizes their numerical values. After a specified interval of 1 s, the program reads out the file with the current measurement data again, deletes the old visualization and displays the current data. In order to provide an overview of the final configuration of the communication, the programs and hardware used, the data structures and the visualization are summarized in Figure 3-35 (right). The systems used are shown in black, the interface in dark gray, the software used for programming the functions in light gray and the functions themselves in white.

3.7.5 Experimental Setup

The experiments are performed on a LPBF machine TruPrint 1000 from the company Trumpf. The used Material is Titan (Ti-6Al-4V). Trumpf provided settings are used as process parameters for all parts and support structures. Operating conditions used in the experiments are given in Table 3-7.

Powder	Titan - Ti-6Al-4V ELI-A
layer Thickness	20 µm
particle size range	25 - 45 µm
laser power border	75 W
laser scan speed border	1000 mm/s
laser power hatch	155 W
laser scan speed hatch	1200 mm/ss
atmosphere	Argon

Table 3-7: LPBF process parameters used for material.

Since the build volume is under a constant inert gas atmosphere the build chamber needs to be gastight. Therefore the sensor platform is designed to fit between a standard build platform and the corresponding adapter plate provided by the machine manufacturer. This has the advantage that no changes have to be made to the machine and with the integrated high temperature accumulators and the Arduino the whole sensor platform is independent and self-sufficient.

To test the system and validate its functionality, it is installed in the printer as shown in Figure3-36. A test part to be printed is chosen that would distribute the different heat loads to the sensors in such a way that well distinguishable readings could be expected.

Three cuboids are chosen as the shape to be printed, two coinciding with sensors 1 to 3 and one coinciding with sensors 7 and 8, as shown in Fig. 3-36.

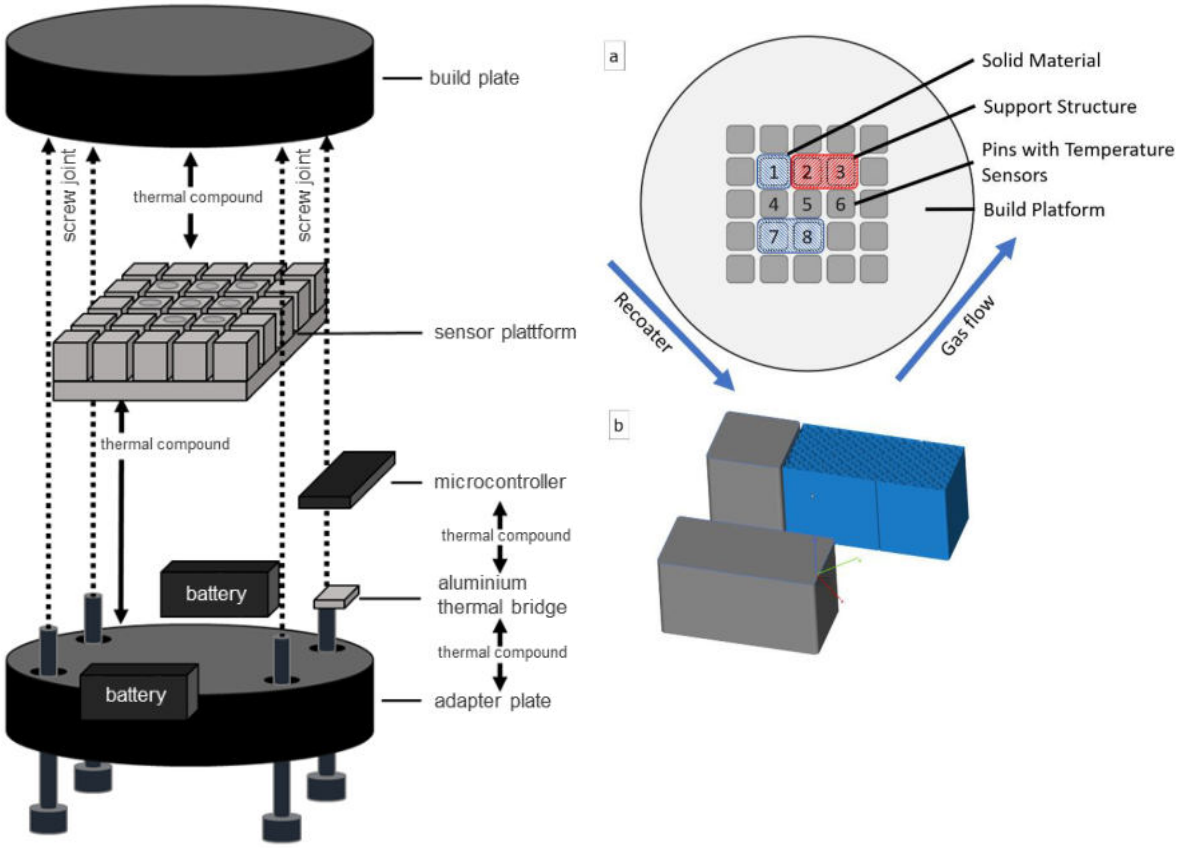

Figure 3-36: Schematic experimental setup (left); a) Sensor and test part layout on the build platform. b) Test part geometry (right).

A support structure is printed over sensors 2 and 3 and no solid material. This division is chosen to ensure well distinguishable heat loads for the respective sensors. Since the support structure conducts less heat and at the same time has a smaller area to be melted by the laser, the pins underneath should experience a smaller temperature increase from the printing process than the others. Of sensors 1, 2 and 3, it is expected that sensor 1 will experience the highest temperature rise and sensor 3 the lowest. For comparison, two adjacent sensors (7 and 8) are printed in the solid material to see if there is a difference between them. To minimize the influence of the two bodies on each other, no body is printed between them (i.e. over sensors 4, 5 and 6). The results of the tests to validate the system show that the design of the prototype fulfils the basic functionality.

3.7.6 Results

Since the focus of this investigation is the observation of thermodynamic relationships during a print job, the main focus of the evaluation is placed on the measured values of the temperature. The temperature sensors showed continuous functionality in this test. In figure 3-37 all eight sensors and their measured values over the entire period can be seen. The print job starts at around 890 seconds, there is a sharp rise in temperature in all sensors shortly afterwards at around 966 seconds. The curves all flatten out towards the end of the print job at about 12000 seconds.

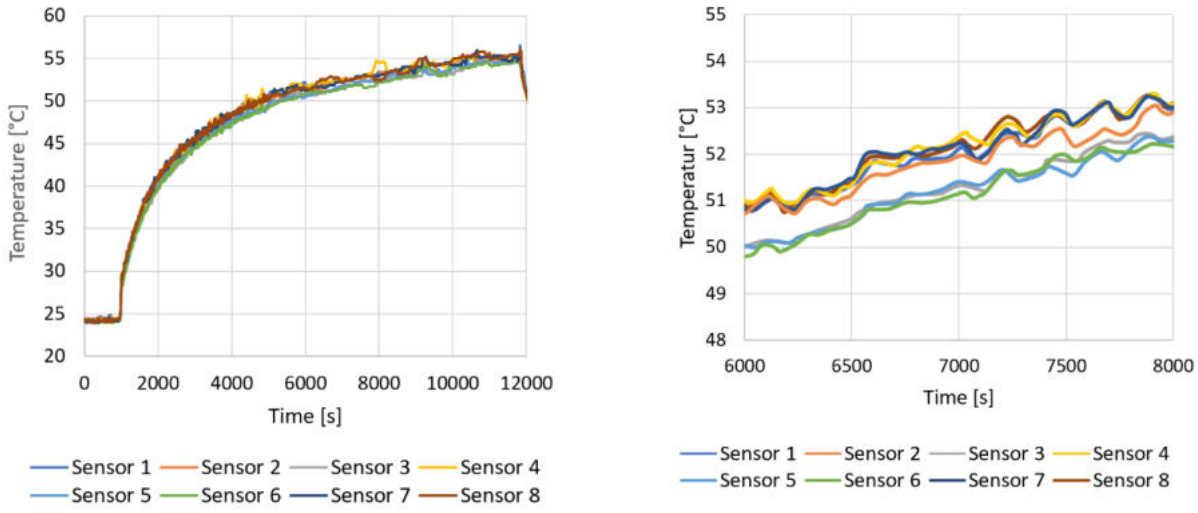

Figure 3-37: measured temperatures during the print job of all sensors (left); Heating levels of all sensors (right).

In figure 3-37 it can be seen that the sensors experience different levels of heating. They are bundled into two groups, one consisting of sensors 1, 2, 4, 7 and 8, which heat up more, and another group of sensors 3, 5 and 6, which heat up less. Within these groups, no clear assignment of the highest temperature seems to be possible in general, the values decrease and increase at different rates, with the exception of sensor 2, which continuously delivers the lowest measured values of the warmer group. In addition, there is a tendency for sensors 1 and 7 to have the highest values of their group, but this trend is often interrupted.

The colder group contains sensors 5 and 6, these two are sensors where no material has been melted above on the build platform. It is therefore plausible that these have lower values than the other sensors.

The third sensor in the group, Sensor 3, is the one which a support structure has been printed on. A small flow of heat is conducted through this. In addition, this sensor has only one neighboring pin which experiences heating; this is also a support structure (above sensor 2).

Sensor 2 provides significantly higher temperature values than sensor 3. In contrast to sensor 3, however, it has two direct neighbor pins from which heat is conducted to it, pin 3 with a support structure and pin 1 with solid material. This allows the assumption that the sensor experiences more heat than sensors 3, 5 and 6 at the beginning of the print job, but less than the other sensors.

Sensor 4, which is in a pin without heat induction from printing, is located in the middle of the warmer group. It seems as if the heat input of the processes via its neighbor sensors 1, 2, 7 and 8 is spreading so far that sensor 4 experiences as much heating as its neighbors themselves.

In general, the predictions made in advance only seem to apply to a limited extent; a distinction between certain sensors based on their temperature is possible, but not between others. It does not appear as if a clear distinction can be made between an area printed with a support structure with only one printed neighbor and an unprinted area around which printing is carried out in several neighboring areas.

What is striking in this section of the measurement data is that the temperature rise has a sinusoidal component. Which can be seen in the temperature data of sensor 1 in figure 3-38. The steep ascent at the beginning of each cycle is caused by the heat provided by the laser and the flattening of the curves immediately afterwards can be assumed to be the time the recoating process step is carried out. Here the time between the peaks is between 24 and 26 seconds. This period is also the recoating time during the print job.

In order to have qualitative comparative values, a process simulation is carried out with the values from Chapter 3.2.1. and based on the work of Möhring et. al [23]. A measuring platform with the real dimensions is implemented, as components with the dimensions of the real components are built (whereby all consist of solid material and none of support structures). The laser changes its power periodically between the maximum and 0 W.

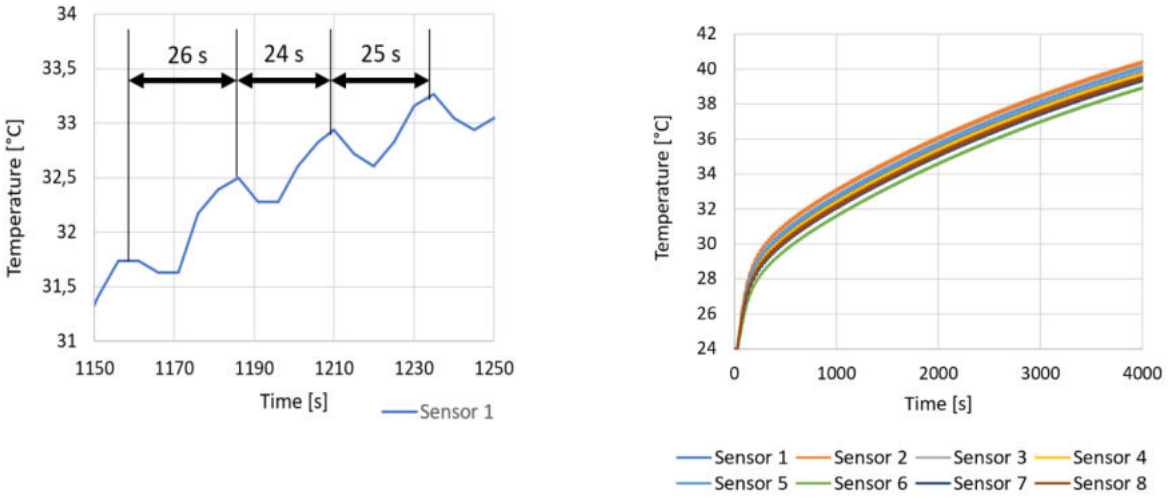

Figure 3-38: Temperature measurement of sensor 1 between 1150 s and 1250 s (left); Thermal simulation results of all sensors (right).

As in the test print, the duration of the laser activity is set at 2 s, the pause in between at 25 s per shift. In the simulation, too, there is a very steep increase in temperature at the beginning compared to the later course which can be seen in Figure 3-38 right. This agrees with the measurement results from the experiment. The flattening of the curve towards a plateau cannot be observed here because the cooling process is dimensioned too small in the simulation.

A wave-like gradient is also visible in the simulation. The period here is 26.54 seconds, which corresponds exactly to the time that is set in the simulation for a shift. Thus, the layers can be clearly distinguished in the simulation. The waveform derives from the short time the laser is active. It heats up in a short time and the heat spreads to the measuring platform. A short cooling down can even be seen after the heat input. The two groups of warmer and colder sensors can still be distinguished. The heating from the laser is also still visible.

3.7.7 Conclusion & Outlook

It can be seen that the measuring system can also record fine thermodynamic processes during a print job and the presented method makes it possible to monitor the mechanical part integrity and heat distribution during the LPBF process inside the powder bed. Also the monitoring of the build platform can be carried out in a cost-efficient way.

Even though the results so far are promising, further experiments are needed in order to gain a complete understanding of the complex thermomechanical interactions during the additive process. Currently ongoing efforts include further tests during long print jobs to observe the functionality of the system as well as the data quality of taller structures. In addition, the system will be used to detect process interruptions caused by delamination. The ability of the system to control the process parameters in the form of the time-related induced energy depending on the measured values is to be examined in the future.

3.8 WP6 Geometric Simulation of the ASM process chain

The geometric simulation of the ASM process chain was carried out with a process simulation of the LPBF process with ANSYS Additive Science to correlate the simulated deformation to the required machining allowance for subsequent machining e.g. reaming. In ANSYS Additive Science, the “thermal strain” calculation method is selected, which takes the laser path and anisotropy directly into account using the production data of the LPBF system. This simulation method provides the highest degree of accuracy by predicting how thermal cycling influences strain accumulation at all locations within the part. ANSYS employs a “thermal ratcheting” algorithm for this purpose. After calculating strain magnitude at each location, the result is passed to the mechanics solver as anisotropic strain based on magnitude and local scan vector direction.

Figure 3-39 visualizes the deviation in shape for 45° and 60° samples in their as-built condition. The simulated results (Fig. 3-39 above) and measurements (Fig. 3-39 below) show good agreement especially in the marked regions (marker A and B). The simulation predicts that there will be a higher displacement in the bottom region which can be measured inside the bore. A deviation up to 120 µm from the nominal cylinder form can be seen. The simulation tool does not consider downskin effects, resulting from the meltpool penetrating several layers instead of just one on each scan pass. This leads to the shape deviation that can be seen at marker C of the measurement plot, but not on the downskin surface

of the simulation. The same agreement between simulation and measured results for 60° samples can also be observed. The magnitude is around 70 µm in this bore orientation and located closer to the bottom of the sample (marker B). Downskin effects are also much less prevalent for this orientation (marker D). The measurement of the vertical bores and the corresponding simulation also show the same agreement, with a lower shape deviation and a symmetrical appearance. The results show that building bores vertically results in a better surface roughness in the as-built condition. The main findings from the bore orientation analysis can be summed up as follows: − Bores in vertical orientation achieve the best cylindricity, straightness and roughness in as-built condition. − Angled bores have lower surface quality in as-built condition not only because of downskin effects, but also because of higher warpage compared to vertical bores. − Simulations show predictions for warpage that closely match the measurements.

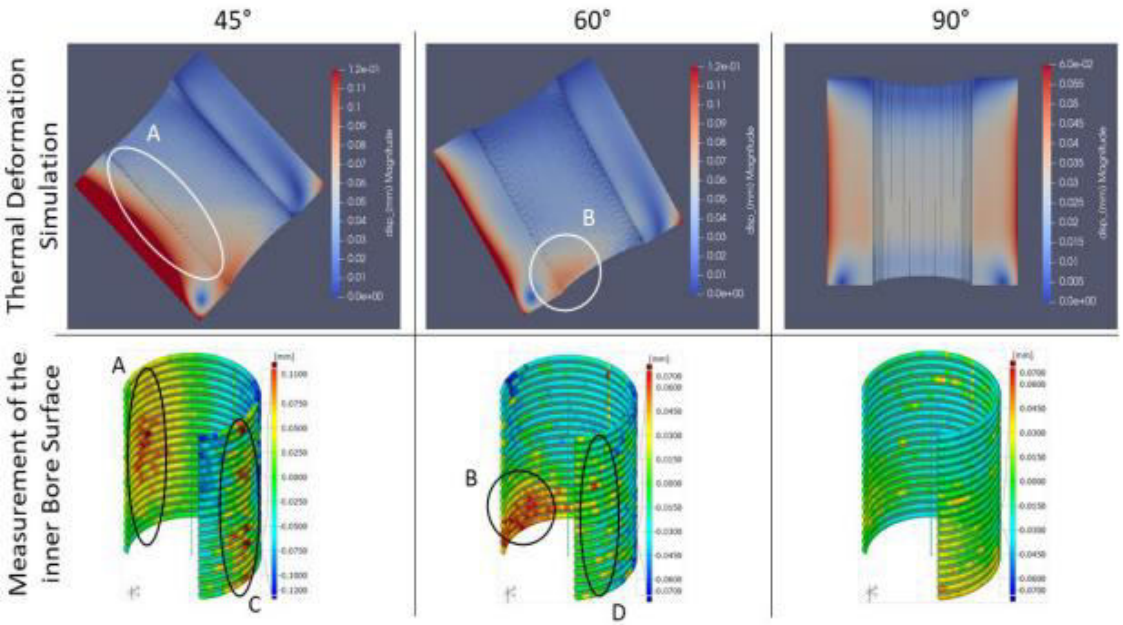

Figure 3-39: Deformation comparison between the LPBF process simulation and the form measurement.

3.8.1 Summary

At the beginning of the process chain under consideration is the additive process, which largely determines the geometry and material properties. As part of the project, a procedure was therefore developed that makes it possible to develop optimal process parameters. In the subsequent process chain, blasting was combined with the aspects of cleaning, smoothing and shot peening. Here, connections between the direction of build-up and the associated surface quality and the blasting processes could be determined. Based on this, practical handouts could be formulated.

In terms of functionalizing processes with a defined cutting edge, orthogonal cutting, drilling, reaming and milling was investigated.

The scope of the orthogonal cut experiments was to investigate anisotropic effects, especially regarding the effect of build-up angles on cutting forces. The anisotropic behavior of the material during cutting could be proven and is visible both in cutting forces as well as in the chip thick-ness. Cutting force varies

by up to 6 % and thrust force by up to 8 % when the orientation of specimens in the build volume is changed. To make cutting force predictable a regression model was fitted to the data gathered by the experiments and a good model fit was achieved.

3.8.2 Outlook

In further investigations, in a follow-up project, the processes in terms of the surface and subsurface properties as well as the use of the additive manufacturing on semi-finished parts must be considered more in detail. This includes the following topics:

- Changing additive manufacturing process parameters to alter in situ material properties in terms of surface and subsurface modification (e.g. density, microstructure, residual stresses, hardness).
- Considering semi-finished parts in the ASM process chain with special focus on the interface surface.
- Adapting support structures for specific subtractive processes.
- Usage of functionalizing processes (e.g. milling) for defined modification of surface and subsurface properties (e.g. density, microstructure, residual stresses, hardness) .

4 Functionalisation by abrasive fine machining processes – Results of the ISF

D. Biermann, M. Tilger

(Institute of Machining Technology - ISF, TU Dortmund University, Germany)

4.1 Introduction

Additive manufacturing is increasingly becoming the focus of industrial applications due to its degrees of freedom and flexibility, with the still young technology spreading very quickly. In its National Industrial Strategy 2030, the German Federal Ministry for Economic Affairs and Energy cites additive manufacturing as a key area in which Germany has a leading role and must maintain it [4-1]. Particularly in high-tech sectors such as the aerospace industry, medical technology and the automotive industry, 3D printing processes are forecast to reach a global market volume of around 17.8 billion euros in 2030 [4-2]. Accordingly, the number of applications and the needs in terms of specific functionalities when using these manufacturing processes are increasing and now include a wide range of different materials [4-3; 4-4].

Additive manufacturing is not a substitute for conventional manufacturing processes, but rather a technological supplement to existing primary forming, forming and separating manufacturing processes due to the associated degrees of freedom. The usually very high demands placed on component parts here lead to the need for a suitable process chain in which the focus particularly lies on the combination of additive manufacturing and machining post-processing.

This necessity is especially evident for functional surfaces, which have to meet high requirements for shape and dimensional accuracy as well as surface quality. For additively manufactured components made of metals, the resulting surfaces are insufficient so that subtractive processes are indispensable [4-5]. As machining processes for this purpose, fine and ultra-fine machining processes, such as grinding and microfinishing, are particularly interesting since they are suitable for generating functional surfaces under tribological aspects [4-6; 4-7; 4-8]. In this context, the subtractive processes are also referred to as functionalization processes.

The following section summarizes the results regarding investigations on abrasive fine machining of additively manufactured parts. Hereby, the abrasive fine machining processes flat grinding, cylindrical grinding, wet abrasive jet machining (WAJM) and microfinishing are considered.

4.2 Description of project results

Flat grinding of additively manufactured parts

For flat grinding of additive manufactured parts, the interactions between the additive manufacturing process and the subtractive process were analyzed by using different build-up directions for the additively manufactured parts. Figure 4-1 shows the schematic layer build-up for additive manufactured prismatic workpieces with an inclination angle of α_b = 0 and 90°. Furthermore, the cross sectional view of additively manufactured workpiece of stainless steel 1.4404 (manufacturer designation 316L) is depicted.

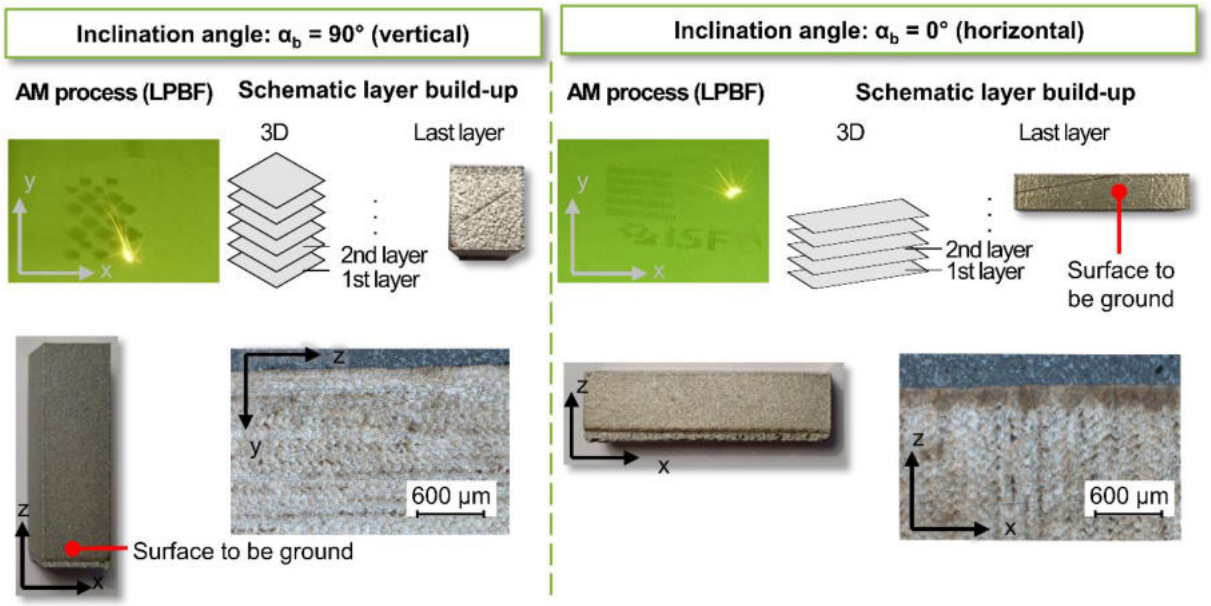

Figure 4-1: Illustration for the build-up of additive components for varying inclination angles.

Based on the inclination angle the surface to be ground is marked. For flat grinding, several experiments were carried out for different materials. For the stainless (1.4404) steel one factor at a time, experiments and space-filling design of experiments (DOE) have been analyzed. In case of the one factor at a time experiments the factor´s cutting velocity v_c, feed velocity v_f and dressing coverage ratio U_d were varied over five stages. The space filling experiments were carried out varying cutting and feed velocity.

Figure 4-2 depicts the results regarding arithmetic mean roughness values Rz, tangential force F_t and normal force F_n for the space filling experiments on 1.4404 within regression models. The Experiments were carried out for both inclination angles α_b = 0° and 90°.

Above the regression models, a schematic illustration of the grain engagement in the layered specimens as a function of the inclination angle is shown. The fundamentally recognizable influences of cutting speed and feed velocity correspond to the interactions known from the state of the art for the grinding of conventionally produced workpieces. Thus, higher cutting speeds tend to result in lower grinding forces and lower Rz values, while an increase in the feed velocity leads to an increase in the process forces in the normal and tangential directions and to lower surface quality.

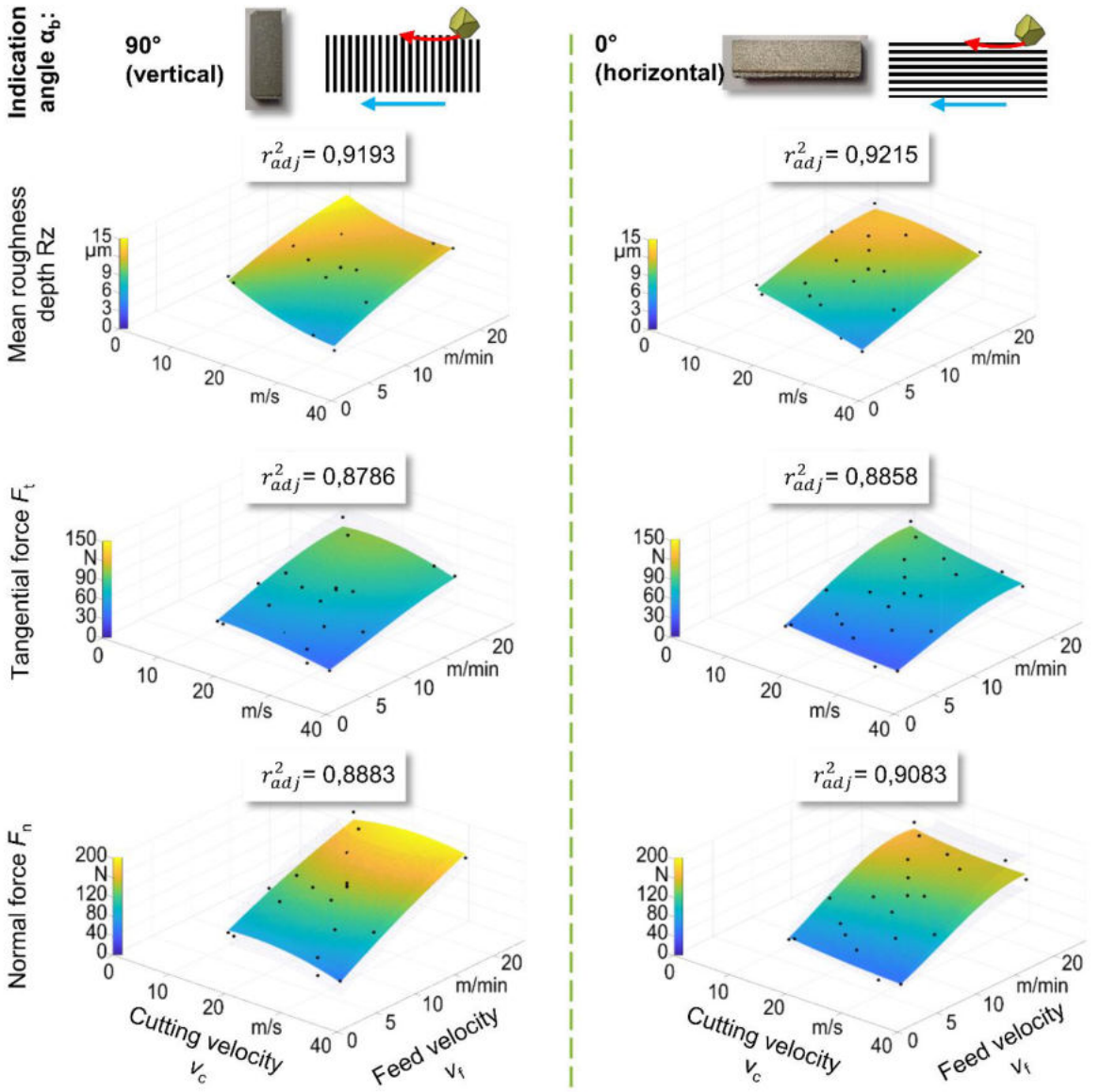

Workpiece material:	1.4404	Grinding wheel:	60C 80/02 H 93 V685A	Cooling:	Emulsion
Dressing depth of cut a_d:	15 µm	Dressing velocity v_d:	var.	Dressing coverage ratio U_d:	3
Grinding depth of cut a_e:	25 µm	Cutting velocity v_c:	var.	Feed velocity v_f:	var

Figure 4-2: Regression models of mean roughness depth Rz and process forces F_n and F_t for grinding additive manufactured 1.4404 parts with different inclination angles.

For the consideration of the influence of additive manufacturing, the regression models of the different inclination angles are compared. Just like the influences of the grinding parameters, which act in the same way for both build-up directions, no clear differences can be identified in relation to the average roughness depth Rz. Only in the range of low cutting speeds with v_c < 20 m/s do slightly higher Rz values result for the specimens with an inclination angle of α_b = 90°. For the process forces, differences can only be observed in the range of normal forces. Here, for the processing of the upright specimens (inclination angle α_b = 90°) compared to the horizontal specimens (inclination angle α_b = 0°) slightly higher normal forces result . This effect is related to a tendency of higher macro hardness of the surface to be machined, which can be detected from a multiple measurement. The following boxplot diagram in Figure 4-3 shows this result for a multiple measurement of macro hardness.

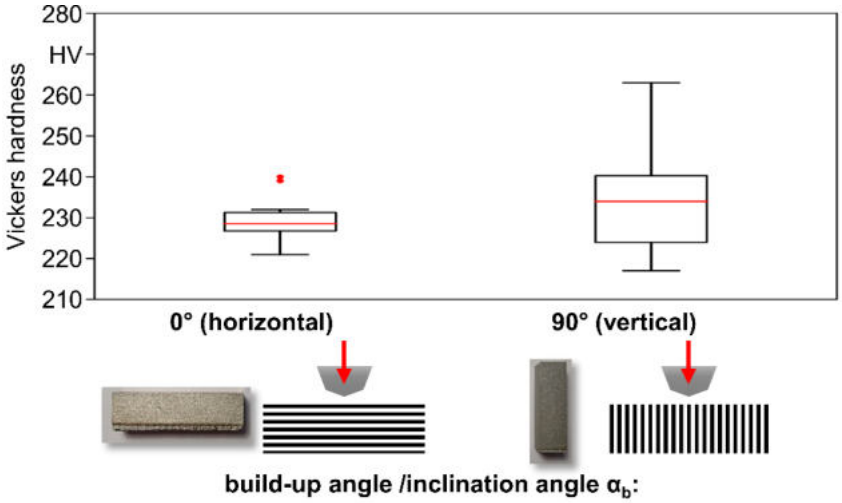

Workpiece material:	1.4404	Vickers hardness measure:	HV10
Measuring load:	10 kp	Holding time:	10 s

Figure 4-3: Macro hardness of additive manufactured stainless steel (1.4404) parts with varying build-up angle.

Based on the present results, grinding chips were collected during grinding investigations and analyzed by means of scanning electron microscopy (SEM). Here, for identical parameter combinations, the resulting grinding chips are to be considered with regard to possible influences of the build up direction on chip formation. The selected grinding chips are depicted in Figure 4-4.

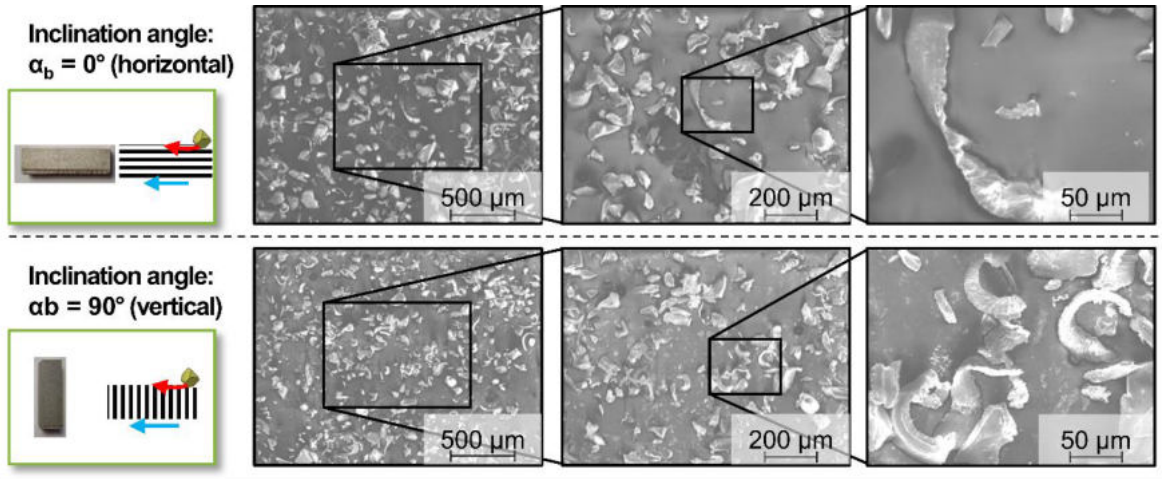

Workpiece material:	1.4404	Grinding wheel:	60C 80/02 H 93 V685A	Cooling:	Emulsion
Dressing depth of cut a_d:	15 µm	Dressing velocity v_d:	var.	Dressing coverage ratio U_d:	3
Grinding depth of cut a_e:	25 µm	Cutting velocity v_c:	35 m*s^{-1}	Feed velocity v_f:	5 m*min^{-1}

Figure 4-4: Scanning electron micrographs of grinding chips.

The representation of the SEM shows that a large number of chips could be collected and recorded well. Here, the chips of the sample with an inclination angle of α_b = 0° tend to be larger, whereas smaller and more deformed grinding chips can be seen at αb = 90°. This effect can be justified by the different material structure due to the layered structure and is explained below based on the schematic representation of the abrasive grains relative movement trough the workpiece (in each case on the left of the Figure 4-4). For the vertical oriented specimens, the abrasive grain almost orthogonally penetrates

through the individual layers. Due to the layer boundaries, a breaking of the material appears to occur here. For the horizontally oriented components, the abrasive grain penetrates the outermost layer. Since the layer thickness d of the additive manufacturing process, d = 30 µm, is greater than the set grinding depth of cut, theoretically no penetration of the layer occurs here. The resulting chip is the outcome of one layer thickness.

Further experiments were carried out for the materials 1.2709 and AlSi10Mg build by powder bed fusion of metal with laser beam (PBF-LB/M) and S355 generated by wire arc additive manufacturing (WAAM). These specimens were manufactured by the other research project partners and made available for the investigations. The following box-plot diagrams in Figure 4-5 show the mean roughness depth Rz for the variation of cutting velocity when grinding tool steel 1.2709.

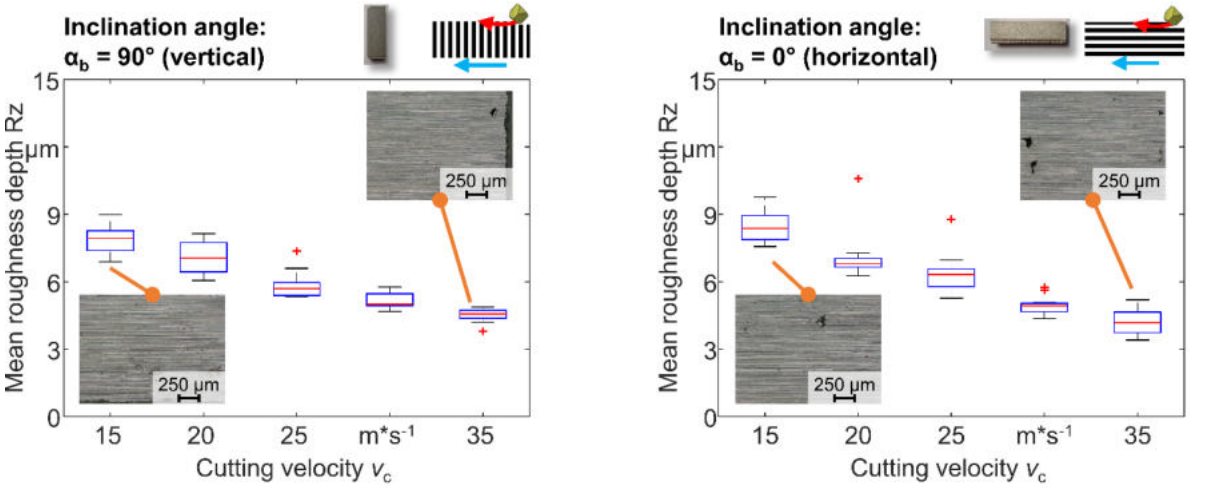

Workpiece material:	1.2709	Grinding wheel:	60C 80/02 H 93 V685A		Cooling:	Emulsion
Dressing depth of cut a_d:	15 µm	Dressing velocity v_d:	var.	Dressing coverage ratio U_d:		3
Grinding depth of cut a_e:	25 µm	Cutting velocity v_c:	var.	Feed velocity v_f:		5 m*min^{-1}

Figure 4-5: Grinding results for varying inclination angles of additive manufactured 1.2709.

Generally, the result is the same for all materials as the Rz-values decrease with increasing cutting velocity. The more interesting point is the optical appearance of the surfaces, where pores become visible through grinding. By analyzing the different inclination angles, there is no influence on the number of pores occurring. Further, cross sectional views show that big pores and surface-near cracks appear in the material structure. These results are depicted in Figure 4-6.

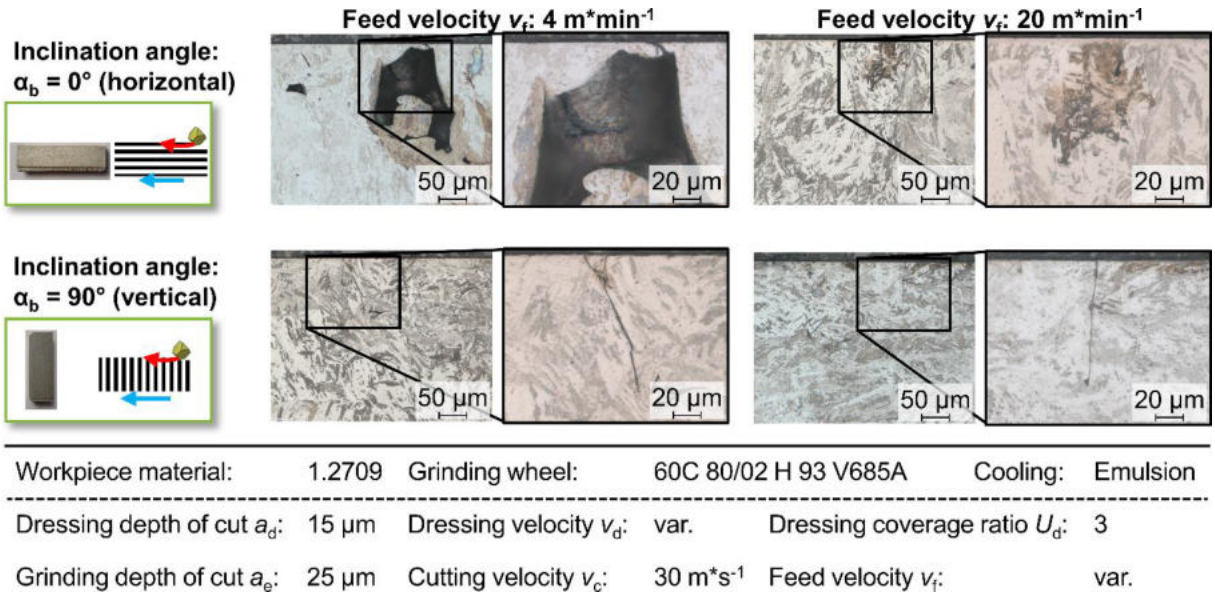

Workpiece material:	1.2709	Grinding wheel:	60C 80/02 H 93 V685A	Cooling:	Emulsion
Dressing depth of cut a_d:	15 µm	Dressing velocity v_d:	var.	Dressing coverage ratio U_d:	3
Grinding depth of cut a_e:	25 µm	Cutting velocity v_c:	30 m*s^{-1}	Feed velocity v_f:	var.

Figure 4-6: Cross sectional view on the additive manufactured 1.2709.

For the horizontal built-up workpiece ground with a feed velocity of v_f = 4 m*min^{-1}, the pore is going to be open as a small crack already appears. The crack shown for the vertical orientation seems to be too big as it might result from grinding. Therefore, it is assumed that these cracks result from the additive manufacturing and thus influence the final surface quality of the ground surface.

Additionally, ground samples of 1.2709 showed surface thermal defects (grinding burn), which indicate a thermomechanical overload of the material. Since the grinding parameters were not changed in this case and previous tests did not produce defects, the thermomechanical resistance of the material seems to be different due to unknown influences which may be caused by the additive manufacturing process or powder aging.

Wet Abrasive Jet Machining of additively manufactured parts

The experiments on wet abrasive jet machining (WAJM) have been carried out for stainless steel and tool steel. With respect to different machine systems and thus varying required jet pressures, it can be assumed that in general, higher jet pressures are preferable for wet abrasive jet machining of the additive manufactured surfaces. The results for a Box Behnken DOE of experiments for higher jet pressures are depicted in Figure 4-7 for the as-built initial surfaces.

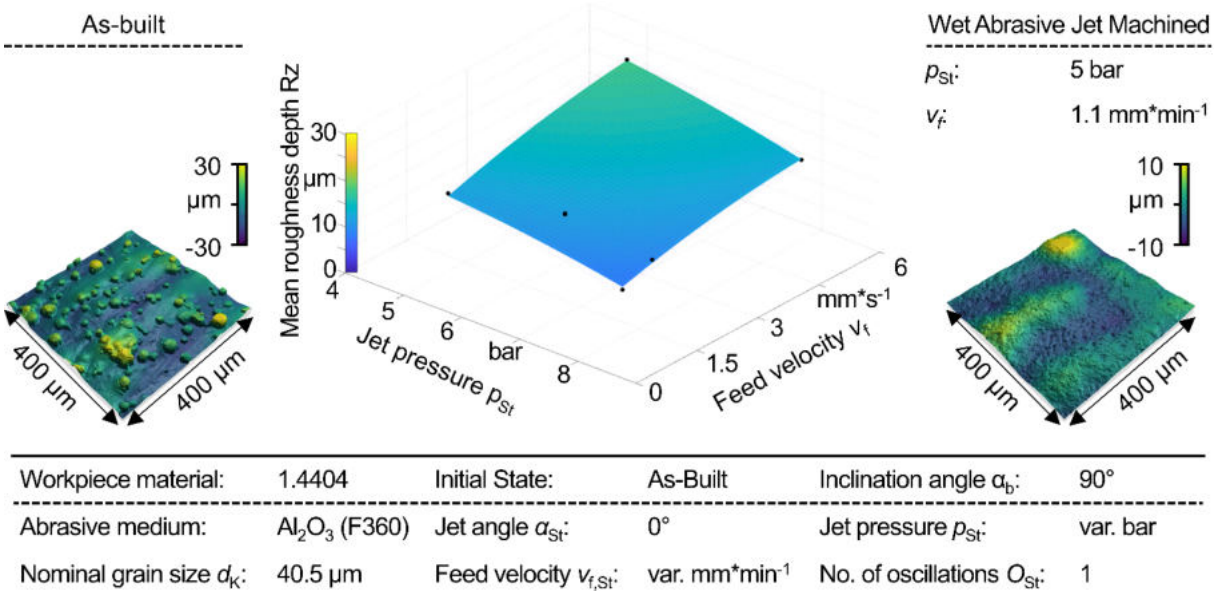

Workpiece material:	1.4404	Initial State:	As-Built	Inclination angle α_b:	90°
Abrasive medium:	Al_2O_3 (F360)	Jet angle α_{St}:	0°	Jet pressure p_{St}:	var. bar
Nominal grain size d_K:	40.5 µm	Feed velocity $v_{f,St}$:	var. mm*min-1	No. of oscillations O_{St}:	1

Figure 4-7: WAJM of As-Built additive manufactured stainless steel (1.4404).

Especially when talking about functionalizing of surfaces, the WAJM processes are not suitable to generate surface topographies comparable to conventional manufactured steel parts for directly machining the as-built surface. Therefore, the resulting mean roughness depth Rz values remain higher than 8 µm. Based on this insight, the process chain of additive-subtractive manufacturing was modified and an additional grinding process was added prior to WAJM. The results are shown in Figure 4-8 within a regression model.

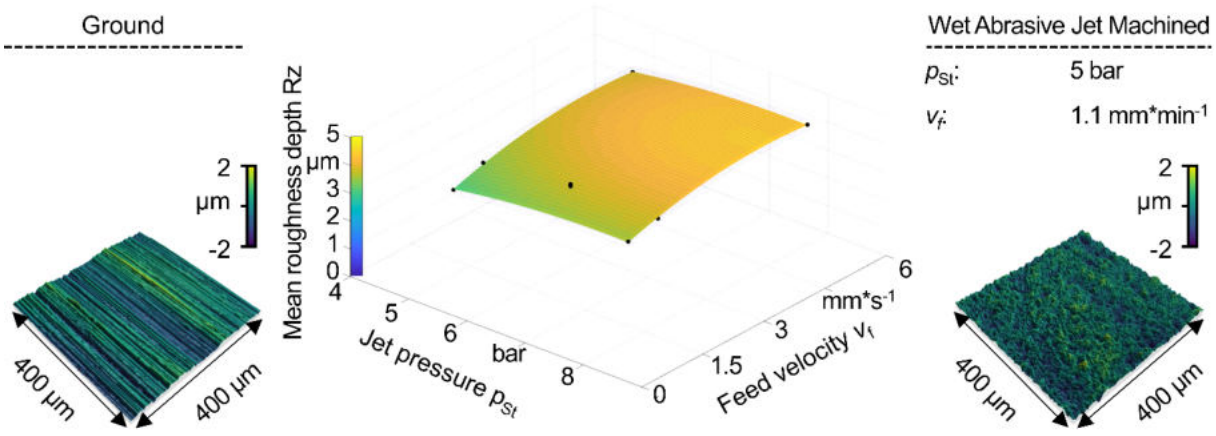

Workpiece material:	1.4404	Initial state:	Ground	Inclination angle α_b:	90°
Abrasive medium:	Al_2O_3 (F360)	Jet angle α_{St}:	0°	Jet pressure p_{St}:	var. bar
Nominal grain size d_K:	40.5 µm	Feed velocity $v_{f,St}$:	var. mm*min-1	No. of oscillations O_{St}:	1

Figure 4-8. WAJM of ground additive manufactured stainless steel (1.4404).

While grinding leads to an initial mean roughness between Rz = 3 and 5 µm, WAJM only has a small effect on the surface roughness. The lowest Rz-values are generated with low feed velocities since the exposure time of the WAJM medium is longest here. In contrast to the machining of the as-built surfaces,

the jet pressure p_{St} has no significant influence on the resulting Rz-values. With respect to the topography, the influence of WAJM is more significant. The typically ground topography with direction depending peaks and valleys is changed to a homogenous and direction-independent topography.

Depending on WAJM of 1.2709 the results are different. Due to the pores already shown after grinding, the WAJM processes seem to be influenced as well. Therefore, the surface roughness increases by means of mean roughness depth Rz and a surface with pores and cracks appears. The results and exemplarily microscopic views of the surface are depicted in Figure 4-9.

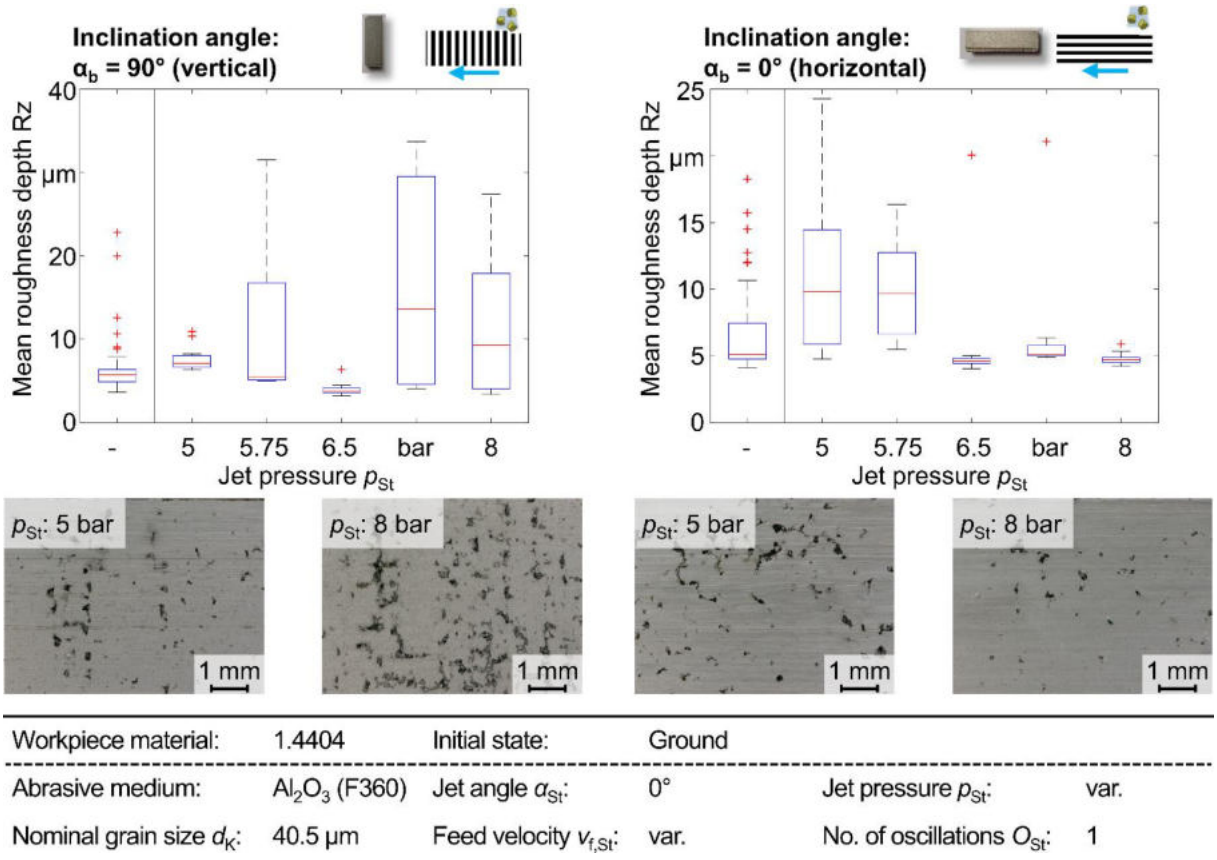

Workpiece material:	1.4404	Initial state:	Ground		
Abrasive medium:	Al_2O_3 (F360)	Jet angle α_{St}:	0°	Jet pressure p_{St}:	var.
Nominal grain size d_K:	40.5 µm	Feed velocity $v_{f,St}$:	var.	No. of oscillations O_{St}:	1

Figure 4-9: Results of WAJM and occurring surface defects for 1.2709.

These results lead to the assumption that additive manufacturing, especially for 1.2709, significantly influences the surface quality along the additive-subtractive process chain. Thus, the machining post-processing at this point is directly dependent on the quality of the additive manufacturing process. While high surface roughness typically can be reduced by means of subtractive processes, defects present in the layer structure, such as pores, cannot be corrected and can lead to insufficient component quality.

At this point, a clear boundary must be drawn for fine machining of additively manufactured components: Subtractive fine machining makes it possible to functionalize additively manufactured components in general. However, subtractive fine machining cannot correct insufficient component properties resulting from the additive manufacturing process and originating in the layer structure.

Cylindrical grinding of additively manufactured parts

For cylindrical grinding a specimen with a cylinder contour and a bore was defined to realize the workpiece clamping on a cartridge mandrel. The defined specimen were build of 1.4404, 1.2709 and

AlSi10Mg. While the components made of AlSi10Mg and 1.4404 were manufactured exclusively with an angle of α_b = 90°, there were specimens with α_b = 90° and 60° for 1.2709.

For the cylindrical grinding tests using the infeed method, a periodic noise emission in the form of a squeak was perceived. The noise emission did not occur until after about one third of the selected total infeed. The amplitude and frequency of the noise emission changed irregularly and depending on the specimen and are presumably due to friction processes between grinding wheel and workpiece or workpiece and mandrel.

In addition, eccentric runout was noticed in some specimens. In the case of the non-pre-machined specimens made of austenitic steel 1.4404, the inner cylindrical surface is a possible cause. Due to particle agglomerations, layer overlaps and elevations occurring in the construction process, the real coaxiality of outer and inner cylinder surface can be lower compared to the CAD model. At the same time, reduced coaxiality in the martensitic specimens used in previous drilling and reaming tests is due to inaccurate alignment of these specimens or clamping failures due to clamping in different systems.

In addition to infeed cylindrical grinding, additional experiments were carried out with axial oscillation by an axial feed velocity v_{fa} and reduced cutting velocity v_c for cylindrical grinding in order to further reduce surface roughness. The comparison of both strategies is illustrated in Figure 4-10.

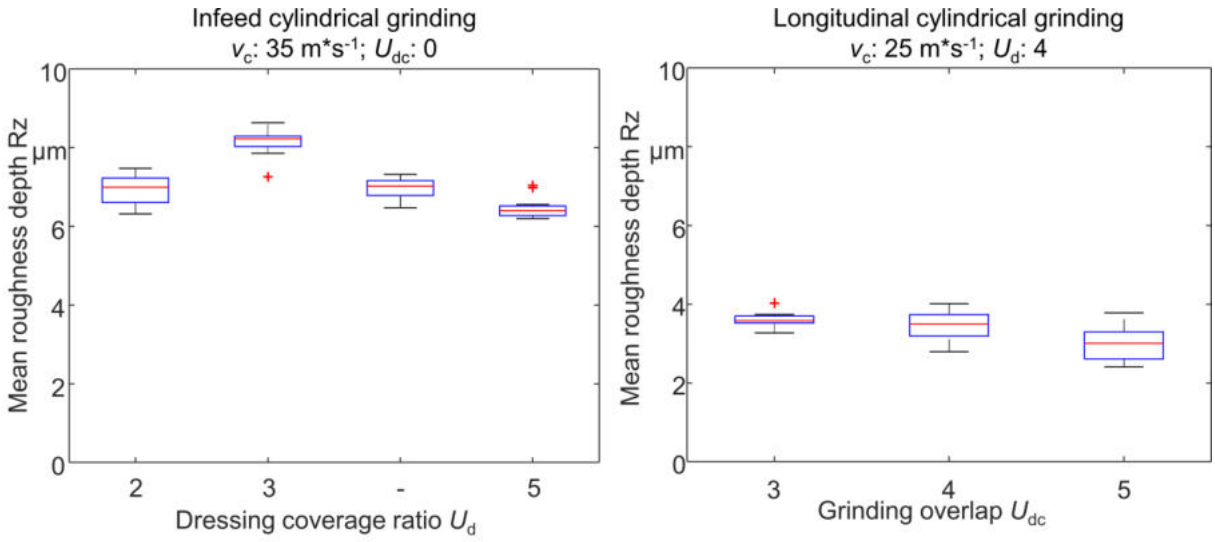

Workpiece material:	1.4404	Inclination angle α_b:	90°	Initial state:	As-Built
Dressing depth of cut a_d:	10 µm	Dressing velocity v_d:	var.	Dressing coverage ratio U_d:	var.
Grinding velocity ratio q_G:	90	Cutting velocity v_c:	var.	Axial feed velocity v_{fa}:	var.
Grinding strategy:	Up grinding	Cooling fluid:	Oil	Grinding Overlap U_{dc}:	var.

Figure 4-10: Results on cylindrical grinding of 1.4404 for different grinding strategies.

Microfinishing of additively manufactured parts

For microfinishing, first a test on as-built 1.2709 was made within a four-stage process. During the different stages of microfinishing, the surface roughness decreases subsequently and a typical honed plateau-structured topography is generated. However, this correlation only applies to the first three microfinishing stages. The additional 4th microfinishing stage using a grain size of d_K = 3 µm results in

lower distributions of the measured values without changing the average values. The measured profile as well as the topography seem less homogenous than after the third microfinishing stage since larger peaks occur. Further analyses with SEM showed that there are breakouts from the surface as well as individual peaks on the surface similar to droplets that occur by coated surfaces. It is assumed that these local defects result from the additive process and were exposed here. Based on the information of industry partners (additive machine manufacturer), these defects result from the use of aged or too moist metal powder that tends to oxidize in the additive process. As such peaks are considered critical for functional surfaces, it can be stated that the quality of additive manufacturing directly influences the opportunities of functionalizing parts by means of fine machining.

Due to the long process time, a pre-machining process by means of cylindrical grinding was installed for further microfinishing experiments. The following experiments were based on the influence of different microfinishing belts using the different grain types diamond (D), alumina (Al_2O_3) and silicon carbide (SiC). In addition, the additive manufactured workpiece material and, for 1.2709, the inclination angle were considered during the experimental investigations.

While the inclination angle does not influence the surface roughness, the workpiece material and the grain types do. Al_2O_3, which is preferred to expensive diamond as a cutting material for machining unhardened steel materials, achieves the lowest material removal. This results in higher roughness for each individual process step. In the comparison of silicon carbide and diamond, the results differ depending on the material being machined. While no difference can be identified for the machining of 1.2709, diamond produces the finest roughness for the machining of AlSi10Mg and SiC tools for 1.4404. For 1.4404 the comparison of the finally finished surfaces is shown in Figure 4-11.

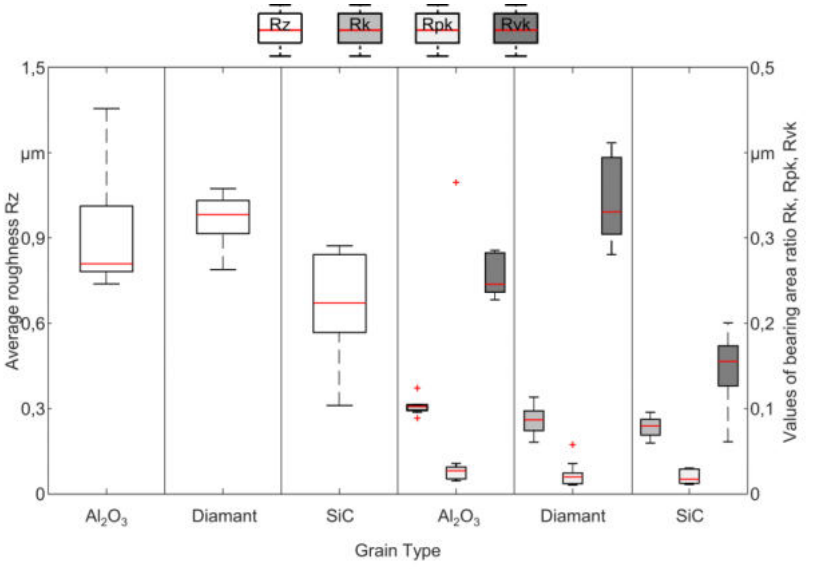

Workpiece Material:	1.4404	Inclination angle α_b:	90°	Initial state:	MF
Grain Type:	var.	Normal force F_n:	120 N	Res. surface pressure $p_{s,res}$:	1,4 N*mm^{-2}
Grain size d_K:	3 µm	Amplitude S:	± 2	Oscillation frequency f_{Os}:	17,2 Hz
Grain application:	Gravity scattered	Tangential vel. v_t:	85 m*min^{-1}	Res. cutting velocity v_c:	86 m*min^{-1}

Figure 4-11: Comparison of the roughness values for 3-stage microfinishing processes with different grain types.

In general, relatively high values of the reduced valley depth Rvk occur for all tools when machining 1.4404, indicating the generation of new grooves by the finishing process. Since low reduced peak

height Rpk values are detected at the same time, there seems to be only a small amount of lateral bulges along the honing grooves. From this, it can be inferred that the material removal mechanism of micro cutting dominates and there are fewer micro ridging and micro ploughing. In terms of grain types, it can be assumed that SiC is particularly well suited for machining the relatively soft steel material 1.4404 due to its sharp cutting edges and tendency to sharp-edged breaking.

Finally, the successive development of surface roughness and topography for 1.4404 is illustrated by means of profile curves, Abbott curves and a 3D topography in Figure 4-12. The profiles and surfaces shown here refer to the use of the SiC finishing tapes.

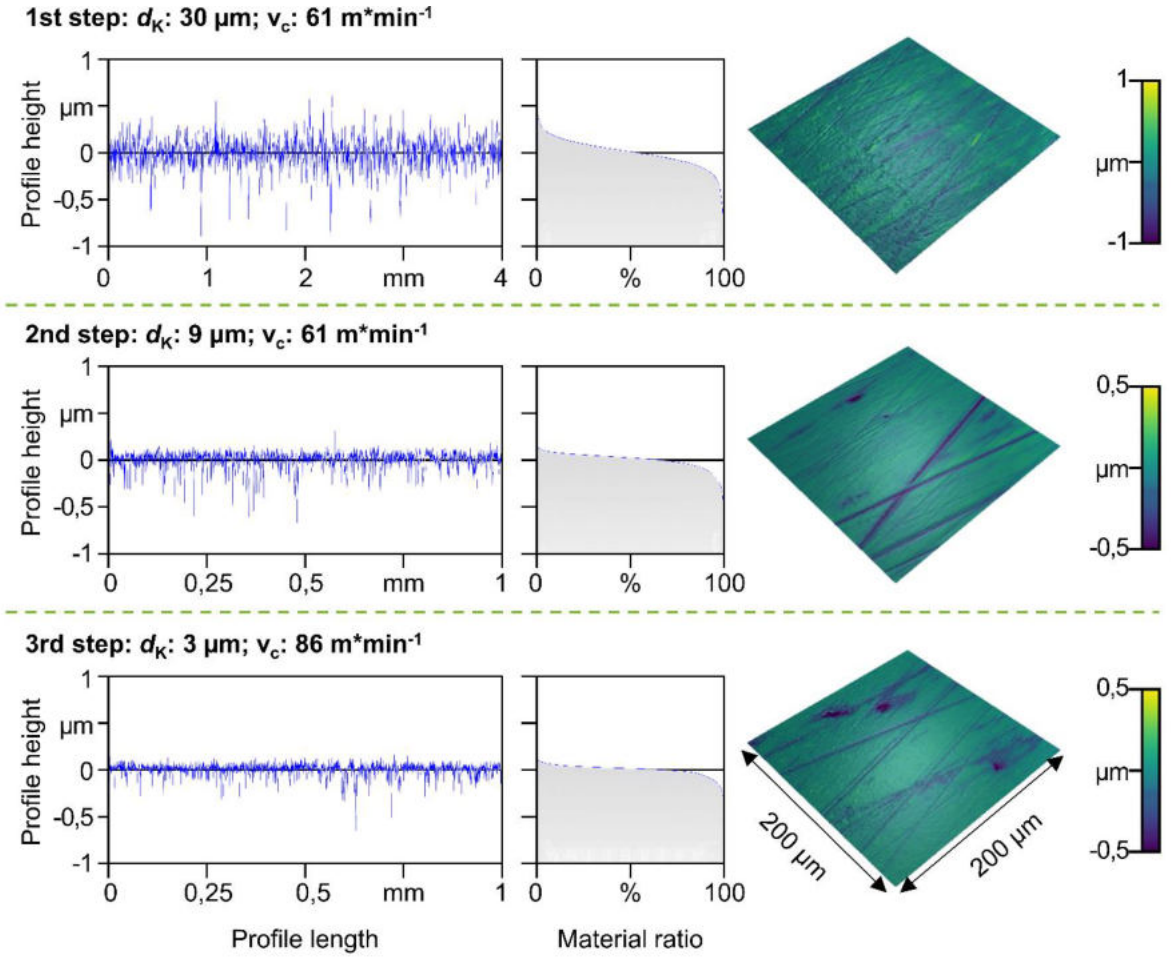

Workpiece Material:	1.4404	Inclination angle α_b:	90°	Initial state:	Ground
Grain Type:	SiC	Normal force F_n:	120 N	Res. surface pressure $p_{s,res}$:	1,4 N*mm^{-2}
Grain size d_K:	var.	Amplitude S:	± 2	Oscillation frequency f_{Os}:	17,2 Hz
Grain application:	Gravity scattered	Tangential vel. v_t:	var.	Res. cutting velocity v_c:	var.

Figure 4-12: Topography change along the multi-stage microfinishing process using SiC-tools for 1.4404.

The 3D topography shows the generation of characteristic crossing honing grooves by the first finishing step. The profile writing also shows that the surface is still characterized by grooves and peaks and that a plateau-structured topography has not yet formed. This happens successively with the second process stage. Here, only a few peaks appear in the profile, and the bearing area ratio curve also becomes flatter in the middle area. The 3D topography clearly shows two crossing grooves and several finer honing

grooves. The strong differences between the fine and the more dominant grooves are here due to the use of the two grain sizes d_K = 30 and 9 µm. In addition, a smaller oval cavity appears, which can be explained by a pore exposed from the layer structure of the additively manufactured workpiece.

For the third microfinish stage, even more of these pores appear and are also expressed in the profile writing by relatively deep grooves with a depth of approximately 0.5 µm. Apart from this, the amount of grooves deeper than 0.25 µm decreases significantly. This can be explained by a successive removal of the previously created plateaus, which in turn leads to a reduction of the valley depth. Ultimately, a homogeneous surface with plateau-structured topography is produced, which corresponds to a functional surface suitable for many applications.

4.3 Summary

The investigations along the additive-subtractive process chain focusing on the functionalization of additively manufactured parts by means of fine machining lead to a large number of results and new findings. These concern both the possibilities of machining and the influence of the initial additive component production. Within the investigations carried out, no clear influence of the build-up direction of the additive workpieces on the machining result was found for grinding WAJM or microfinishing. However, the analysis of collected microchips shows tendency differences for flat grinding of 1.4404. It can be assumed here that the influence on process behavior and process result increases with increasing material hardness.

The greatest recognizable influence of the machining is on the quality of the additively manufactured component. In particular, very high porosity was found to cause surface defects and insufficient surface quality after fine machining. While this effect still occurred slightly after grinding 1.2709, it was dominant for the subsequent WAJM. The pores present in the coating structure are mainly attributed to possible powder aging or excessive powder moisture. Microfinishing also exposed defects in the component in the form of oxidized powder material, which finally cause disturbances in the functional surface of the component.

In addition to these influences, difficulties were also encountered in the machining of rotationally symmetrical components. An additively produced clearance bore is considered unsuitable for clamping by means of a mandrel due to the high roughness values Rz > 30µm and the resulting diameter deviations and insufficient contact surface due to the many roughness peaks. For the use of already reworked bores, in contrast, a high eccentricity was found, which was attributed to reclamping errors.

In addition to these influences on the part of additive manufacturing, it was shown that the grinding of additively manufactured components in principle is suitable for post-processing and is particularly recommended as an intermediate step for the generation of functional surfaces. Due to the high output roughness and the low material removal rate in WAJM or microfinishing, an intermediate grinding process is considered economically necessary.

Especially for microfinishing, typical honing topographies with plateau character could be generated via the grinding-microfinishing process chain. In particular, the cutting material SiC proved to be advantageous for the machining of 1.2709 and 1.4404. Due to the lower costs, this cutting material is preferable

to diamond even with the same process result. For AlSi10Mg, on the other hand, diamond proved to be the best cutting material.

4.4 Outlook

Based on the findings, there are further investigation possibilities for increasing the understanding of the interactions of additive-subtractive manufacturing. The focus of additive manufacturing parameters and powder properties can be placed on the change in material properties and the machinability of the additively produced components. This could be used to examine how the defects in the layer structure revealed by the WAJM can be reduced and whether, for example, the use of aged powder reduces the thermomechanical load capacity and thus increases the risk of thermal defects (grinding burn) caused by the grinding process.

Furthermore, an extension of the investigations into the influence of the buildup direction would be useful, in which harder or additionally heat-treated materials are used in addition to further angles in order to increase possible effects. In this case, single-grain scoring tests could be carried out for a detailed investigation of chip formation during grinding.

In addition, it should be investigated to what extent the different build-up directions can generate a possible preferred direction for the grinding process. In this context, differentiations between down and up-cut grinding should also be considered.

In the context of component functionalization, surface conditioning should also be taken into account. This means that, in addition to surface topography, the influence on boundary zone properties such as residual stresses and microhardness is specifically considered. Thus, the surface integrity moves into the focus of further considerations. This is particularly interesting with regard to the thermal history of additively manufactured components. Due to the effect of WAJM and microfinishing, which usually generate residual compressive stresses in the boundary zone, advantages for the functionalization processes could arise. This hypothesis should be investigated taking into account the thermal history of the components.

In addition, it is conceivable to investigate more complex component geometries and to use NC form grinding processes for machining free-form surfaces. This enables additive manufacturing to come closer to industrial applications, since simple geometries generally are not used here. The increase in component complexity also draws into focus the support structures required in additive manufacturing. It should be investigated how these must be designed in order to achieve the necessary support and at the same time be easy to remove. In addition to NC form grinding, robot-guided WAJM processes are also conceivable for this purpose.

5 Surface functionalizing with milling and hard coating technology – Results of the GFE

S. Lutze, H. Frank, M. Ambos, M. Uhl; GFE - Gesellschaft für Fertigungstechnik und Entwicklung Schmalkalden e.V.

5.1 Introduction

When manufacturing additively manufactured components, the entire additive-subtractive manufacturing (ASM) process chain must be take into account. Various pre- and post-treatment and components are of great importance. For example, the used materials, necessary heat treatment processes after additive manufacturing, processes for removing necessary support structures, subtractive processes for surface functionalization and finishing processes for setting defined surface properties are of importance. By varying these processes, it is possible to influence the properties of the manufactured components. Use the different processes, the entire process chain shown in Figure 5-**1** was considered by the various research institutions as part of the Ad-Proc-Add project. Regarding the process chain for the additive-subtractive processes, some aspects were investigate more closely.

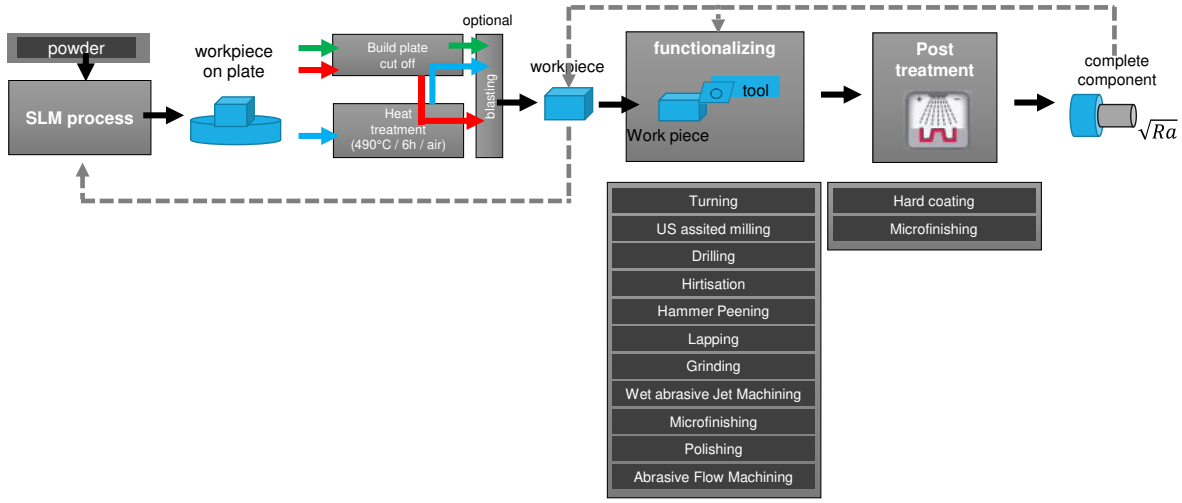

Figure 5-1: Complete additive-subtractive process chain in Ad-Proc-Add.

At the beginning of the project, the process chain was specified with regard to the used materials, the selection of the component geometries, as well as the heat treatment and the parameters of the used functionalization processes. The aim of the project was to determine the relationships between process parameters and component properties and to determine process parameters for specific modification of component properties. The analysis of the additive process was carried out taking into account various parameter variations (e.g. scan speed, build-up rates, laser energy and focus size, geometry, orientation) Subsequent process steps (e.g. heat treatment, blasting, grinding) were also considered and evaluated. The focus of the GFE's investigations was on

- Use of the maraging steel 1.2709 with the laser powder bed fusion (LPBF) method
- Analysis of the influence of the LPBF method on component properties
- Surface functionalization by milling processes with and without ultrasonic assistance
- Surface finishing with PVD hard coating

In order to get a detailed understanding of the correlations in additive manufacturing, the additive-subtractive process chain shown in Figure 5-2 was used. The LPBF process is used to produce components from the material 1.2709. After the AM process, the components were separate from the build plate. The boundary conditions for the processes were set in relation to machining scenarios, tool selection, the definition of process parameter areas and the specification of the measurement technology as well as work piece analysis. The design of experiment (DoE) method was used to create statistical test plans.

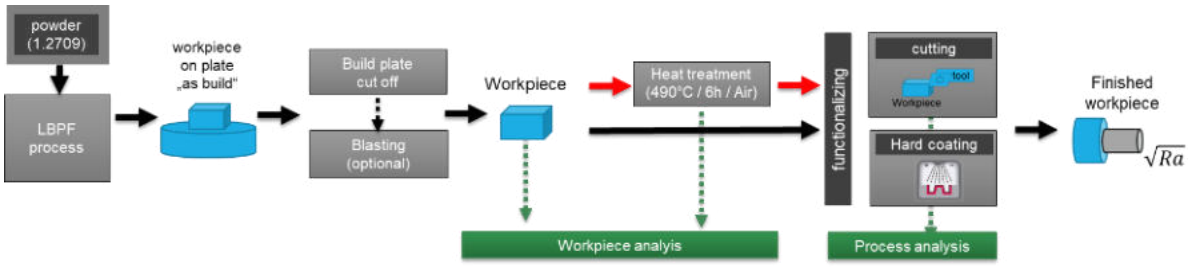

Figure 5-2: Specific process chain for surface functionalizing by milling processes and hard coating technology.

Analysis of the influence of the LPBF method on component properties

The LPBF machine Lasertec 30 SLM 2nd from the company DMG MORI Germany was used to produce the AM samples from the material 1.2709. Simple geometries (discs, hollow cylinders, rods) produced for the basic analyzes and in order to determine the influence of the process parameters on the geometry, structure and roughness of the manufactured components. Used initial process parameters, based on the recommendations of the manufacturer of the AM system is show in Table 5-1. Regarding the AM process parameters, also different buildup-directions (0°, 90° to the build plate) used.

Process conditions		work piece geometry
Material	1.2709	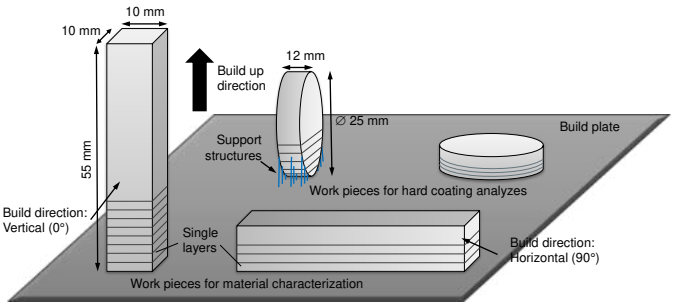
Layer thickness	65 µm	
Work piece orientation	0°, 90°	
Atmosphere	Argon	
Build plate temperature	200 °C	
Laser power (hatch)	275 W	
Scan speed (hatch)	750 mm/s	

Table 5-1: LPBF process conditions and work piece geometry.

Surface functionalization by milling processes

The post-machining with defined cutting edges are also analysed in terms of milling of AM parts of the material 1.2709. An appropriate definition of tools, tool holders and fixtures, as well as an initial parameterization were work out. Main goals of the investigations were to identify process influences on the workpiece properties and optimum parameter sets for the functionalizing. The milling test are carried out on the machining center DMG 125 P DUO with an ultrasonic (US) module. Various process variants (peripheral milling, face milling) as well as cutting conditions (cutting speed, feed rate) are analyzed

based on the used DoE. Range of the used parameters as well as the used machine are given in Table 5-2.

Machine	parameter	Parameter range
 DMU 125 P DUO	Cutting Speed v_c	80 - 240 m / min
	Tooth feed rate f_z	0.04 - 0.16 mm
	radial depth of cut a_e	0.1 – 0.4 mm (peripheral milling)
		2.5 mm (face milling)
	axial depth of cut a_p	15 mm (peripheral milling)
		0.1- 0.4 mm (face milling)
	Ultrasonic amplitude γ	0 %

Table 5-2: used machine, machine parameters and variation range for cutting processes.

Surface finishing with PVD hard coating

The hard coating process carried out using the PVD process on the commercial coating machines π^{211} and π^{411} from the company PLATIT. The objective is the analysis of the thermal influence of the coating deposition on the additively manufactured components as well as the combination of surface functionalization, hard coating and heat treatment in a single process. Relevant influencing factors are surface roughness and surface hardness after the additive process (before coating deposition), coating composition, coating structure and deposition temperature. Used machines for coating deposition as well as major process variants given in Table 5-3.

Machines		Parameter	Parameter variant
 π^{211}	 π^{411}	Heat treatment before coating	Without, 490°C/6h
		Pre treatment	Blasting, grinding, polishing
		Post treatment	Without
		Deposition temperature	100°C - 550°C
		Coating thickness	1 -5 µm

Table 5-3: Used machines for coating deposition and major process variants.

Main goals with industrial relevance

Main goals for the investigation of surface functionalization by milling processes and hard coatings are the analysis of the relationships between additive manufacturing and machining process, the analysis of the influence of the hard coating on the work piece properties and the development of a technology for the precise production of components with additive manufacturing. Based on the project goal of the Ad-Proc-Add project, expected results with a significant relevance for the industry with respect to the additive-subtractive manufacturing (ASM) are:

- Fundamental insights regarding influences on workpiece properties in ASM chains
- Methodologies for characterization of ASM process influences on workpiece properties
- Basics for the targeted application of ASM for innovative cutting and forming tools
- Requirements and approaches for future machine concepts for post-machining of AM parts

5.2 Description of project results

5.2.1 Analysis of the AM process

AM process technology and characteristic values

In order to evaluate the additively manufactured and post-treated components according to the process chain, it is necessary to analyze the LPBF process and the components. Goal of the investigations is the determination of the influence of process conditions on the geometrical properties, the necessary and possible accuracy and the mechanical properties of the workpiece, as well as on the functionalization process. In the investigations of the GFE the following points were of particular interest:

- Conditions of the LPBF process
- Work piece geometries and material
- Characteristic workpiece properties

Conditions of the LPBF process

Based on the recommendations of the manufacturer of the AM system, the main parameters are layer thickness, laser power and scan speed (see above Table 5-1). However, other parameters of the LPBF process can influence the component properties. Important are the conditions for the material, the laser and the laser scanning as well as the environment (Table 5-4).

Due to the high complexity of the process, in the investigations the focus was only on red coded parameters in Table 5-4. To the analyses carried out, in Figure 5-4 the explanation of the different values are given as well as the used LPBF machine and an example of the build job in the chamber of the AM machine.

material	Laser	Scan	Environment
Composition	Mode	Scanning speed (v)	Pre-heating
Powder density	Wavelength	Hatch distance (h)	Pressure
Morphology	Power P	Layer thickness (t)	Gas type
Diameter of grains	Frequency	Scan strategy	Oxygen level
Distributions	Pulse width	Scan-sectors	
Thermal properties	Offset (+/-)	Pulse distance	
Flow properties	Spot-∅ (d)	Scaling factors	

Table 5-4: influencing parameters on the LBPF process.

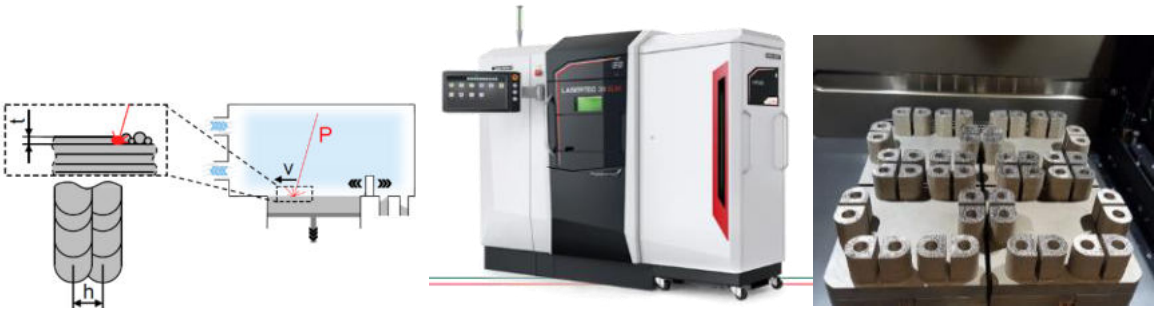

Figure 5-4: explanation of main LBPF influencing parameters (left), used LPBF machine (middle) and example of the build job (right).

Workpiece geometry and material

In cooperation between the project partners and the committee responsible for the project, test specimen and workpiece geometries were defined for the experimental and theoretical analysis. Available test parts (e.g. ASME part for the qualification of AM systems) were taken into account. Here, specimens were specified for basic tests (e.g. tensile test, impact test, density), the definition of components for the comparative analysis of additive manufacturing and the construction of test workpieces (prismatic and cylindrical), which were created additively functionalized. Exemplary features (e.g. flat, inclined and curved surfaces, cavities, ribs, struts, holes, lattice structures) come from typical and challenging applications in industry.

Figure 5-5 shows the geometries for fundamental investigations of the material analysis (notch impact strength, tensile strength, density). These test pieces were additive manufactured with an orientation 0° and 90° to the build-up direction (see Table 5-1). Figure 5-6 represent examples of simple geometries (holes, channels, thin structures) that should be used to compare the system technology used in accordance with ASTM 52902). These structures can use to analyze the accuracy, the resolution and the surface quality.

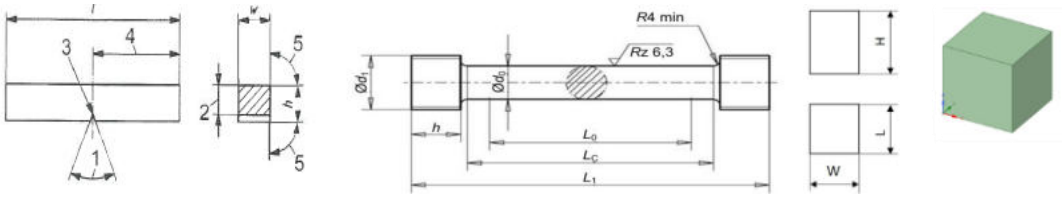

Figure 5-5: Sample geometry for the analysis of notched impact strength (left), tensile strength (middle), density (right).

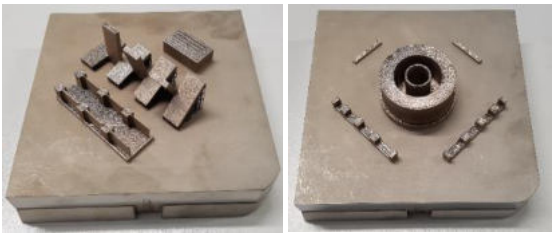

Figure 5-6: Sample geometry for the analysis of resolution, accuracy and surface quality in accordance with ASTM 52902

The geometry of the components for the functionalization process milling and PVD hard coating is shown as an example in Figure 5-7. These test pieces were additive manufactured with an orientation 0° and

90° to the build-up direction (see Table 5-1). The aim is to produce the additively manufactured components with a high level of geometrical accuracy, a roughness Rz <20 µm with a layer thickness of 60 µm.

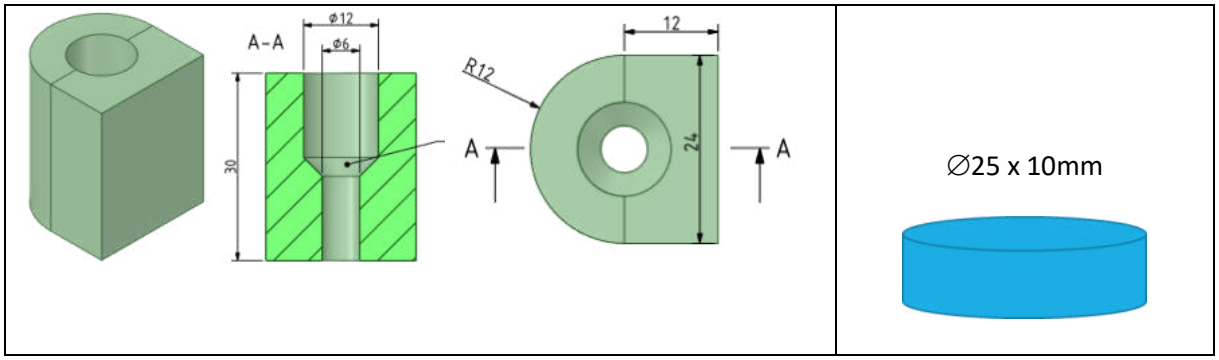

Figure 5-7: Geometry of test specimen functionalizing with milling (left) and hard coating technology (right).

The material specification and the heat treatment chose to compare the various alternative process chains of additive manufacturing and functionalization in the project. The investigations of milling and hard coating technology were carried out with the margaring steel powder as well as without and with a heat treatment at 490°C for 6h in Air. To compare the properties of different materials, the research partners produced work pieces from different, industrially relevant materials. The materials and heat treatment conditions as well as the additive process to produce test specimen for the material analysis is summarized in Table 5-5. The material mainly used for GFE investigations is **bold** marked.

Material	Heat treatment parameters	Process
G42 3 M21 13 S1	Without / 620°C/2h/Ar	WAAM (wire arc additive manufacturing)
AlSi10Mg (3.2381)	Without / 300°C/2h/Air	LPBF (laser powder bed fusion)
TiAl6V4 (3.7165)	Without / 650°C/3h/Ar	LPBF (laser powder bed fusion)
X3NiCoMoTi18-9-5 (1.2709)	**Without / 490°C/6h/Air**	**LPBF (laser powder bed fusion)**
1.4404 (X2CrNiMo17-12-2)	Without / 490°C/6h/Air	LPBF (laser powder bed fusion)

Table 5-5: Used materials and heat treatment parameter.

Characteristic workpiece properties

The parameters to be characterized when functionalizing the surface are determined by the application. With regard to the characterization of the properties of the additively manufactured components, there are a number of options for analysis. This includes both mechanical and structural properties of the manufactured components as well as geometric and surface parameters after functionalization and coating. In addition, the various component properties also influence the respective functionalization process, which is why essential parameters of the functionalization are also important. Table 5-6 shows the characteristic parameters that were determined in the investigations. With regard to comparability, bold marked analyzes were carried out respectively by one research partner.

Powder analysis	• **Particle size distribution (FOTEC)**	• Composition
Mechanical properties	• **Notched impact strength (GFE)** • **Hardness (GFE)**	• **Density (IFT)** • **Tensile strength (IfW)**
Microstructure	• Microstructure • Structure	• Porosity • Composition
Macrogeometry and accuracy	• Shape • Roundness	• Cylindricity • Straightness
Roughness and topography	• Topography (2D/3D)	• **Roughness (ISF)**
Functionalizing	• Cutting forces and moments • Process temperature • Vibrations	• Use of energy • Wear • Optical analysis
Hard coating (GFE)	• Coating thickness • Coating structure • Coating adhesion	• Micro hardness • Elasticity • Wear coefficient

Table 5-6: Characteristic values determined in the project processing.

Material Qualification

Powder Analysis

The analysis of the powders used included the determination of the composition and shape of the various powders as well as the particle size distribution. In the GFE scanning electron microscopy (SEM) and the energy-dispersive X-ray spectroscopy (EDX) were used to measure the composition and shape. The particle size distribution (PSD) was carried out at the research institute INSPIRE with laser diffraction methods.

In Figure 5-8, typical particle shapes of the used powders are shown. Also in the pictures a uniform particle distribution with different particle sizes is visible. The particles are also predominantly ideally spherical. The results also show that the powder present in the powder cycle shows only small changes in particle shape and distribution after longed use (material 1.2709 used). Corresponding particle size distribution, measured by the research partner INSPIRE (Figure 5-9) confirm, that the all PSDs are within the range of a typical SLM powder.

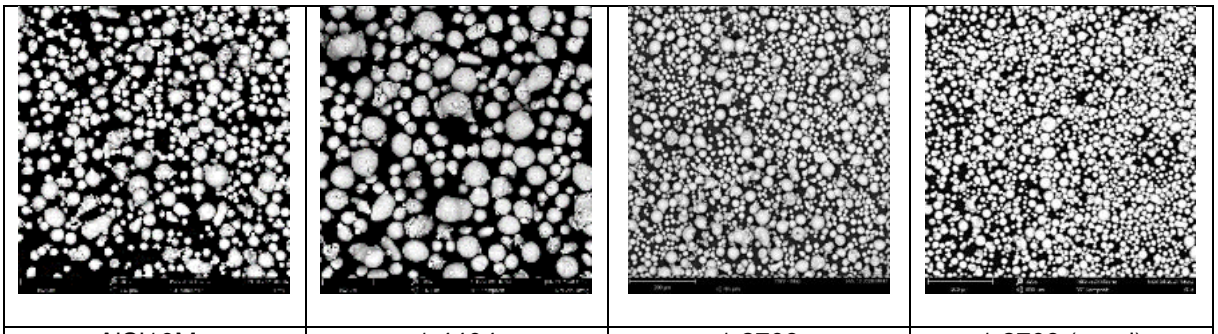

AlSi10Mg	1.4404	1.2709	1.2709 (used)

Figure 5-8: typical particle shape of different powders.

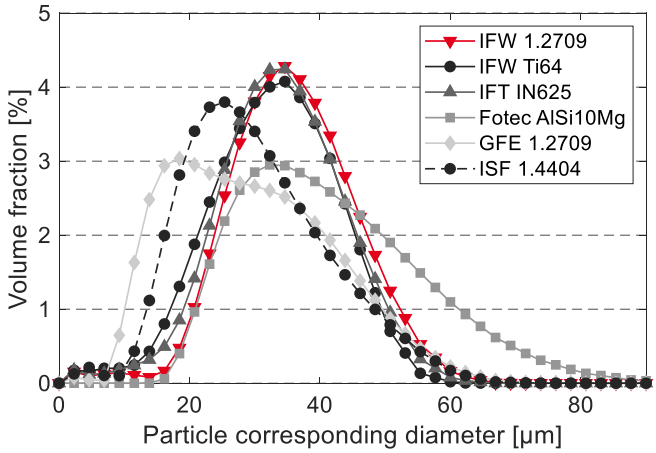

Figure 5-9: Particle size distribution of different used powders (measured by INSPIRE).

Results of EDX analysis of the used powders 1.2709, 1.4404, AlSi10Mg given in Table 5-7. The results show, that the chemical composition meet expectations of the powder supplierer without significant deviations.

Remarkable is the composition of the powder material 1.2709 after a long period of use (800 h operating hours). Changes in the composition arise here, which can be cause by oxidation processes and contamination, for example. Here, the aging of the various powders should be analyzed more precisely in further analyzes and projects.

1.2709		C	Ni	Co	Mo	Ti	Fe
Data sheet (supplier SLM)	Wt-%	≤ 0,03	18,0 – 19,0	8,5 – 9,5	4,7 – 5,2	0,5 – 0,8	bal.
EDX measurements	Wt-%	-	16,9 – 17,7	8,8 – 9,2	4,5 – 5,3	0,6 – 1,0	bal.
Used powder (Batch #5)	Wt-%	-	14,2 – 15,0	10,7 – 10,9	3,9 – 4,3	0,7 – 0,8	bal.
Used powder (800 op. hours)	Wt-%	-	17,7 – 18,4	9,6 – 9,7	5,7 – 6,7	0,9 – 1,1	bal.

1.4404	Wt-%	C	Ni	Cr	Mo	Mn	Si	Fe
Data sheet (supplier SLM)	Wt-%	≤ 0,03	10,0 – 14,0	16,0 – 18,0	2,0 – 3,0	≤ 2,0	≤ 1,0	bal.
EDX measurements	Wt-%	–	12,3 – 13,1	17,2 – 18,2	2,2 – 3,2	0,8 – 1,2	0,5 – 0,9	bal.

AlSi10Mg		Si	Mg	Fe	Mn	Al
Data sheet (supplier SLM)	Wt-%	9,0 – 11,0	0,2 – 0,45	≤ 0,55	≤ 0,45	bal.
Supplier analysis (r IMR)	Wt-%	10	0,35	0,06	≤ 0,01	bal.
EDX measurements	Wt-%	9,0 – 15,0	(0 – 0,8)	–	–	bal.

Table 5-7: Chemical composition of the used powders and comparison with supplier data sheet.

Roughness and Geometry

The analyses of roughness and geometry carried out and evaluated in collaboration between the research institutes ISF Dortmund and GFE Schmalkalden e.V. The roughness and the geometric characteristics were measured on components manufactured by the research partners GFE Schmalkalden e.V., ISF Dortmund, IfW Stuttgart, FOTEC and IFT, TU Wien from the materials 1.2709 (GFE), 1.4404 (ISF), AlSi10Mg (FOTEC, IFT), TiAl6V4 (IfW). The produced geometries correspond to the components of the ASTM 52902 standard (see Figure 5-6). Measured geometrical parameters are

- Roughness / different orientations in relation to the build-up directions
- Dimensional accuracy of solid structures
- Dimensional accuracy of round structures
- Dimensional accuracy of small structures (holes, pins, slots, walls)

The results for roughness measurement is shown in Figure 5-10 for the roughness R_z. Here the orientation of the structure varies between 0° and 90° in relation to the build-up direction (see small picture in Figure 5-10). The diagram demonstrate, that with exception of AlSi10MG /IFT (unfavourable parameter set) the orientation of the structure has only a small influence on the resulting roughness R_z, the roughness is in a similar range. But there are differences of the roughness in the various materials. These document different parameter sets in additive manufacturing (e.g. laser power, hatch). Based on

the results of these roughness measurements, the research partners subsequently also optimized the respective parameters.

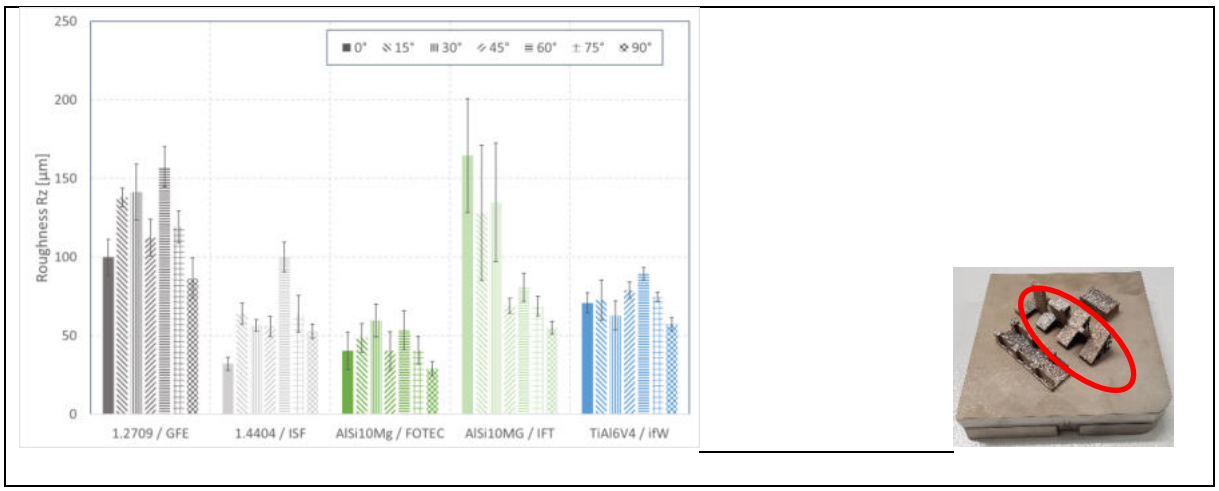

Figure 5-10: Roughness Rz on different oriented structures of various materials.

In Figure 5-11 the structural size of solid blocks with a defined length in the range 2.5 -12.5 mm is shown. There are only minor differences in the generated lengths compared to the target size. For better visualization, the deviations of 0.1 – 0.2 mm from the target size showed in Figure 5-11 on the right. In the case of the material AlSi10MG / FOTEC are higher variation due to errors in the data entry. These sizes represent the good dimensional accuracy of the additively manufactured probes.

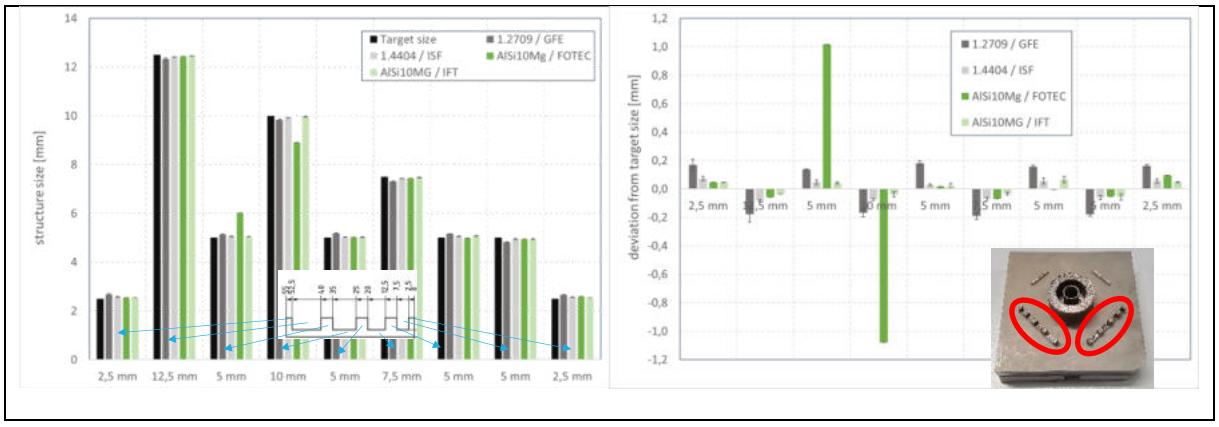

Figure 5-11: Dimensional accuracy of solid structures of various materials.

The determine the dimensional accuracy of round structures the inner and outer diameter as well as the concentricity of rings with a diameter 14-16 mm (thickness of the ring 2 mm, Figure 5-12, left) and 30-47 mm (thickness 15 mm, Figure 5-12, right) of structures of different materials were measured. The deviations from the target size in figure 5-12 are in the range between 0.1-0.2 mm. The deviation from the concentricity of with<0.2 mm is also small. These sizes confirm the good accuracy in the producibility of round structures.

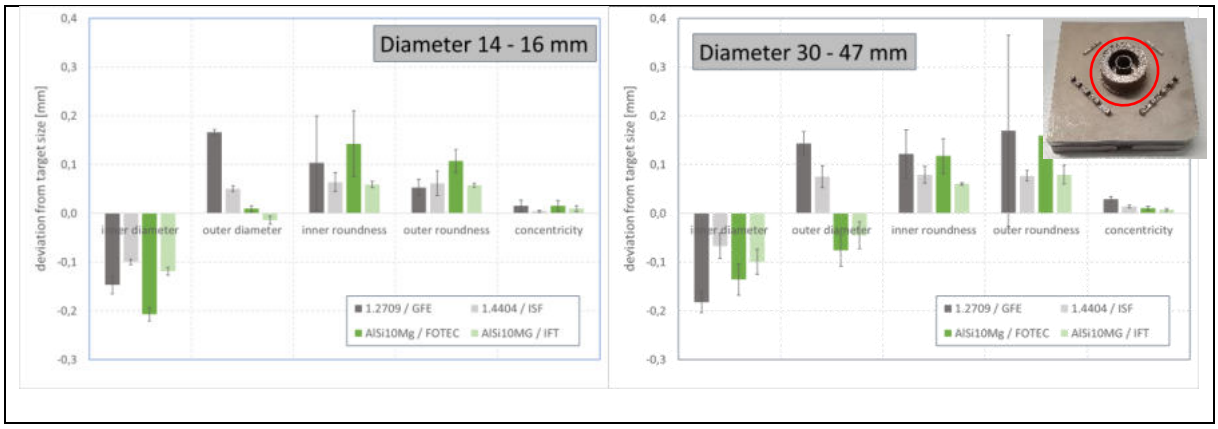

Figure 5-12: Dimensional accuracy of round structure of various materials for round structures with 14-16 mm (left) and with 30-47 mm (right).

In the case of additive manufacturing of thin walls (Figure 5-13 left) it can be seen, that the measured wall thickness is normally higher than the target size. Usually the generated thickness is about 0.1-0.2 mm larger than desired. With a reduced wall thickness, variations get higher. Walls with a thickness of 0.1 and 0.2 mm are not manufacturable with a sufficient accuracy. A similar behavior are visible for small slots (Figure 5-13, right). Here the measured width is usually 0.1 - 0.2 mm smaller than the target size. An exception is the material 1.4404, in which the width deviates only very little from the target size. The additive manufacturing of slots with a width of 0.2 mm is possible, but requires more effort in the determination of suitable parameters.

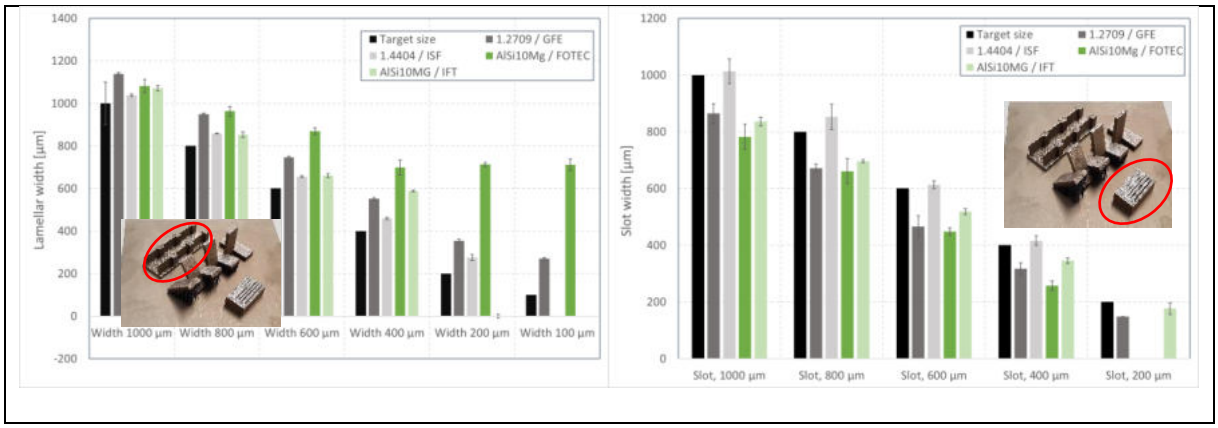

Figure 5-13: Dimensional accuracy of thin structures of different materials: lamellar walls (left) and small slots (right) compared with a target size.

The production of small pins and holes is more challenging. Like shown in Figure 5-14, left, there are large deviation from the target size for pinholes with a diameter <500 µm. The diameter of the pinhole is always in the range of 500 µm. The production of small holes is not possible in a reproducible manner. Additive manufacturing of pins with smaller diameters of pins is possible (Figure 5-14, right), but there are also large deviations from the target size especially when using AlSi10Mg. Often a worse geometry of smaller structures can be observe, smaller diameters can bend and break very quickly.

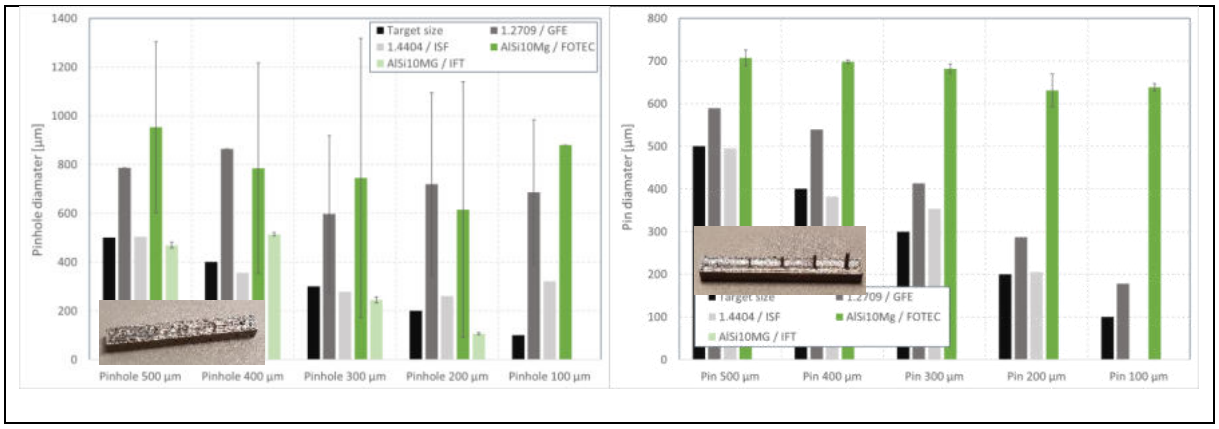

Figure 5-14: Dimensional accuracy of thin structures of different materials: pinholes (left) and pins (right) compared with a target size.

The conditions and restrictions for additive manufacturing of thin structures (rings, walls, slots, pins, pinholes) of different materials given above were taken into account for the manufacturing of components for the functionalization in the next investigations

Mechanical properties

According to the test specimen geometry (see Figure 5-5), the research partners manufactured samples for the analysis of the mechanical properties density, tensile strength and notched impact strength. The measurement of the hardness was carried out on the printed samples. For the structural examinations, printed samples were separated and a cross-section was made. To improve the visibility of the structure, the samples were etched (with NaOH). The sample production was varied according to:

- Material: G42 3 M21 13 S1, AlSi10Mg, TiAl6V4, 1.2709 and 1.4404
- Orientation of the probe to the build-up direction: 0° and 90°, see Table 5-1)
- Heat treatment: with and without (see Table 5-5)

The hardness of the additive manufactured samples showed and compared with the literature in Figure 5-15, all materials are in good agreement with the values from the literature. The lowest values can see for the AlSi10Mg-Alloys. For AlSi10Mg, the hardness is nearly independent form the build-up direction and slightly decreases after heat treatment. For TiAl6V4 there are large differences in the hardness between vertical (0° to build-up direction) and horizontal (90° to the build-up direction): horizontal orientation lead to a lower hardness. With a heat treatment, hardness for Ti-Al6V4 is independent from the build-up orientation. For the material G42 3 M21 13 S1 (WAAM processed) the hardness is nearly independent from orientation, with heat treatment the hardness is slightly reduces. The hardness for 1.4404 is independent from the orientation.

For the materials 1.2709, the orientation to the build-up direction and the heat treatment is essential (Figure 5-15, grey bars). Without a heat treatment, the hardness is lower and there are larger differences between orientation of 0° and 90° to the build-up direction. Vertical (0° to build-up direction) orientation leads to a higher hardness. With a hardening heat treatment, the hardness increases significantly and the differences between the orientation are reduced. The heat treatment leads to a significant increase in hardness, which can be explained by the intermetallic segregations formed during age hardening. After heat treatment, the hardness is independent from the orientation.

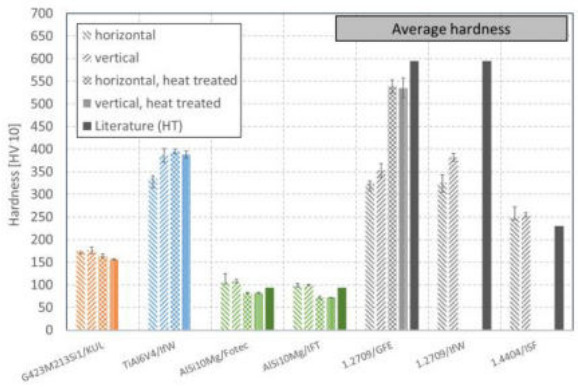

Figure 5-15: Hardness of different AM materials, with and without heat treatment, different orientations to the build-up direction.

Results for measurement of the notched impact strength are shown in Figure 5-16. The highest strength was measured for the WAAM material G42 3 M21 13 S1 due to the density structure of the material caused by the higher heat input. AlSi10Mg and TiAl6V4 show a low notched impact strength, which can slightly increase by heat treatment. For the material 1.2709 and 1.4404, the notched impact strength without heat treatment is less in horizontal direction (90° to build-up). As result of the heat treatment, the impact energy for the material 1.2709 is reduced, and there is no longer any significant difference between the workpieces produced in different orientations. The reduced impact energy after the heat treatment correlates with the increase in hardness and is due to the formed intermetallic segregations, which limit the deformability of the material and lead to a more brittle material behaviour.

The fracture surfaces generated during the notched impact tests (Figure 5-17 and 5-18) can be used to give information about ductility. With a build-up direction of 0° without heat treatment, more dimples occur and the work pieces are more ductile. Heat-treated samples have fewer or smaller dimples, regardless of the build-up direction, and therefore have a significantly lower ductility. These results are consistent to the measured impact energy. Higher porosity in vertical build direction and without heat treatment can be seen in the SEM images as well. In the case of TiAl6V4 the material show brittle behaviour.

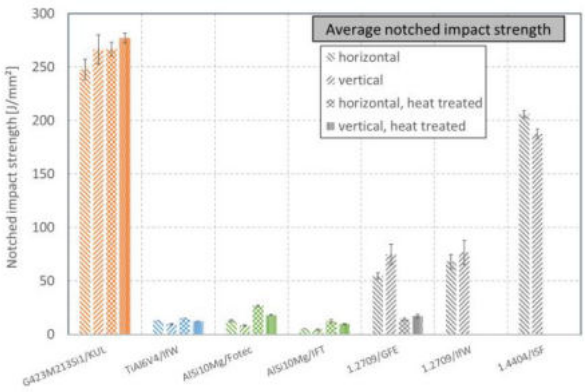

Figure 5-16: Notched impact strength of different AM materials, with and without heat treatment, different orientations to the build-up direction.

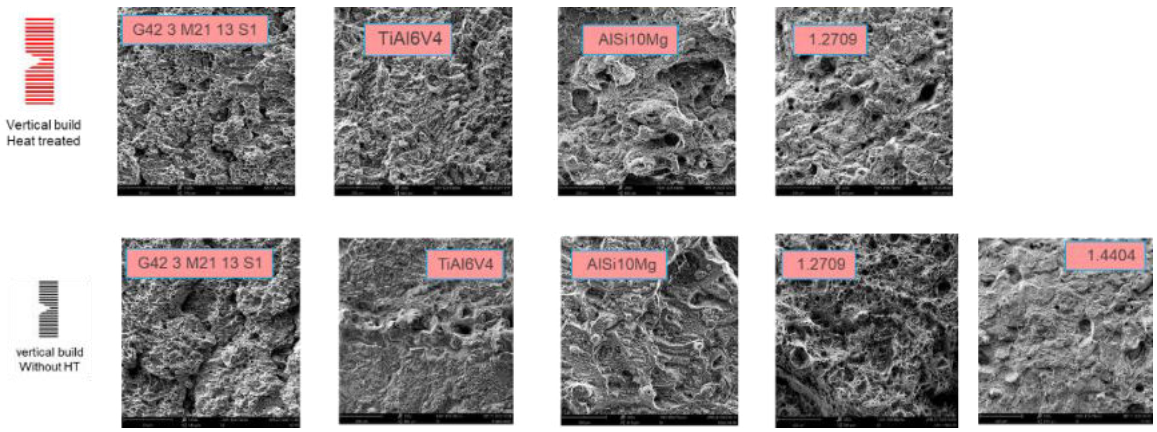

Figure 5-17. SEM images of the fracture surfaces of the notched impact work pieces with and without heat treatment 0° to build plate (vertical orientation).

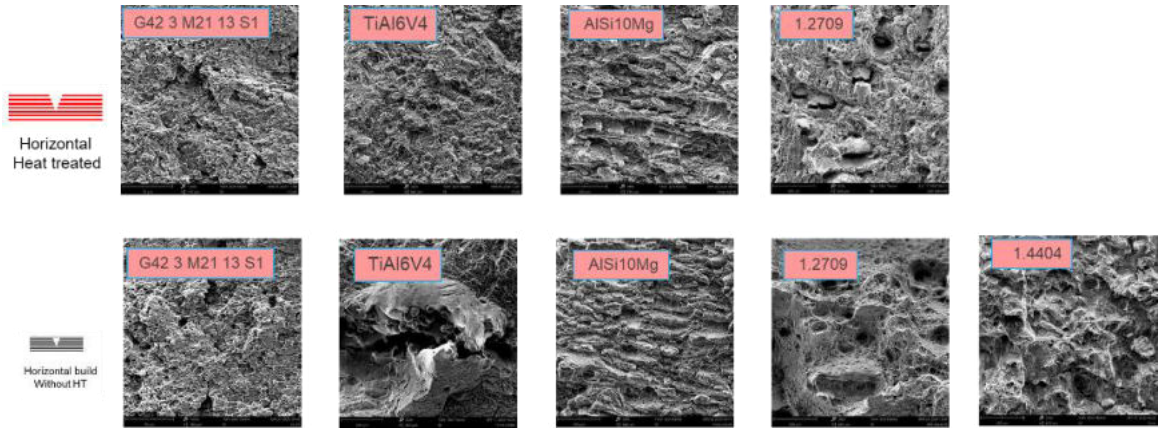

Figure 5-18. SEM images of the fracture surfaces of the notched impact work pieces with and without heat treatment 90° to build plate (horizontal orientation).

Results of tensile strength confirm the results of hardness and notched impact strength. In Figure 5-19, the tensile strength and the Young's modulus of the materials can be seen. For tensile tests, the materials AlSi10Mg and TiAl6V4 without heat treatment and 1.2709 with and without heat treatment examined. Compared with the literature the values of the tensile strength are in the same range (Figure 5-19, left). The AlSi10Mg-Alloys show the lowest tensile strength and Young's modulus, TiAl6V4 and 1.2709 have higher values.

For the material 1.2709 is important that tensile strength and Young's modulus are influenced by heat treatment and direction of build-up. There are differences in the Young's modulus between vertical and horizontal position before and after heat treatment, in horizontal direction the Young's modulus is higher (Figure 5-19, right). Furthermore, tensile strength and Young's modulus are higher after heat treatment.

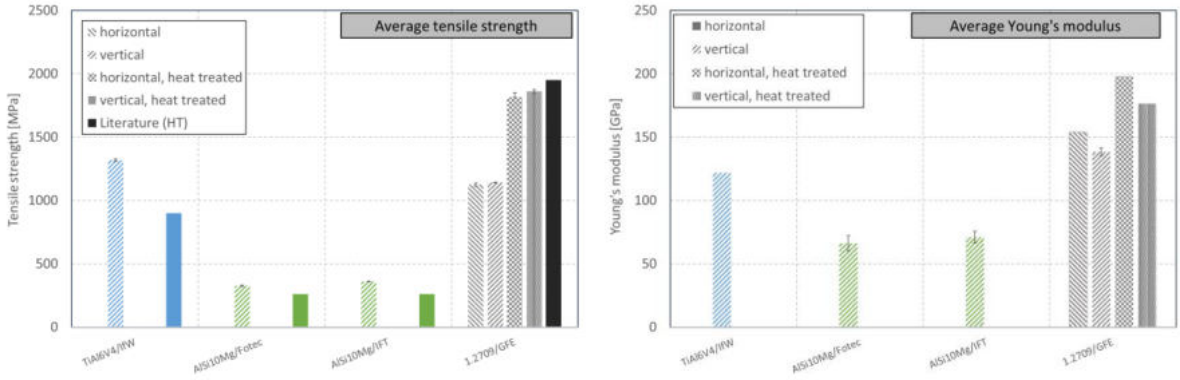

Figure 5-19: Tensile strength (left) and Youngs modulus (right) of different AM materials, with and without heat treatment, different orientations to the build-up direction.

Microstructural Analysis of different AM work pieces

Figure 5-20 shows a cross-section through the structure of the different additively manufactured and heat-treated workpieces in horizontal and vertical build-up direction. The analyzed materials were G42 3 M21 13 S1, AlSi10Mg and 1.2709. For a better visibility of grain boundaries and structural components, the structure was etched using the etchant Nital (solution of 3% HNO3 in ethanol). For the different materials and build-up directions, the grain boundaries of the individual layers are particularly visible in the variants without heat treatment (Figure 5-20). After the heat treatment, no differences in metallographic phases at different build-up directions are visible, the build-up direction has no influence on the resulting structure. The structure is homogenized with heat treatment (Figure 5-21). The greatest changes in the microstructure after heat treatment occur in the material 1.2709, here martensitic structures results.

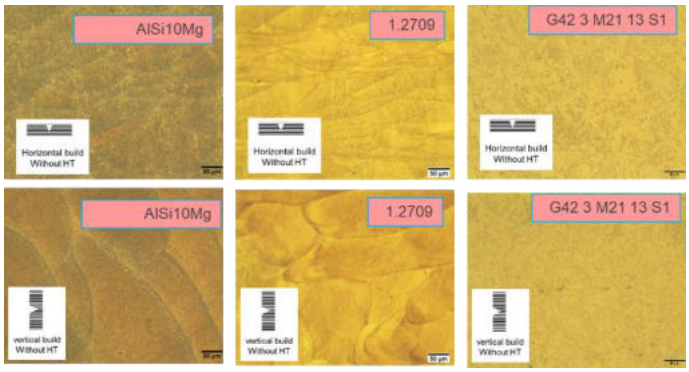

Figure 5-20: microstructure of AM samples of AlSi10MG, 1.2709 and G42 3 M21 13 S1 without heat treatment; horizontal (upper) and vertical (lower) build-up direction.

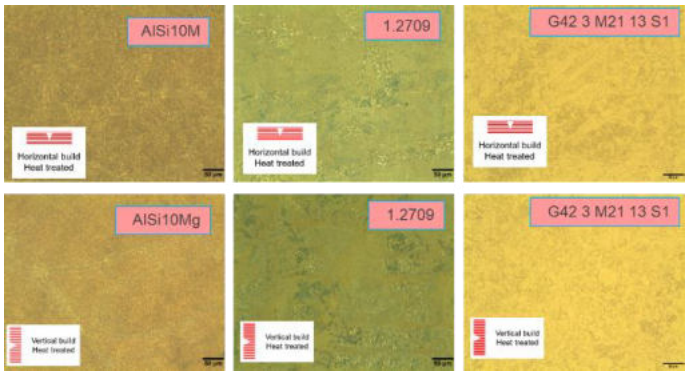

Figure 5-21: microstructure of AM samples of AlSi10MG, 1.2709 and G42 3 M21 13 S1 with heat treatment; horizontal (upper) and vertical (lower) build-up direction.

Relative Density

Results for density measurements are given in Figure 5-22. Here the measurements were carried out at the IFT, TU Wien with Archimedes method. With this method, the density is measured in air and in water and a comparison to the theoretical density given from the supplier of the used powder (see figure 5-22). The results show that ISF density probes of the material 1.4404 have achieved the highest relative density with an average of 99,78%. The density results show as well, that parameter optimization is necessary for each SLM machine in detail.

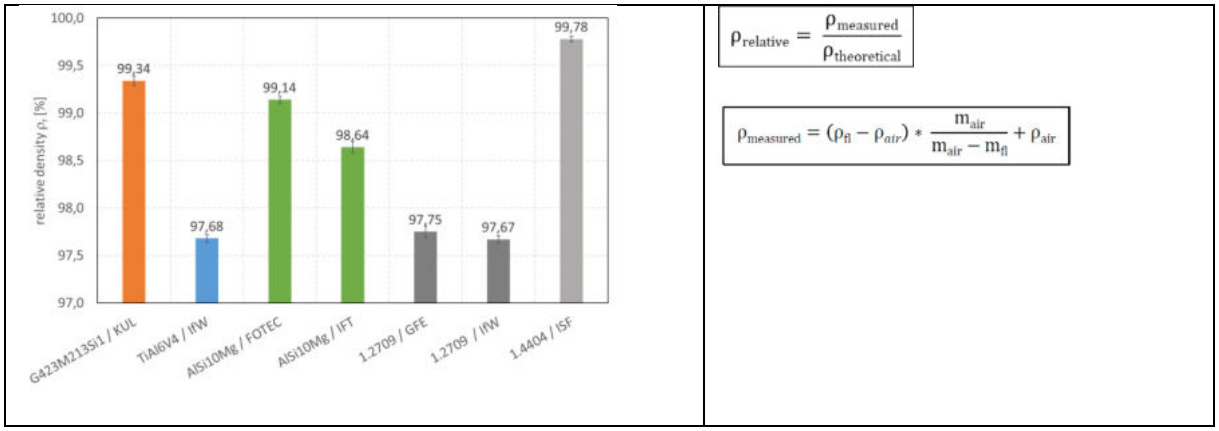

Figure 5-22: Relative density of AM samples (left) and calculation rule for determining the density (right).

Analysis and optimization of the LBPF technology

In the GFE, a systematic analysis of the process was carried out to optimize the ASM in order to determine interactions between process boundary conditions and workpiece properties. The analysis results were used to obtain statements on process reproducibility through correlations with sensor and control data and to optimize the AM process. As an example of the analyses carried out, Figure 5-23 (left) shows the component densities determined at different positions for the additive manufacturing of the material 1.2709. The results show greater fluctuations in the component density between the worst and the best variant

The SLM process itself depends from essential influencing factors, in particular scanning speed, scan strategy and hatch distance, but also by the design of the SLM system (component positioning, optimized supply of gas and powder). This modified factors in an modified batch an increase in the density

from to 7.81 g/cm³ (relative density 98,05), a reduced density variance: 95.6 - 98.7% (7.7 - 7.9 g/cm³) was reached. Optimal positions with an even density distribution are in the middle of the installation space. Density and relative density results in next batch are shown in Figure 5-23 (middle).

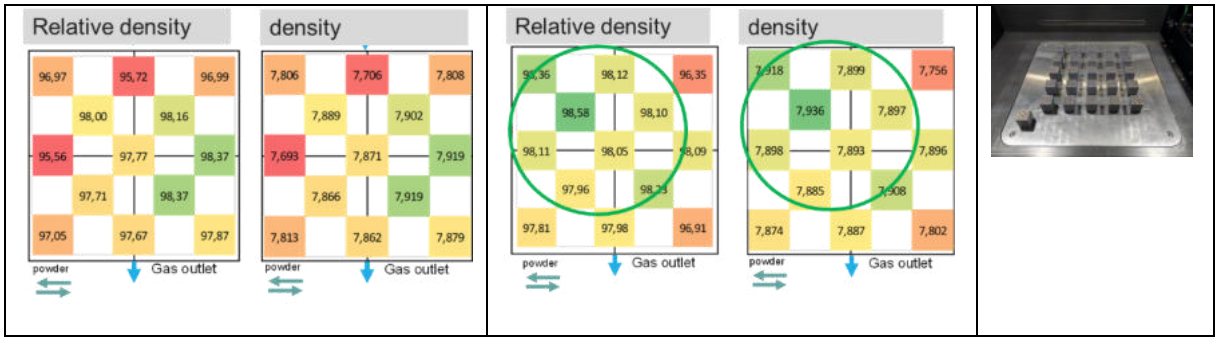

Figure 5-23: Component density at different positions in different batches: left: batch #1; middle batch #2; position of density cubes with the batch.

Conclusion for material qualification and process optimization

The analysis of both the SLM process and the material properties show the influence of the various parameters on the component properties. Although it was possible to realize comparable component properties with the literature for all additively manufactured materials (G42 3 M21 13 S1, AlSi10Mg, TiAl6V4, 1.2709 and 1.4404) in the project consortium, there is still considerable potential for optimization.

The analysis of the powder used shows only a slight change in the powder distribution as the period of use progresses. However, due to oxidation and moisture, powder aging can occur with a slightly different powder composition. This should be the subject of further investigations. Furthermore, there is still insufficient accuracy, particularly in the production of small structures (0.1 -0.2 mm structure size). Here, further optimization of the SLM process is necessary by adjusting the SLM parameters (e.g. scanning speed, power, hatch distance, layer thickness, scan strategy, scan strategy, spot diameter). The modification of the parameters should be carried out to influence the thermal behavior and to reduce thermal effects (e.g. distortions, pores) in additive manufacturing.

The mechanical properties (hardness, tensile strength, impact strength) of the additively manufactured materials (G42 3 M21 13 S1, AlSi10Mg, TiAl6V4, 1.2709 and 1.4404) show the expected results. Nevertheless, the orientation of the work pieces according to the build-up-direction as well as a further heat treatment plays an important role for the properties of the AM components.

- With heat treatment, the micro structure will homogenized
- For the material TiAl6V4 heat treatment is necessary to reduce thermal stresses
- For the material 1.2709 heat treatment is necessary
    - to achieve a high hardness and a high tensile strength,
    - material properties are independent from the build-up direction
- Material 1.2709 without heat treatment
    - lower hardness and notched impact strength for horizontal work-piece direction (90° to the build-up direction)
    - Has a higher notched impact strength

5.2.2 Surface functionalizing by milling

Technological setup for the milling process

Ultrasonically assisted machining has a great potential with regard to tool life, process stability, machining quality and productivity. The surface and subsurface properties of AM parts can modified by adjusted machining conditions. To investigate the relationships between workpiece properties and machine conditions, the surface functionalizing of AM parts are analyzed with defined cutting edges in terms of ultrasonic assisted machining (milling and hammer peening.

The milling as well as tests with ultrasonic-assisted machining are carried out on the machining center DMG 125 P DUO with an ultrasonic (US) module. Various process variants (peripheral milling, face milling) as well as cutting conditions (cutting speed, feed rate) are analyzed based on the used DoE (see also Table 5-2). An appropriate definition of tools, tool holders and fixtures, as well as an initial parameterization were work out. Figure 5-24, left shows the experimental setup as well as the used tools for the machining operations. For the tests, a standard milling tool with a diameter of 8 mm was used.

Due to a defect in the ultrasonic module, there was a delay in ultrasonic processing in the project. Even after the repair, the US parameters could not be set reproducibly. Because of the clearly limited possibility of ultrasonically supported processing, this task was only used in a random test. This made it possible to carry out a significantly higher number of tests, especially in the area of cutting tests without ultrasound support. Especially in the field of investigations into the generated surface qualities, the gain in knowledge could be significantly increased.

For the cutting, the processes face milling and peripheral milling were chose do analyze the properties of different surfaces. In Figure 5-24, right, the used milling path for the functionalizing processes is shown. Here all specimens were clamped in the same direction.

Setup	Tool	Peripheral milling	Face milling
	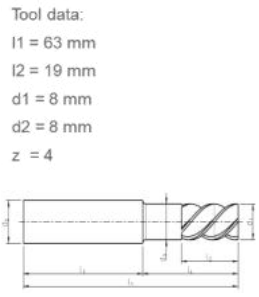	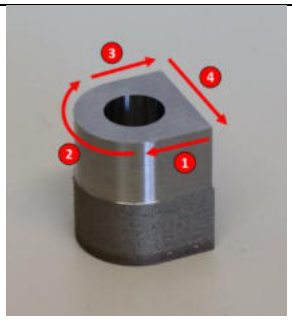	

Figure 5-24: experimental setup and used tools (left) and milling path for peripheral and face milling (right).

Main goals of the investigations were to identify process influences on the workpiece properties and optimum parameter sets for the functionalizing. Of special interest are the parameters of roughness and topography, cutting process conditions (force and moments, vibrations), sub-surface properties (microstructure) and workpiece hardness. The geometries developed within the project were used for additive manufacturing of the work pieces with different orientations and LPBF parameters sets (see also Figure

5-7). The direction of build-up was varied from 0° up to 90° (45° steps). The AM workpieces for the cutting test as well as the orientation of the work pieces are shown in Figure 5-25.

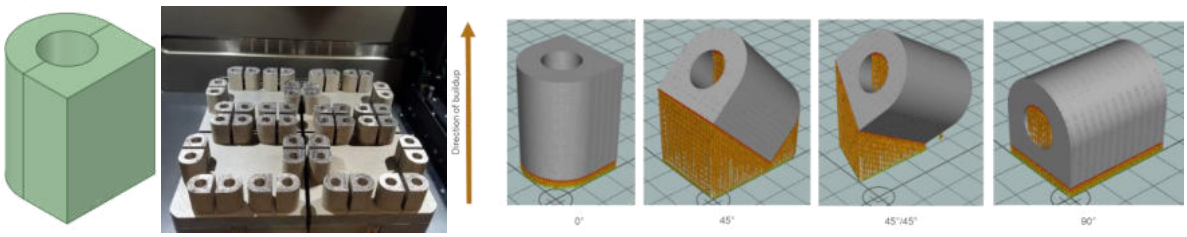

Figure 5-25: Used work pieces for cutting test in the AM chamber (left) and orientation of the work pieces (right).

During and after the milling process the roughness and the cutting forces were measured. It has been found that the roughness in particular is influenced by the processing parameters. Procedure for the roughness measurement are given in Figure 5-26. For the data acquisition of the roughness, the measuring device Alicona Infinite Focus SL was used (Figure 5-26, left). Profile and roughness as well as surface texture were measured by means of focus variation.

Measured surfaces and the measuring directions for peripheral and face milling are given in Figure 5-27. Depending on the process and the feed direction, different surface structures are formed. The direction of the measurement as well as of the feed is important to determine the influence of the LPBF process on the work piece properties.

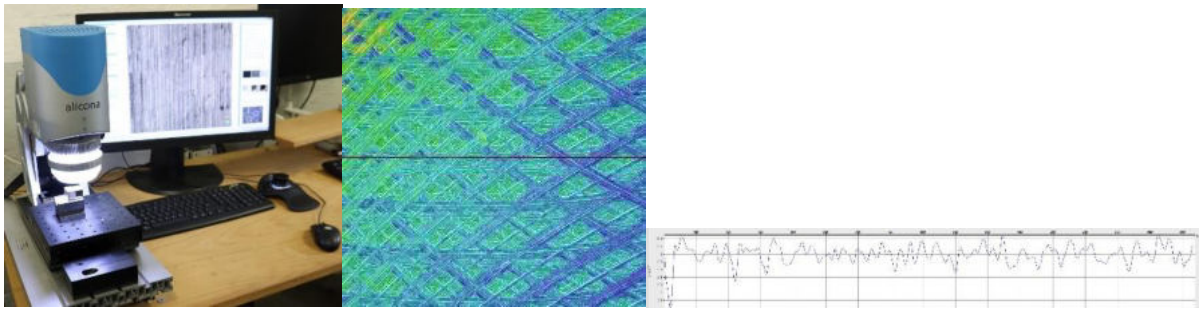

Figure 5-26 measuring device Alicona Infinite Focus SL (left) and example of measured area roughness and roughness profile (right).

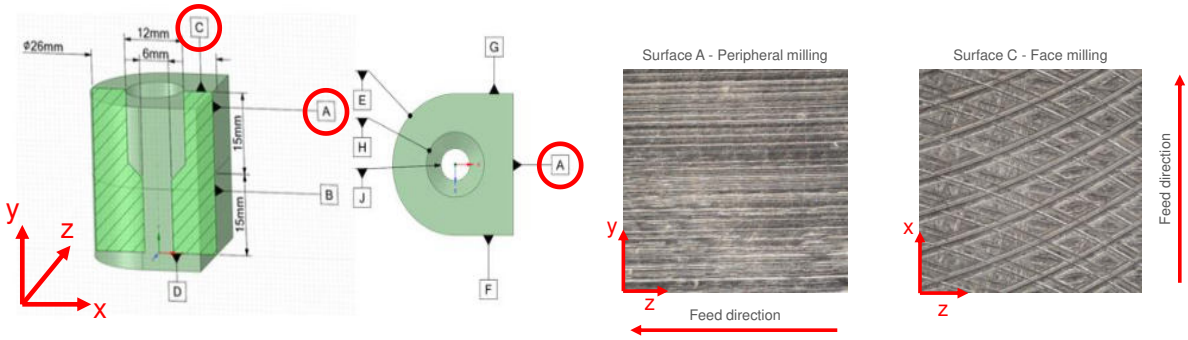

Figure 5-27: Surfaces and measuring directions.

For the following investigations of the relationships between workpiece properties and machine conditions different boundary conditions were used:

- Tested materials: 1.2709, AlSi10Mg, 1.4404 without heat treatment (Non-heat treated samples show a greater dependence on the LPBF parameters; see results of the material analysis)
- Functionalizing processes: Peripheral milling, Face Milling
- Buildup directions: 0° 45° 45/45°, 90° (with support structures if needed)
- Cutting with cooling lubricant

Milling of AM parts of the material 1.2709

Variation of the machining parameters - Peripheral milling

First investigations in peripheral milling were done to set optimized cutting conditions with effect on surface quality and low roughness. All of the milled parts additively manufactured in vertical (0° to the build-up direction) direction (see Figure 5-25, right, 0°). As relevant parameters for the first cutting tests in peripheral milling were used:

- Cutting speed v_c 80 – 240 m/min
- Tooth feed f_z 0.04 – 0.16 mm
- Radial depth of cut a_e 0.1 – 0.4 mm
- Axial depth of cut a_p 15 mm
- Ultrasonic amplitude γ 0 %

In Figures 5-28 and 5-29, the measured roughness after variation of f_z, v_c, a_e and a_p is shown for a measuring direction perpendicular to the feed direction and in the direction of feed.

The roughness R_z perpendicular to the direction of feed (Figure 5-28) show, that lower values of tooth feed f_z increases the resulting roughness. With higher radial depth of cut, the roughness can be reduced. In this case, a consistently high surface quality (lower roughness r_z) under variation of the cutting speed can be reached. Best results are achieve with a radial infeed of 0.4 mm and a tooth feed of 0.04 mm.

In comparison with roughness perpendicular to the feed direction, in feed direction (y-direction) the roughness show a higher surface quality (lower roughness, Figure 5-29). The results are comparable to the measurement results perpendicular to the feed direction.

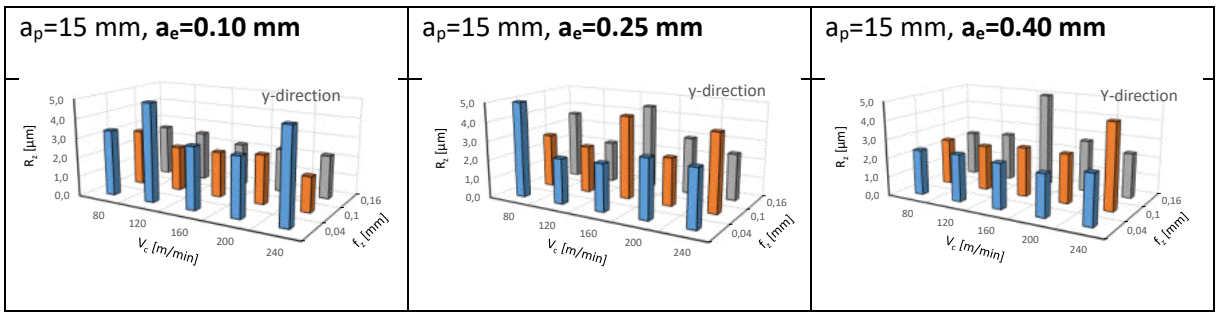

Figure 5-28: Surface roughness R_z in y-direction (perpendicular to feed direction) for different radial depth of cut a_e after peripheral milling.

a_p=15 mm, **a_e=0.10 mm**	a_p=15 mm, **a_e=0.25 mm**	a_p=15 mm, **a_e=0.40 mm**
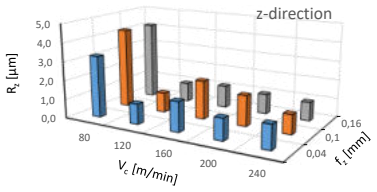	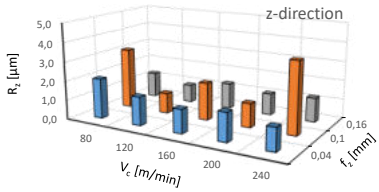	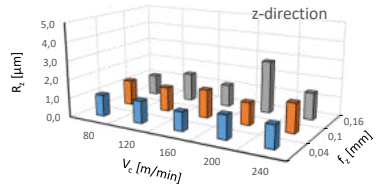

Figure 5-29: Surface roughness Rz in z-direction (in feed direction) for different radial depth of cut ae after peripheral milling.

Based on the measurements, for further systematic investigations of the influence of the SLM proves on the work piece properties, parameters were be defined. The best results (lowest roughness) can be achieved with a cutting speed v_c=80 m/min, tooth feed f_z=0.04 mm and radial depth of cut a_e=0.4 mm. These parameters were used in the next investigations.

Variation of the direction of buildup - Peripheral milling

To determine the influence of the build-up direction on the surface roughness after surface functionalizing with peripheral milling, the parameters determined in the previous tests were used. The direction of orientation of the work pieces were 0° (direction of the build-up) 45°, 45°/45° (diagonal) and 90° (perpendicular to the build-up) (see Figure 5-25).

The measured roughness after milling with the given parameter is presented in Figure 5-30. It can be seen, that in both measuring directions the roughness decreases with the increasing angle of orientation of the work piece to the build-up direction. Higher surface qualities in peripheral milling can reached when the build-up direction is not equal to the feed direction.

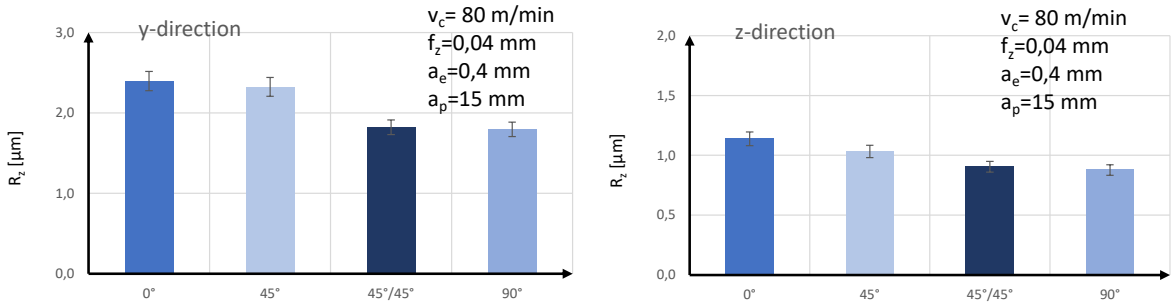

Figure 5-30: Roughness rz after peripheral milling for different orientations of the work-pieces during build-up within the LPBF process, left: Rz in perpendicular to the feed direction; right: Rz in feed direction.

Variation of the direction of buildup - Face milling

Start of the investigations in face milling were done analogous to the peripheral milling to set optimized cutting conditions with effect on surface quality and low roughness. All of the milled parts additively manufactured in vertical (0° to the build-up direction) direction (see Figure 5-25, right, 0°). As relevant parameters for the first cutting tests in peripheral milling were used:

- Cutting speed v_c 80 – 240 m/min
- Tooth feed f_z 0.04 – 0.16 mm
- Radial depth of cut a_e 2.5 mm

- Axial depth of cut a_p 0.1 – 0.4 mm
- Ultrasonic amplitude γ 0 %

In Figures 5-31 and 5-32, the measured roughness after variation of f_z, v_c, a_e and a_p is shown for a measuring direction perpendicular to the feed direction and in the direction of feed.

The roughness R_z perpendicular to the direction of feed (Figure 5-30) show not clear connections between cutting conditions and resulting roughness. For higher values of the axial depth of cut a_p or higher tooth feed rates f_z the roughness is slightly higher. A higher surface quality (lower roughness r_z) under variation of the cutting speed. Best results are achieve with a radial infeed of 0.25 mm and a tooth feed of 0.1 mm.

a_e=2.5 mm, **a_p=0.10 mm**	a_e=2.5 mm, **a_p=0.25 mm**	a_e=2.5 mm, **a_e=0.40 mm**
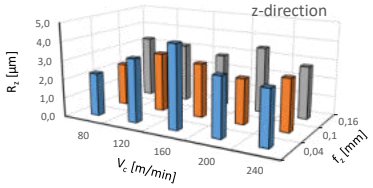	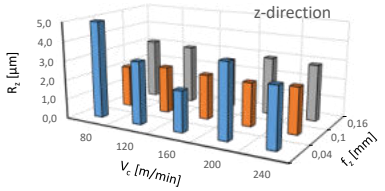	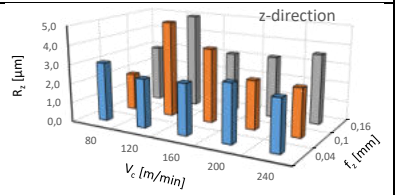

Figure 5-31: Surface roughness Rz in y-direction (perpendicular to feed direction) for different axial depth of cut ae after face milling.

In feed direction (y-direction), the results are comparable to the measurement results perpendicular to the feed direction (Figure 5-32). The best results (lowest roughness) can be achieved with a cutting speed v_c=80 m/min, tooth feed f_z=0.04 mm and axial depth of cut a_e=0.4 mm. Variation of the cutting speed has no clear effect on the surface roughness. The developed parameter used in the next investigations.

a_e=2.5 mm, **a_p=0.10 mm**	a_e=2.5 mm, **a_p=0.25 mm**	a_e=2.5 mm, **a_e=0.40 mm**
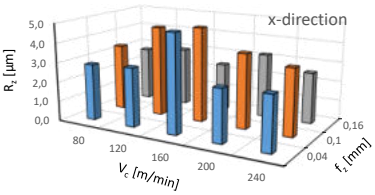	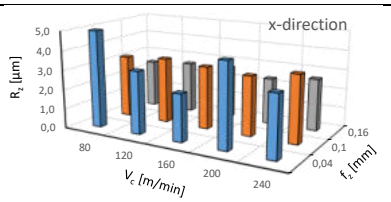	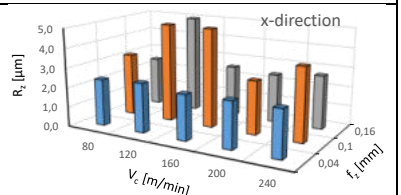

Figure 5-32: Surface roughness Rz in x-direction (in feed direction) for different radial depth of cut ae after face milling.

Variation of the direction of buildup - Face milling

To determine the influence of the build-up direction on the surface roughness after surface functionalizing with pface milling, the parameters determined in the previous tests were used. The direction of orientation of the work pieces were 0° (direction of the build-up) 45°, 45°/45° (diagonal) and 90° (perpendicular to the build-up) (see Figure 5-25).

The measured roughness after milling with the given parameter is presented in Figure 5-33. It can see, that in both measuring directions the roughness is higher, if feed direction equal to the build-up direction

as well as perpendicular to the build-up direction. For a good surface quality for face milling, the feed direction >0° und <90° to the build direction.

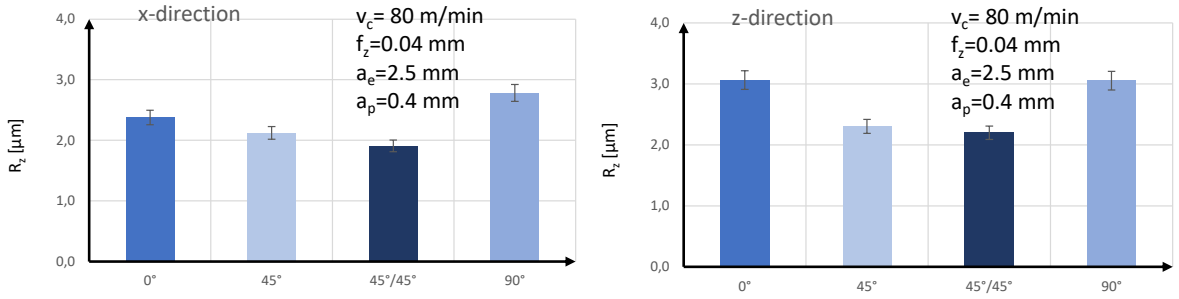

Figure 5-33: Roughness Rz after face milling for different orientations of the work-pieces during build-up within the LPBF process, left: Rz in feed direction; right: Rz perpendicular to the feed direction.

Milling of AM parts of the material 1.4404 and AlSi10Mg

The results for peripheral milling and face milling of the material 1.2709 use to test the transferability to the materials 14404 and AlSi10Mg. The material was milled without a heat treatment process after the additive manufacturing. Also different orientations of the work-pieces (0°, 90°) during build-up within the LPBF process of the material were used. The cutting conditions correspond to those of the previous investigations for peripheral and face milling:

- Peripheral milling: v_c= 80 m/min, f_z=0.04 mm, a_e=0.4 mm, a_p=15 mm
- Face milling: v_c= 80 m/min, f_z=0.04 mm, a_e=2.5 mm, a_p=0-4 mm

In Figure 5-34 the roughness r_z after peripheral milling of the materials AlSi10Mg, 1.2709 and 1.4404 with different orientations of the work-pieces during build-up within the LPBF process is presented. The results show, that a lower roughness can be reached, if the feed direction not equal the build-up direction of the work piece. The lowest roughness has the material 1.4404. With this material, there are also only small differences in the various build-up direction. This correlates with the mechanical properties of the material 1.4404 for the different build-up directions. The highest roughness as well the highest roughness differences between different build-up directions can be seen for the material AlSi10Mg.

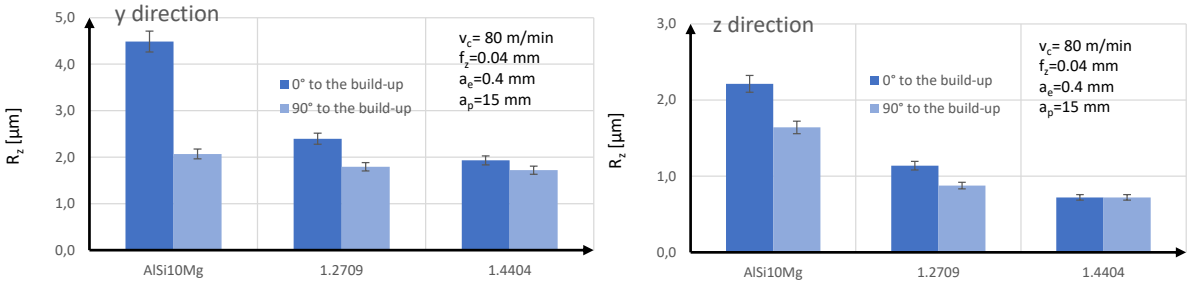

Figure 5-34: Roughness Rz after peripheral milling of the materials AlSi10Mg, 1.2709 and 1.4404 for different orientations of the work-pieces during build-up within the LPBF process, left: Rz perpendicular to the feed direction; right: Rz in feed direction.

In face milling (Figure 5-35), the differences in roughness in different build-up directions are smaller than in peripheral milling. The feed direction influences the component quality (roughness) only marginally. Components made of the material 1.4404 also have the lowest roughness during face milling, the highest roughness measured for the material 1.2709.

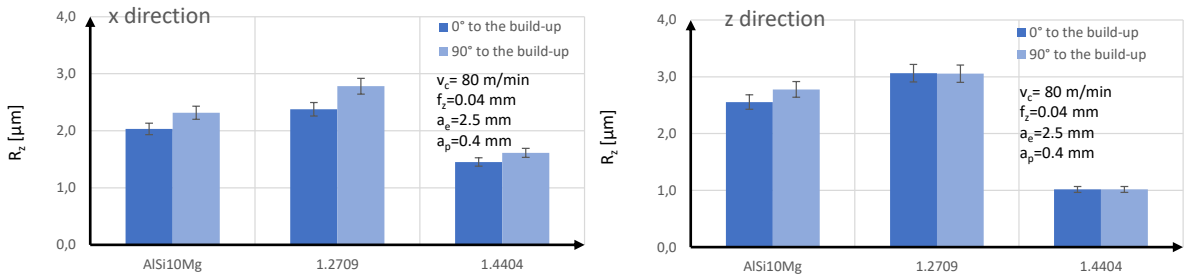

Figure 5-35: Roughness Rz after face milling of the materials AlSi10Mg, 1.2709 and 1.4404 for different orientations of the work-pieces during build-up within the LPBF process, left: Rz in feed direction; right: Rz perpendicular to the feed direction.

Conclusion of the results of the milling processes

The analysis of the ultrasonic assisted machining and especially in milling show that work piece properties and surface quality depends on cutting parameters as well as the LPBF conditions. Results of the variation of the machining parameters during machining of the material 1.2709 show that

- For peripheral milling, the best results were achieved with a higher feed and a low tooth feed rate.
- In face milling, different optimum parameters were determined due to the surface quality (lowest toughness) in and perpendicular to the feed direction.

After determination optimized cutting conditions, the influence of the build-up- direction on machining with peripheral and face milling were determined during cutting the materials 1.2709, 1.4404 and AlSi10Mg. The results show a small influence of the build-up direction on the surface quality for the material 1.2709 and a larger influence for the material AlSi10Mg. In detail for the variation of the direction of build-up it can concluded, that

- Cutting conditions for 1.2709, 1.4404 and AlSi10Mgare comparable
- Best surface quality can reached with the material 1.4404
- In peripheral milling, a higher surface quality can reached when the feed direction is not equal to the build-up direction.
- In face milling the surface quality improves when the feed direction is >0° und <90° to the build-up direction

The results show, that the direction of build-up has a measurable influence on the surface quality during milling. For the post processing of functional surfaces by means of milling, it is therefore advisable to take the direction of buildup into account. Machining should not carried out in the build-up direction of the additive manufactured components.

5.2.3 Surface functionalizing with PVD hard coating systems

Hard coating technology and heat treatment

Surface functionalizing of AM parts with PVD hard coatings can used for a further improvement of the surface e.g. high hardness, low friction. The motivation for investigations of PVD-hard coatings on AM parts is the analysis of the influence of LPBF conditions on the surface and subsurface properties and finally on the properties on the deposit PVD hard coatings. The objective is the analysis of the thermal

influence of the coating deposition on the additively manufactured components as well as the combination of surface functionalization, hard coating and heat treatment in a single process.

With consideration of the process chain for the complete additive-subtractive process chain (see Figure 5-1) for hard coating technology some additional process steps are taken into account (Figure 5-36). After the LPBF procedure and the remove of the work pieces from the build plate, additional process are necessary. To achieve a sufficient coating adhesion a defined surface quality (pre-treatment procedure) and surface hardness (heat treatment) are needed. To ensure good coating properties and, in particular, to remove contaminations from the LPBF and the pre-treatment steps, an intensive cleaning process is required. In the investigations, the material 1.2709 were used to generate the AM workpieces, the heat treatment / coating deposition conditions are based on a conventional heat treatment.

For the development of the hard coating technology and the heat treatment of the AM parts, different variants of pre-treatment and for the deposition and heat treatment were selected (Figure 5-36).

- Generation of different surface qualities before coating deposition by different mechanical pre-treatment processes (blasting, grinding, polishing)
- Heat treatment and coating deposition using different deposition temperatures and PVD coating systems (110 -550 °C)

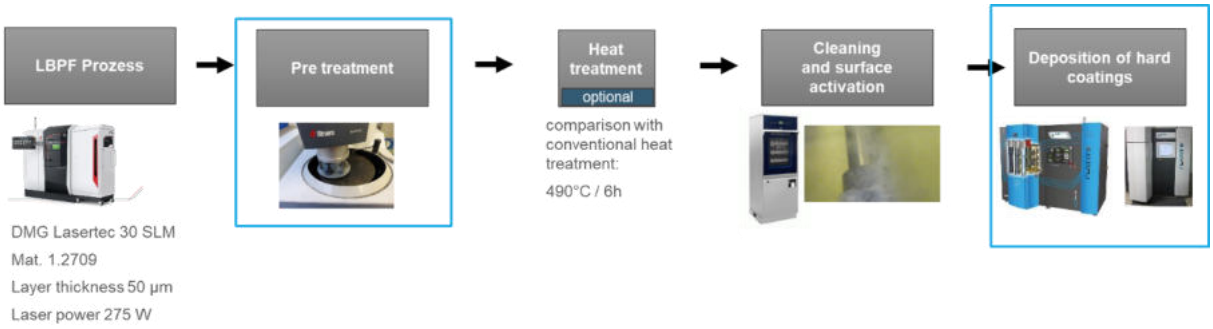

Figure 5-36: Modified process chain for PVD hard coating deposition on additively manufactured parts.

The pre-treatment procedures were used to determine their influence on the coatability of the AM work pieces (e.g adhesion, full coverage of the surface), different heat treatment / coating systems can have an significantly influence on the workpiece and coating properties (e.g. hardness, wear resistance, residual stresses). The hard coating process carried out using the PVD process on the commercial coating machines π^{211} and π^{411} from the company PLATIT. Relevant influencing factors are surface roughness and surface hardness after the additive process (before coating deposition), coating composition, coating structure and deposition temperature. Conditions and parameters for the hard coating technology and heat treatment according used machines, process temperatures, pre-treatment processes and relevant parameters are summarized in Table 5-8.

Machines for PVD deposition	Process temperatures	Pre-treatment processes	Analyzed parameters

 π^{211}  π^{411}	110°C 300°C 480°C 550°C	Without, Blasting, grinding, polishing	Composition and structure (REM Zeiss EVO MA-15, EDX) Hardness (DiaTestor 7521) Adhesion (Rockwell indentation, GFE) Micro hardness (Picodentor HM500) Wear coefficient (KaloMax NT)

Table 5-8: machines, process temperatures, pre-treatment processes and relevant parameters.

Hard coating / heat treatment procedure

In order to enable optimal coating development, the temperature profile of the classic heat treatment of the used material 1.2709 analyzed and then transferred to a PVD deposition process. The influence of the PVD deposition on the surface and component properties was determined by varying the deposition conditions.

Based on the usually hardening procedure for the used material 1.2709 (hardening temperature 490°C, holding time 6 h, in Air), PVD-hard coatings with different deposition temperatures developed and analyzed with regard to various properties. The selection of the coatings also made under the aspect of good wear protection. In Table 5-9, the different coating systems used in the investigations with their expected mechanical properties summarized. Here the deposition temperature varied between 100 and 550°C. The lowest deposition temperature of 110°C shows the coating ta-C (tetrahedral amorphous carbon), which is a diamond like carbon coating with a very high hardness and abrasion resistance. The coating TiCN-LT is a good combination of wear resistance and reduced friction at a deposition temperature of 300°C. The coating nACo2, deposited at a temperature of 480°C, consist nanocomposite structures of TiAlN in an amorphous matrix. Due to these structures, the coating show a high hardness even at higher temperatures. AlCrON coatings (deposition temperature 550°C) contain thermally stable oxynitride structures. All coatings expected to have a high hardness and high wear resistance.

coating	deposition temperature	Hardness	Application
ta-C	110°C	65 GPa	High wear resistance, reduced friction
TiCN-LT	300°C	34 GPa	Wear resistance, reduced friction
nACo2	480°C	41 GPa	Wear resistance at high temperatures
AlCrON	550°C	39 GPa	Wear resistance at high temperatures
HT	490°C		Heat treatment temperature for 1.2709

Table 5-9: Used PVD coatings for hard coating technology and heat treatment.

Based on the used coating systems with the different deposition temperatures, the deposition procedure and the temperature profile during coating deposition were determined.

Figure 5-37 show the developed temperature profile of the different coating systems / deposition temperatures and a comparison with the conventional heat treatment. The nACo2 layer with a deposition temperature of 480°C shows the best agreement with conventional heat treatment in terms of temperature profile.

Based on the boundary conditions of the used coating machines (e.g. deposition is in vacuum), the heating and cooling rates between the conventional heat treatment and the hard coatings are different. For conventional processes heating and cooling rates in the range of 2 K/min, for PVD-coatings the rates are higher between 4 and 7 K/min. No significant influence of the heating and cooling raters on the component properties expected, since the hardness mainly influenced by the holding time.

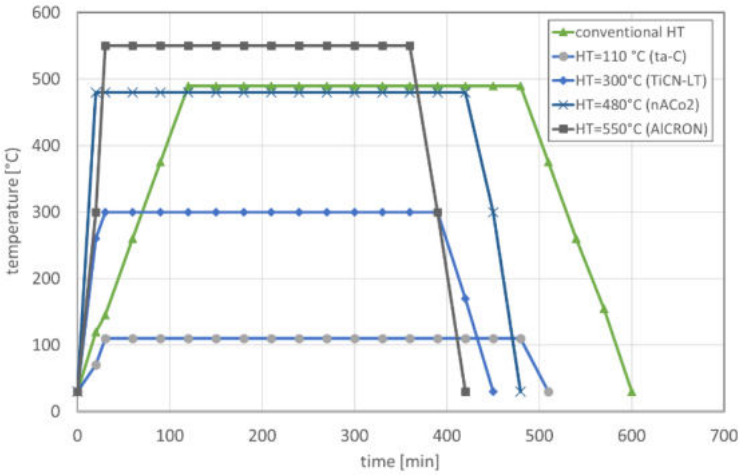

Figure 5-37: Temperature profiles of the developed PVD coatings and comparison to conventional heat treatment.

The different coatings with the temperature profile were deposit on additive manufactured test probes (geometry: see Figure 5-7, right, Chapter 5.2.1.1). The resulting structure after calo grinding and the coating sequence are given in Figure 5-38. The deposited coating consist of an adhesive layer to achieve a high adhesion, a core layer that acts as a support and a top layer as the essential functional layer. In the case of the TiCN and ta-C coatings, top-layer and core layer combined in one structure. In Figure 5-38 it can be seen as well, that with the lower deposition temperatures (110°C and 300°C) the surface show a slightly rougher and inhomogeneous surface. This can partly indicate an insufficient structural change in the material for these deposition temperatures.

Temp.	**550°C**	**480°C**	**300°C**	**110°C**
Coating	**AlCrON**	**nACo2**	**TiCN-LT**	**Ta-C**
Adhesion	CrN	TiN	TiN	Cr-C
Core	AlCrN	TiAlN	TiCN	C
Top	AlCrON (10%O)	nc-TiAlN / α-Si3N4	TiCN	C

Structure	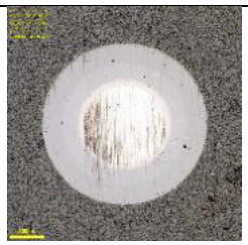	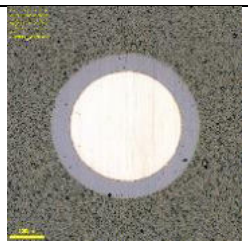	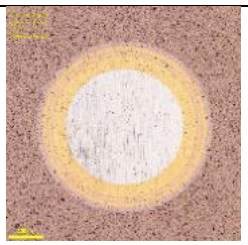	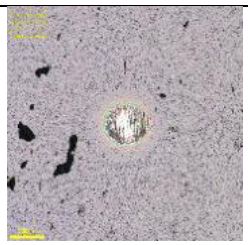

Figure 5-38: Coating sequence and coating structure of the on AM workpieces of 1.2709.

Influence of the pre-treatment procedure

In the next step, the influence of the mechanical post-treatment of the additive manufacturing / pre-treatment before the coating on the coating properties and in particular the roughness was analyzed. Of interest here were the guarantee of coating adhesion and a complete surface coating for uniform coating properties.

For investigations on the pre-treatment procedures before coating, various methods were used after additive manufacturing and the separation of the manufactured component from the build-plate in order to gradually reduce the roughness. The pre-treatment processes used to remove remains of the support structures, to remove surface imperfections and to reduce the roughness are given more in detail in Table 5-10. For the different pre-treatment processes, additive manufactured probes given in Figure 5-7, right (see Chapter 5.2.1.1) were used as well.

process	machine	parameter	Expected effects
Without	-	-	Shortened process chain
Blasting	HGH 750 Duo	Al2O3, p = 3 bar, t=1 min	Remove of support structures
Lapping	Okamoto AeroLap	MultiCone, d=150 mm, p=2 bar, t=1,5 min	Smoothing of surface imperfections
Grinding	Tegramin-20	SiC-Paper, diamond suspension 9+3 µm, p=30 N, t=7,5 min	Reduced roughness
Polishing	Tegramin-20	Polishing cloth, diamond suspension 1 µm , p=30 N, t=12,5 min	Lowest roughness, best coating adhesion

Table 5-10: Pre-treatment processes and parameters.

After the additive process and before coating deposition, different samples were treated with the conditions given in Table 10. The resulting initial roughness R_a and R_z of the surface is given in Figure 5-39. It can be seen, that under the given boundary conditions, blasting and lapping does not lead to a significant reduction in roughness compared to the initial state. A significant reduction of roughness can

reached only with grinding and polishing. Sufficient coating properties expected only with grinding / polishing.

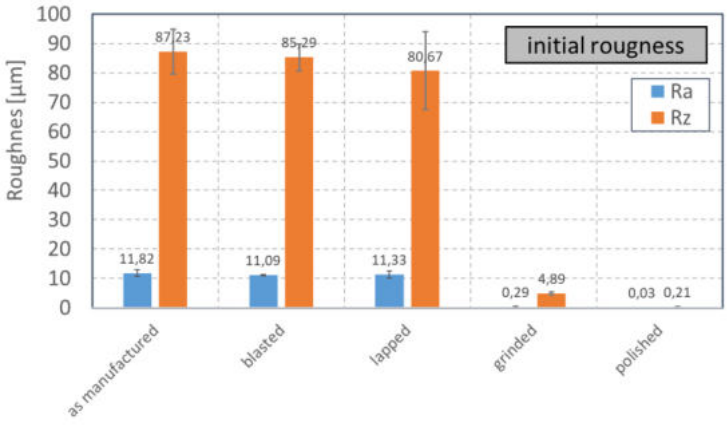

Figure 5-39: Initial roughness before coating deposition after different pre-treatment processes.

The roughness after deposition is shown in Figure 5-40. For coatings on blasted, lapped and as manufactured surfaces (Figure 5-40, left), PVD-coatings have no significant influence of the work piece roughness. Also there are large fluctuations in the roughness values. Furthermore, for these surfaces with the higher roughness there is also poorer coverage and inhomogeneous coating thickness distributions. These surfaces with the higher roughness therefore not considered further in the investigations in the project.

Coating deposition on surfaces with a lower initial roughness (Figure 5-40, right), lead to an increase of the roughness on polished and a small decrease on grinded workpieces. The reduction in roughness due to the coating on grinded surfaces is remarkable. This can possibly explained by a leveling of pores.

Due to the lower roughness values and the smaller fluctuations in the roughness, for the next investigations AM workpieces with a polished surface used.

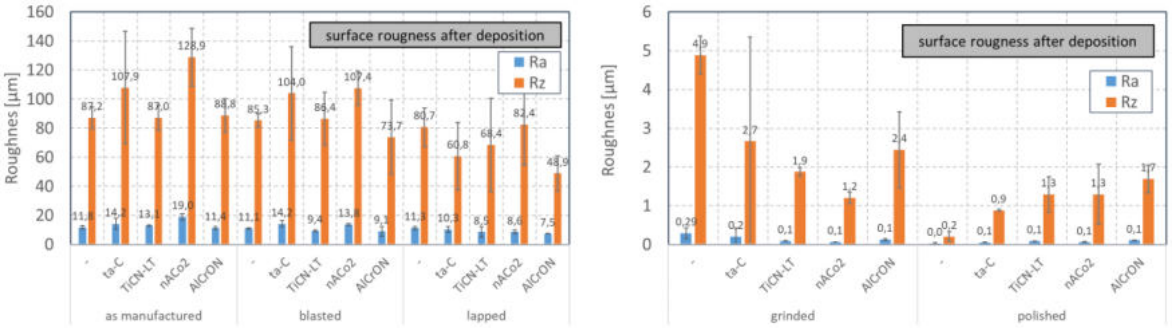

Figure 5-40: Roughness after coating deposition on different pre-treated workpieces; left: blasted and lapped, right: grinded and polished.

Optimization of coating technology

During deposition of the different PVD-coatings with the different deposition temperatures between 110 and 550 °C the resulting temperature profile was recorded and evaluated. It can see in Figure 5-41 that the real temperature profile differs from the theoretical temperature profile. In the real coating process, the holding time at the relevant temperatures are shorter than expected. Furthermore, short passages

of cooling steps can be observed by a decrease in the process temperature. Also the temperature for the coating TiCN-LT is a higher than 300°C.

To optimize the deposition process and to adapt the temperature profile to the real heat treatment process, deposition temperatures and deposition times were modified as well as heating and cooling rates. The optimization of the coating process was also carried out taking into account the adhesion of the coating, by pre-treatment and slightly modified adhesion layers.

For the adjustment of the deposition process temperatures, longer times for lower deposition temperatures (110°C, 300°C) and shorter time for higher deposition temperature (550°C) were set. The resulting temperature profile after deposition is shown in Figure 5-41, right. The comparison of the different temperature profiles shows that the temperature of the nACo2 coating (deposition temperature 480°C) is comparable with conventional heat treatment regarding temperatures, holding time and cooling rate.

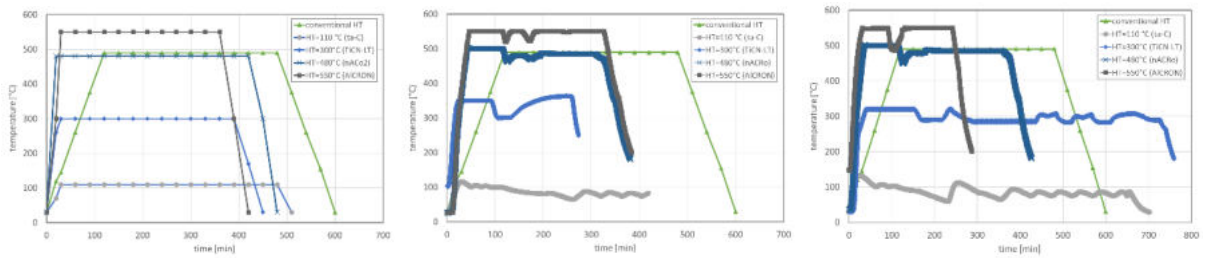

Figure 5-41: theoretical temperature profile (left), measured temperature profile (middle) and optimized temperature profile (right) during deposition of different PVD coatings on AM 1.2709.

According to the different deposit coatings and the process and coating optimization, the different used variants as well as the holding times on maximal temperature and the resulting coating thickness given in Table 5-11. For the coatings ta-C (110°C) and TiCN-LT the longer holding time increases the coating thickness to 1.3µm (ta-C) and 4.6 µm (TiCN-LT). The coating nACo2 shows the coating thickness usually used (2.7 µm). The AlCrON coating has a higher coating thickness due to the larger part of formed oxides within the coating during the deposition process.

Coating	**Depositon Temperature**	**Step 1**		**Step 2: Optimization**	
		Holding time at T_{max}	Coating thickness	Holding time at T_{max}	Coating thickness
ta-C	110°C	400 min	0.7 µm	630 min	1.3 µm
TiCN-LT	300°C	220 min	3.9 µm	690 min	4.6 µm
nACo2	480°C	270 min	2.5 µm	340 min	2.7 µm
AlCrON	550°C	280 min	2.6 µm	210 min	5.5 µm

HT	490°C	360 min			

Table 5-11: Holding time and coating thickness for different deposition processes.

For the different coatings and optimization processes, the coating adhesion was evaluated as well. Important for the applicability of the coating is a very good coating adhesion. The pre-treatment, the adhesion layer system, the deposition temperature as well as the substrate properties (e.g. hardness) influence the adhesion strength. Therefore, the influence of various parameters such as the coating temperature, the coating thickness, but also the build-up direction and the hardness of the additively manufactured workpieces on the adhesion was analyzed. It was also examined if an improvement in coating adhesion could be achieved by optimizing the coating process. The coating adhesion of additive manufactured and coated parts were measured by indentation test with a Rockwell indenter (HRA). According to the resulting crack network, the adhesion class were determined based on the DIN 4856.

Figure 5-42 shows examples of the crack network after Rockwell indentation test for the different coatings and the different process steps (Step 1, Step 2 optimization) and a comparison with usually used HSS steel (1.3343). It can see that on the AM steel 1.2709 without heat treatment there are a larger crack network compared to a HSS steel. The ta-C coating on the AM 1.2709 shows the lowest adhesive strength with very large coating delamination. After the optimization process (step 2) the crack network on AM 1.2709 was reduced, the coating adhesion was increased. The best adhesion, which could be comparable with common used HSS, have the coatings AlCrON and TiCN-LT.

The resulting adhesion class according to the DIN 4856 for the different coating, heat treatment before deposition (HT) and different orientations of the workpieces during the AM process (vertical / 0° and horizontal / 90° to the build-up direction) is summarized in Figure 5-43. An adhesion class 1 and 2 is equivalent to a good coating adhesion, an adhesion class of 5 and 6 are not allowed due to large crack and coating spallation. In comparison with coatings on conventionally produced high speed steel (HSS) material 1.3433, which is a common substrate material for PVD coatings, on the AM material 1.2709 the coatings show a lower coating adhesion (higher adhesion class).

For the ta-C coating with the lowest deposition temperature, large-scale flakes and insufficient coating adhesion are visible. The reason for this are the high internal stresses of the coating due to the extremely high coating hardness. All other heat treatments / coatings show adequate adhesion, the coating adhesion is enhanced with increasing deposition temperature. In addition, it can be seen that the orientation of the components as well as a heat treatment before deposition (HT) to increase the substrate hardness only have a small influence on the adhesive strength.

Temp.	**550°C**	**480°C**	**300°C**	**110°C**
Coating	**AlCrON**	**nACo2**	**TiCN-LT**	**Ta-C**
Substrate	1.3343 / Reference			

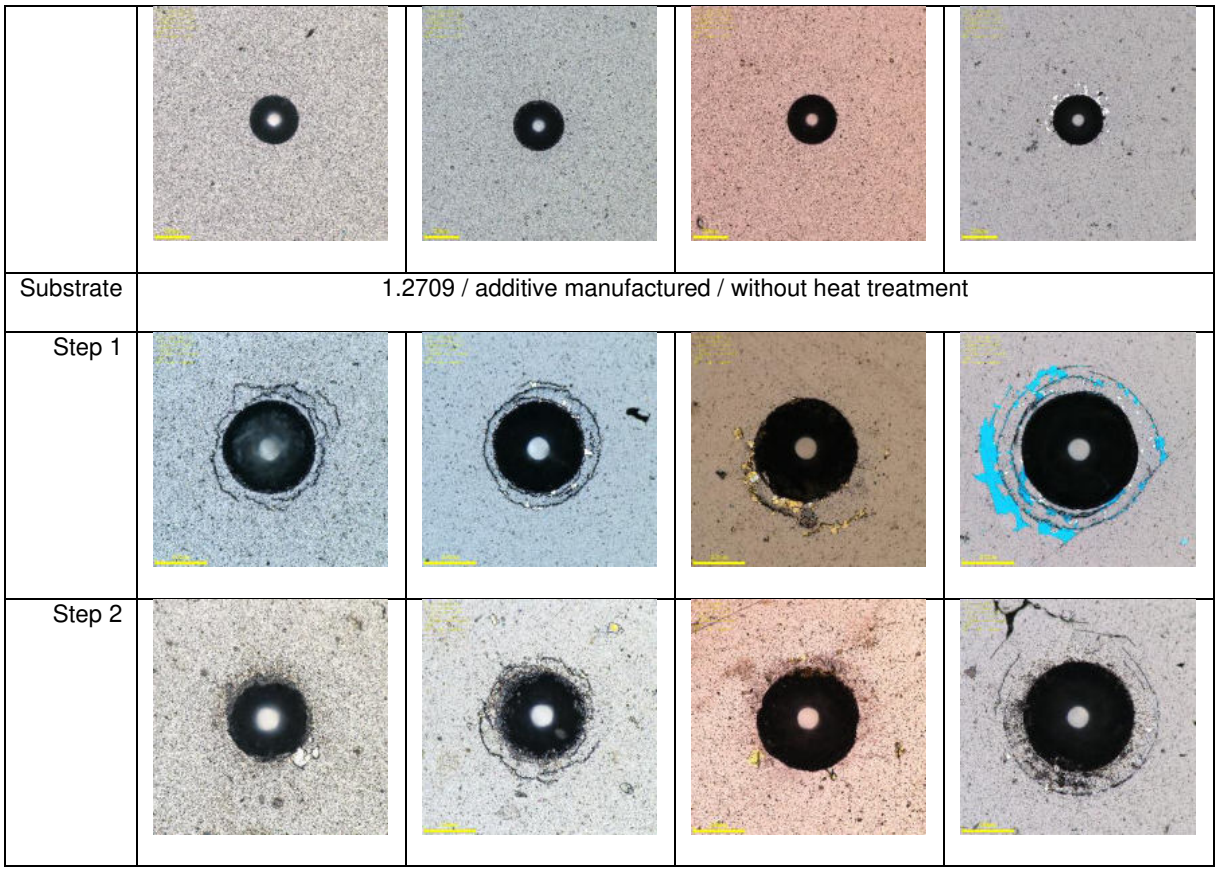

Figure 5-42: Crack network after rockwell indentation test for the different coatings and process steps and a comparison with usually used HSS steel (1.3343).

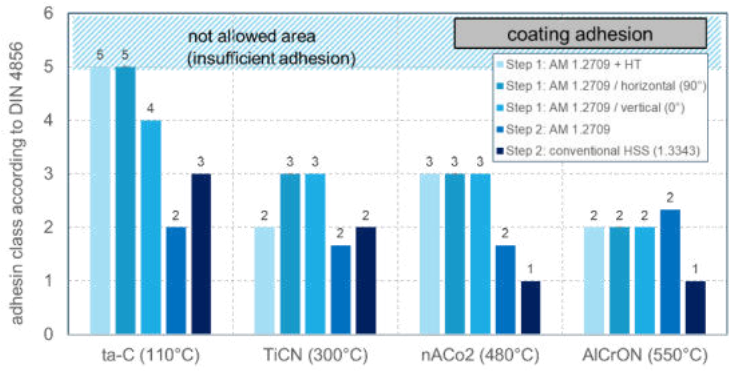

Figure 5-43: Mean value of adhesion class for the different coatings and steps, heat treatment (HT) and orientations of the work-pieces (0° / 90°).

With optimized deposition procedure with optimized temperature profile in step 2, the coating adhesion was increased. The adhesion of the coatings on additively manufactured parts is comparable with commonly used substrates.

Influence of hard coating on work piece properties

The results of the optimization of the coating technology show, that the temperature profile during deposition correspond to the temperature profile of heat treatment / hardening of the in additive manufacturing used material 1.2709. As a result, the heat treatment influences the mechanical and structural properties of the additively manufactured workpieces. Microstructural analyzes have shown that the

PVD coating is suitable as a simultaneous heat treatment to set a structure similar to conventional heat treatment for the material 1.2709.

Figures 5-44 and 5-45 shows the microstructure in an etched cross section of different heat-treated / coated material in different magnifications for the different orientations of the workpieces during the AM process (vertical / 0° and horizontal / 90° to the build-up direction). Etching was done with 3% nital solution. In Figure 5-45 the cross section with a magnification x250 shows, that for lower deposition temperature and without a heat treatment, the microstructure is similar. The layer structure of single additively manufactured layers are also visible. For this temperature profiles, differences between vertical and horizontal build direction are visible. With higher deposition temperatures, the microstructure in the substrate of coated samples is similar to the conventional heat treatment, differences between horizontal and vertical build-up reduced.

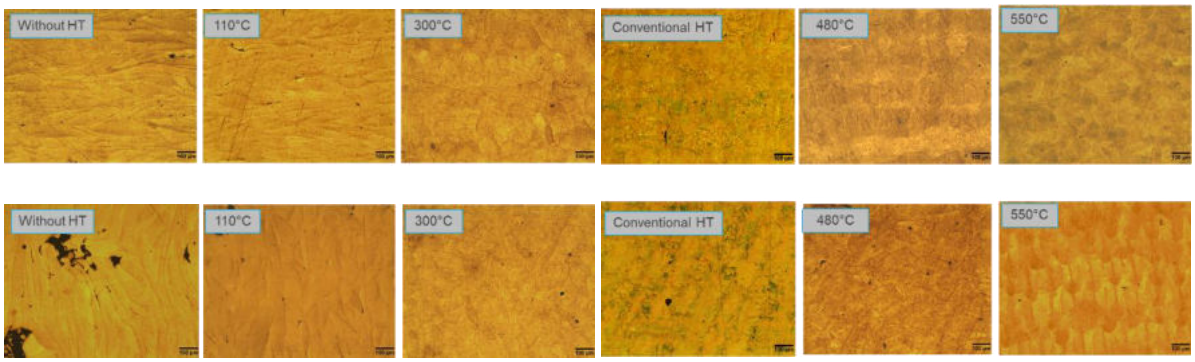

Figure 5-44: microstructure in an etched cross section of different heat-treated / coated material (magn. x50) upper line: horizontal orientation (90°), lower line vertical orientation (0°).

The martensitic microstructure is shown in more detail with higher magnification in Figure 5-46 for different layers and deposition temperatures. Due to the different coating temperatures, the segregation of intermetallic phases varies in strength and thus an increase in hardness. The segregation become coarser with higher coating temperatures. There are no differences between the horizontal and vertical construction direction of the additively manufactured components.

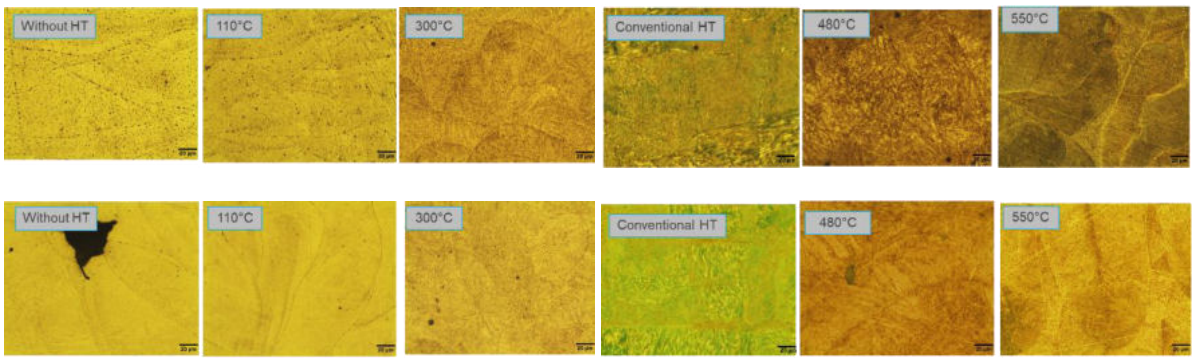

Figure 5-45: detailed microstructure / martensitic structure in an etched cross section of different heat-treated / coated material (magn. x250) upper line: horizontal orientation (90°), lower line vertical orientation (0°).

As result of the microstructural analysis, it can be prove that coated samples with higher deposition temperature show a similar microstructure as conventionally heat-treated samples. With regard to the

structure of the additively manufactured work pieces, the PVD coating technology can used as a heat treatment process.

A further important aspect for of the heat treatment is the hardening of the workpiece. With a conventional heat treatment at 490°/6h at air, the hardness of 1.2709 can increased to from 350 HV10 to about 540 HV10.

As result of various investigations, it was found that the temperature during the deposition is mostly relevant for the hardness of the additively manufactured components with the PVD coating. The hardness of the components of the different coatings and heat treatment variants are compared in Figure 5-46. Small differences between different build-up-orientations are visible for workpieces without a heat treatment and for low coating deposition temperatures (110°C, 300°C). For a conventional heat treatment as well as for higher temperatures during coating deposition the build-up direction has no influence on the workpiece hardness.

Optimization of the temperature profile during deposition in step 2 has a low effect on the hardness, except the coating TiCN-LT. Here the reduced deposition temperature form 340°C to 300°C (see also Figure 5-41) lead to a reduced hardness. Highest hardness reached for coating nACo2 with deposition temperature 490°C (nearly conventional HT). Here the hardness is comparable to conventional heat treatment. The build-up direction has no influence on the component hardness.

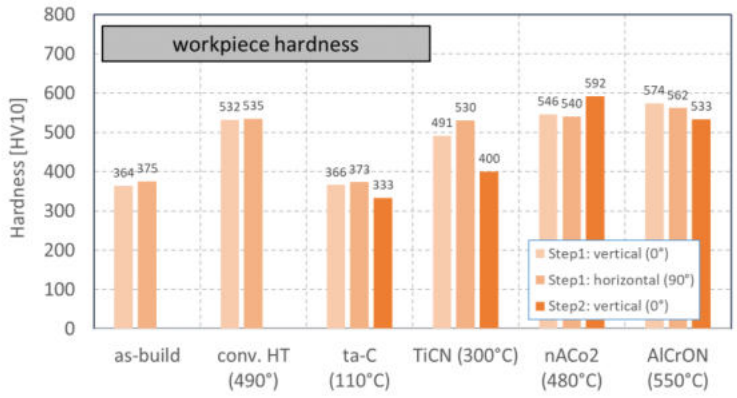

Figure 5-46: Hardness of the different coatings and steps, heat treatment (HT) and orientations of the workpieces (0° / 90°).

The results of the structural analyzes and the component hardness confirm that the PVD hard coating with a deposition temperature of 480°C with a nanocomposite coating (nACo2) can be used for heat treatment of additively manufactured parts of the material 1.2709.

Influence of hard coating on surface and coating properties

Beside the workpiece properties, the hard coating has influence of the surface properties, particularly the mechanical properties. Of special interest are the coating hardness and the wear resistance of the surface to improve the wear behavior of the additively manufactured parts. In the following investigations, the parameters coating thickness, surface roughness, coating hardness and elasticity as well wear rate as well as their correlation with the boundary conditions in coating and additive manufacturing processes were determined.

Roughness after the deposition with optimized parameters can be seen in Figure 5-47. The different PVD-coatings have no significant influence of the work piece roughness. With deposition the different coatings on a polished AM substrate of the material 1.2709, the roughness was increased (Ra: from 0.03µm to about 0.2µm, Rz: from 0.2 µm to about 2.7µm, Rpk from 0,02 mm to 0.4 µm). Due to the higher amount of droplets for the AlCrON and insufficient adhesion (coating delamination) for ta-C, the roughness for these coatings as well as the roughness variations higher compared to the other coatings.

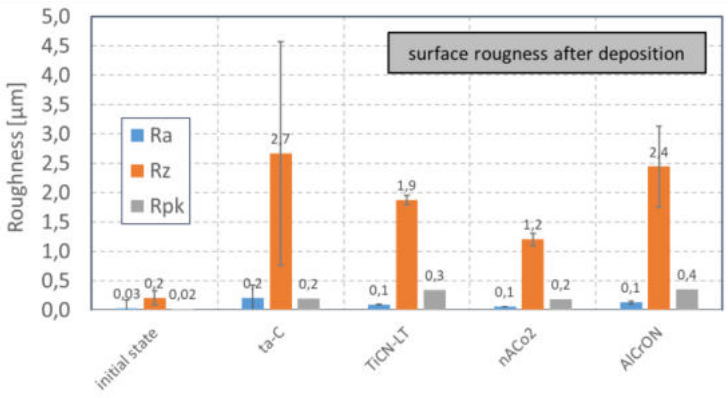

Figure 5-47: Surface / coating roughness of the AM work pieces with different heat-treatments / coatings.

The results for the coating thickness of the different coatings is given in Figure 5-48. In the first step, the coating thickness is in the range of about 0.8 µm (ta-C) and 4.0 mm (TiCN. With process optimization with an adapted temperature profile (step 2), the thickness was increased for all coatings. The higher coating thickness allows compensating small surface defects. The highest thickness shows the coating AlCrON. No or small differences in coating thickness can detected between different orientation to the build-up directions, different heat treatments and substrate materials.

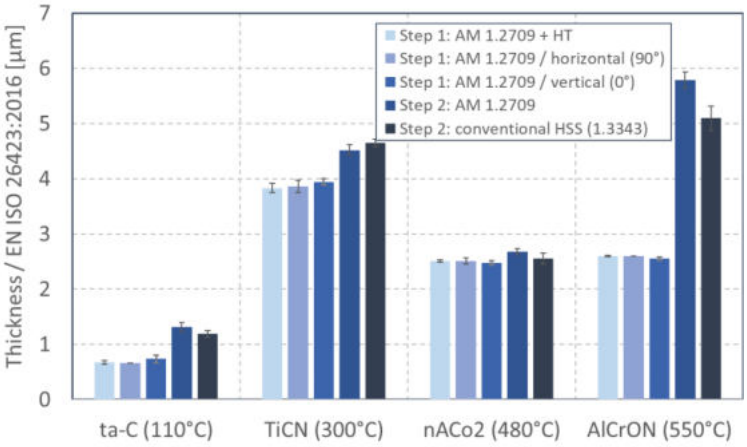

Figure 5-48: Coating thickness of the AM work pieces with different heat-treatments / coatings in different build-up directions (0° / 90°).

Elasticity of the PVD coatings can estimated based on the indentation modulus during hardness measurement. Figure 5-49 gives the result for the indentation elasticity EIT for the different coatings. The highest elasticity (highest stiffness) were measured for the for ta-C coating. For the other coatings, the elasticity is lower and in a similar range. As well as the results for the coating thickness, no or small

differences in coating elasticity can detected between different orientation to the build-up directions, different heat treatments and substrate materials. Furthermore coating elasticity is comparable to coatings on conventional substrates.

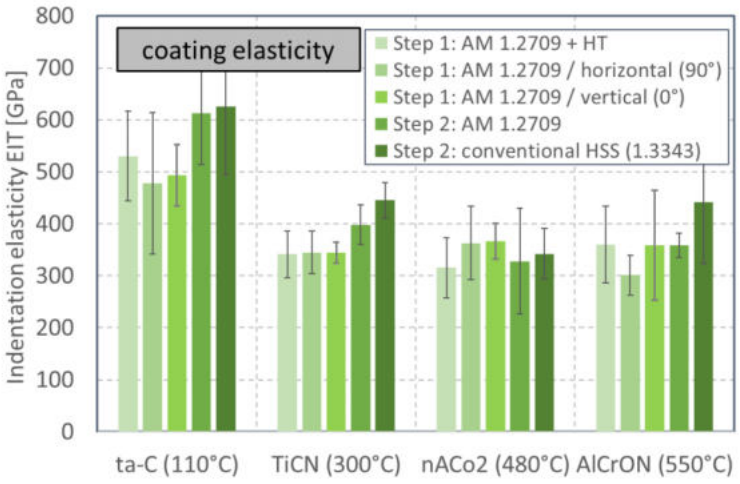

Figure 5-49: Coating elasticity (indentation modulus) of the AM work pieces with different heat-treatments / coatings in different build-up directions (0° / 90°).

The hardness of the coatings with different deposition temperatures is shown in Figure 5-50. For the same coating system, there are only small variations with respect to the build-up direction and a previous heat treatment. The highest hardness of about 60-80 GPa shows the ta-C coating. The strong variations in the hardness are due to the poor coating adhesion. The coating hardness for the ta-C coating can be increased by conventional heat treatment before coating deposition, because of the better support due to the higher substrate hardness. All other coatings show significantly lower coating hardness between 20 and 30 GPa. After optimization of the temperature profile of the coating deposition, the hardness of coatings on AM workpieces can compared to hard coatings on conventional base material.

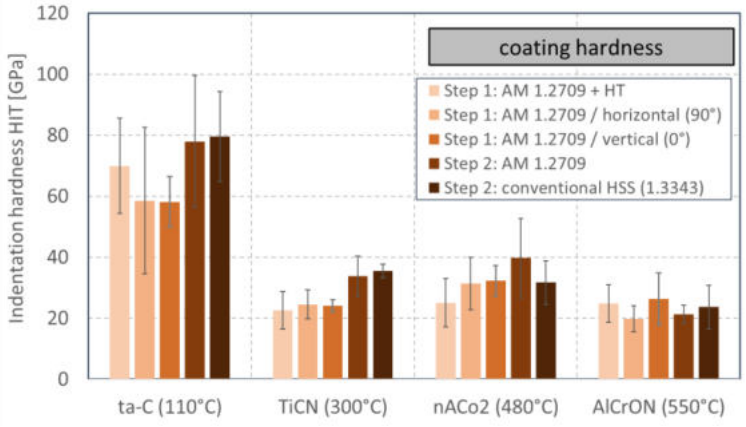

Figure 5-50: Coating hardness (indentation hardness) of the AM work pieces with different heat-treatments / coatings in different build-up directions (0° / 90°).

The wear resistance to abrasive wear is shown in Figure 5-51. Compared to an uncoated, additively manufactured component, all coatings reduce the wear rate (increase the wear resistance). Wear rates on AM parts comparable to usual used substrates (HSS) The results show, that the ta-C coating can strongly reduce the abrasive wear. As well as it can be seen, that the build-up direction or a previous

heat treatment has only a small influence on the wear rate. The results show that the coating nACo2 with an deposition temperature of 480°C, which correspond to the heat treatment of 1.2709, can used to improve wear resistivity of AM parts of the material 1.2709.

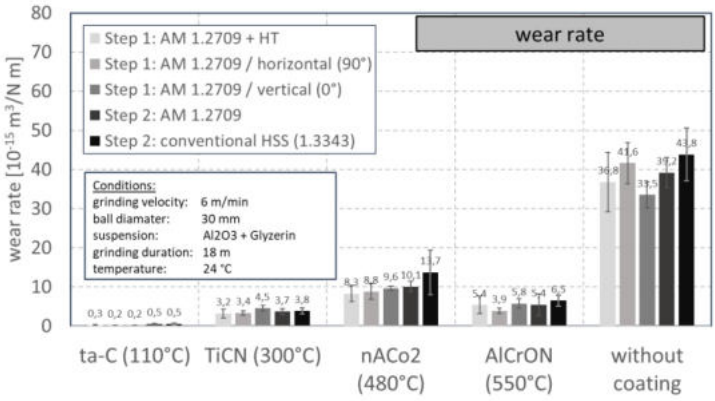

Figure 5-51: Surface wear resistance (wear rate) of the AM work pieces with different heat-treatments / coatings in different build-up directions (0° / 90°).

Conclusion hard coating technology

The deposition of PVD coatings on additively manufactured parts is possible by a defined pre-treatment procedure and hard coatings with a special temperature profile during the coating deposition. The pre-treatment before deposition is necessary to reduce roughness after the AM process. The roughness Ra should be less than 0.2µm and Rz less than 3µm. With such an pre-treatment before deposition, a good coating adhesion is achievable. Furthermore, the coatings have no significant influence on surface roughness after deposition. The development and deposition of different coatings with different wear resistances on AM substrates of the material 1.2709 show the following results

- The coating properties are comparable to hard coatings on conventional produced substrates
- No significant differences in coating properties by different build-up directions, heat treatments and substrate materials
- PVD hard coating can use for a significant increase in wear resistance and surface hardness

To use the PVD deposition technology as a heat treatment process it is necessary to reach the conventional hardening temperature profile for the used material 1.2709. With a deposition temperature during the hard coating process of about 480-490°C (nanocomposite coating nACo2):

- A substrate hardness of about 590HV10 can be reached, which correspond to the hardness of conventionally heat treated material 1.2709 for a PVD coating with a deposition temperature of 490°C
- The microstructure of the material 1.2709 show a similar microstructure as conventionally heat-treated samples
- The build-up direction of the workpieces during the AM process has no influence on the component hardness and microstructure after coating deposition / heat treatment

It was show, that the PVD coating can used for heat treatment and as surface functionalization to improve wear resistance of additively manufactured parts of the material 1.2709. The properties that can achieved are comparable to conventional heat treatment and coatings on conventionally manufactured components.

5.3 Summary

The aim of the project was to determine the relationships between process parameters and component properties and to determine process parameters for specific modification of component properties when manufacturing additively manufactured components. Here the entire additive-subtractive manufacturing (ASM) process chain must be take into account.

At the beginning of the project, the main priorities were worked out in the project and industrial consortium of the entire Ad-Proc-Add project. The ASM process chain and different additive and subtractive processes was analyzed were taken into account by the research institutes. The GFE Schmalkalden was concerned with the following research tasks.

- Use of the maraging steel 1.2709 with the laser powder bed fusion (LPBF) method
- Analysis of the influence of additive manufacturing on component properties
- Surface functionalization by milling processes
- Surface finishing with PVD hard coating

Based on the research topics, a modified ASM process chain with considered process steps was developed. The relevant steps for workpiece and process analysis are marked in Figure 5-52 in the specific ASM process chain. The process chain was modified with regard to the LBPF parameters, the build-up direction of the additively manufactured components, the heat treatment, the machining parameters of functionalizing by milling and the deposition conditions of PVD coatings.

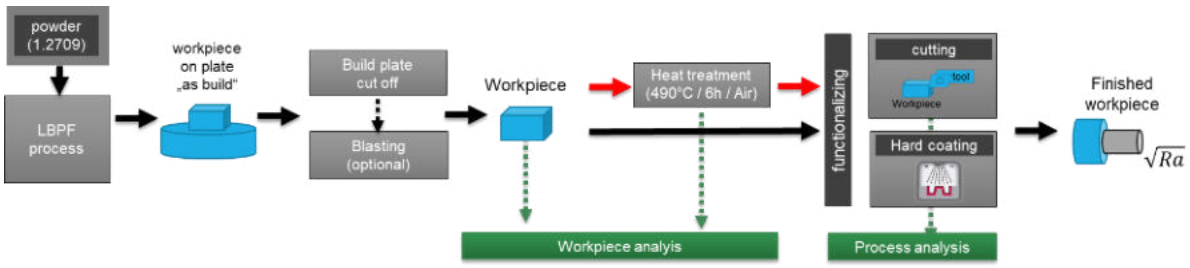

Figure 5-52: Specific process chain for surface functionalizing by milling processes and hard coating technology.

Exemplary results for the influence of the LPBF conditions on component properties is shown in Figure 5-53. It has been shown that both the direction of build-up and the heat treatment have an influence on hardness and impact strength for various additive processes (WAAM, LPBF) and different materials (1.2709, Alsi10Mg, TiAl6V4, G423M213S). In particular for the very often used material 1.2709 it could be shown that

- using without heat treatment the hardness and notched impact strength is lower for horizontal work-piece direction
- to achieve a high hardness and a high tensile strength, a heat treatment is necessary.

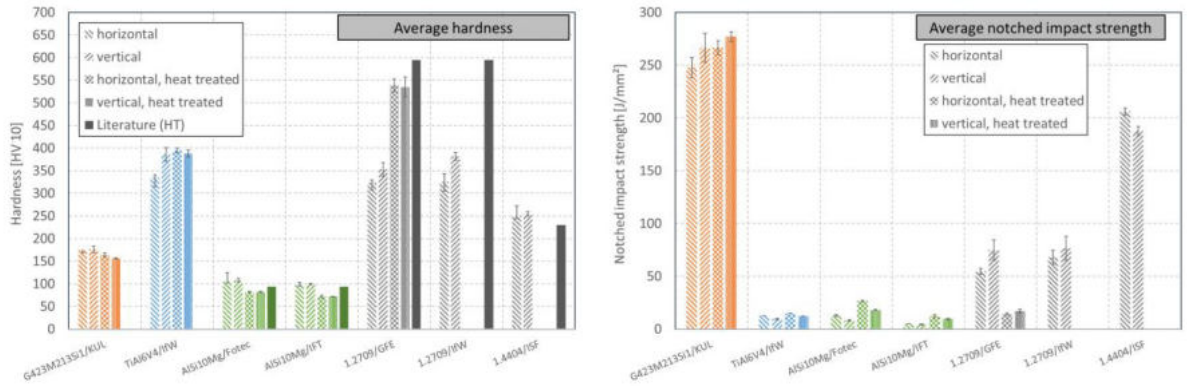

Figure 5-53: Hardness (left) and notched impact strength (right) of different AM materials, with and without heat treatment, different orientations to the build-up direction.

The analysis of the ultrasonic assisted machining and especially in milling show that work piece properties and surface quality depends on cutting parameters as well as the LPBF conditions. Variation of the machining as well as the LPBF parameters during machining of the materials 1.2709, 1.4404 and AlSi10Mg were used to define optimized cutting conditions. The results show a small influence of the build-up direction on the surface quality for the material 1.2709 and a larger influence for the material AlSi10Mg (Figure 5-54). In detail for the variation of the direction of build-up it can concluded, that

- cutting conditions for 1.2709, 1.4404 and AlSi10Mgare comparable
- Best surface quality can reached with the material 1.4404
- In peripheral milling, a higher surface quality can reached when the feed direction is not equal to the build-up direction.

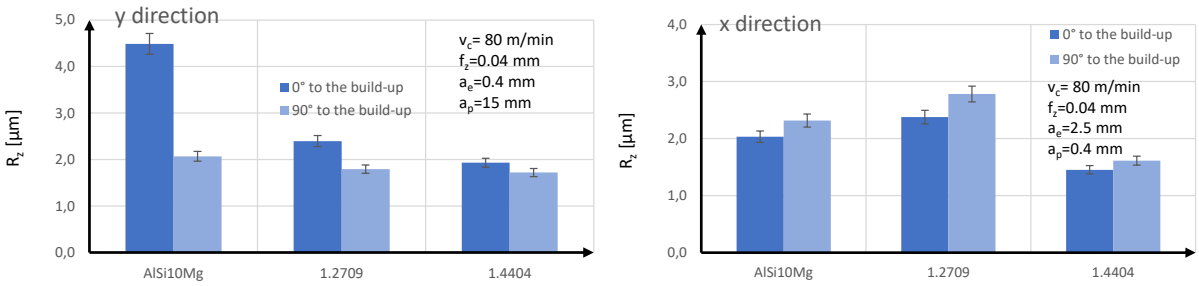

Figure 5-54: Roughness R_z perpendicular to the feed direction after peripheral milling (left) and face milling (right) of the materials AlSi10Mg, 1.2709 and 1.4404 for different orientations of the work-pieces during build-up within the LPBF process.

The results of surface functionalizing by PVD hard coatings show, that the PVD coating can used for heat treatment and as surface functionalization to improve wear resistance of additively manufactured parts of the material 1.2709. To use the PVD deposition technology as a heat treatment process it is necessary to reach the conventional hardening temperature profile for the used material 1.2709. With a deposition temperature during the hard coating process of about 480-490°C (nanocomposite coating nACo2) a substrate hardness of about 590HV10 can be reached. The properties that can achieved (e.g.

workpiece hardness and wear resistance, Figure 5-55) are comparable to conventional heat treatment and coatings on conventionally manufactured components.

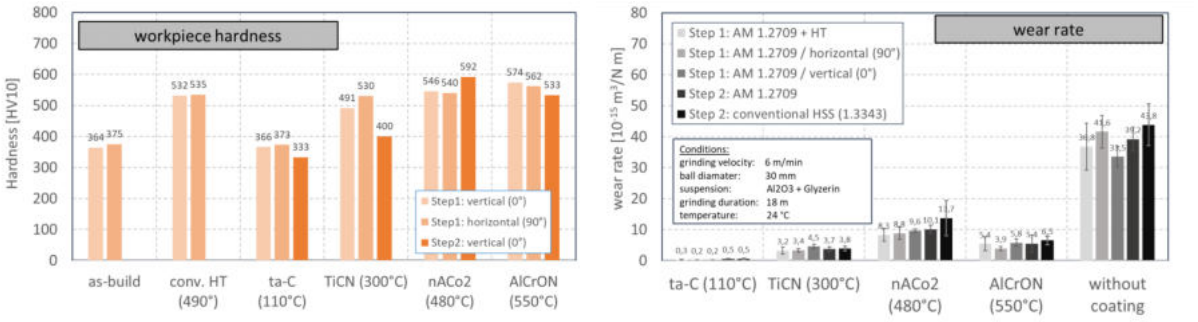

Figure 5-55: Workpiece hardness (left) and surface wear resistance / wear rate (right) of different coatings, heat treatment (HT) and orientations of the workpieces (0° / 90°).

5.4 Outlook

During the research, a modified process chain was used to investigate the influence of different process conditions on the properties of additively manufactured work-pieces after the LPBF process and surface functionalizing by milling and by PVD hard coating technology. Further investigations are necessary to research for a better understanding of the connection between process behaviour on the material properties and sub-surface properties after the subtractive and finishing processes.

In further investigations, in cooperation with industrial partners, the optimization of the surface and subsurface properties as well as the use of the additive manufacturing on semi-finished parts must considered more in detail. Of special interest are:

- Optimization of the additive manufacturing process
    - to determine and modify the influence on AM process conditions on surface and subsurface properties (e.g. density, microstructure, residual stresses, hardness)
    - to improve the interface to on semi-finished parts
    - to generate defined support structures as clamping point as well as for easy removal
- Use of surface functionalizing processes by milling for defined modification of surface and subsurface properties (e.g. density, microstructure, residual stresses, hardness)
- Development of PVD coating technologies with influence on subsurface properties on the additively manufactured parts
    - Reduction of surface roughness by thick hard coatings (> 10 µm)
    - Modification workpiece properties (e.g. density, microstructure, residual stresses, hardness) by hard coatings

Some of these aspects (Optimization of the additive manufacturing process on semi-finished products) will examined in detail in the Ad-Proc-Add II project.

6 Analysis of additive process technology – Results of the IFT

D. Nikolaev https://orcid.org/0000-0003-3877-694X,

I. Yavuz

(TU Wien, Institute of Production Engineering and Photonic Technologies)

6.1 Introduction

Powder-bed printing processes provide many advantages over conventional manufacturing processes such as improved product design or manufacturability of complex geometries. However, the actual printing process comes along with many challenges to produce parts that show high material density and minimize the risk of microcracks which might lead to component failure over the lifecycle. In the course of this project, several powder materials, process parameters and post-treatment technologies have been investigated, to identify optimal process parameters leading to high density and high-quality printed parts.

In this work package, impact of various process parameters (e.g., scanning speed, build-up rate, laser power, part alignment) on the additive process technology has been investigated. A testing part geometry has been produced based on the defined DoE.

6.2 Description of project results

6.2.1 Analysis of powder-bed-based process technologies

One of the widely (e.g. [1], [2]) used process parameter metrics for selective laser melting is the volumetric energy density (VED). VED can be calculated using the simplified state-of-the-art formula:

$$ED_{vH} = \frac{P_L}{v\, H_S\, L} \tag{1}$$

where:

P_L is the laser power,

v is the scanning speed,

H_S is the hatch spacing

and L is the layer thickness.

Parameters in this formula describe the laser induced energy level as well as layer thickness of the used powder.

In order to ensure valid process parameter's comparability between different machines, a more detailed method is required for more realistic energy density calculation. First, the induced laser energy needs to be modelled using fundamentals from fiber-optics and Gaussian beams. In powder-based applications, Ytterbium based fiber laser are frequently used due to their small beam quality factor which provide good convergence towards ideal Gaussian beams.

For instance, Figure 6-1 illustrates the power distribution in Gaussian Beam for various laser power (blue line) and intensities (red line) over increasing spot radius. Respective combinations of the laser

power and spot radius are depicted with same color shades. It is shown that larger spot radius results in lower intensity gradient, thus, is advantageous if the energy input is sufficient to melt the powder material.

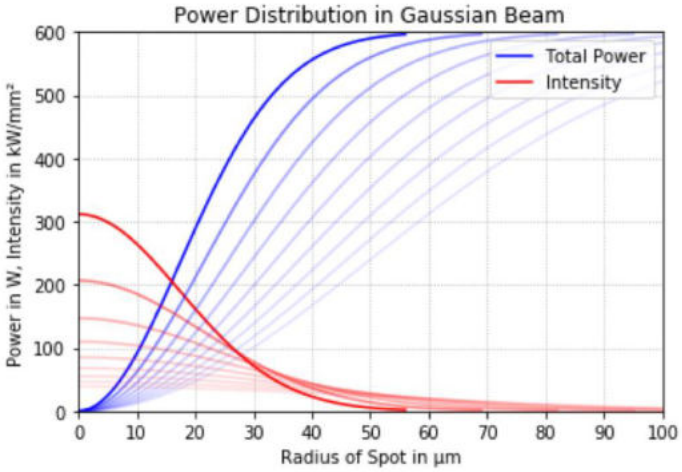

Figure 6-1: Laser power and intensity over increasing spot radius.

Second, a literature-based material model is required, reflecting temperature gradients in the powder material caused by the laser. For the specific experiments in this work, an exemplary material model for AlSi10Mg has been developed. The Gaussian-based power distribution of the laser and the temperature dependent material parameters have been used to setup a simulation model in ANSYS Workbench. Figure 6-2 highlights first simulations in ANSYS utilizing the Gaussian distributed laser power and the described material model.

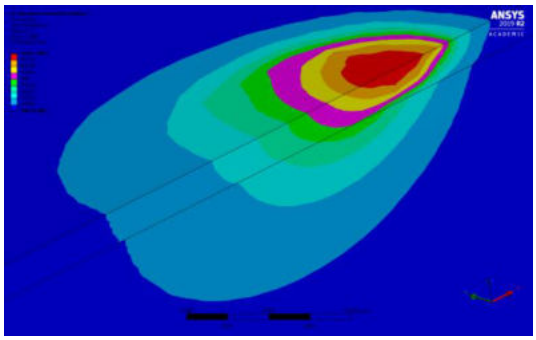

Figure 6-2: Temperature distribution results for a developed laser melt pool material model for AlSi10Mg [3].

A digital signal acquisition (DAQ) chain for temperature measurement possibly close to the melted layer has been developed by M. Prießnitz during his Master's thesis [3] as a part of the project. The developed numerical simulation allows to estimate the position of the temperature sensors to the plate surface in order to prevent their irreversible damage. The measured thermal history and heat dissipation of the additive machined parts, supports numerical analysis by providing novel process information for powder-based applications. For simulation validation, an experiment has been conducted, using 10-15 temperature sensors (PT1000) with minor reaction time and high sampling rates. First simulation results supported fitting position of the sensor in the machine tool. For sufficient sample rates, roughly 5 kS/s are required.

The experimental setup is positioned in the printer's build chamber instead of the standard plate and will be covered with powder during the process. The sealed machine infrastructure and moving recoater make any wired connection from inside the chamber difficult and thus require an autonomous DAQ system including a power supply, sufficient memory for the data and thermal isolation of the electronic components.

Figure 6-3: Sensory part of the developed DAQ chain [3].

The sensory part of the developed DAQ chain is depicted on Figure 6-3. SLM-printed sensor housing contains an array of 16 temperature sensors and can be mounted on the building plate inside of the SML machine while several layers will be printed directly on top of this housing.

Investigation of SLM process parameters for the selected powder materials for T 1.1 has been conducted based on a standardized process using a DMG LASERTEC 30 2nd Generation powder bed printer. The workflow is illustrated in Figure 6-4.

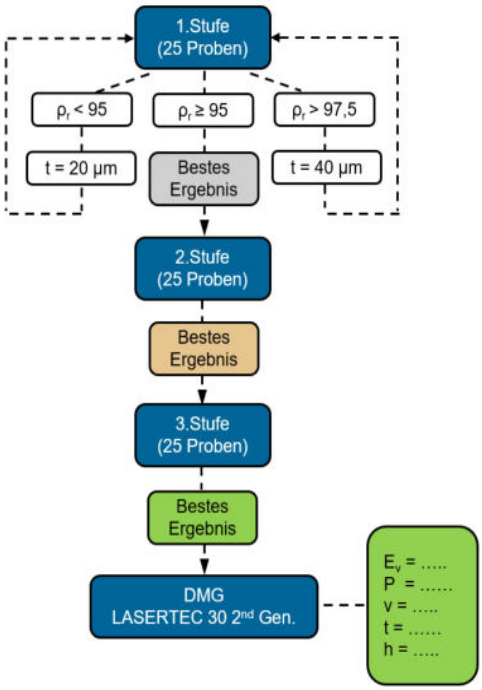

Figure 6-4: General workflow for a parameter optimization study.

In the experiment, laser power P_L, scanning speed v and layer thickness L were varied in a three-staged experiment. In each stage 25 cubic specimens are printed, then polished and weighed in air and in water for investigation of their relative density ρ_r according to the Archimedes' method. The best result of each

printing stage sets the starting point for the next stage. Each following stage aims the refinement of the process parameters from the previous one and uses a narrower range for parameter variation (see Figure 6-5).

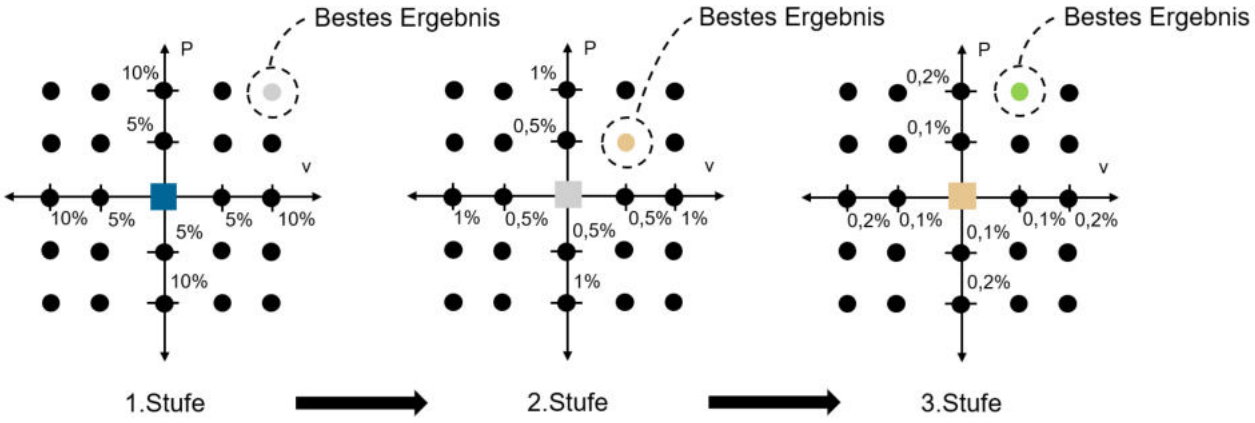

Figure 6-5: Parameter variation and refinement stages.

The described methodology has been used for development and optimization of various powder materials, targeting higher relative density of the printed specimens.

6.2.2 Use-case IMR – a parameter study for aluminum alloy powder AlSi10Mg

One of the process parameter optimization studies during the project was carried out on behalf of the powder manufacturing company IMR and covers a most widely used for powder bed manufacturing aluminum alloy AlSi10Mg. The aim of the study was to reach an improved density of test geometry as well as to increase the productivity of the printing process itself. Starting with the benchmark parameter set, provided by machine manufacturer DMG MORI, laser power P_L, scanning speed v and layer thickness L were varied. Figure 6-6 illustrates the workflow of the study (left) and respective density testing procedure according to the Archimedes' method (right). This study was initially carried out in a reduced manner (only the first stage) to ensure a short-term parameter availability for the company and has been completed afterwards.

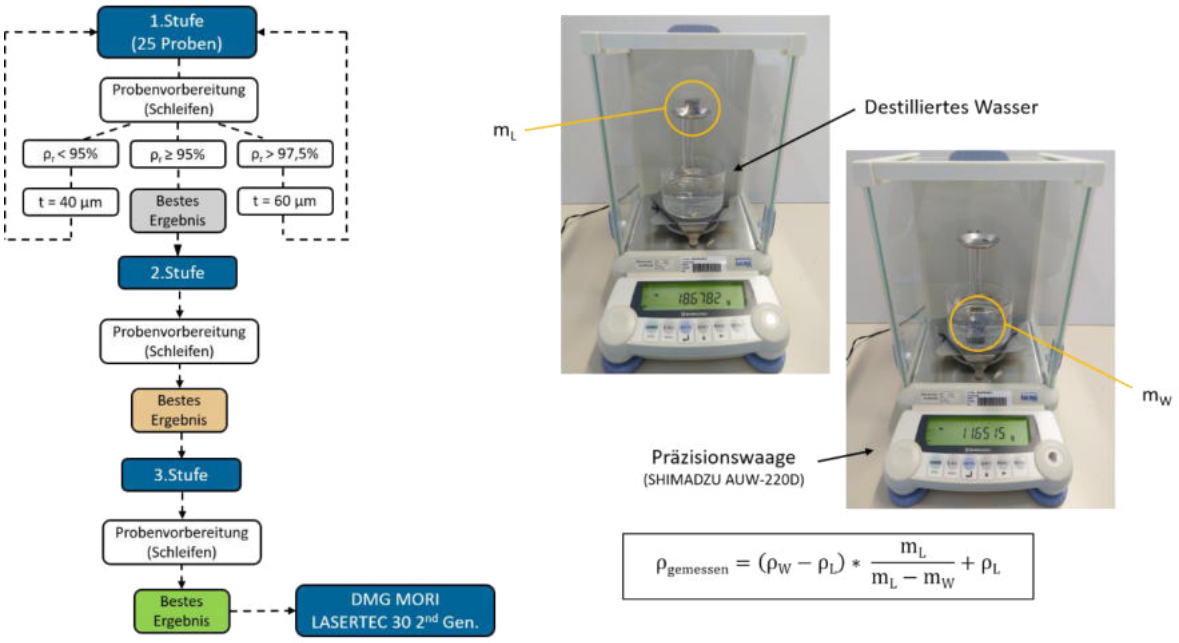

Figure 6-6: IMR parameter optimization workflow (left) and Archimedes density estimation (right).

During the first stage, layer thickness of 50 µm has been used and laser power and scanning speed have been varied by ±5 %. Using the benchmark parameter, a relative density of 98,21 % has been achieved. Since this value exceeds the defined threshold of 97,5 %, an increased layer thickness can improve productivity of the process. A second iteration of the first stage was printed with an increased layer thickness of 60 µm and best results for relative density are used as a baseline for the second printing stage (see Figure 6-7).

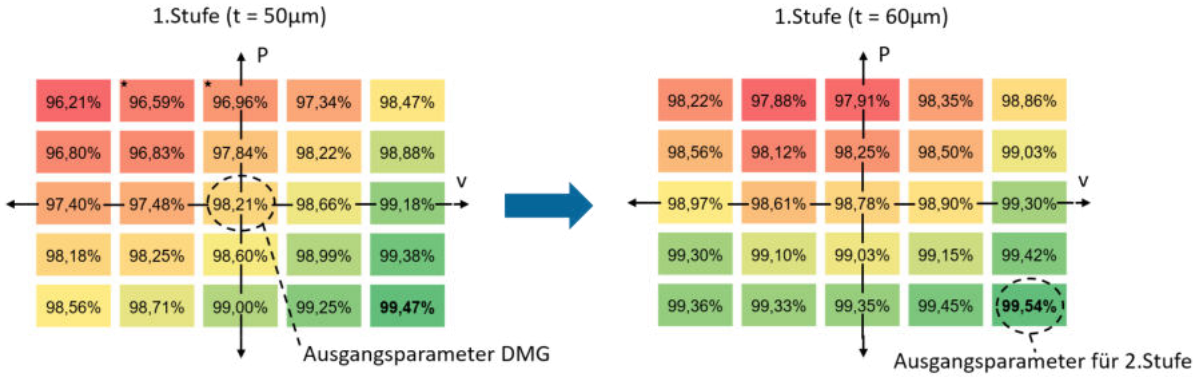

Figure 6-7: Interpretation of the relative density measurement results of the 1st workflow stage.

Again, laser power and scanning speed have been varied by ±5 % starting with the best parameter set from the first stage. In this experiment, a mutual influence of neighbored specimen on their relative density has been observed.

Figure 6-8 illustrates better density results for a printed specimen with two other specimens nearby, compared to a specimen, printed with the same process parameters, but surrounded with four other specimens (see Figure 6-8 grey squares). Further investigations confirmed the negative influence of too close placement of the specimens to each other on the specimen's relative density. Thus, a safety margin between specimens must be considered.

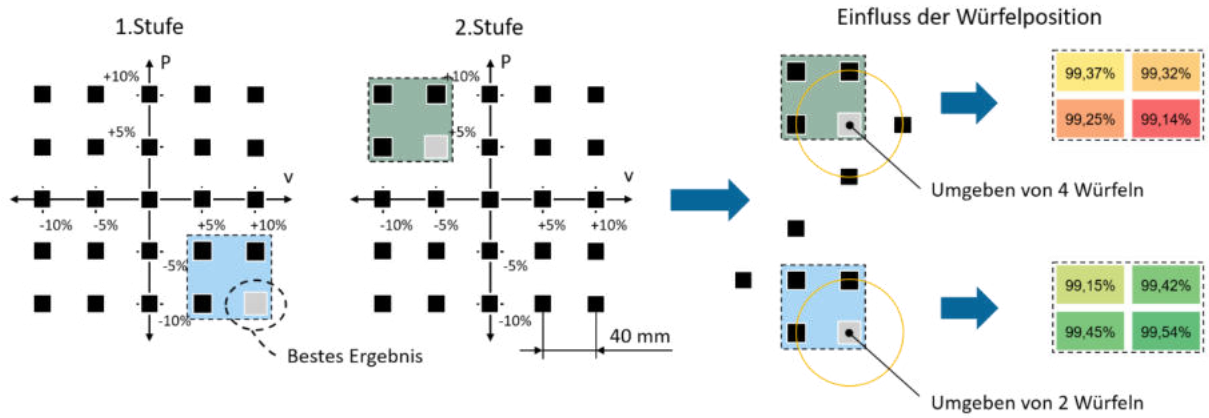

Figure 6-8: Influence of the neighbored cubes on the relative density of each other.

Five process parameter sets from the 2nd printing stage, which have shown the highest relative density, have been selected and manufactured again using larger distances to each other. Figure 6-9 shows the estimated relative density of these specimens among with values measured for closer placed specimens (values in parentheses). The parameter set "P2", related to the specimen with best relative density, was selected as initial set for the last optimization stage.

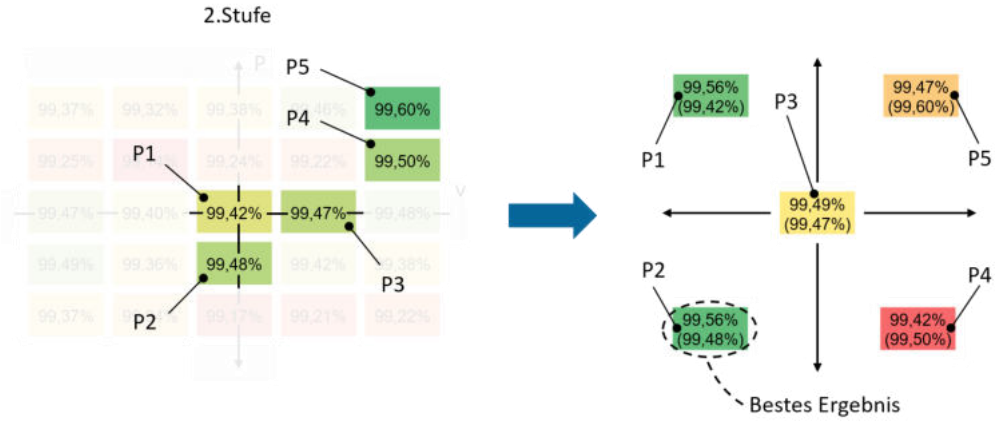

Figure 6-9: Interpretation of the 2nd stage density measurements for AlSi10Mg under consideration of the mutual influence of the neighbored specimens.

For the stage 3, the total number of specimens was reduced to 9 in order to maintain a larger margin between them. Laser power and scanning speed were varied by ±2,5 %. The best parameter set (see Figure ***6-10***) could be identified for optimal printing of the powder material AlSi10Mg of company IMR.

Figure 6-10: Interpretation of the density measurements of the 3rd workflow stage (refinement) for AlSi10Mg

Results of investigations on powder material AlSi10Mg can be summarized as followed:

- Optimized parameter over several printing stages for AlSi10Mg with $ED_{vH} = 38{,}7\ J/mm^3$.
- Relative density has been increased by 1,46 %, while increasing layer thickness by 10 µm, compared to the initial parameter set from DMG MORI SLM Lasertec 30 2nd Gen.
- Improvement of productivity due to increased layer thickness by +35 %.
- Impact of distance between printed cubes identified and investigated. Identical process parameter may result in different relative densities depending number of surrounding specimens (e.g., 2 or 4) and distance between them.

6.2.3 Process parameter transformation approach

However, the identified parameter set is only valid for the used DMG Mori SLM machine and cannot be transferred in a trivial way for using with machine of another type or different vendor. A formula, enabling automated transformation of parameter sets between various SLM machines and system specifications would save time and costs during the engineering process. For instance, the utilization of the optimized parameter set for AlSi10Mg powder on an EOS M400 SLM machine, which is also available in consortia, was taken into account. Both machines were supplied with the same charge of the AlSi10Mg powder material by IMR. In the context of this work, two different approaches for parameter transformation have been identified and evaluated.

First of all, the technical differences between these two SLM machines were investigated and summarized into four groups (powder material, laser source, scan and environment) as follows:

		DMG MORI Lasertec 2nd gen.	**EOS M400**
Laser spot diameter	$d, \mu m$	65	82
Maximum laser power	$P_{L,max}, W$	600	1000
Overpressure in printing chamber	$p, mbar$	20	30
Residual oxygen level	$O_{2,max}, \%$	0,25	1,3

Table 6-1: Technical properties of the machines used in parameter transformation study.

The state-of-the-art formula for calculation of the volumetric energy density ED_{vH} (1) does not take the spot diameter into account. The approaches investigated in this study focus on inclusion of the spot diameter into volumetric energy density calculation. Two approaches have been considered and parameter transformation has been tested. For the reference experiment the optimized parameter, identified for DMG MORI Lasertec 30 2nd Gen., has been used without any adaptions on the EOS M400 machine. The achieved relative density on the EOS M400 was higher compared to the original tests. Details about the test are depicted in Figure 6-11.

Versuch	Formel	Einheit	Einflussfaktor	Umsetzung
Referenz-versuch	$E_v = \frac{P}{t * h * v}$	(J/mm³)	-	Direkte Übertragung der Parameter

DMG-Parameter	
P	314 W
v	1,35 m/s
t	60 µm
h	100 µm
$\rho_{r\,(Ar)}$	99,67%

Referenz

EOS-Parameter	
P	314 W
v	1,35 m/s
t	60 µm
h	100 µm
$\rho_{r\,(Ar)}$	99,76%

Figure 6-11: Reference experiment for parameter transformation.

First experiment targeting a parameter transformation has been conducted focusing influence of the spot diameter d adaptation to the hatch distance h. In the first test, the ratio h/d from parameter set for DMG Mori machine has been used for adjusting the hatch distance on EOS machine using the known spot diameter. A significantly lower relative density of 99,49 % (see Figure 6-12) has been evaluated for specimens printed with this new parameter set.

Versuch	Formel	Einheit	Einflussfaktor	Ansatz
1	$E_v = \frac{P}{t * h_{EOS} * v}$	(J/mm³)	Spot-Durchmesser	$h_{EOS} = \frac{h_{DMG}}{d_{DMG}} * d_{EOS}$

DMG-Parameter	
P	314 W
v	1,35 m/s
t	60 µm
h	100 µm
d	65 µm
$\rho_{r\,(Ar)}$	99,67%

1.Versuch

EOS-Parameter	
P	314 W
v	1,35 m/s
t	60 µm
h	126 µm
d	82 µm
$\rho_{r\,(Ar)}$	99,49%

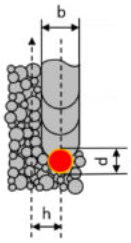

Figure 6-12: 1st experiment of the parameter transformation approach.

Second experiment focused on the adaption of the meld pool width b in relation to hatch spacing h. In order to estimate this ratio, several isolated laser tracks were welded on each machine using the same reference parameter set. Micrographs was used for estimation of the actual seam width at several points. The calculated mean value of the seam width was finally used for estimation of the h/b ratio, which was kept constant during the hatch distance adjustment on the “target” machine EOS M400. An adjusted parameter set with $h = 225\ \mu m$ has been found to produce the specimen on target SLM machine with the same relative density of 99,67 %, as the specimen produced with the DMG MORI Lasertec 2nd gen (see Figure 6-13).

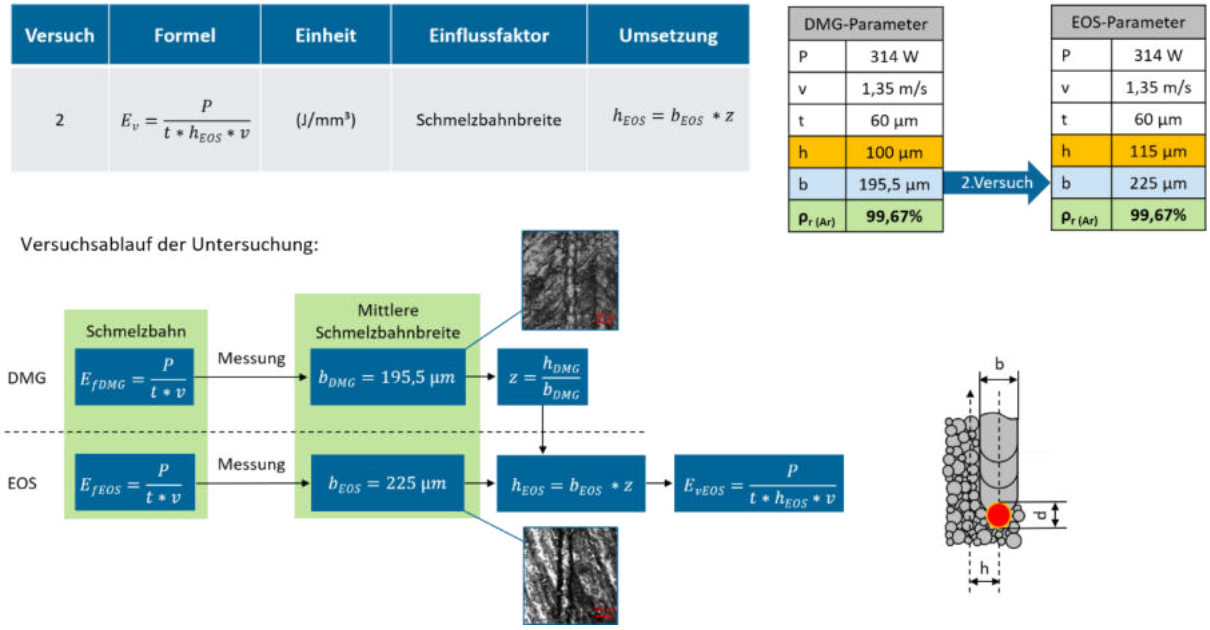

Figure 6-13: 2nd experiment for parameter transformation.

6.2.4 Use-case voestalpine Böhler Edelstahl GmbH & CO KG –powder M789 AMPO

Further parameter optimization study has been carried out for powder material M789 AMPO on behalf of the company voestalpine Böhler Edelstahl GmbH & CO KG. Similar to previous experiments, laser power P_L, scanning speed v and layer thickness L were varied in a multi-staged workflow. As a reference for parameter optimization for usage on DMG Mori Lasertec 2nd gen machine, a parameter set from a TRUMPF TruPrint 1000 was proposed by the company. However, these parameters led to unwanted termination (see Figure 6-14) of the printing job and could not be used as reference for further trials.

Figure 6-14: Job failure on DMG MORI Lasertec 2nd Gen. using the process parameters from TRUMPF SLM machine for M789 AMPO.

The chemical composition of the powder M789 AMPO appears to be similar (except of cobalt usage instead of chrome) to another alloy, widely used for powder bed additive manufacturing – 1.2709 (see Table 6-2). Hence, a parameter set available for 1.2709 has been used for further optimization.

	Fe	C	Si	Mn	Cr	Co	Mo	Ni	Cu	Ti	Al
							[wt %]				
M789 AMPO	bal.	0,009	0,44	0,02	12,20	-	1,02	10,38	<0,02	0,98	0,60
1.2709	bal.	<0,03	<0,10	<0,10	<0,25	8,5	4,50	17,0	<0,5	0,8	0,15

Table 6-2: Chemical compositions of M789 AMPO and 1.2709.

Similar to previous studies, laser power P_L, scanning speed v and layer thickness L were varied by ±5 %. Some estimated relative density values from the 1st stage (see Figure 6-15) exceed 100 %, which is likely caused by the usage of theoretical density of the alloy claimed by the manufacturer but not experimentally proved as a reference for estimation of the relative density of the specimens. After the first printing stage, where all estimated relative density values exceeded the threshold of 97,5 %, layer thickness could be increased by 10 µm. Specimens printed with increased layer thickness showed the relative density of 99,95 %. This parameter set have then been used as starting point for the second printing stage.

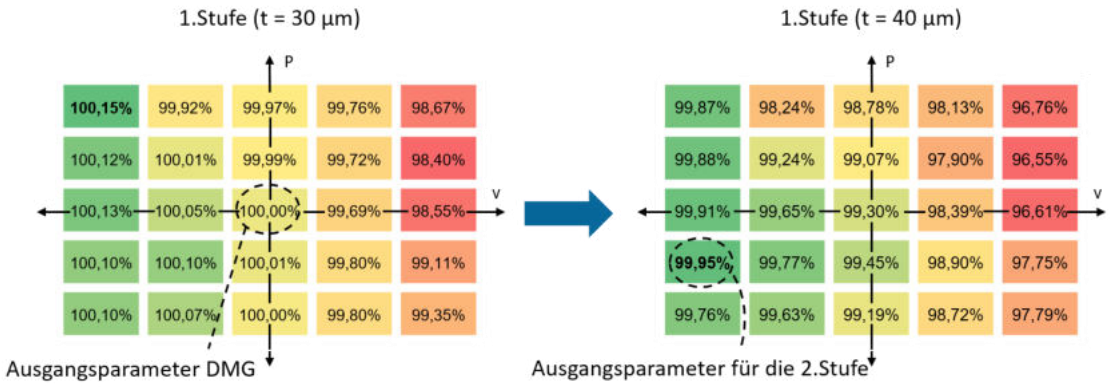

Figure 6-15: Relative density measurements interpretation of the 1st stage parameter optimization workflow for M789 AMPO.

In the second optimization stage, an impact of the neighbored specimens has been considered. Thus, the printing job has been split up into two, in order to maintain a necessary margin between the specimens during one job. The best result of the parameter study shows a relative density of 100,15 % (see Figure 6-16).

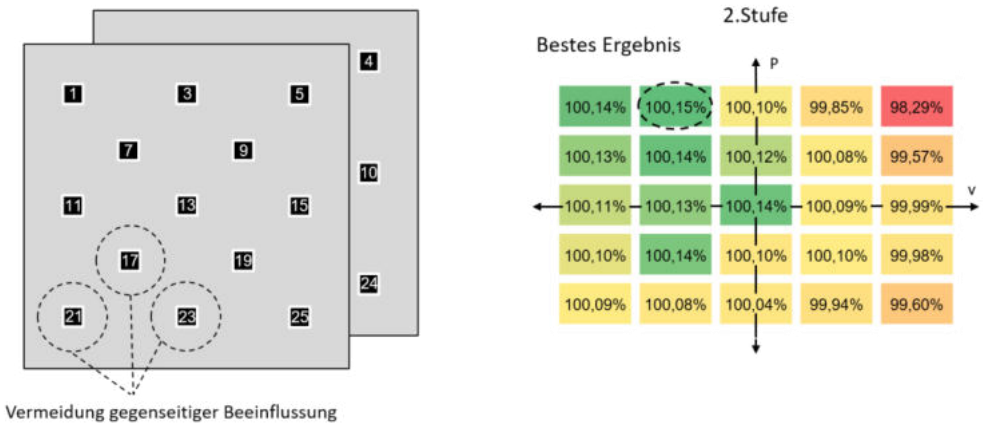

Figure 6-16: Relative density measurements interpretation of the 2nd stage parameter optimization workflow for M789 AMPO.

In the last printing stage, parameters have been varied by ±2,5 % and number of specimens has been reduced to 9. The experiment highlights worse results compared to the previous stage, which might be caused by the new powder which has been used for this stage. The best parameter set allowed to achieve the relative density of 100 % (see Figure 6-17).

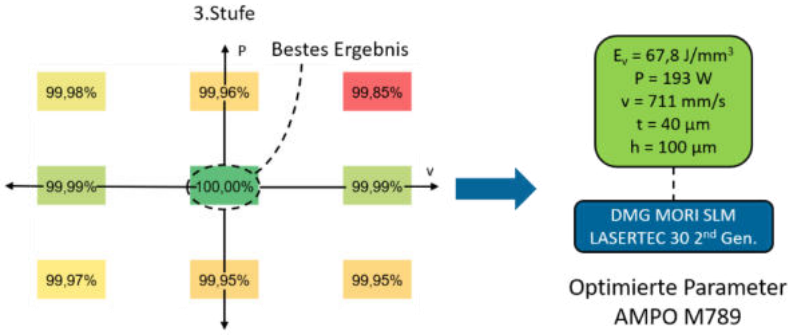

Figure 6-17: Relative density measurements interpretation of the 3rd stage parameter optimization workflow for M789 AMPO and identification of the resulting parameter set.

The summary of parameter study for powder material M789 AMPO:

- Optimized parameter set found through multiple optimization stages for M789 AMPO with $ED_{vH} = 67{,}8\,J/mm^3$.
- Increased relative density by 0,15 % while increasing layer thickness by 10 µm compared with original reference parameter set from DMG MORI SLM Lasertec 30 2nd Gen.
- Productivity increased by +8 % due to the parameter optimization.

6.2.5 Use-case globalHydro – type13-X.03 stainless steel

Further parameter optimization study was carried out for an Austrian hydro power supplier company Global Hydro Energy GmbH. A widely used for hydropower parts stainless-steel alloy, chemically similar to the 1.4313 (see Table 6-3 for detailed chemical composition), was investigated in this case. Parameter optimization has been carried out for a selective laser melting machine SLM solutions SLM 500.

	Fe	Cr	Ni	Mn	Mo	Si	C
				[wt %]			
Nominal min.	balance	12,0	3,5	-	0,3	-	-
Nominal max.		14,0	4,5	1,50	0,7	0,70	0,05
Charge	balance	13,4	4,0	1,07	0,5	0,36	0,03

Table 6-3: chemical composition of the stainless-steel alloy m4p 13-X [4].

There are three values for the layer thickness as defined for the study by the company: 30 µm for fine detailed parts, 50 µm for average prints and 70 µm for large scaled parts, where resolution of the surface may be traded off for shorter manufacturing time. According to the sieve analysis of the powder charge (see Table 6-4), the size of the powder grains was found to be between 53 µm and 20 µm with 96% probability. Assuming the minimum thickness, achievable with specific granularity of the powder being 1,87 times the mean grain size [5, p. 106], required layer thicknesses of 50 µm and 70 µm should be achievable. Layer thickness of 30 µm may result in recoating issues or longer manufacturing time due to the lack of suitable powder in the tank.

	+63 µm	+53 µm	+45 µm	-53 µm +20 µm	-20 µm
Nominal min.	-	-	-	-	-
Nominal max.	0,5%	2%	-	-	10%
Charge	0%	0,2%	11,8%	96,0%	3,5%

Table 6-4: sieve analysis results of the powder and fractions distribution [4].

There is no parameter set, which would be suitable for the investigated powder, provided either by the powder manufacturer nor by the manufacturer of the SLM machine. Thus, the initial parameter set was chosen according to a standard parameter set for a stainless-steel powder 316L (see Table 6-5) with the most similar chemical composition to the alloy 13-X.

Laser power	Scanning speed	Layer thickness	Hatch distance	Volumetric energy density
P_L [W]	v [mm/s]	L [µm]	H_S [µm]	ED_{vH} [J/mm³]
250	950	50	100	52,6

Table 6-5: Initial parameter set.

The machine SLM 500 is equipped with four separate laser sources and allows simultaneous exposure of the laser tracks in order to leverage the material deposition rate. Build plate size of the SLM 500 allows to print up to 28 cubic specimens (20 x 20 x 20 mm) in the same job under consideration of the safety margin of 70 mm between the specimens, as described in chapter “Use-case IMR – a parameter study for aluminum alloy powder AlSi10Mg” Furthermore, in order to understand possible environmental influences on the resulting workpiece density caused by design of machine or build chamber, the whole build plate, containing 28 specimens was manufactured twice during two different days.

Results of the estimated relative density of those specimens are shown in Figure 6-18. Measurement results repeatability of 0,02(05) % between the days one and two (see Figure 6-18 right, upper and lower charts respectively) are in agreement with the average measurement uncertainty and confirm an overall stable machine performance. Also, no negative influence of the recoater could be found, since the relative density measurements in this direction (top side of the plate to bottom) is found to be stable (compare values in each column of both tables in Figure 6-18 right). No significant influence has been found for the workpiece placement in the “overlapping” areas (see blue areas on the Figure 6-18 middle), where either of two or both neighbored laser sources may be active.

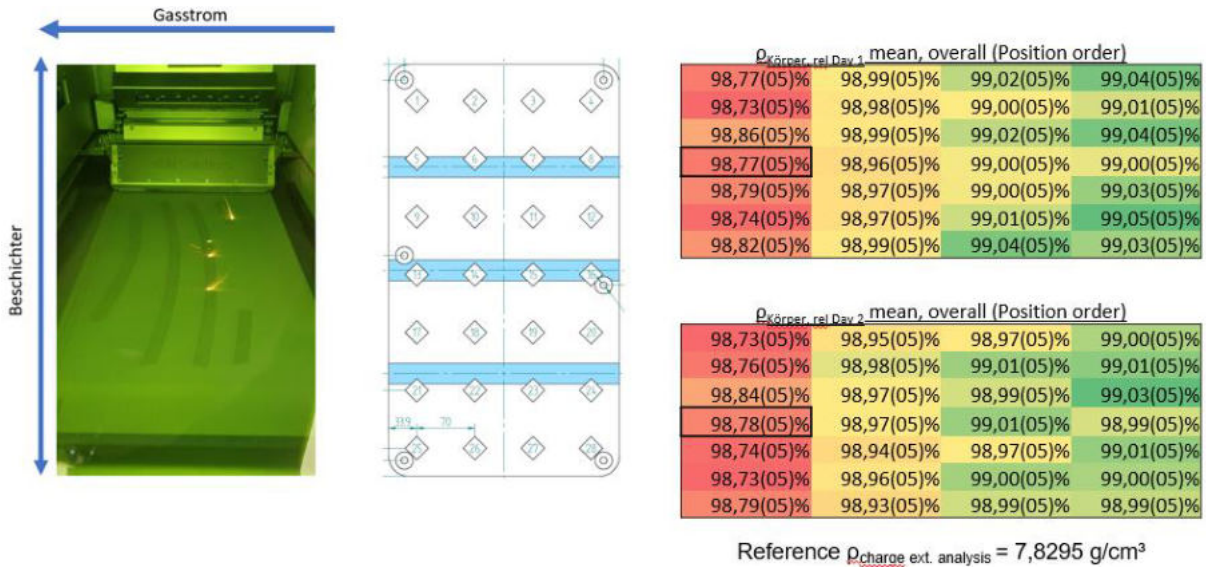

Figure 6-18: SLM 500 build chamber (left), specimen's positions on the build plate (middle), relative density estimation results (right).

A strong dependency of the specimen’s relative density on their location respective to the shielding gas flow direction has been found. The specimens, which were located closer to the gas inlet valve (see Figure 6-18 right side respectively), will likely be less porous, compared to the specimens closer to the gas outlet valve on the opposite side of the build plate. The achievable density in this machine may vary for up to 0,30 % within a single print job for this reason.

First stage of the parameter optimization workflow was performed the same way, as described previously in chapter “Use-case IMR – a parameter study for aluminum alloy powder AlSi10Mg”. Laser power P_L and scanning speed v were both varied in 5 % steps in a wide range from - 10 % to + 10 % of the values defined in initial parameter set (refer to the Table 6-5).

Results of the relative density estimation are depicted in Figure 6-19 to Figure 6-21. The relative density value, which corresponds to the initial parameter set, is represented in the center, while the density values for specimen printed with different laser power P_L are aligned bottom to top in ascending order (last table row – lowest laser power) and for different scanning speed v are aligned left to right in ascending order (first table column – lowest scanning speed).

All experiment series have shown repeatable and significant lower relative density values for the specimen #25, which was located on the bottom corner of the plate. This is in agreement with shielding gas flow issue, however the exact reasons cannot be explained sufficiently yet.

Following interpretation considers this specimen to be an outlier.

$\rho_{Körper, rel}$ mean, overall (P-V order), Interpolated

99,12(05)%	98,92(05)%	98,92(05)%	98,94(05)%	**99,11(05)%**
98,86(05)%	98,86(05)%	98,90(05)%	99,02(05)%	98,88(05)%
98,86(05)%	98,89(05)%	99,08(05)%	98,89(05)%	98,84(05)%
98,90(05)%	99,09(05)%	98,90(05)%	98,88(05)%	98,87(05)%
99,12(05)%	98,90(05)%	98,87(05)%	98,83(05)%	98,65(05)%

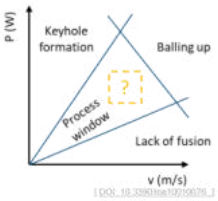

Figure 6-19: Relative density results for the layer thickness of 30 µm.

$\rho_{Körper, rel}$ mean, overall (P-V order), Interpolated

98,90(05)%	98,68(05)%	98,69(05)%	98,74(05)%	98,87(05)%
98,66(05)%	98,67(05)%	98,74(05)%	98,83(05)%	98,75(05)%
98,64(05)%	98,70(05)%	98,86(05)%	98,73(05)%	98,71(05)%
98,72(05)%	98,86(05)%	98,73(05)%	98,74(05)%	98,75(05)%
98,92(05)%	98,74(05)%	98,74(05)%	98,76(05)%	97,73(05)%

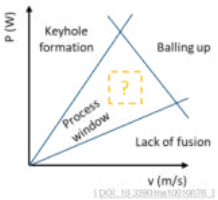

Figure 6-20: Relative density results for the layer thickness of 50 µm.

The estimated relative density for specimens printed with layer thickness of 30 µm and 50 µm are depicted on Figure 6-19 and Figure 6-20 respectively. A similar distribution of the estimated relative densities over the P_L/v field could be observed in these cases: the relative density deviation between specimens, which was printed with same volumetric energy density (located diagonally bottom left to top right corner), does not exceed the measuring uncertainty of the applied method. Thus, no significant difference by the means of resulting relative density of the specimen can be observed between slower parameter set with less energy input (lowest left value) and a parameter set with proportionally increased laser power and scanning speed (top right value).

Considering the isolated influence of the changing laser power or of the scanning speed within the P_L/v field, the relative density deviation of 0,12 % and 0,17 % for the specimen, printed with 30 µm and 50 µm layer thickness respectively. Both deviation ranges are found not to exceed the density deviation within a group of specimens printed with the same parameter set, which shows so significant influence of the parameter variation within an ±10% range from initial parameter set. This indicates, that the observed process parameter range likely lays within the process window [6], as defined by Trevisan et. al. Thus, for the layer thickness of 30 µm and 50 µm a parameter set with laser power and scanning speed both increased by 10 % can be considered as optimized, coming along with equally increased productivity.

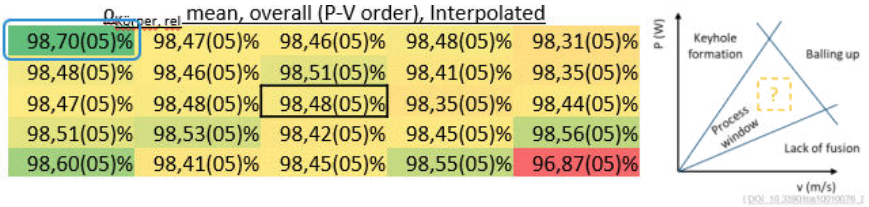

Figure 6-21: Relative density results for the layer thickness of 70 µm for the group of specimens printed with layer thickness of 70 µm.

A different relative density distribution has been observed. The deviation of the estimated values of 0,52 % slightly exceeds the density deviation within a group of specimens printed with the same parameter set and thus confirms the influence of the process parameter variation within described range on the relative density in this particular case. However, the further parameter optimization by varying the process parameters in narrower range cannot be considered as reliable. Higher volumetric energy density (top left value) due to increased laser power and lower scanning speed results into increased relative density of the specimen. This parameter set (-10 % scanning speed and +10 %laser power) may be considered as optimal one.

Optimized process parameters are summarized in the Table 6-6 for all three investigated layer thicknesses.

Laser power	**Scanning speed**	**Layer thickness**	**Hatch distance**	**Volumetric energy density**
P_L [W]	v [mm/s]	L [µm]	H_S [µm]	ED_{vH} [J/mm³]
220	880	30	120	69,4
275	1045	50	100	52,6
385	855	70	120	53,6

Table 6-6: Optimized parameter sets for m4p 13-X.

Results of the use-case for parameter optimization for m4p 13-X show the limitations of the proposed method. In case if the relative density of specimens printed with initially selected parameter set is around 99%, no meaningful parameter mapping to the P-V density map [6] according to Trevisan et. al can be performed anymore. Thus, the direction for the parameter optimization isn't clear either. Furthermore, at this point the influences caused by process conditions such, as the shielding gas flow, may have greater impact on the print job quality by the means of specimen's relative density, than the parameter variation itself.

6.2.6 Parameter optimizations for consortium project partners

The parameter optimization study has also been conducted for scientific partners in the consortia. A shorter single-staged study design with 9 cubic specimens was considered in order to provide a quick estimation of how well the currently used parameter set has been defined respectively to the process

window [6] and allow to identify a possible optimization approach in each case. Laser power P_L, scanning speed v and layer thickness L were varied by ±10 % from values of the currently used parameter set. A possible mutual influence of neighbored specimens was taken into account and a reference specimen featuring the same parameter set as the initial one was printed outside of the test field (see Figure 6-22 to Figure 6-24, blue square).

Optimization results for FOTEC (AlSi10Mg, EOS M400)

Results of this study for a AlSi10Mg powder used in an EOS M400 SLM machine by FOTEC are depicted in Figure 6-22. A mutual influence of the specimens on each other's relative density has been found. The specimens printed with initial parameter set show significantly (0,15 % deviation) different results. An optimization approach by reduction of the laser power and increase of the scanning speed can be considered in this case.

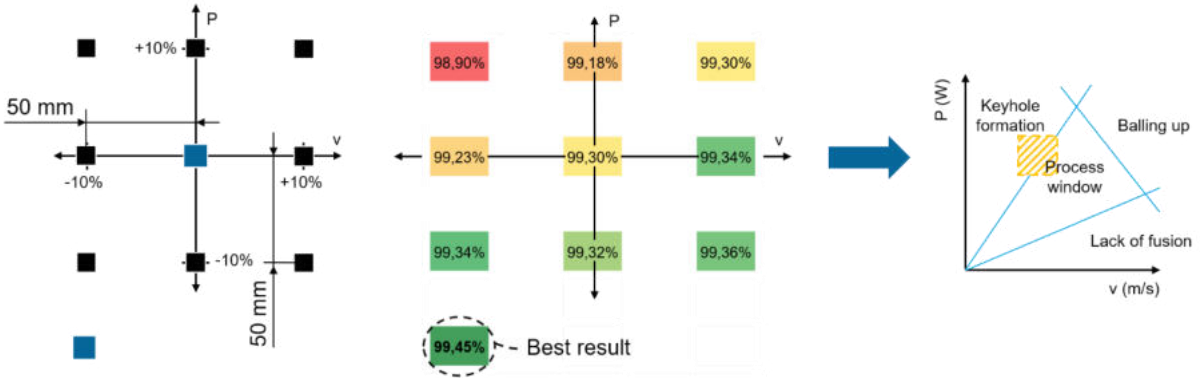

Figure 6-22: Results of the single-staged parameter mapping and optimization for AlSi10Mg on EOS M400 (FOTEC).

Optimization results for GfE (1.2709, DMG MORI Lasertec 30 2nd Gen.)

Overall relative density results (see Figure 6-23) estimated for the specimens printed by GFE (Gesellschaft für Fertigungstechnik und Entwicklung Schmalkalden e.V.) on a DMG MORI Lasertec 2nd gen. SLM machine using a 1.2709 powder have been found to be suboptimal, as the values do not exceed 97,5 %. The distribution of the estimated values over the testing field indicates the occurrence of the balling-up issue, thus reduced scanning speed and laser power would be necessary as an optimization measure. Again, a significant mutual influence of the specimens on each other's relative density has been found: specimens printed with initial parameter set show density deviation of 0,9 %.

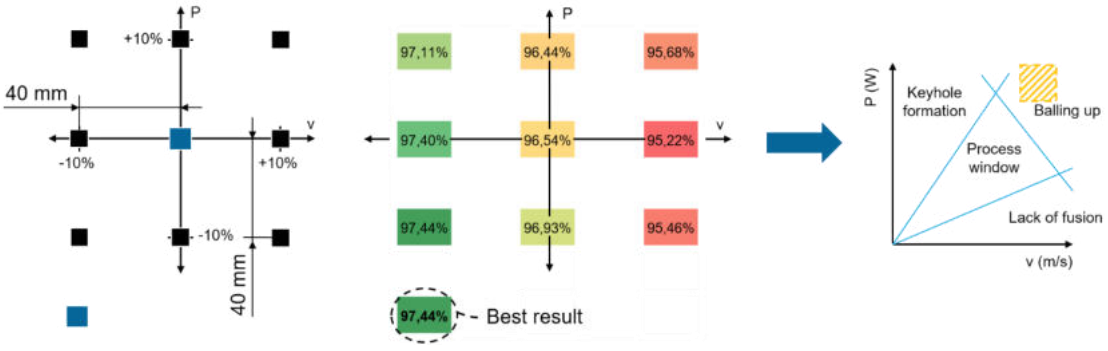

Figure 6-23: Results of the single-staged parameter mapping and optimization for 1.2709 on DMG MORI Lasertec 2nd Gen. (GfE)

Optimization results for ISF (1.4404, SLM 280)

The parameter study for ISF (Institut für Spanende Fertigung, TU Dortmund) on the specimens printed with 1.4404 powder in a SLM 280 machine showed highest results (see Figure 6-24) by the means of relative density. A very low deviation of 0,04 % between the reference and control parameter set shows no mutual influence of the specimens. The overall results of >99,6 % indicate, that the parameter set is optimally defined in process window and has a high process stability.

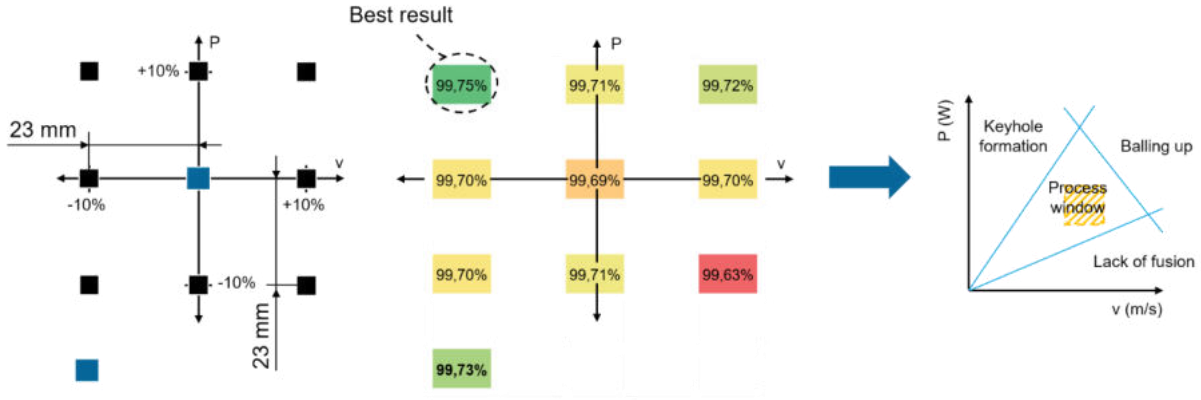

Figure 6-24: Results of the single-staged parameter mapping and optimization for 1.4404 on SLM 280 (ISF).

Analysis of the intermediate workpiece treatment

In this task, tensile and impact probes have been manufactured in different orientations using AlSi10Mg powder material and machine manufacturer's standard process parameters. For tensile testing, 15 specimens have been printed in vertical orientation and 10 probes in horizontal orientation. For impact testing, 10 specimens have been printed in both orientations. Additionally, 3 cubic specimens have been printed for estimation of the achieved relative density of this print job (see Figure 6-25).

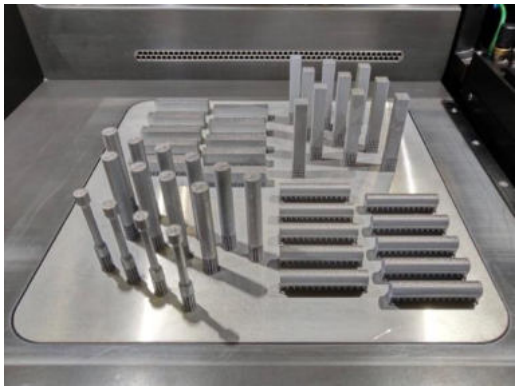

Figure 6-25: Specimens for tensile, impact and density testing manufactured out of AlSi10Mg.

For each probe type and build up orientation, 5 specimens undergo a heat treatment (stress-relief annealing, 300°C for 2 hours). The specimen was then machined to achieve the standardized shape and dimensions for respective mechanical testing method. Unfortunately, due to project delays caused by the COVID-19 pandemic situation, the impact of the heat treatment on build-up direction and material strength have not been investigated as planned.

Hot Isostatic Pressing (HIP)

A further possibility to improve density of additively manufactured parts, beside parameter optimization, has been investigated in the project. In the Hot Isostatic Pressing (HIP) process, material is treated under high temperature and high pressure in order to increase material density due to compression of the pores.

Investigation in this project focused on manufacturing various density cubes using different SLM machines and materials, which are available in consortium. Respective relative density of the printed cubic specimens has been evaluated according to the Archimedes' method before and after the HIP treatments has taken place. Figure 6-26 highlights the results of the different probes.

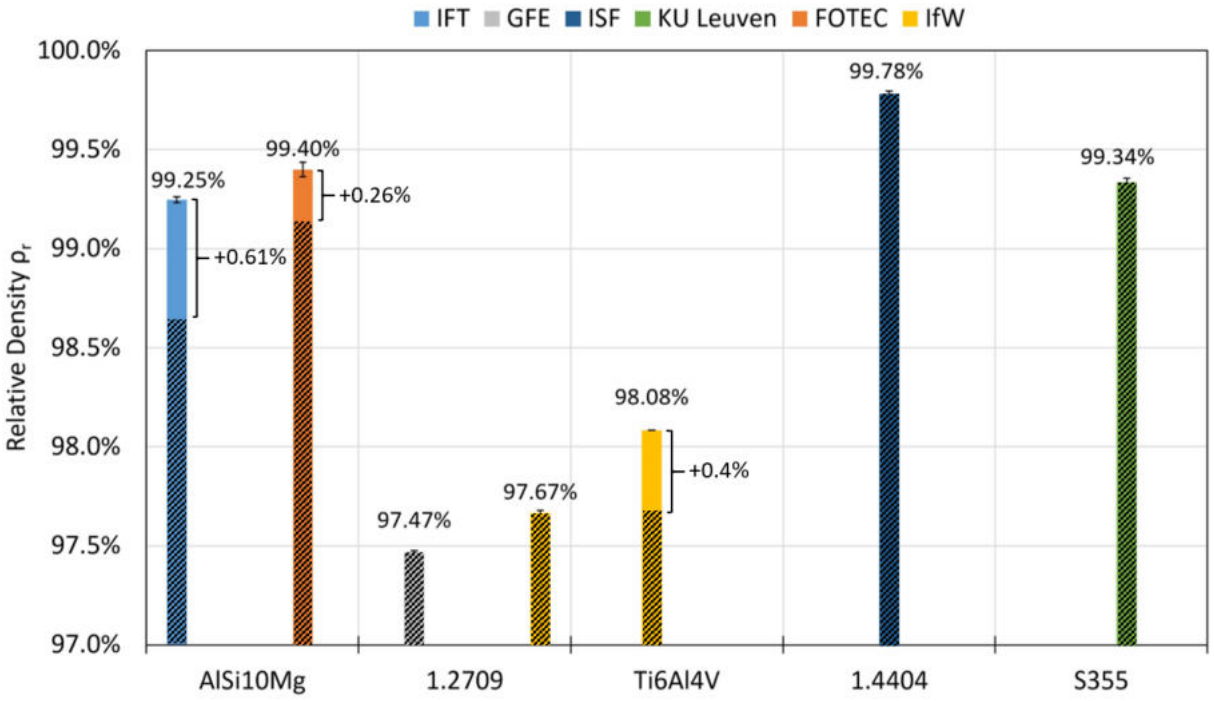

Figure 6-26: Results of the relative density measurements on specimens after HIP treatment.

For aluminum and titan alloys, a significant increase in density due to the HIP process has been determined. Specimens out of AlSi10Mg powder, printed and tested by IFT, indicate a density increase of 0,61 %. Specimens printed by FOTEC showed an improvement of 0,26 %. Titan specimens by TU Stuttgart (IfW) achieved an improvement in relative density by 0,4 %.

All other specimens, including both steel powder materials 1.2709 and 1.4404 and WAAM steel specimens out of S355, did not show improvement of density due to HIP process. Possible reasons are the selection of unfit process parameters for HIP treatment, because of the simultaneous treatment of all steel specimens.

The HIP treatment also influenced the surface appearance of some specimens. For aluminum probes, which were polished before, surface turned rough. Such phenomenon is caused by the closure of the pores directly under the surface or their dislocation toward the surface under conditions of applied pressure and temperature. Figure 6-27 highlights the change of surface conditions for aluminum probes after HIP process treatment along with allied parameters for the treatment.

AlSi10Mg	Densal II Cycle (Fa. Bodycote) Ähnlich einer T6 Wärmebehandlung Schutzgas: Stickstoff
Ti6Al4V	Haltephase: 920°C, 100 MPa, 120 min Schutzgas: Argon
1.2709 14404 S355	Aufheizphase: 9°C/min → 600°C Haltephase: 1150°C, 100 MPa, 240 min Kühlphase: 1,2°C/min → 300°C Schutzgas: Argon

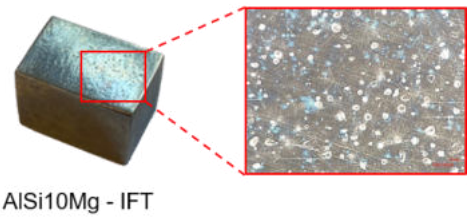

Figure 6-27: Applied HIP process parameters (left), changed surface texture after HIP treatment (right).

6.3 Summary

A reliable, inexpensive and machine-independent method for parameter optimization on novel or given powder materials has been developed in course of the study on additive process technology of the laser powder bed process, carried out at the institute of production engineering and photonic technologies. The method consists of a multi-staged iterative investigation of the relative density of the printed specimen and aims its optimization towards at least 99%. Further optimization has been found to be less reliable, since the influence of the local process conditions might exceed the influence of a finer parameter variation. The workflow can be also carried out in a reduced manner in order either to benchmark machine and powder performance, or to provide a quick estimation if and how the process parameter set can be optimized.

A parameter transformation approach, suitable for transferring given SLM process parameter from a specific machine to another machine type or vendor has been developed. The transformation approach takes major differences of the equipment and process environment into account in order to achieve a similar appearance of the isolated welded seam and thus to adjust two different process situations and provide conversion coefficients for selected parameters. A further parameter optimization study may be considered afterwards.

Both methods have been validated in studies, carried out for parameter optimization in scientific and industrial consortium of the Ad Proc Add project.

Aside of the parameter optimization, an intermediate workpiece treatment with hot isostatic pressing has been confirmed to be a considerable possibility to increase the relative density of the LPBF additively manufactured components.

6.4 Outlook

All carried out optimization studies have indicated, that the local circumstances, such as too narrow placement or process deviations along the shield gas flow, may affect the quality of the printed part in a negative manner. Thus, further investigations should be considered to better understand of these phenomena and develop an effective counteracting strategy.

Further on, an alternative reference value or a general calculation method should be considered for the estimation of relative densities of the powder materials. Since its manufacturer frequently only provide no information on the actual alloy density of the charge, or only the general alloy information, this fact

limits the applicability and result transparency of the developed method. As a short-term measure towards better transparency of the scientific results dealing relative density of the additively manufactured parts, the specification of the reference alloy density along with its estimation way should be considered.

7 Analysis of functionalizing process technology – Results of the IFT and FOTEC

D. Nikolaev https://orcid.org/0000-0003-3877-694X,

I. Yavuz

(TU Wien, Institute of Production Engineering and Photonic Technologies)

7.1 Introduction

In this work package, varying process parameters and their geometrical and thermomechanical impact on the printed parts has been investigated. Research is based on the part characteristics and process conditions including the respective process chains for the workpieces, which were manufactured during WP 2. Energy use for selected post-treatments was measured or estimated simultaneously.

7.2 Description of project results

7.2.1 Analysis of the abrasive flow machining (AFM) and hirtisation

Based on previous experience gained during the research project, a new demonstration part (see Figure 7-1) has been designed, containing different features and considering upcoming treatment. The part has been manufactured on behalf of the company IMR using AlSi10Mg powder material. Features on the outer side of the demonstration part are focused on investigation of design limitations for an SLM process on possible wall thickness, angles and hole diameters. The demonstration part consists of two halves, which provides a good access for optical and contact investigation of the treated surfaces of the inner channels in various shapes and dimensions. All inner channels are represented at least twice, which allows to optimize the treatment parameters.

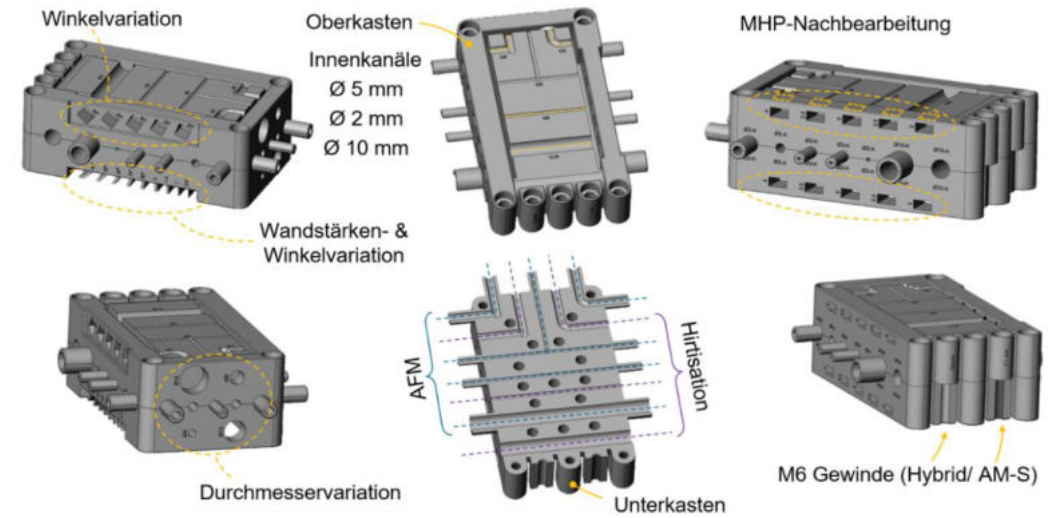

Figure 7-1: Demonstration part representing various embedded functionalities and applied post-processing steps.

All features have been aligned and defined in cooperation with the project partners. For instance, Bosch Rexroth designed a curved cooling channel for comparison with a conventional design with two connected boreholes. Also, tapping processes can be analyzed using the given demonstration part. Based

on the given designs, different post-treatment technologies and their impact on the features' integrity have been investigated (e.g., hirtisation, abrasive flow machining or machine hammer peening).

Compared to conventional manufacturing processes, additive manufacturing show various advantageous opportunities for design and production of complex parts. Using additive technologies, high complex free-form surfaces, thin-wall structures and very detailed features can be manufactured in a single manufacturing step. Additionally, new opportunities for design of cooling channels within the part are created, which can be used for new designs in regards of hydraulic and pneumatic control units, as well as for parts with special requirements to the heat dissipation efficiency.

Depending on the application, defined surface quality on inner cooling channels might be required. Currently there are just several specialized treatment methods, which are suitable for such complex geometry as inner cooling channels. Two such methods (see Figure 7-2) have been evaluated in course of the project: a novel hirtisation method and the abrasive flow machining (AFM) process.

Hirtisation is an electro-chemical discharge process, combined with hydro-dynamic abrasive flows, resulting in respective material removal on the features. Three different process stages allow to achieve different material removal rate and different process goals, such as removal of the remaining support structures of surface polishing.

For comparison, the abrasive flow machining (AFM) is using a viscous abrasive fluid flowing through the workpiece. However, no removal of support structures is possible using this technology.

Figure 7-2: Abrasive flow machining principle (left), surface appearance after three Hirtisation steps (right).

For comparison of the two processes, a demonstration part has been printed out of AlSi10Mg powder and heat treated afterwards. All cooling channels exist twice, and have been printed without supporting structures. Various diameters (3 mm, 5 mm and 10 mm) and finishing allowance of 300 µm have been used for the channels. A channel featuring 90° orientation change has been printed as well as machined conventionally. For utilization of hirtisation process, special fastening features had to be designed. For investigation, 28 measurement points have been defined to measure the cooling channels before and after the abrasive treatment. Surface roughness as well as 3D geometry measurements have been carried out. Figure 7-3 shows the demonstration part and illustrates the major features for the experiment.

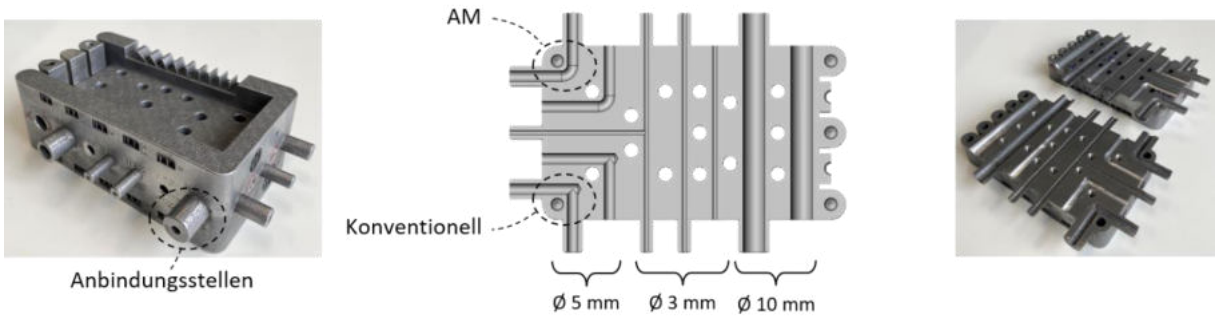

Figure 7-3: Example part featuring various cooling channels.

Surface texture (Sa) has been measured in the measurement points before and after the respective treatment. Figure 7-4 illustrates the measurement results for hirtisation process.

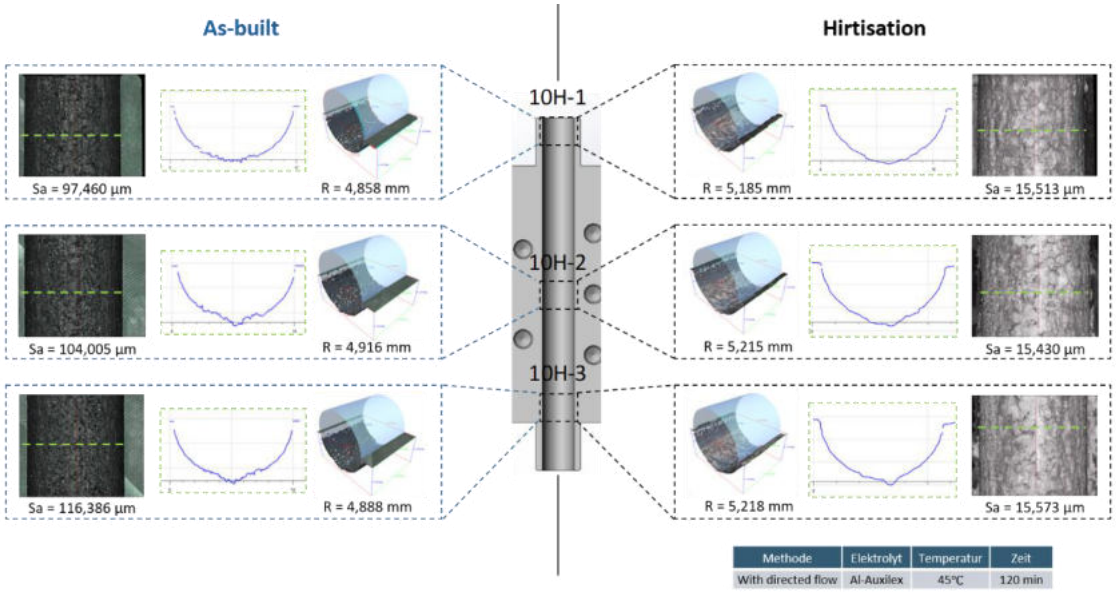

Figure 7-4: Optical measurement of the shape and surface texture of the ⌀10 mm cooling channel after hirtisation.

Comparing the two process technologies hirtisation and abrasive flow machining (AFM), it is shown that AFM achieves significantly better surface roughness of Sa=1-3 µm, than hirtisation (Sa=12 µm). Neither of the technologies was able to reach the targeted diameter tolerances. Due to suboptimal process parameter for AFM, the channel diameter after the treatment was exceeded almost twice. Investigations showed, that the final diameter, as well as the achievable surface quality after post-treatment, are strongly dependent to their initial condition in as-built state. The designed dimensions of the channels also weren't achieved in as-built state. A summary of the results is shown in Figure 7-5.

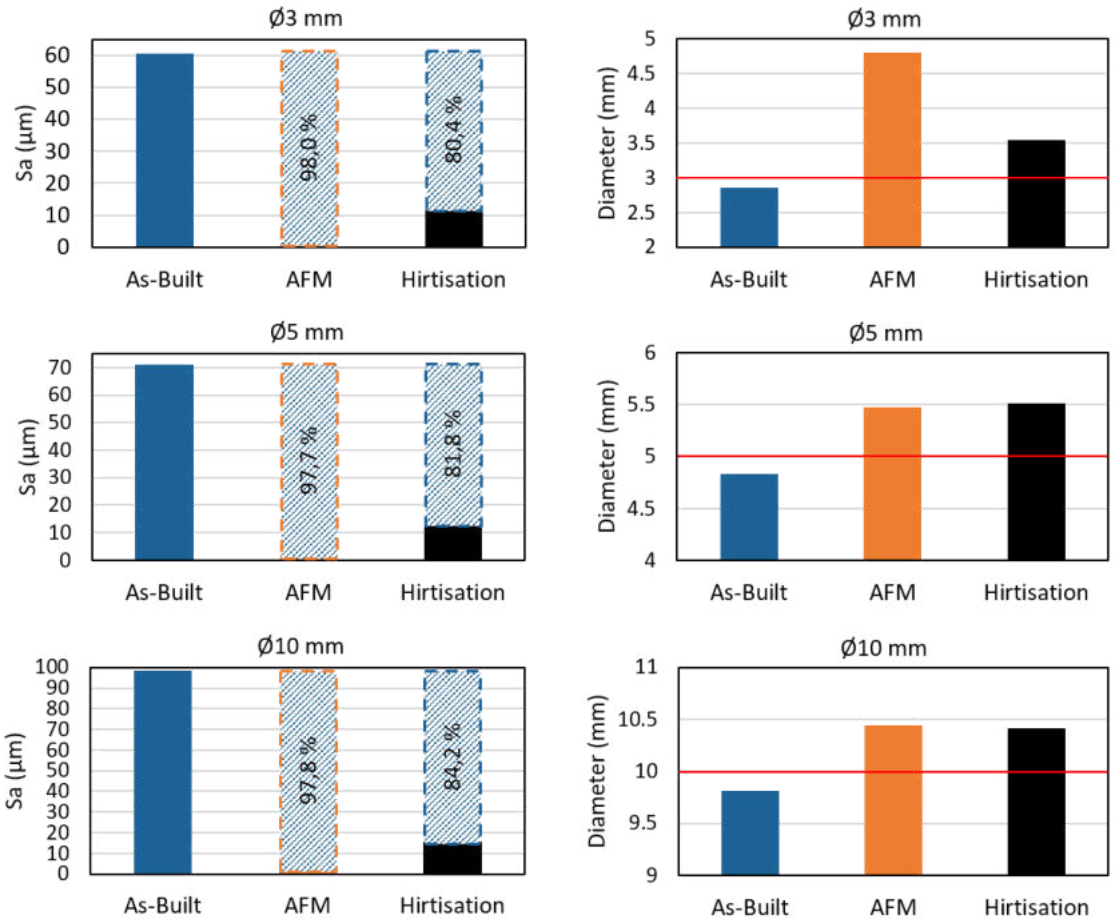

Figure 7-5: Summary of the AFM and hirtisation post-processing of the cooling channels.

The main results of the comparable study can be summarized as follows:

- Post-treatment with hirtisation process requires special fastening features ⌝ post-treatment is done within one setup.
- Hirtisation can be considered suitable for technical applications with highly complex shape and geometries of inner cooling channels and outer features.
- Abrasive flow machining cannot be applied for removal of support structures. Different diameters require different setups.
- Abrasive flow machining is especially advantageous in high-tech applications, when high polished inner channel surface is required.

Already mentioned design flexibility, applicable for additively manufactured parts, includes the possibilities for manufacturing threads additively instead of conventional tapping procedure. Different situations have been investigated, when an additively manufactured part features M6 screw threads and shall undergo an abrasive post treatment in order to identify the best possible option. Figure 7-6 illustrates the thread conditions:

1. When the borehole was manufactured additively and the thread was cut conventionally afterwards.
2. When the thread geometry was manufactured additively.

3. …and used once for joining purpose.
4. When conventionally manufactured thread undergoes a hirtisation treatment.
5. When additively manufactured thread undergoes a hirtisation treatment.

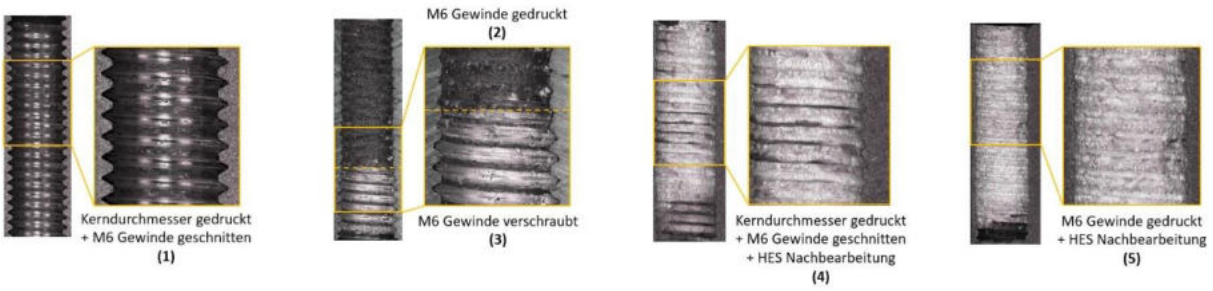

Figure 7-6: Results on treatment of the threads in AM parts. 1 – conventionally manufactured, 2 and 3 – additively manufactured in its final condition and joined once, 4 – conventionally manufactured after hirtisation, additively manufactured after hirtisation

Optical inspection shows, that the hirtisation treatment of the thread leads to complete removal of the thread profile (see Figure 7-6, pos. 4 and 5), disregarding the initial state or manufacturing method and thus should be avoided. Additively manufactured thread geometry may be insufficient detailed or have poor surface quality depending on the selected thread diameter, as for the case of an M6 thread additively manufactured in AlSi10Mg using the default process parameters (see Figure 7-6, pos. 2). However, if the necessary manufacturing allowance is still met, such “pre-manufactured” threads may undergo the conventional tapping procedure and can still be used for joining. The best possible results can be achieved, if only the borehole for the thread is manufactured additively and the thread is manufactured in a conventional way (see Figure 7-6, pos. 1). Profile metrics are summarized in Table 7-1.

#	Major diameter D_{maj}, mm	Borehole diameter D_{min}, mm	Pitch P, mm	Flank angle $2 \cdot \theta, °$	Profile heigh H, mm
nom.	6	5	1	60	0,541
(1)	6,067	5,039	1,00	58,91	0,538
(2)	5,432	4,941	0,987	84,82	0,369
(3)	5,968	5,088	1,028	58,88	0,427
(4)	-	-	-	-	-
(5)	-	-	-	-	-

Table 7-1: Measured and nominal screw thread M6 metrics.

7.2.2 Analysis of hirtisation parameter and resulting part properties

For the investigations of the Hirtisier process, the component ("benchmark part") was basically defined together with the company RENA Technologies Austria GmbH (formerly Hirtenberger Engineered Surfaces GmbH).

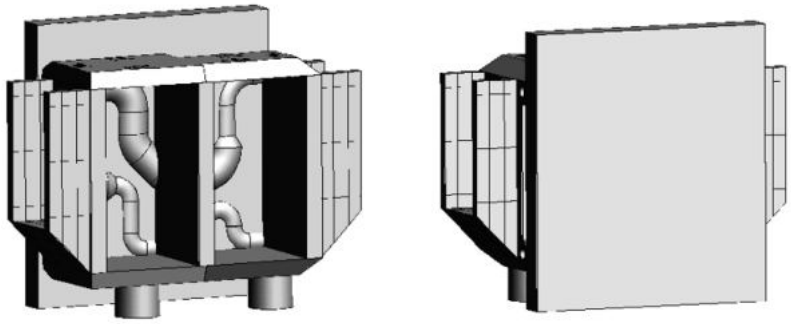

Figure 7-7: Use-Case Company RENA Technologies Austria GmbH („benchmark part").

This was designed within the framework of the use case (WP6) together with the company Rena and was primarily used for investigations of the material AlSi10Mg. However, for further analyses of the hirtisation process, tests were also carried out with Ti6Al4V and 1.4404 and 1.2709. A detailed consideration of 1.4404 and 1.2709 within a DOE could not be performed by FOTEC, as their hirtisation process does not include these materials. However, Rena, which already has process know-how for 1.4404 and 1.2709, was able to post-treat test parts by inkind services they brought into the project. So FOTEC was also able to determine the component properties that could be achieved here.

From the hirtisation process parameters previously defined in the project, the following DOE plans were derived for the AlSi10Mg and Ti6Al4V experiments (see the next two tables). For each of the samples defined in the plan, one process parameter was changed (in red) to consider its effects. The "reference" sample was used as the basis for the analysis.

Sample	Basin 1	Basin 2	Basin 3
	time / amperage / temperature	time / ~~amperage~~ / temperature	time / amperage / temperature
AlSi10Mg part #1 (reference)	**60 min / 80 % / 40 °C**	**15 min / ~~100~~ % / 21 °C**	**60 min / 80 % / 23 °C**
AlSi10Mg part #2	60 min / 100 % / 40 °C	15 min / ~~100~~ % / 21 °C	60 min / 80 % / 23 °C
AlSi10Mg part #3	60 min / 80 % / 40 °C	30 min / ~~100~~ % / 21 °C	60 min / 80 % / 23 °C
AlSi10Mg part #4	60 min / 80 % / 40 °C	15 min / ~~100~~ % / 21 °C	180 min / 80 % / 23 °C
AlSi10Mg part #5	60 min / 80 % / 40 °C	15 min / ~~100~~ % / 21 °C	180 min / 120 % / 23 °C
AlSi10Mg part #6 (cold built)	60 min / 80 % / 40 °C	15 min / ~~100~~ % / 21 °C	60 min / 80 % / 23 °C

Table 7-2: DOE-Plan Hirtisieren – AlSi10Mg.

Sample	Basin 1	Basin 2
	time / amperage / temperature	time / amperage / temperature
Ti6Al4V part #3 (reference)	**120 min / 80 % / 22 °C**	**15 min / 80 % / 22 °C**
Ti6Al4V part #4	**120 min / 80 % / 22 °C**	**15 min / 100 % / 22 °C**
Ti6Al4V part #5	**120 min / 120 % / 22 °C**	**15 min / 80 % / 22 °C**

Table 7-3: DOE-Plan Hirtisieren – Ti6Al4V.

For the investigation of the analysis aspects present on the benchmark parts (see next figure), with the exception of the support removal percentage (% support removal), the following measuring devices were defined:

- Alicona InfiniteFocusSL (measurement of edge radii and surface roughness).
- Faro Quantum M (measurement of allowance/material removal)

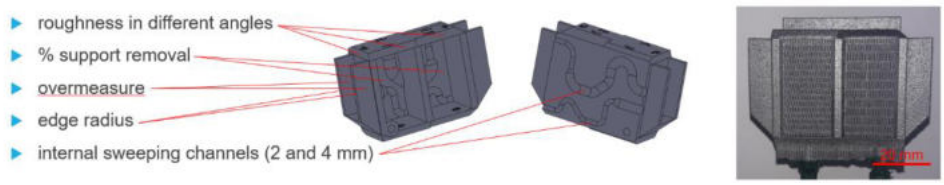

Figure 7-8: Analysis aspects on the benchmark part.

The support-removal was assessed visually from photographs.

In contrast to AlSi10Mg, the Ti6Al4V tests had to be carried out on samples printed by Schiebel Elektronische Geraete GmbH. The specimen design was provided by FOTEC. n principle, the use case components from company RENA would also have been planned here. However, this could not be implemented due to delivery difficulties at the University of Stuttgart (Institute for Machine Tools), triggered by the pandemic situation.

For the Ti6Al4V samples, the same measuring equipment as for AlSi10Mg was used to analyze the components.

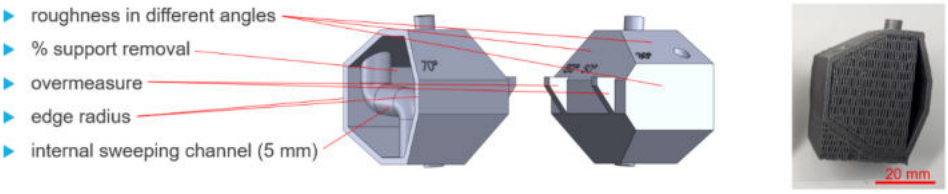

Figure 7-9: Analysis aspects on the samples printed by company Schiebel (part design from FOTEC).

According to the defined DOE plan, the use case components for RENA ("benchmark part") were 3D printed by FOTEC from AlSi10Mg and hirtisation tests were performed. The results were analyzed in terms of support removal, material removal (necessary allowance), surface smoothing (inside and outside) and edge radius. Finally, tensile specimens were fabricated and treated by hirtisation to investigate mechanical properties. These samples were tested in as-built condition and after hirtisation.

In addition, hirtisation tests were performed by FOTEC on the Ti6Al4V specimens (manufactured by Schiebel), and by RENA on 1.4404 specimens (manufactured by ISF) and 1.2709 specimens (manufactured by GFE). The treated specimens were also analyzed at FOTEC for necessary allowance, surface smoothness, edge radius and mechanical characteristics (tensile test).

The results for all these tests are shown below.

AlSi10Mg

The support removal was documented with a photo after each treatment basin. The amount of support left behind in each case was marked in red in Paint.net (version 4.2.14) (see next Figure). Based on the covered area in relation to the originally covered area, a statement about the support removal percentage could be made.

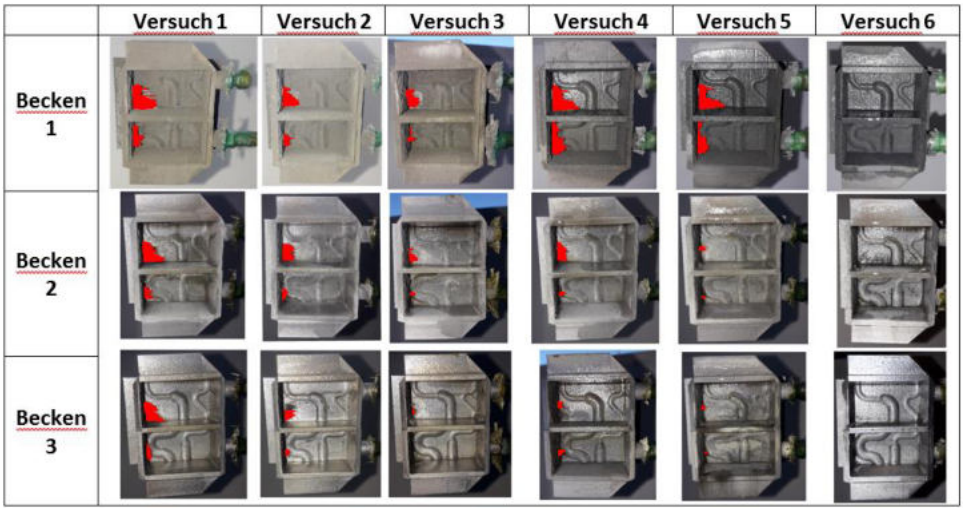

Figure 7-10: Determination support removal.

An important finding in the investigations on support removal was that printed samples with minimum build platform heating (cold-built, 45 °C) could be removed significantly better than printed samples with maximum build platform heating (hot-built, 200 °C). For material removal and edge radius, cold-built samples also showed better results (lowest material removal and low edge radius).

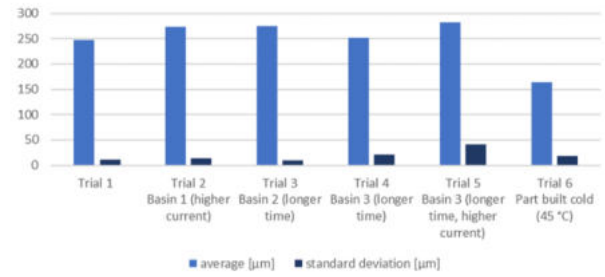

Figure 7-11: material removal.

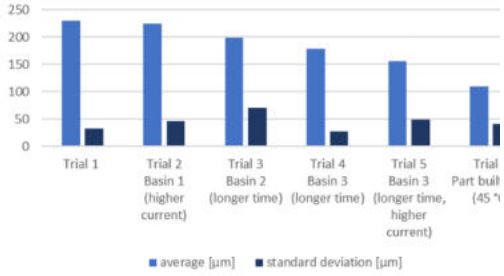

Figure 7-12: edge radius.

Despite a relatively inhomogeneous initial roughness (10-30 µm Sa) of the as-built upskin, surfaces with a angle between 25° and 90° could be smoothed significantly (6-10 µm Sa) in almost all tests.

The high roughnesses at 0° result from the fact that the melt paths cannot be completely leveled during etching. At 10°, the high roughnesses result from the staircase effect, which can even be intensified, as in trial 6 for AlSi10Mg.

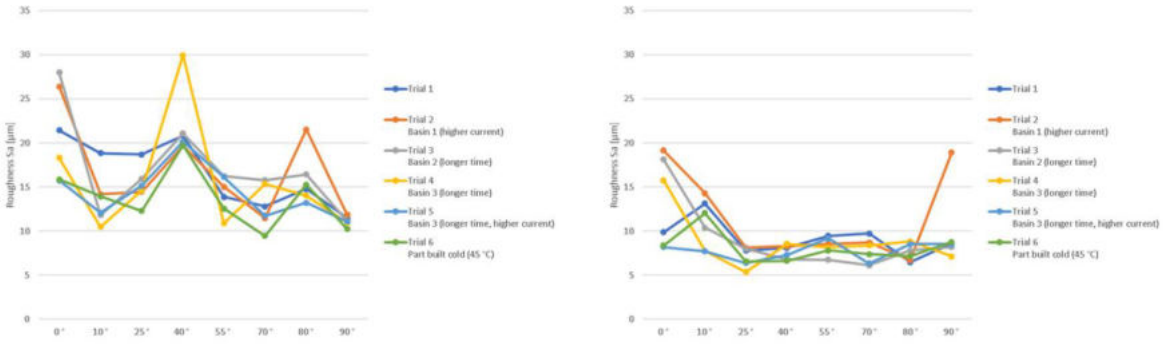

Figure 7-13: Roughness (Sa) Upskin surfaces and vertical surfaces (90°) - Trials 1-6 (left: as-built, right: after hirtisation).

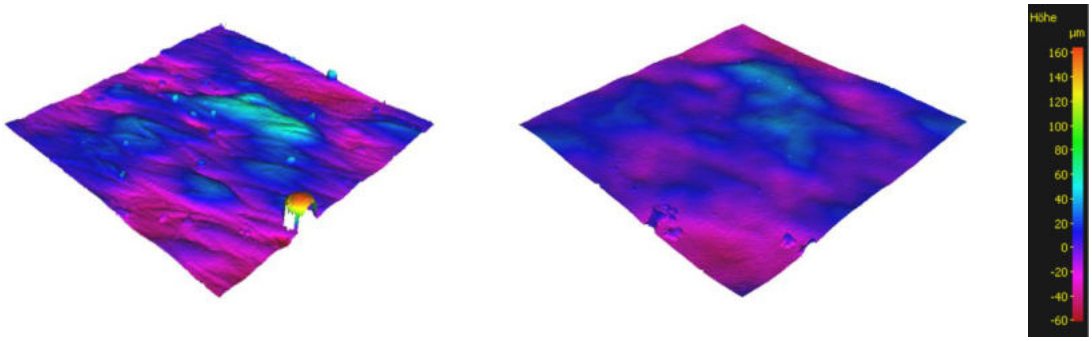

Figure 7-14: not completely leveled melt pool lines at 0 ° (left: as-built, right: after hirtisation) based on test 6.

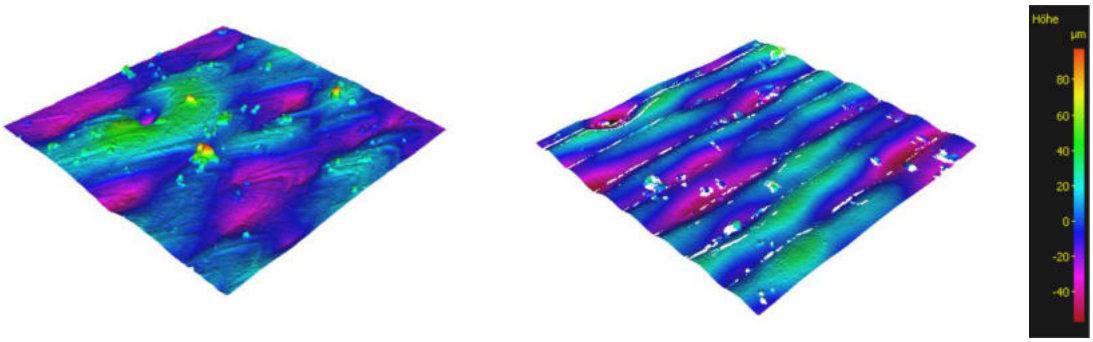

Figure 7-15: increased staircase effect at 10 ° (left: as-built, right: after hirtisation) based on test 6.

For unsupported downskin surfaces (45°- 80°), roughnesses about < 30 µm, could generally be achieved. For the cold-built specimens, the lowest as-built roughnesses could be achieved. With hirtisation, results of 17 µm Sa at 45° and below 10 µm Sa at 55° - 80° could be achieved.

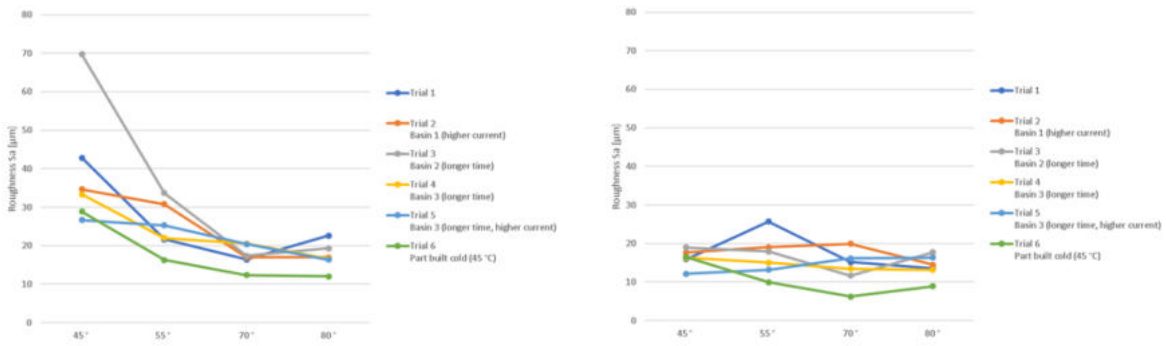

Figure 7-16: Roughness (Sa) downskin surfaces without support - tests 1-6 (left: as built, right: after hirtisation).

With regard to internal channel roughness, except for the tests with longer treatment times in the basins, 3 times roughnesses of less than 10 µm Sa are shown.

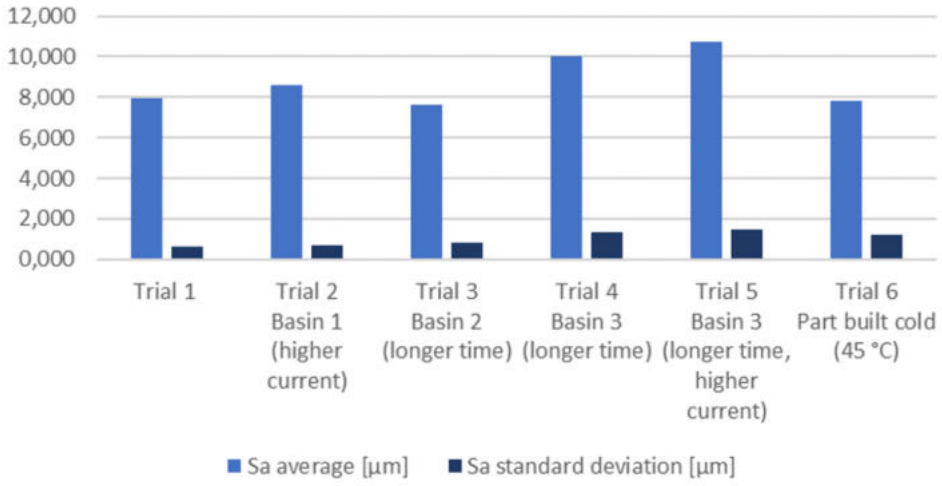

Figure 7-17: Inner channel roughness.

The inner channel roughness measurement points are exemplarily shown for Trail 1 in the figure below.

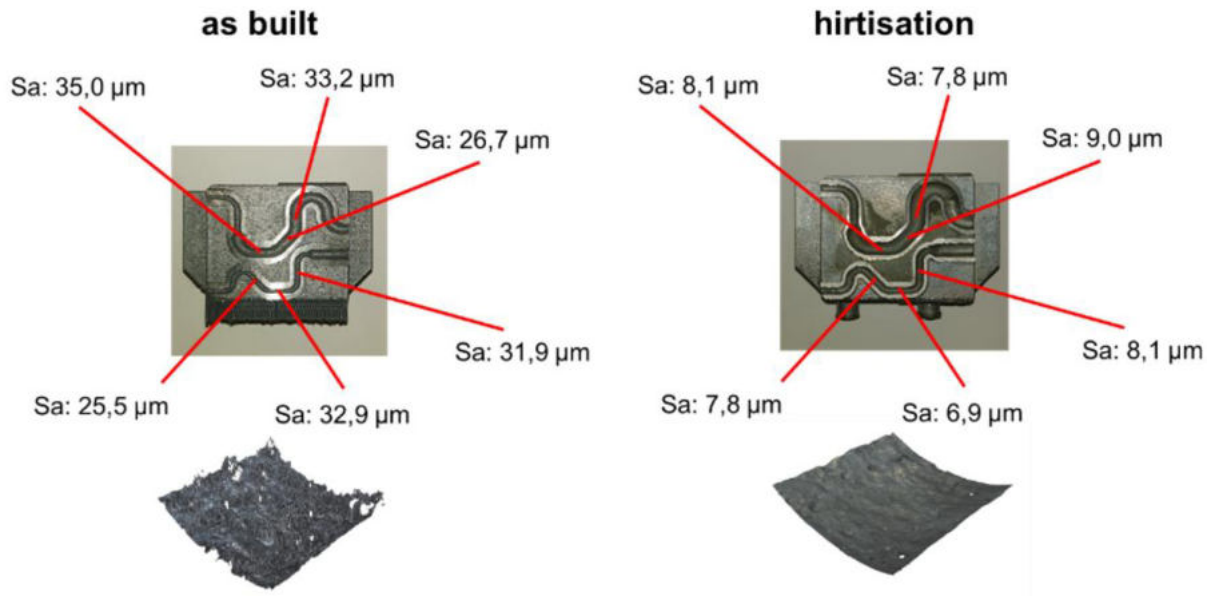

Figure 7-18: Comparison of internal channel roughness on as-built components and components after hritisation (test 1 exemplary).

Ti6Al4V

Based on the hirtisation results, the following effects of the process settings are apparent:

- Higher support removal at higher current in basin 1 (see part #5).
- No significant effect of different treatment currents on Sa roughness or edge radius detected
- Good smoothing of melt pool lines for horizontal surfaces (0 °, see Figure 2-13)
- Heat treatment in as-built condition on not completely de-powdered samples can cause powder aggregates and thus a reduction of support removal

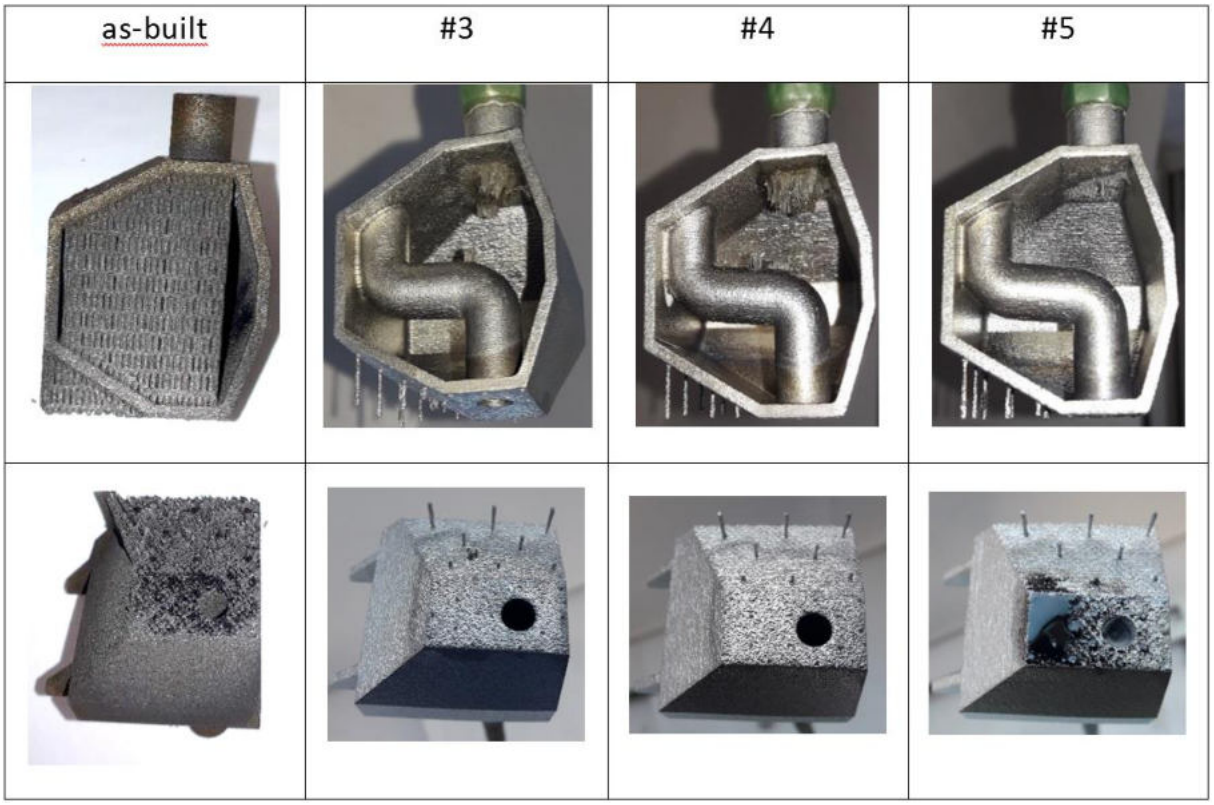

Figure 7-19: support removal Ti6Al4V.

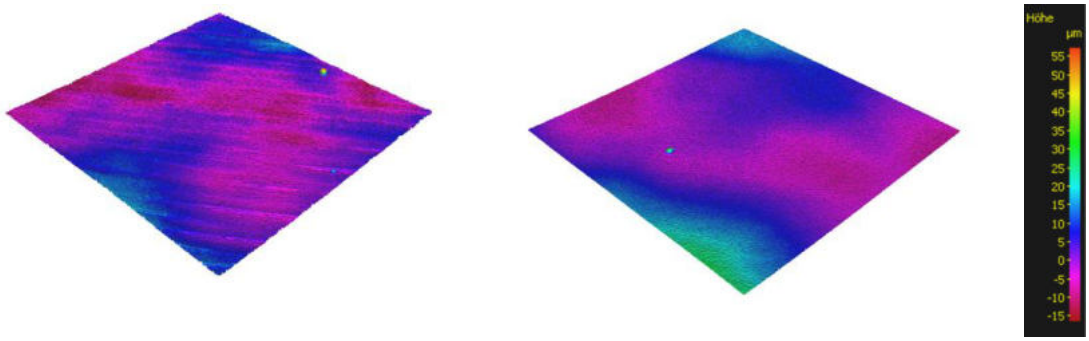

Figure 7-20: Smoothing on horizontal surfaces Ti6Al4V.

1.4404

With regard to 1.4404, ISF first had to develop suitable support geometries that would enable components to be printed without defects.

At the University of Dortmund, Institute for Machining Technology (ISF), the printing tests of the support geometries were carried out. Finally, a sample with optimized support geometries was manufactured for hirtisation.

Company RENA carried out the hirtisation tests (in-kind service). Based on their know-how, the parameters were adjusted in such a way that the complete support (with exception of the cone support) could be removed and the surface optimally smoothed.

Figure 7-21: Development stages of support geometries 1.4404.

Figure 7-22: Samples 1.4404 (left: as built, right: after hirtisation).

1.2709

The samples from 1.2709 were printed at GFE (Gesellschaft für Fertigungstechnik und Entwicklung Schmalkalden e.V.). The hirtisation was performed by company Rena (in-kind service).

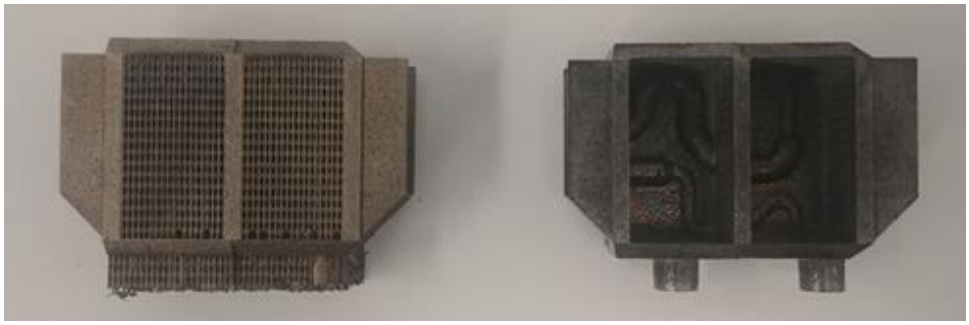

Figure 7-23: Samples 1.2709 (left: as built, right: after hirtisation).

Summary of hirtisation results

The overall results determined for the hirtiation tests, such as the necessary allowance, feasible edge radius and achievable surface roughness, based on as-built properties, can be summarized in general terms as follows. The data are based on exemplary results of the respective promising component treatment parameters of the series of measurements at FOTEC.

		as-built				Hirtisation			
	Angle [°]	AlSi10Mg (50 µm)	1.4404 (30 µm)	Ti6Al4V (60 µm)	1.2709 (50 µm)	AlSi10Mg (50 µm)	1.4404 (30 µm)	Ti6Al4V (60 µm)	1.2709 (50 µm)
Allowance [µm]	90	-	-	-	-	164	547	183	316
Allowance Standard Deviation [µm]	90	-	-	-	-	18	9	2	16
Edge radius [µm]	90	281	115	135	80	171	43	66	107
Edge Radius Standard Deviation [µm]	90	62	11	42	16	51	10	29	12
Sa roughness upskin [µm]	0	16	18	4	18	8	5	2	17
	10	14	22	-	24	12	29	-	29
	25	12	24	-	26	7	18	-	32
	30	-	-	26		-	-	13	-
	40	20	24	-	20	7	6	-	9
	45		-	-		-	-	-	-
	50		-	41		-	-	14	-
	55	13	11	-	10	8	8	-	4
	70	9	9	15	7	7	5	7	2
	80	15	9	-	10	7	4	-	4
	90	10	7	11	8	9	4	5	4
Sa roughness downskin [µm]	80	12	supported	-	11	9	25	-	8
	70	12	supported	20	18	6	28	11	5
	55	16	supported	-	24	10	16	-	23
	50	-	-	39		-	-	16	-
	45	29	supported	-		16	8	-	37
	40	supported	supported	-	62	48	18	-	39
	30	-	-	supported			-	32	-
	25	supported	supported	-	56	92	21	-	54
	10	supported	supported	-	supported	69	19	-	63
	0	supported	supported	supported	supported	44	8	24	-
Sa inside 4 mm channel [µm]	90	32	10	-	13	8	3	-	9
Sa inside 2 mm channel [µm]	90	30	8	-	12	7	7	-	11
Sa inside 5 mm channel [µm]	90	-	-	13		-	-	6	

Table 7-48: Summary results (AlSi10Mg - parts 9-1 and 9-2, 1.4404 - parts 1b and 2b, Ti6Al4V - parts 2 and 3, 1.2709 - parts 1 and 2).

In addition to the necessary allowance and edge radius (as-built and hirtized), the table above also shows the as-built and hirtisation roughnesses determined depending on the surface angle (0°= horizontal, 90°= vertical, upskin and downskin), so far as these surfaces were accessible for measurement or these geometries were present on the specimen. The results show that the hirtisation process reduced the edge radius of all materials (down to 1.2709) and lowered the overall surface roughness. The upskin surfaces at 10° have to be evaluated critically, because a certain roughness remains due to the staircase effect structures.

In addition, the table shows roughnesses of the internal channels as-built and after hirtisation in comparison. Here, the vertical region of the circular channel was used for the roughness analysis. It can be seen that the external roughnesses in the hirtisation state (despite partially higher as-built roughnesses as with AlSi10mg) can also be achieved in the channels if the channels are not too narrow (compare the hirtized roughnesses at 90° and in the channel "Sa inside..." with AlSi10Mg = blue and Ti6Al4V = orange).

In the case of 1.4404 (=green), it can be seen that the 2mm channel in the hirtisation state shows no roughness reduction, which suggests that it is already too narrow for hitrisation (compare also the data 90 ° and in the channel "Sa inside..."). In the case of 1.2709, both channel diameters are probably already too small for an optimum hirtisation treatment on the basis of this comparison.

Tensile tests

In the following, the comparisons of the tensile test results in the as-built condition and after hirtisation are shown.

For AlSi10Mg and 1.2709, there are hardly any relevant differences between as-built condition and after hirtisation. For Ti6Al4V, the hirtisation samples show a slightly higher yield strength and reduced elongation at break. Hirtisation results in a significant reduction of the Young's modulus for 1.4404, but a higher elongation at fracture.

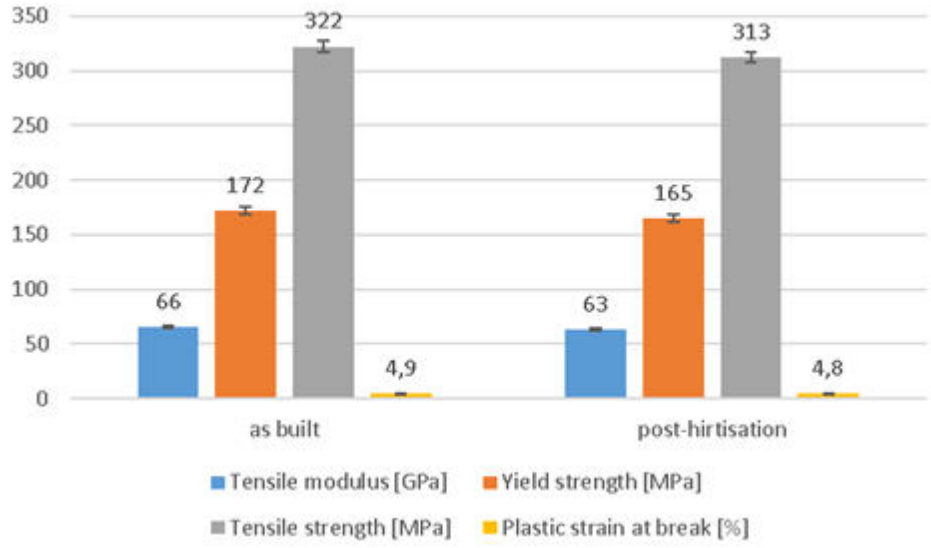

Figure 7-24: Results tensile tests AlSi10Mg.

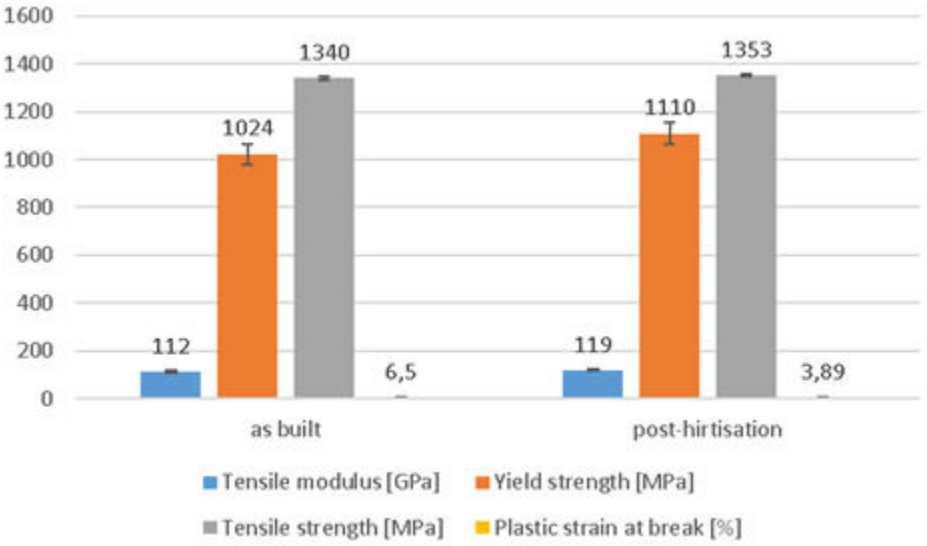

Figure 7-25: Results tensile tests Ti6Al4V

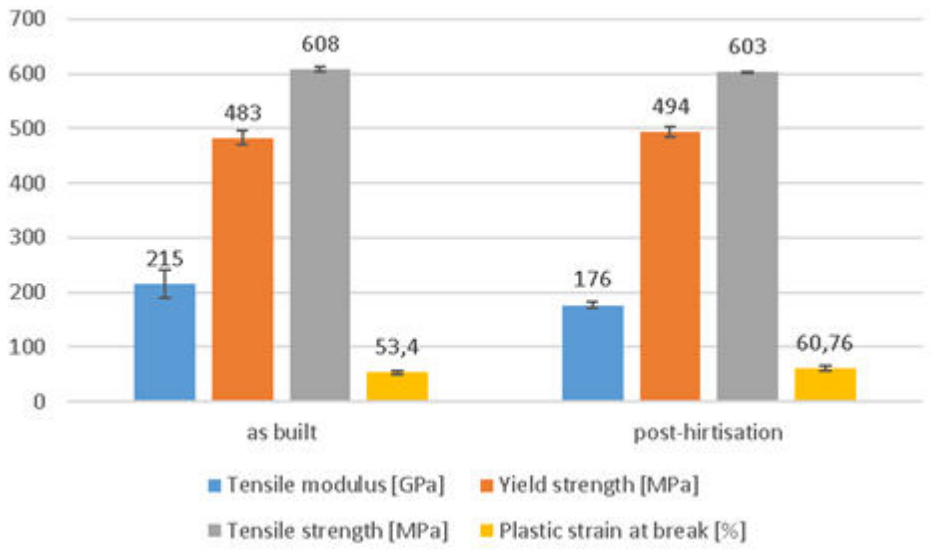

Figure 7-26: Results tensile tests 1.4404.

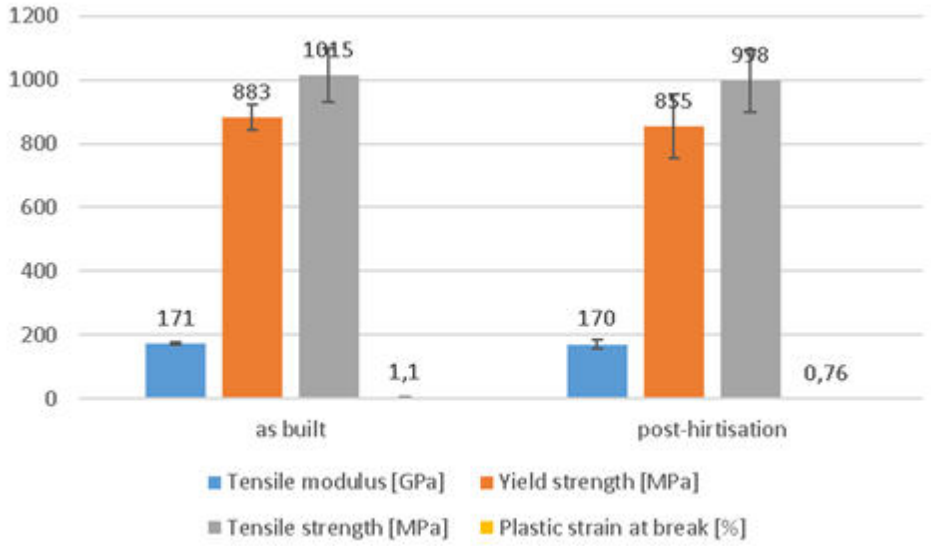

Figure 7-27: Results tensile tests 1.2709.

Hirtisation Usecases

Based on the analysis of the hirtisation parameters and resulting part properties some usecases were carried out, which are briefly described in the following section.

For company Rena, the use case currently shown in Figure 7-, a benchmark part for deriving hirtisation parameters for new materials, was developed, printed from AlSi10Mg and intensively tested at FOTEC. The results of the tests have already been shown in the previous sections.

In the course of the project, company RENA also performed hirtisation treatments as in-kind services for the following parts:

- AlSi10Mg, 1.4404, 1.2709, benchmark parts.

- AlSi10Mg, 1.4404, 1.2709, Ti6Al4V - tensile specimens

- Buhler usecase component (dough pourer)

- Testfuchs usecase part (flame arrestor)

As described in the previous section hirtisation tests were also carried out for Schiebel on the test components made of Ti6Al4V (see Figure 7-9) in order to determine suitable parameters for hirtisation of their usecase "Injector Housing".

Figure 7-28: Injector Housing as-built.

The use case printed at Schiebel was treated by hirtisation at FOTEC. The majority of the support structures could be removed by the process and adhering powder was removed from the channels.

Figure 7-29: Injector Housing after hirtisation.

For Bühler, the main components of a dough pourer with internal channels were designed for 3D printing. The design was then 3D printed from 1.4404 at ISF (University of Dortmund), the internal channels were smoothed by hirtisation at RENA, and functional surfaces were finished by milling.

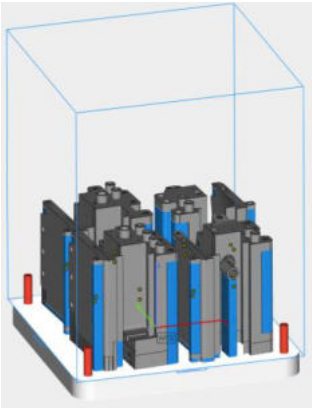

Figure 7-30: Bühler dough pourer components - print job.

Concerning Testfuchs a support concept for their usecase “flame arrestor” was developed. The component was then 3D printed from 1.4404 at ISF (University of Dortmund) and the hirtisation was carried out at company RENA.

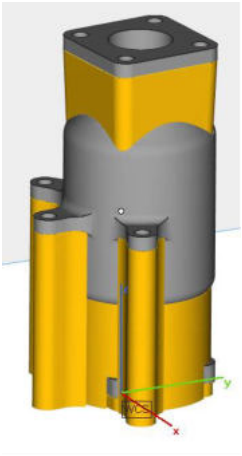

Figure 7-31: Flame arrestor Design with supports.

Figure 7-32: Flame arrestor 3D-printed.

7.2.3 Analysis of the micro finishing

Functional surfaces of a part might have the requirements on maximal surface roughness. In case if surface roughness about Ra (or Sa) = 1 µm is specified, the micro finishing manufacturing steps, such as lapping, must be applied to these surfaces.

In course of the investigation on lapping as a functionalizing process for additively manufactured parts, the 30 x30 mm cylindrical specimens with a pre-built inner borehole were manufactured by all scientific consortia partners on their SLM machines using the default SLM process parameters, recommended by the machine manufacturer. The top surface of these specimen was first grinded, then polished and lapped prior to the optical investigation of achieved surface quality. Two-dimensional surface quality metrics, arithmetical mean height (Sa) and root mean square height (Sq) were chosen for result evaluation.

A very smooth, reproducible and uniform surface has been achieved for specimens manufactured out of Ti6Al4V and 1.4404 powders (see Figure 7-33). Two titanium specimens, B1 and B4, were excluded

from further investigation because of the large diagonal cracks, which were exposed after the grinding operation.

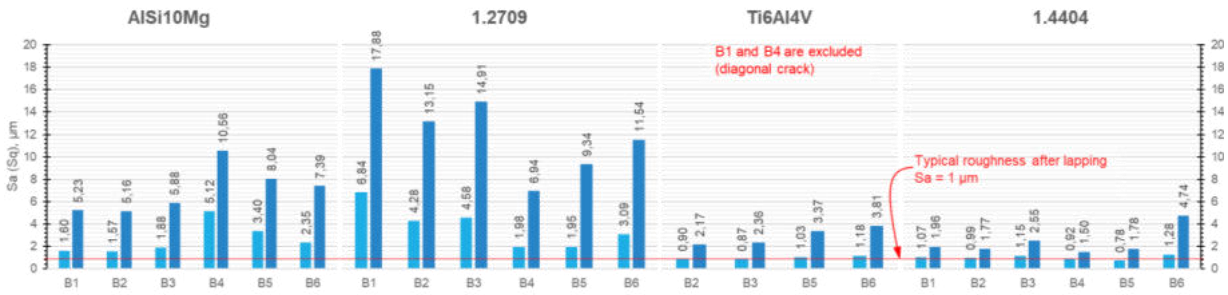

Figure 7-33: Overview lapping results for all materials [7].

Remarkable poor surface quality, achieved for specimen out of AlSi10Mg and maraging steel powder 1.2709 (see Figure 7-33), is related to highly porous core material of the specimen (hatch area). Since the lapping procedure requires a preparatory grinding operation with much coarser abrasive particles, these particles may be trapped inside exposed pores and transferred to the next manufacturing step, where finer abrasive particle are used. Especially during the lapping, where these particles are transported with a fluid, the extraction of the trapped coarse abrasive particles can occur, leaving the scratches and grooves on the polished surface. Long lateral scratches, which start in the exposed pores (see Figure 7-34) illustrate the described phenomenon.

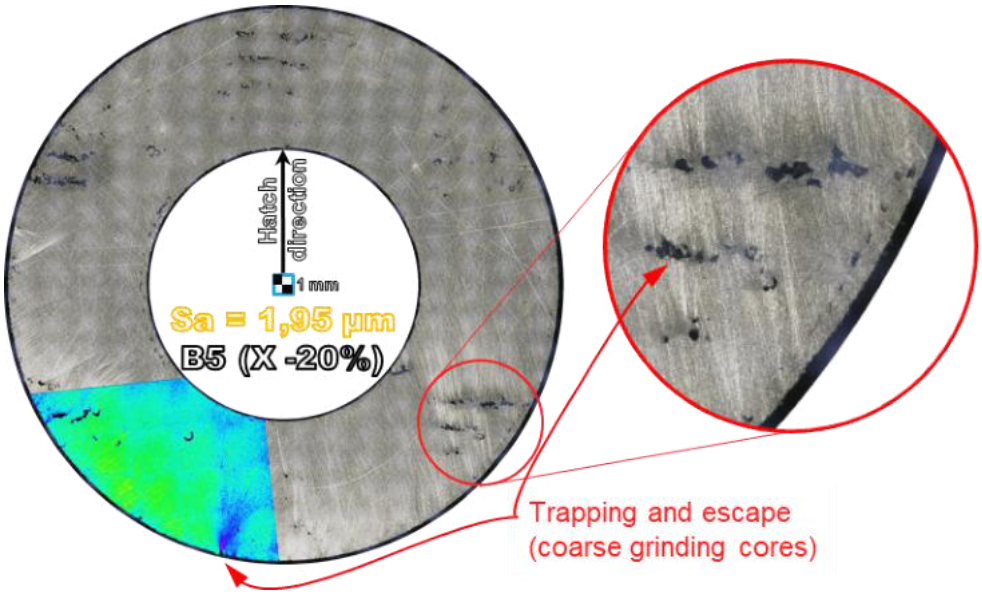

Figure 7-34: Surface micrograph of a specimen made of 1.2709 after lapping [7].

Furthermore, the micro finishing surface treatment reveals the occasional material porosity, which can occur between boundary layers and hatch area, since these seams aren't usually exposed simultaneously. This kind of porosity has been observed for each specimen disregarding, which powder of which machine has been used, and thus can be considered as a common issue. As a possible countermeasure against the sub-skin porosity, the variation of the margin between boundary and hatch laser tracks was investigated in course of this project and in context of micro finishing.

For the SLM process parameters, recommended by the machine manufacturers, the margin is set equally to the laser spot diameter. This value was considered as a reference and was varied in a range of ±20 %. The investigation was carried out only for stainless-steel and titanium specimens, which showed no or only minor porosity in core material and overall good surface quality after lapping (compare Figure 7-33).

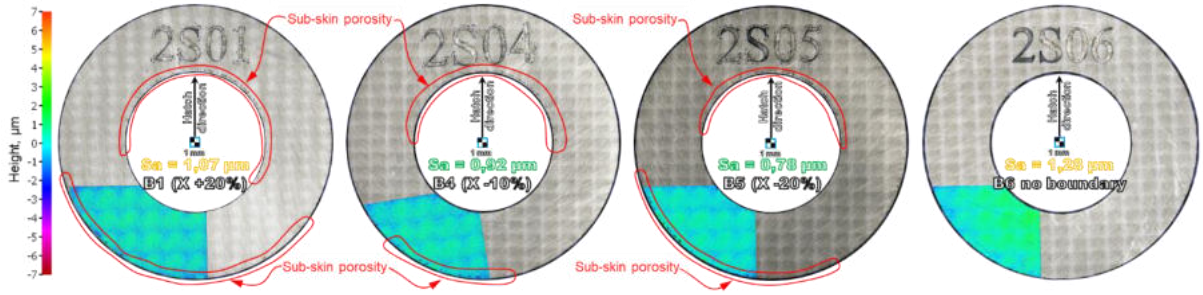

Figure 7-35: Sub-skin porosity distribution in specimens made of stainless-steel 1.4404 [7].

Figure 7-35 illustrates results for 1.4404 specimens. Neither occurrence nor morphology of the sub-skin porosity is found to be affected by the margin variation. For the specimens made of stainless-steel 1.4404 powder especially in the areas, where the laser tracks of the hatch begin or end (see Figure 7-35 bottom and top specimen side respectively), sub-skin porosity has been observed. Thus, the workpiece geometry optimization towards the sub-skin porosity minimization is also expected to be ineffective.

Either the manufacturing without boundary tracks or mechanical post-treatment targeting the pore's compression as described in chapters “

Hot Isostatic Pressing (**HIP)**" and "Analysis of ultrasonic assisted machining and machine hammer peening" should be considered in case if the sub-skin porosity is an important issue.

An overall applicability and respective good surface quality were confirmed for lapping of additively manufactured parts.

7.2.4 Analysis of ultrasonic assisted machining and machine hammer peening

Ultrasonic assisted machining of LPBM parts

Vibration assisted machining (VAM) and ultrasonic assisted machining in particular, are known to be advantageous for machining of materials, which tend to produce long flow chips since they can be broken apart and evacuated from cutting zone much easily without leaving damage on the machined surface. One further advantage of the VAM, which is related to the size of chips, is the recycling possibility. Smaller chips could be easier compressed into rods and used as raw material for stir friction additive manufacturing. Till now the investigations on this technology were limited to conventionally manufactured parts and respective materials only. Investigations on VAM in course of this project pursue the goal to evaluate the applicability of this technology to the additively manufactured components and related materials. For instance, the drilling operation and respectively Vibration Assisted Drilling (VAD) were investigated.

Two commonly used for SLM alloys were taken into account: a 1.2709 maraging steel and AlSi10Mg. Cylindrical specimens were manufactured in vertical and horizontal orientation relative to the Z build direction. A two staged drilling operation should be performed with and without vibrational assistance, including an initial drilling operation with ⌀8 mm drill and a drill out operation with ⌀12 mm drill. However, the vibration assisted drilling with a ⌀12 mm drill was cancelled because of the hardware limitations on the side of magnet bearings of the spindle.

Reference drill experiments in AlSi10Mg without VAD (see Figure 7-36 top row) have shown, that this material, being brittle, do not tent to produce long chips. Nevertheless, their size and shape were affected by VAD in the same manner for specimens additively produced in vertical and horizontal orientation. Moreover, the cutting force was found to be about 3 times lower for drilling with vibrational assistance.

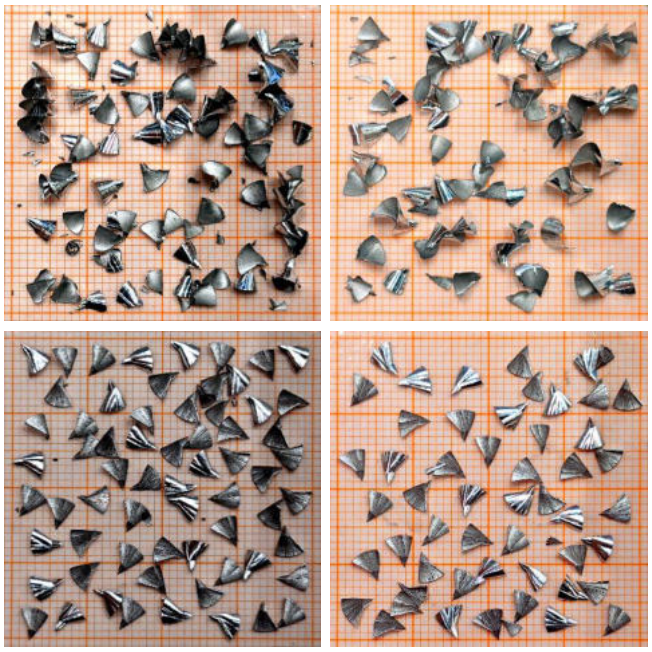

Figure 7-36: Chips produced by the drilling operations without and with VAD (top and bottom rows respectively) in vertically and horizontally (left and right columns respectively) additively manufactured specimens out of AlSi10Mg powder [8].

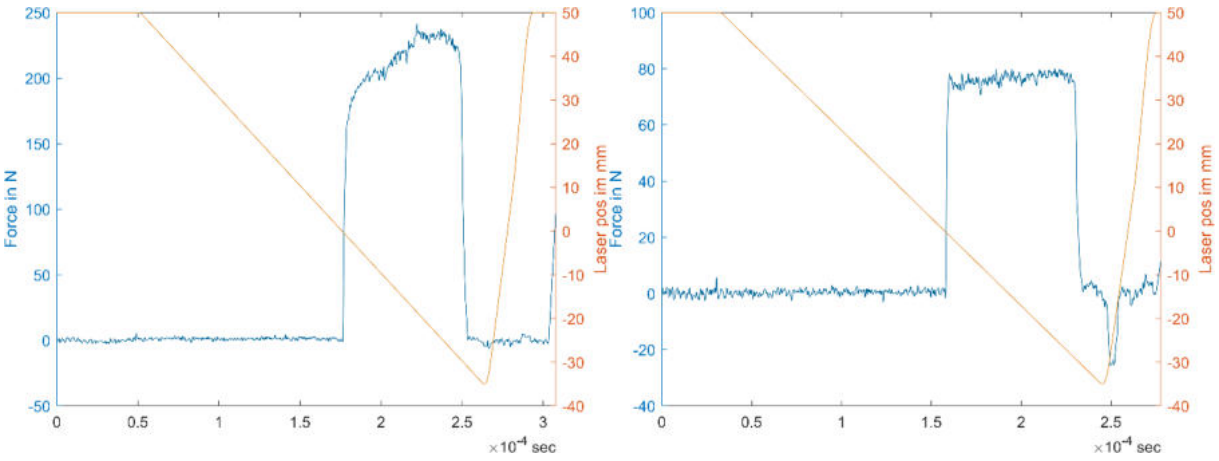

Figure 7-37: Cutting force during a conventional (left) and VAD operation (right) in AlSi10Mg [8].

For the maraging steel alloy 1.2709 the importance of the chip segmantation is more obvious, since this material tends to produce long flow chips during machining in a conventional way. Application of the VAD led to uniform chip form and size (see Figure 7-38). Again, no differences have been found for machining specimens, built vertically or horizontally. Also in this case a cutting force reduction by 30 % compared to the conventional drilling operation has been observed (compare Figure 7-39).

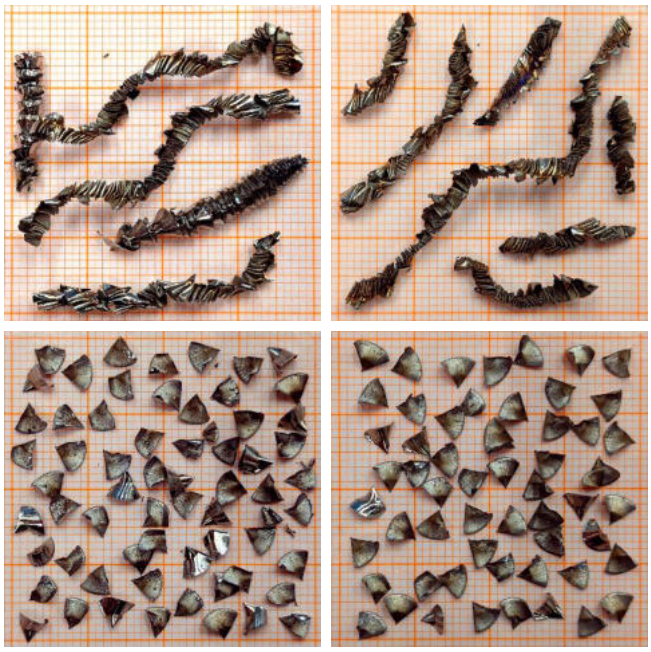

Figure 7-38: Chips produced by the drilling operations without and with VAD (top and bottom rows respectively) in vertically and horizontally (left and right columns respectively) additively manufactured specimens out of 1.2709 powder [8].

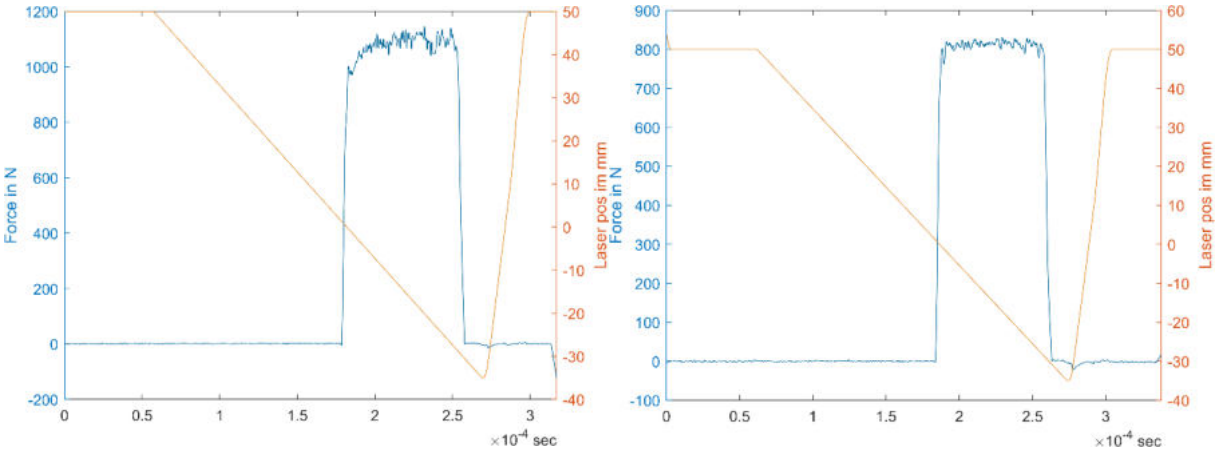

Figure 7-39: Cutting force during a conventional (left) and VAD operation (right) in 1.2709 [8].

Thus, the applicability of the vibration assisted drilling to the additively manufactured parts has been confirmed and suggested for application on additively manufactured parts.

Machine hammer peening of LPBM parts

In course of the project machine hammer peening has been investigated as a possible treatment of additively manufactured parts. Surface texture by the means of its arithmetical mean height (Sa) was chosen as a key performance indicator for a MHP treatment for parameter optimization study. Square specimen 50 x 50 x 10 mm (component 3) were manufactured in vertical and horizontal orientation by scientific partners in consortium. Both steel alloys, 1.2709 and 1.4404, and AlSi10Mg powder available in consortium were taken into account. Each of the specimen features four fields treated using different MHP process parameters, feedrate v, stroke amplitude h and impactor head diameter d.

Figure 7-40 represents the results achieved for specimen made of AlSi10Mg alloy. Due to the hatch segmentation, which is exposed on the top surface in case of horizontally built specimens, worse initial

conditions for MHP treatment were given for those specimens. Since the initial condition of the surface is important for the results of the MHP treatment, the achieved Sa values were almost two times worse compared to the vertically built specimens.

Regarding to the process parameters, better surface quality has been achieved if bigger impactor head, shorter stroke amplitude and higher federate parameter were applied, which indicates a good machinability of the AlSi10Mg.

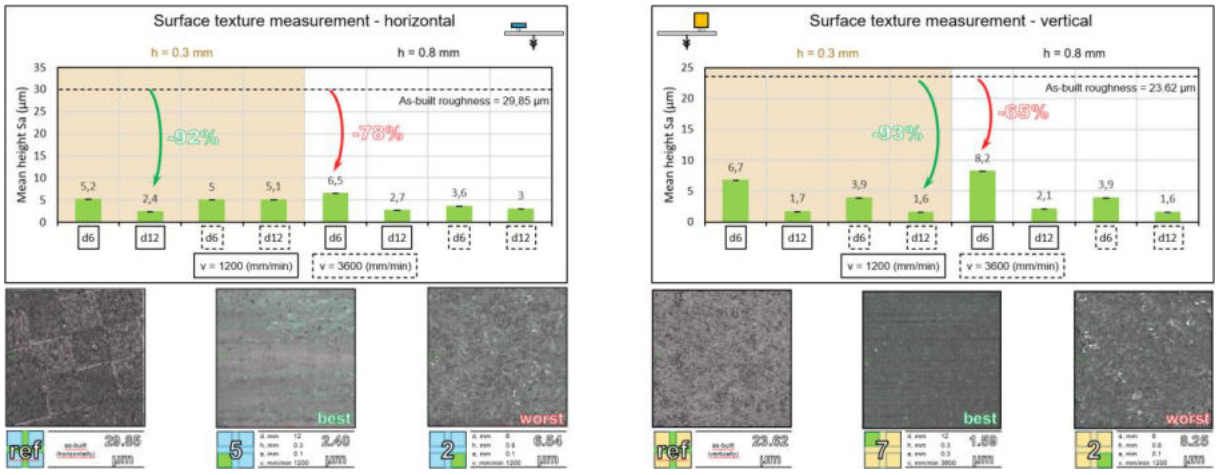

Figure 7-40: Results of the MHP treatment of AlSi10Mg specimens.

Results for specimens, made of stainless-steel powder 1.4404, are shown on Figure 7-4128. The best surface quality among all experiments (Sa=1,09 µm) could be archived for this material with MHP treatment, which indicates its excellent machinability. Favorable MHP process parameters for treatment of 1.4404 parts are found, when using bigger impactor head and slower feedrate, while the stroke amplitude seems to have less impact on the resulting surface quality in this case.

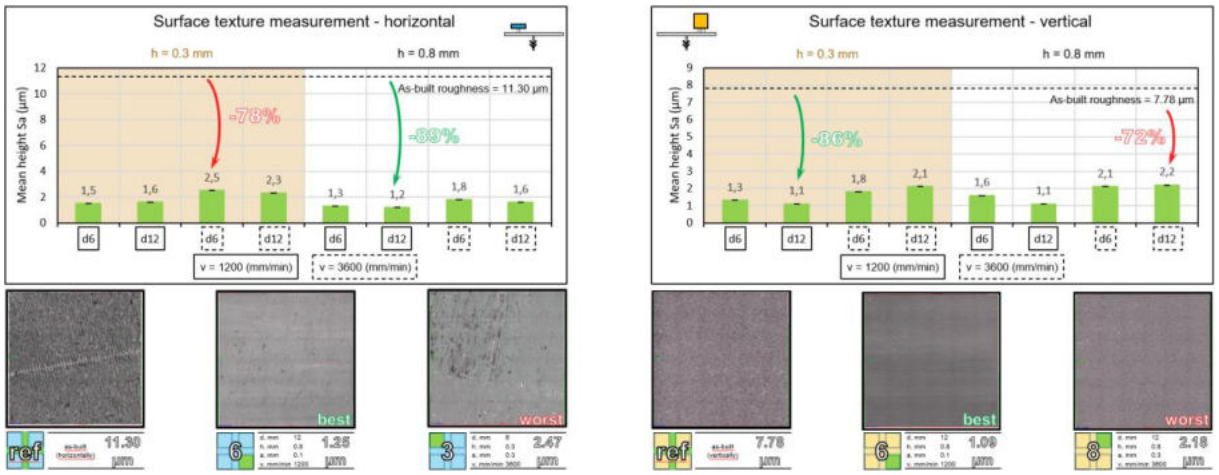

Figure 7-4128: Results of the MHP treatment of 1.4404 specimens.

Figure 7-42 shows the results of MHP treatment on specimens made of maraging steel 1.2709. Since in every experiment only default SLM parameters were used for specimen manufacturing, which cause high core material porosity in case of 1.2709, a poor initial condition of the surface was found for these

specimens. Exposed pores and their boundaries were clearly observable after MHP treatment, especially for horizontally manufactured specimens, thus this data is less reliable regarding to the treatment efficiency or optimal parameters for MHP. However, the vertically built specimen with better initial surface roughness of Sa = 9,55 µm show the roughness reduction by at least 52 % after MHP treatment.

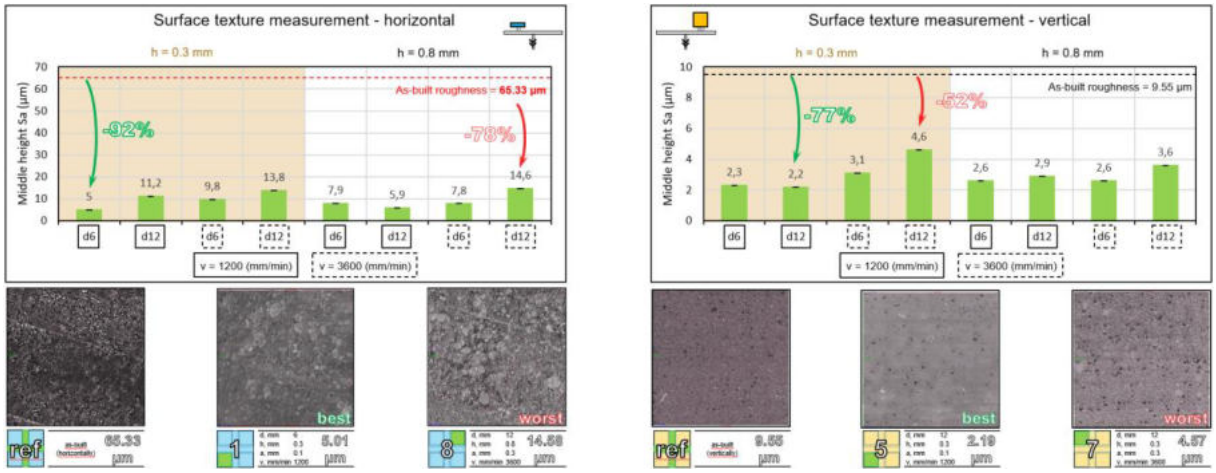

Figure 7-42: Results of the MHP treatment of 1.2709 specimens.

In all experiments, good surface smoothening results have been achieved due to MHP treatment of the additively manufactured specimens. The arithmetical mean height of the treated surface could be reduced by at least 52 %, and under the optimal circumstances by 93 %, compared to the as-built condition. Thus, machine hammer peening can be recommended as treatment for function surfaces of the LPBF manufactured parts.

Use-case IMR – Machine hammer peening

Further complementary investigation of MHP treatment of LPBF manufactured parts was carried out on behalf of the company IMR on the demonstration part made of AlSi10Mg powder and described previously. An important aspect for a surface treatment, which is based on the principle of plastic surface deformation, is the minimal material thickness underneath. Thus, two experiment series, one with ⌀12 mm impactor head and another with ⌀6 mm impactor head was carried out on both halves of the demonstration part, where the material thickness was varied from 4 to 2 mm as shown on the Figure 7-43 in order to estimate the necessary material thickness for MHP treatment without damage for the part.

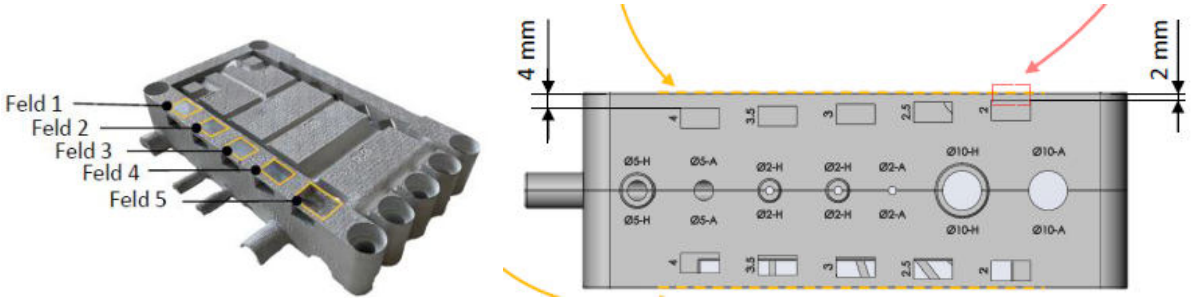

Figure 7-4329: Experiment design for estimation of the minimum required materiel thickness of AlSi10Mg for MHP treatment.

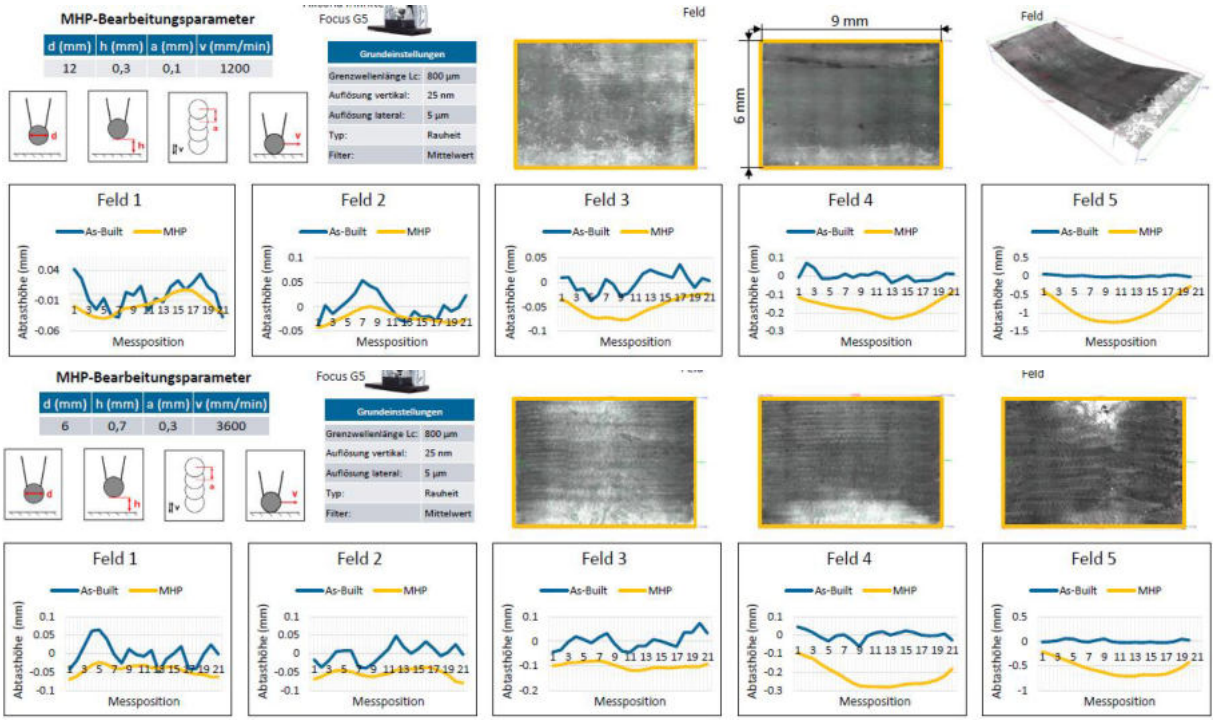

Figure 7-44: Surface height after MHP treatment of the fields 1 to 5 with ⌀12 mm (top) and ⌀6 mm (bottom) impactor heads.

Surface height measurement results (see Figure 7-44) indicate, that for the selected MHP parameter set the minimum required material thickness of 3,5 mm can guarantee no plastic deformation of the cantilevered surface made of AlSi10Mg in LPBF process and heat treated afterwards. In case of more distant impacts (e.g., a parameter set with higher feedrate and lower oscillation frequency), the material thickness of 3 mm may be sufficient even if using smaller impactor head. Thin-walled components made with AlSi10Mg under described conditions with wall thickness below 3 mm should not undergo MHP treatment because of the high risk of damage due to plastic deformation.

Use-case voestalpine Böhler Edelstahl GmbH & CO KG – maraging steel powder Böhler M789

On behalf of the project partner voestalpine Böhler Edelstahl GmbH & CO KG, a demonstration part for post-treatment using machine hammer peening (MHP) process has been defined. The demonstration part 55 x 35 x 20 mm is designed to be used for marketing events to illustrate various application scenarios of MHP for additively manufactured parts out of powder AMPO M789. Two different surface conditions have been prepared for the MHP process (as-built printed surface and milled surface). For each surface condition, two different sets of process parameter for high surface quality and high surface material hardness have been applied each on the separate halve of the demonstration part. Results are represented in Figure 7-45.

Figure 7-45: Use-case part for MHP treatment of the AMPO M789.

7.3 Summary

The applicability of the vibration assisted drilling to the LPBF additively manufactured parts has been confirmed and suggested for application. In course of this study a cutting force reduction by 30 % compared to the conventional drilling operation has been observed during the drilling the maraging steel alloy 1.2709. No differences have been found for machining specimens, built vertically or horizontally.

The machine hammer peening of the LPBF additively manufactured parts shows good surface smoothening results and can be recommended as treatment for function surfaces of these parts. The arithmetical mean height of the treated surface could be reduced by at least 52 %, and under the optimal circumstances by 93 %, compared to the as-built condition for the specimens during this study.

A minimum required material thickness of 3,5 mm, which should guarantee no plastic deformation, has been confirmed for the cantilevered surface of a part, made of heat-treated AlSi10Mg in a LPBF process. A thickness of 3 mm may be sufficient if using smaller impactor head and a parameter set with more distant impacts. Thin-walled components made with AlSi10Mg under described conditions with wall thickness below 3 mm should not undergo MHP treatment because of the high risk of damage due to plastic deformation.

7.4 Outlook

The achived small and uniform chip size due to application of the vibration assisted machining can be considerable for further chip recycling approaches.

The machine hammer peening application on further materials should be taken into account for further investigations. A local alternation of the physical material properties (e.g. ferromagnetism or specialized surface appearance) of the additively manufactured parts due to MHP treatment might offer even higher customisation and functionalization level, compared to the conventional manufacturing.

8 ASM of parts produced by WAAM – Results of the KUL, TM, BIL and Sirris

8.1 Introduction

Wire and Arc Additive Manufacturing (WAAM) is an additive manufacturing technique that uses an electric arc as a fusion source to melt a filler wire and build a component layer by layer. For WAAM standard welding technologies are usually used, such as Gas Metal Arc Welding (GMAW), Gas Tungsten Arc Welding (GTAW) and Plasma Arc Welding (PAW). The standard welding robot or NC machine tool can be used as a motion system.

WAAM allows to produce a medium to large metal parts in both material- and cost-efficient way. It is characterized by high material usage efficiency (up to 90%), high deposition rates (1-4 kg/min) and increased energy efficiency [1],[2]. However, after deposition, the WAAM parts have low dimensional accuracy and surface quality (waviness up to 0.5 mm [1]) and require further post-processing.

During this project, the impact of the different processes withing the ASM process chain on the quality of the final part were investigated for the components produced by GMAW WAAM. The following section summarizes the results regarding investigations on the additive and subtractive manufacturing processes of the WAAM parts.

8.2 Description of project results

8.2.1 Analysis of WAAM technology[4]

To produce the part with the help of WAAM, a 3D CAD model is sliced into 2.5D layers. To slice the part, the layer height should be known. The layer height is defined by the weld bead height (Figure 8-1) and depends on the welding parameters. Contrary to the SLM process, the WAAM parameters, such as wire feed speed (WFS) and travel speed of the robot (TS), can be varied in a wide range to obtain the required geometry of the weld bead. Thus, the WAAM parameters set are selected based on the thickness of the part to be produced. After slicing the CAD model, a deposition path is generated within each layer and a program for a robot (or NC machine tool) is obtained. The robot program controls both the motions of the robot and the welding power source. The WAAM process chain is shown in Figure 8-2.

[4] This chapter is adopted from the paper: Chernovol, N., Lauwers, B., Van Rymenant, P. (2020). Development of low-cost production process for prototype components based on Wire and Arc Additive Manufacturing (WAAM). Procedia CIRP, 95, 60-65. https://doi.org/10.1016/j.procir.2020.01.188

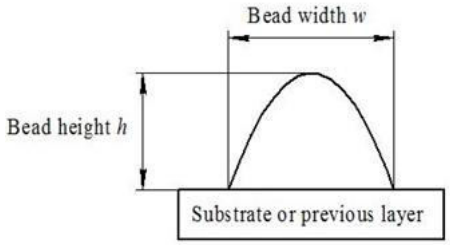

Figure 8-1: Weld bead geometry.

In order to slice the 3D model and generate the deposition path for part production, dimensions of the weld bead geometry are required. Dimensions of the weld bead depend on the WAAM process parameters shown in Figure 8-3 and are usually determined experimentally for each type of wire material and diameter.

Weld bead geometry was experimentally determined for two welding technologies: conventional GMAW (Qineo pulse 450A machine) and Cold Metal Transfer (CMT, Fronius TPS 3200 CMT machine). Both power sources have a synergic control, meaning the current and voltage are automatically assigned based on the selected synergic program, wire feed speed, wire diameter and composition, gas composition and flow rate. That is why the impact of the wire feed speed (WFS) and travel speed of the robot (TS) on weld bead geometry was studied.

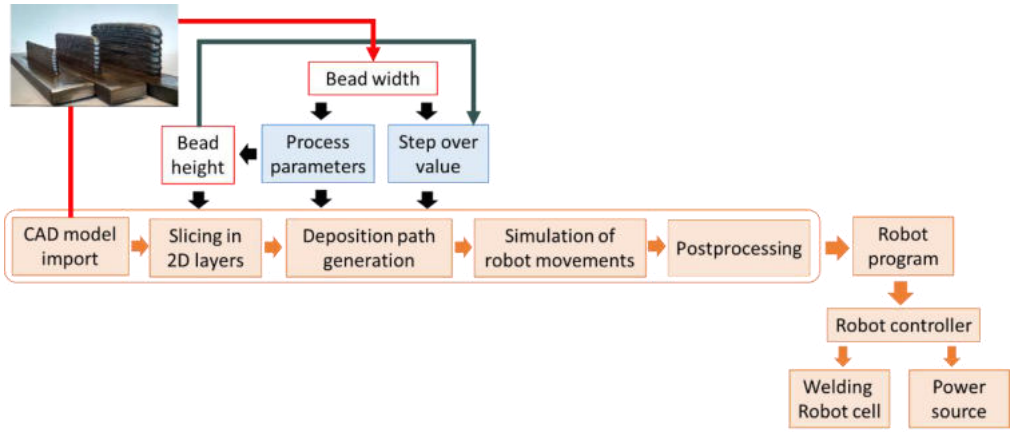

Figure 8-2: WAAM process chain.

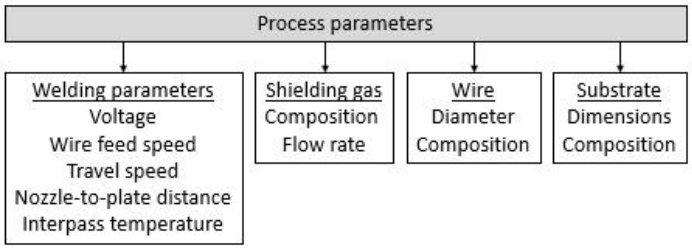

Figure 8-3: Main process parameters for GMAW WAAM.

As filler material, a 1.2 mm diameter wire EN ISO 14341-A (G 42 4 M21 3Si1) was used (Table). The shielding gas was an 85% Ar with a 15% CO_2 mixture at a constant flow rate of 15 l/min. Contact tip to

work distance was equal (CTWD) was equal to 15 mm for both processes and was kept constant during deposition. Temperature between the passes (interpass temperature) was kept below 120°C.

C	Si	Mn	P	S	Cu
0.088	0.9	1.51	0.012	0.012	0.19

Table 8-1: Chemical composition of the wire electrode, % (by mass).

Central Composite Design (CCD) was used to design the experiment. The second-order regression models for bead height and bead width determination for both conventional GMAW and CMT processes were obtained using the response surface methodology. The impact of welding parameters on weld bead geometry is shown in Figure 8-4 for the conventional GMAW process and Figure 8-5, Figure 8-6 for the CMT process.

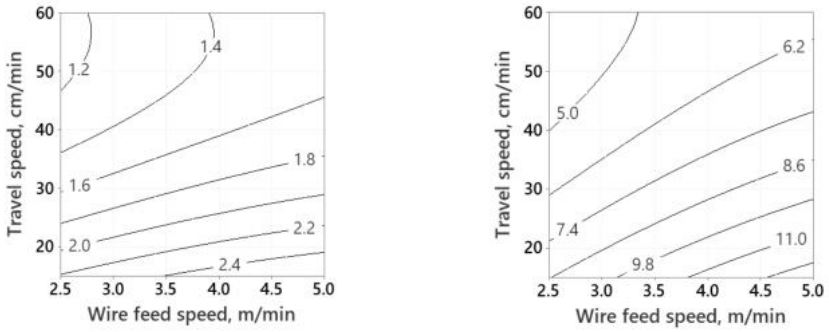

a) b)

Figure 8-4: Impact of welding parameters on a) bead height, mm and b) bead width, mm for conventional GMAW process

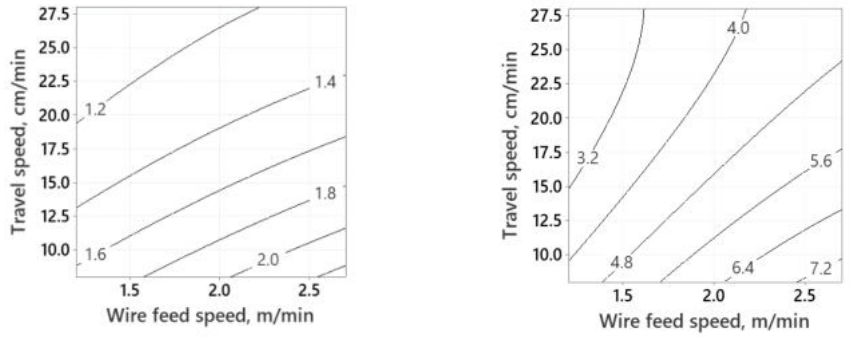

a) b)

Figure 8-5: Impact of welding parameters on a) bead height, mm and b) bead width, mm for CMT process, range 1.

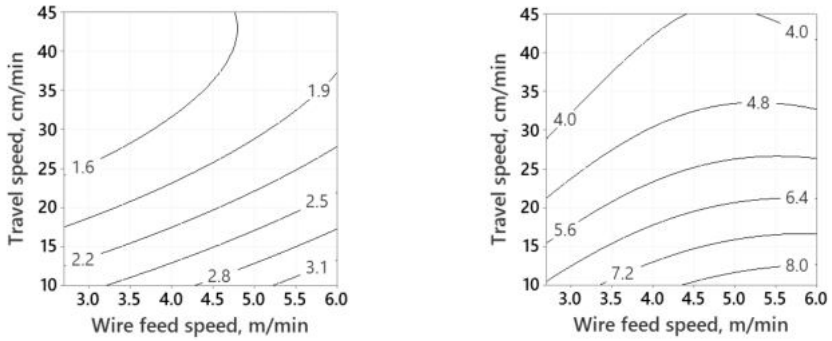

a) b)

Figure 8-6: Impact of welding parameters on a) bead height, mm and b) bead width, mm for CMT process, range 2.

Table 8-9 present the summary of the analysis of two additive process technologies. Lower heat input during the CMT process leads to lower deposition rates and significantly smaller bead widths compared to the conventional process. CMT process is beneficial for the production of the thin-walled components with more complex geometries as the inclined walls can be deposited in any orientation from 0° to 180° without using support structures and external axes (i.e., positioner or rotary table). It also allows to reduce the interpass time. Nevertheless, with an increase in the number of simultaneously produced parts, the time that is spent for cooling of one piece has less influence on the total welding time. For the solid components that require multiple passes within the layer, the conventional GMAW process will be more efficient due to the higher deposition rates and lower number of the adjacent passes to be deposited.

WFS, m/min	TS, cm/min	Height, mm		Width, mm		Minimal deposition rate		Maximal deposition rate	
		Min	Max	Min	Max	kg/h	cm^3/h	kg/h	cm^3/h
Conventional GMAW process									
2.5 - 5	15 - 60	1.14	2.6	4.25	12.84	0.23	29.1	1.56	200

CMT process									
1.2-2.7	8 - 28	1.09	2.27	2.45	7.62	0.084	10.7	0.54	68.9
2.7 - 6	10 - 45	2.37	3.37	6.47	8.55	0.48	61.4	0.899	115.3

Table 8-9: Summary of the analysis of additive process technology.

8.2.2 Investigation of ASM process chain for parts produced by WAAM

WAAM parts are characterized by the significant surface waviness, angular distortions and buckling of the substrate plate after deposition. Due to this, it is hard to accurately position and align as-deposited parts on the NC machine tool. Moreover, a certain problem occurs during clamping of the part in jigs leading to the release of the workpiece.

To machine the WAAM samples, the optimal Additive-Subtractive process chain was determined experimentally and is shown in Figure 8-7.

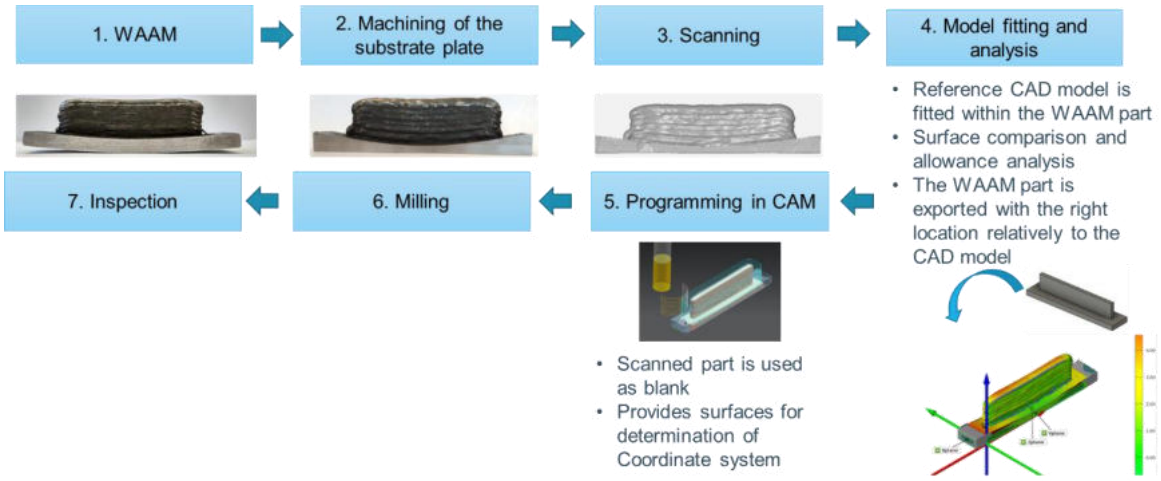

Figure 8-7: Additive – Subtractive Manufacturing process chain.

To provide the reference surfaces both for positioning and alignment, the surfaces of the substrate or the WAAM part might be pre-machined. As an alternative solution, jigs with flexible jaws might also be used (e.g., Vario Tec Jaws). After pre-machining or clamping of the workpiece in a fixture, 3D scanning is implemented. Further, the reference CAD model is fitted into the scanned WAAM part, and the distribution of the stock material is analyzed to evaluate the quality of the alignment. Once the scanned WAAM component is properly aligned, it is exported with the right location relatively to the reference CAD model. In CAM software used to generate toolpath for the required subtractive operations, the aligned WAAM component is imported and used as a blank. The work coordinate system (WCS) is defined in CAM software and further on the NC machine tool using the reference surfaces (i.e., the pre-machined surfaces of the part or the surfaces of the fixture). Finally, the WAAM part is post-processed on the CNC machine. The proposed process chain requires the multi-axis NC machine tool due to the optimal location of the reference CAD model within the WAAM part.

When the 3D scanning is not available, bigger allowances should be foreseen for the machining step. Positioning and levelling of the WAAM part are then implemented manually on the machine. To define

the WCS, the as-deposited WAAM surface might be used. In this case, the small allowance is first removed, and the distribution of stock material is evaluated. Then, the WCS is manually corrected on the NC machine tool and the machining is implemented.

8.2.3 The amount of stock material to be removed during machining

After determining the weld bead geometry, the amount of stock material to be removed was investigated. In general, there are three types of allowances to be assigned: (1) allowance to remove the initial wavy WAAM surface, (2) additional allowance to compensate the impact of deformations of the dimensional and geometrical accuracy, (3) machining allowance for the finishing operations (Figure 8-8).

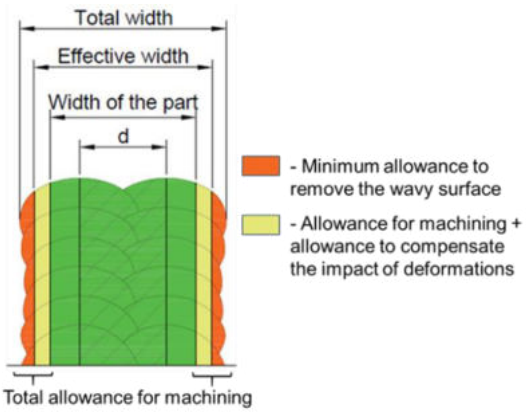

Figure 8-8: Schematic representation of the allowances to be assigned for WAAM parts.

The first goal was to determine the minimum allowance to remove the wavy WAAM surface. For the WAAM samples, the form errors and waviness are much larger; thus, the roughness of the surface is not important. Instead, the *Effective Wall Width* (EWW) is the main characteristic of the WAAM parts. EWW is the maximal wall width after the finishing operations, achievable for a given set of welding parameters. The EWW could be determined only by milling. The study of the cross-section area of the sample could not provide a reliable result as the EWW varies along the component (Figure 8-9).

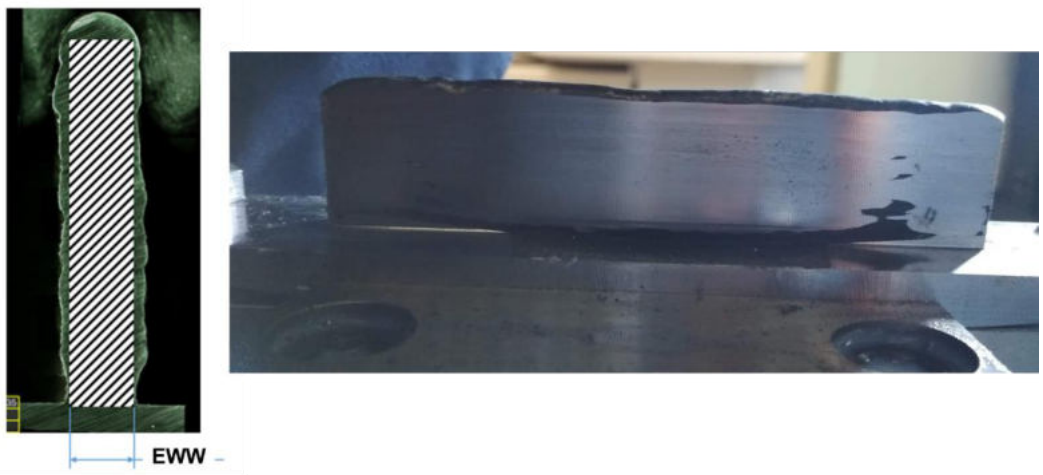

Figure 8-9: Effective Wall Width of the WAAM sample.

To determine the EWW, samples produced by the conventional GMAW process during the previous experiment were used. The second-order regression model for EWW vs WAAM parameters was obtained. Using the regression models for the bead width and EWW, the minimum allowance to be removed per side was estimated. The results showed that the allowance to be removed significantly depends on the WAAM process parameters. Moreover, the relationship between the WAAM process parameters, the EWW and minimal allowance is non-linear (Figure 8-10). An increase in TS has a positive impact on the surface flatness of as-deposited components, thus allows to reduce the amount of stock material. To limit the allowance to be removed per side to 1 mm, the TS should be kept in the range of 30 – 50 cm/min and WFS should be limited to 4 m/min.

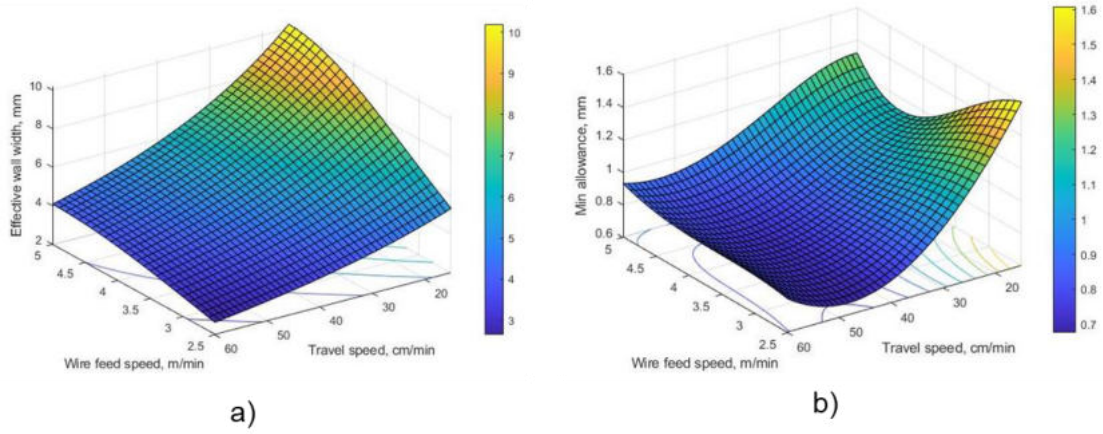

Figure 8-10: Impact of the WAAM parameters on (a) EWW and (b) minimal allowance to be removed per side.

The second goal was to determine the impact of the substrate deformations on the dimensional and geometrical accuracy and EWW of the WAAM parts. For this purpose, three types of specimens were produced (Figure 8-11). Each type of specimen was deposited using different WAAM parameters (Table 10). After deposition, parts were post-processed by milling using the methodology described in chapter 8.2.20.

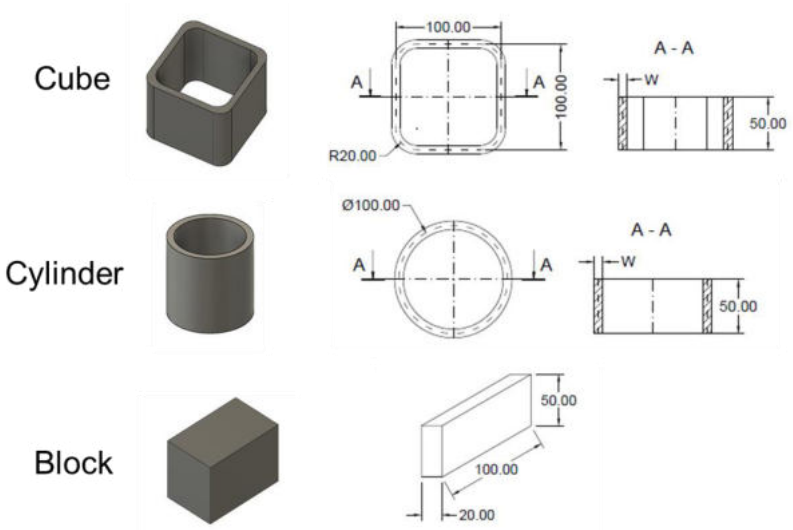

Figure 8-11: Test specimens.

WFS, m/min	TS, cm/min	HI, kJ/m	Bead width, mm	Step-over value, mm	Number of passes	Total width, mm
2.9	22	0.448	7.98	5.57	4	24.68
4.6	22	0.762	10.62	7.32	3	25.27
2.9	53	0.186	4.74	3.16	6	20.545
4.6	53	0.316	6.16	4.11	5	22.596

Table 10: Experimental design matrix and corresponding characteristics.

As the wall width (i.e., weld bead width) varied with WAAM parameters, the dimensions of the reference surfaces shown in Figure 8-11 were used for analysis. Reference dimensions are significantly impacted by the distortions of the substrate plate and are smaller than the programmed one (98.5 mm << 100 mm). Moreover, the dimensions of the cubes in X and Y directions differ due to the non-uniform deformations. The difference in dimensions depending on the welding heat input (HI): 1.18% for the low HI and 0.14% for the high HI. After post-processing, the outer dimensions are smaller than the theoretical values by up to 2% (2.04 mm) for cubes and 3.1% (3.25 mm) for cylinders causing the lack of material. With an increase in HI difference between the experimental and theoretical values reduces. Inner dimensions are also smaller than theoretical ones, but in this case an excessive amount of material is observed leading to lower material efficiency. The difference does not exceed 1.96% for cylinders and 2.03% for cubes.

Outer surfaces are characterized by bigger flatness, cylindricity and perpendicularity values than inner surfaces in an as-deposited state. The post-processing step leads to the redistribution of the residual stresses within the component resulting in lower geometrical accuracy of the inner surfaces compared to the outer surfaces. Moreover, the flatness and perpendicularity of post-processed surfaces depend on the WAAM parameters. For high TS values (TS = 53 cm/min), the geometrical accuracy of the inner surfaces improves with the reduction in WFS. Contrary, the geometrical accuracy of the outer surfaces

reduces with the decrease in WFS. When the TS is low (22 cm/min), welding parameters do not significantly impact the flatness and perpendicularity of the surfaces (Figure 8-12).

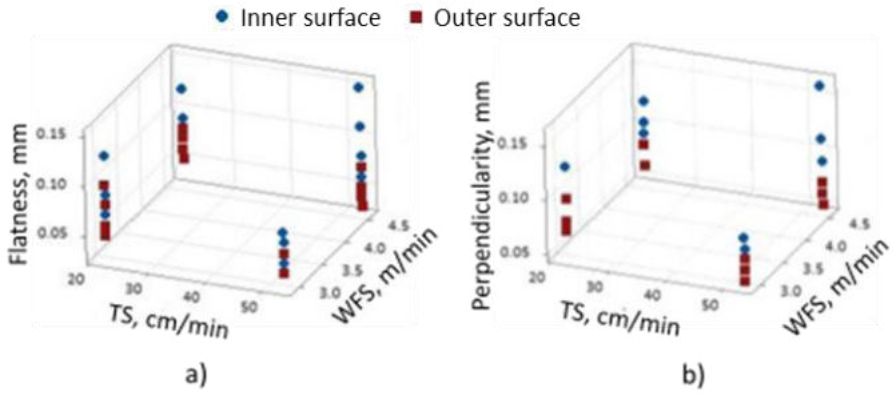

Figure 8-12: (a) flatness and (b) perpendicularity of the surfaces after post-processing.

Distortions lead to the more significant impact of the WAAM parameters on EWW of thin-walled components: (1) high TS leads to reduction of EWW by up to 17.4%, (2) low TS in combination with low WFS provides the best result (error does not exceed 4.37%). Bead width (or total wall width) is not affected by the substrate plate deformations (the error between the predicted and experimental values does not exceed 6%).

Based on the results of the current investigation, the following design rules for WAAM parts were developed:

- The EWW of the WAAM part should include:
  - Width of the part
  - Allowance to compensate the impact of deformations (per side)
    - 1.3…2 mm for outer surfaces
    - 0.2…0.5 mm for inner surfaces
  - Allowance for finishing operations (e.g., grinding) if required
  - For solid components, the reduction of EWW by 7-8% while using high TS values for deposition should be considered.
- Welding parameters and the number of adjacent passes are selected based on the required effective width (or EWW for thin-walled components).
- The minimum allowance to remove the wavy WAAM surface depends on the WAAM parameters and equals 0.7…1.8 mm per side.

8.2.4 Machinability of the WAAM components[5]

Introduction

Surface roughness obtained after machining depends on the properties of the workpiece (e.g., hardness, roughness, etc.), cutting tool, cutting parameters and dynamic behavior of the system (i.e., vibrations excitation). It is well known for carbon steels that machinability improves with an increase in hardness because of the reduced adhesion tendencies and improved chip formation [3-5]. The initial state of the surface determines the variation in the chip thickness and corresponding cutting forces. Inhomogeneous surface hardness, waviness, and low geometrical accuracy that cause the variation in cutting forces also can lead to the excitation of chatter vibrations of the system, including the workpiece, cutting tool, fixture, and CNC machine. Additionally, for thin-walled components, the stiffness that depends on the geometrical configuration of the part and material properties impacts the amplitude of the forced and chatter vibrations. An increase in chatter vibrations amplitude results in a rough surface and lower tool life due to the fatigue cracking of the tool contact surfaces.

On the other hand, the welding heat input (HI), which depends on the wire feed speed (WFS) and travel speed of the robot (TS), and the interpass temperature (IT) have a direct relation with the heating and cooling cycles. The heating and cooling cycles during deposition determine the mechanical properties of the component, weld bead geometry and the surface modulations.

Current investigation aimed to determine the impact of the WAAM and milling parameters on final quality obtained after machining. For this purpose, the WAAM parameters' effect on as-deposited surface properties and thickness of the thin-walled components are determined. Further, the impact of the initial surface state and component's stiffness and milling parameters on the final surface roughness is analyzed.

Methodology

As a motion system for WAAM, a six-axis industrial robot arm CLOOS QRC320H was used. Samples were deposited using a Qineo pulse 450A welding power source with synergic control in standard GMAW mode. The substrate plate was a mild steel plate with dimensions 200 x 30 10 mm. A 1.2 mm diameter wire EN ISO 14341-A (G 42 4/M21 3Si1) was used as a filler material. The shielding gas was 85% Ar and 15% CO2 mixture at a constant flow rate of 15 l/min. The distance between the contact tip and the workpiece was set to 15 mm and kept constant during the process. The dimension of the deposited walls was 45 x 100 mm (height x length). The wall width varied according to the welding parameters. The interpass temperature during the WAAM process was controlled using a FLIR A315 thermal IR camera (Figure 8-13). Once the maximum temperature of the deposited upper layer had reached a specific value, the next pass was applied.

The milling process was implemented on a DMG DMU 50 5-axis machine centre. The tool was a square shoulder end mill R390-016A16-11L (Sandvik) with exchangeable inserts (R390-11T3 08MPM 4330

[5] This chapter is adopted from the paper: Chernovol, N., Sharma, A., Tjahjowidodo, T., Lauwers, B., Van Rymenant, P. (2021). Machinability of wire and arc additive manufactured components. CIRP Journal of Manufacturing Science and Technology, 35 (C), 379-389. https://doi.org/10.1016/j.cirpj.2021.06.022\

(carbide coated - CVD TiCN + Al2O3+TiN)), diameter 16 mm, helix angle 15° and two teeth. Milling of the samples was implemented in two steps: (i) face milling of the top surface of the WAAM component to provide accurate values of axial depth of cut during the side milling and to remove the upper zone, which is characterized by the higher hardness values (ii) side milling using cutting order 'level first' (in case of multiple numbers of cuts). The down-milling strategy that is recommended for the machining of carbon steels was applied. To evacuate the chips from the cutting zone, compressed air was used during machining (i.e., dry cutting was performed). The cutting tool manufacturer recommends dry cutting for machining the selected material. It allows to avoid thermal cracking of the cutting edge, increase tool life, and improve the surface quality.

Figure 8-13: Deposition of the WAAM samples.

To analyze the effect of welding parameters vis-à-vis wall width and surface modulations on the machining process dynamics, the displacement signals of the parts during the milling of the WAAM components were recorded using a proximity probe. A 7200 Proximity transducer system from Bently Nevada was used as a probe (Figure 8-14). Additionally, a custom-made sensor was developed to monitor the contact between the tool and a workpiece. Displacement and contact signals were acquired using a NI 6361 data acquisition system from National Instruments with 50 kHz sampling frequency.

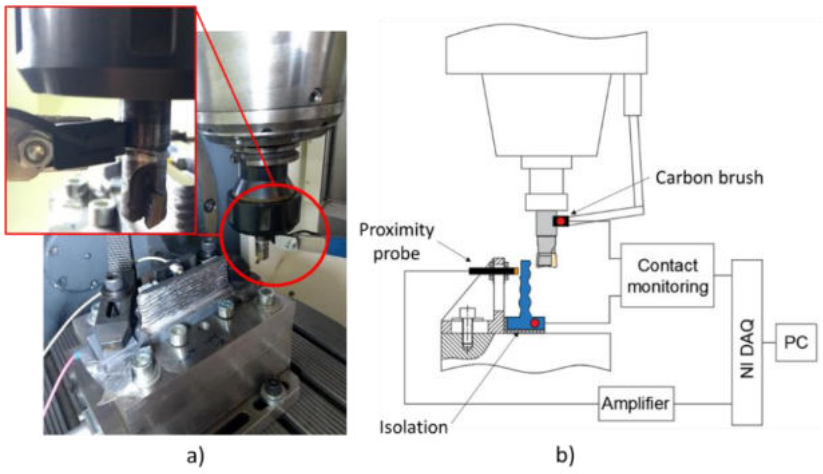

Figure 8-14: Machining process (a) set-up, (b) schematic.

Definitive Screening Design (DSD) was used as a 'design of experiment' to determine the welding and milling parameters' collective impact. Input welding process parameters were wire feed speed WFS, travel speed of the robot TS, and interpass temperature IT. For the milling process, the input process parameters were cutting velocity Vc, feed per tooth Fz, axial depth of cut a_p, and the number of passes n. The number of passes is used instead of the radial depth of cut a_e due to the WAAM components' characteristics. The total wall width (TWW) and effective wall width (EWW) of the WAAM components depend on the WAAM parameters. The total allowance to be removed per side also depends on the WAAM parameters and could not be controlled separately. By setting the number of passes, the radial depth of cut for a specific pass is determined as the total allowance to be removed divided by n. The seven factors DSD requires 17 runs for which the process parameters and their limits are given in Table 11.

	Factor levels		
Factor	-1	0	1
Wire feed speed, m/min	2.9	3.8	4.7
Travel speed, cm/min	22	38	54
Inter-pass temperature, °C	50	175	300
Cutting speed V_c, m/min	280	325	370
Feed per tooth Fz, mm/t	0.05	0.105	0.16
Number of passes	1	3	5
Axial depth of cut a_p, mm	1	3	5

Table 11: Process parameters and their limits.

After milling, roughness measurements were carried out on a Mitutoyo Formtracer CS-3200. Low force Vickers hardness test of HV1 based on EN ISO 6507-1 (2018) was performed on the machined surfaces. Tests were implemented on a Shimadzu HMV – 2000 micro-hardness measurement machine with 1 kgf load applied for 13 s.

Results

Characteristics of the deposited surface

The WAAM surface obtained after the deposition is characterized by the flatness deviation, which is a quantification of geometric quality. Wire feed speed, travel speed, and interpass temperature impact the flatness deviation and thickness of the component as shown in the contour plots (Figure 8-15).

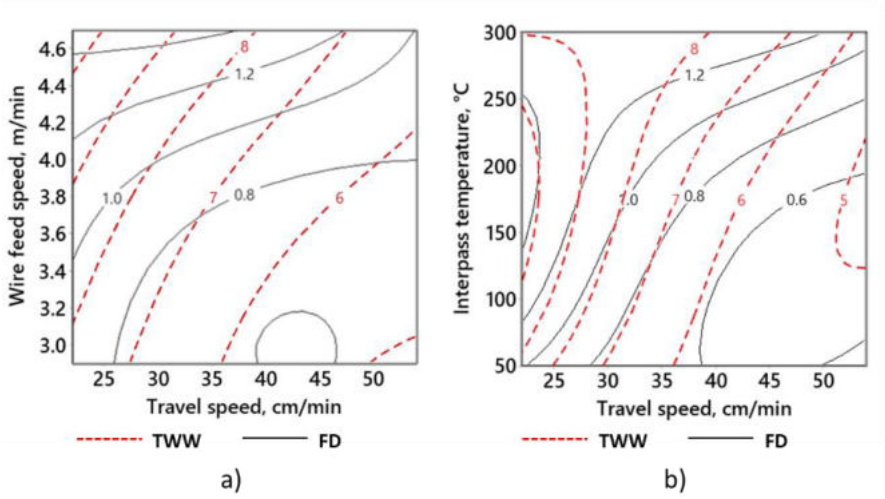

Figure 8-15: Impact of process flatness deviation (FD) and total wall width (TWW).

An increase in WFS increases flatness deviation. The welding current increases in proportion to the WFS to increase the melting rate of the filler wire, causing the spread of a large chunk of molten weld metal with a degree of randomness, resulting in a wide wall with an increased flatness deviation. Therefore, the total wall width (*TWW*) and flatness deviation show similar trends with a change in process conditions (Figure 8-15a). A slow travel speed results in increased heat input as the arc remains on a point for a considerable duration (Figure 8-15a). The material remains in a molten state for a longer duration and spreads to increase the wall width and the flatness deviation. High travel speed causes faster cooling and a limited spread of molten material, leading to a narrow bead and less flatness deviation.

The rise of the interpass temperature leads to an increase in weld width and flatness deviation (Figure 8-15b). An increase in interpass temperature results in an increase in the cooling time from 800°C to 500°C ($\Delta t_{8/5}$, EN 1011-2) causing the overflow of the molten material along the weld width because of the melt pool's increased fluidity [6]. In conjunction with the weld bead shape and flatness deviation, the welding parameters and the interpass temperature also impact the hardness.

The influence of the cooling time on hardness and flatness deviation is shown in Figure 8-16. The increase in cooling time up to 10 s leads to the material softening from 204 HV to around 165 HV (hardness reduction of 19%). Further increase in cooling time does not show a significant impact on the

hardness. At the same time, the flatness deviation of the WAAM surface rises drastically with an increase in cooling time (around 230%), thus having a more significant effect on the final surface obtained after milling.

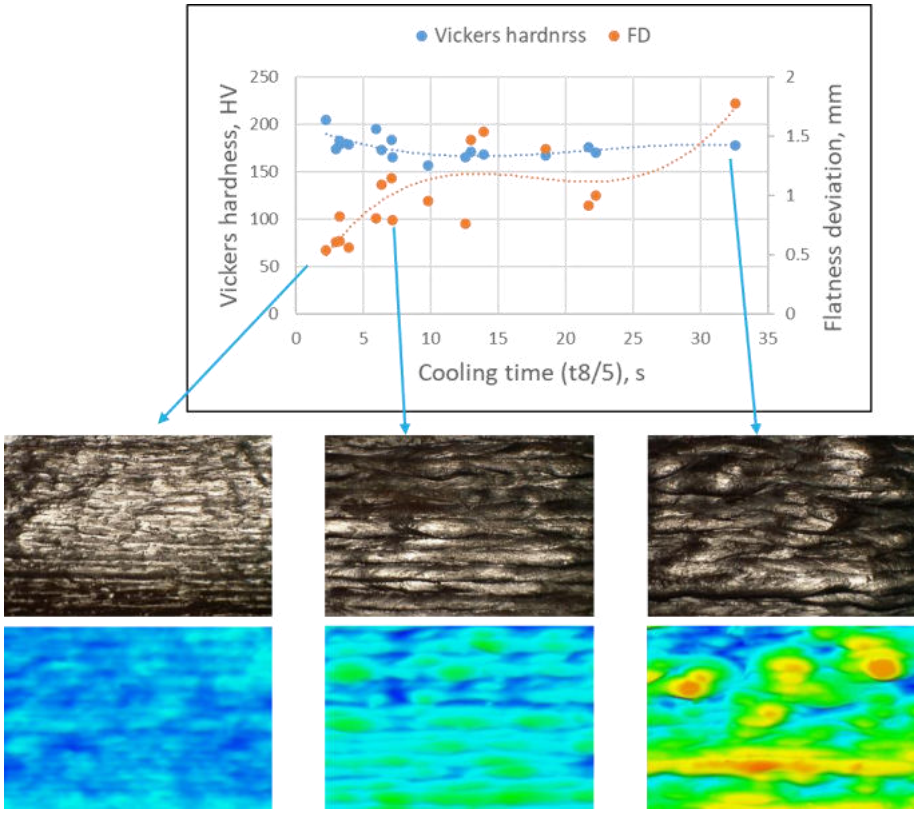

Figure 8-16: Impact of cooling time ($\Delta t_{8/5}$) on hardness and flatness of the WAAM components.

Characteristics of the machined surface

The machined surface quality results from the machining parameters and the quality of the as-deposited surface. The welding parameters directly influence the machined surface quality as they are responsible for forming the deposited surface. Figure 8-17 shows that the rise of the cooling time leads to an increase in surface roughness of the machined WAAM surfaces. This is due to the (1) increase in as-deposited flatness deviation resulting in variation of radial depth of cut, thus the variation of cutting forces and (2) reduction of hardness that has a negative impact on the chip formation during milling. Nevertheless, four samples with significantly higher surface roughness were observed, as highlighted in Figure 8-17. For these samples, increased roughness was caused by the instability of the milling process and is discussed in section ‘Dynamics of milling process’.

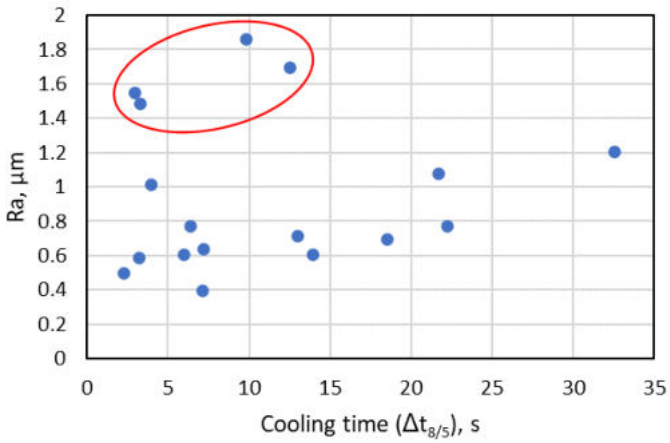

Figure 8-17: Impact of cooling time ($\Delta t_{8/5}$) on the roughness of machined WAAM surfaces.

The impact of milling parameters on final surface roughness is following (Figure 8-18):

- With an increase in the cutting velocity (*Vc*) to 325 m/min, surface roughness improves. Nevertheless, further increase in *Vc* shows negative impact on the surface quality.
- An increase in axial depth of cut (a_p) leads to the coarsening of surface quality. The change in a_p is related to the stability of the milling process. The cutting system becomes unstable, and chatter develops when the axial depth of cut exceeds a limit for a given cutting speed and width of cut.
- Low values of feed per tooth (*Fz*) lead to an increase in the Ra. With an increase in *Fz*, surface quality improves. It is well known that with an increase in chip thickness (i.e., *Fz*), the amplitude of the chatter and forced vibrations reduces leading to better process stability and surface quality.
- Number of passes (n) determines the radial depth of cut a_e = (*TWW* - *EWW*) / (*2n*). With an increase in the number of passes, surface roughness improves.

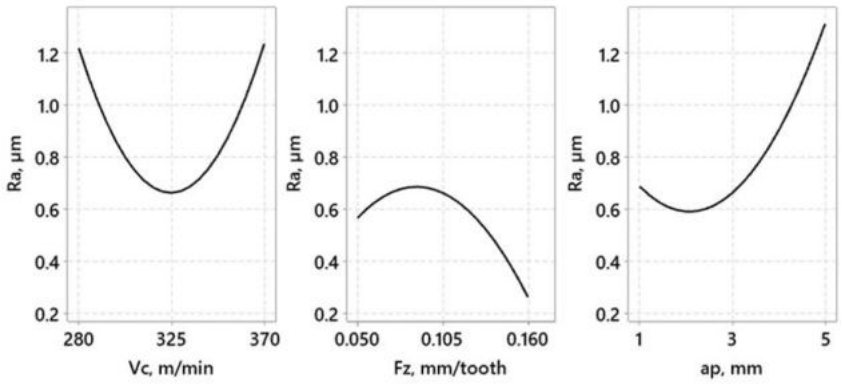

Figure 8-18: Impact of milling parameters on the surface finish of machined WAAM surfaces.

Dynamics of milling process

Three types of oscillations can occur during milling, namely forced vibration, self-excited or chatter vibration, and free damped oscillation (Figure 8-19) [7]. Forced vibration occurs when the mill's tooth is in contact with the workpiece, and it removes the allowance, causing the deflection of the thin-walled part.

The frequency of forced vibration corresponds to the tooth passing frequency f_z (or tooth passing period T_z). In contrast, self-excited vibration occurs when the tooth passes through the allowance on top of the forced oscillation at one of the natural frequencies. The free damped oscillation occurs in the absence of external force, causing the vibration to dissipate, and the thin-walled part tends to return to its equilibrium position. The frequency of the free damped vibrations corresponds to the natural frequency of the system comprising machine tool, clamping device, and workpiece (i.e., stiffness of the system).

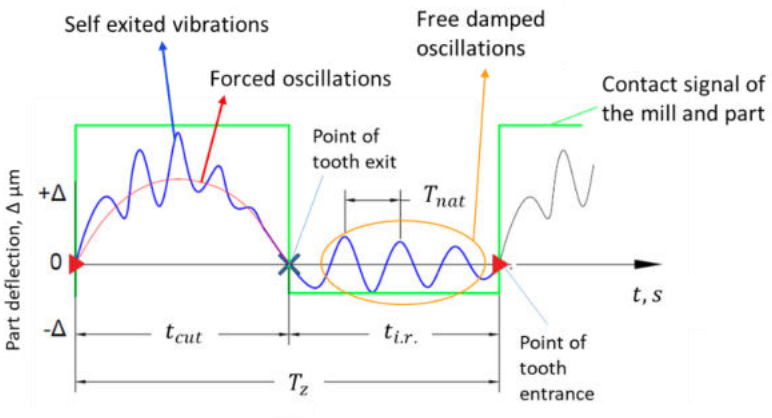

Figure 8-19: Types of oscillations that occur during milling (t_{cut} – cutting time for one tooth of the mill, $t_{i.r.}$ –time of idle run when the previous tooth exited the allowance and the next one has not yet entered; T_z – tooth passing period; T_{nat} - period of one natural oscillation).

As mentioned before, chatter vibrations occur at one of the system's natural frequencies. In thin-walled components, the part stiffness is much lower than the stiffness of the cutting tool. Thus, the part's stiffness has a more significant impact on the frequency range of chatter vibrations excitation. For the deposited WAAM walls, the component's stiffness is determined by the material properties and workpiece configuration (i.e., height *H*, thickness *W*, length *L*). As the components' length and height were fixed, the width that varied with WAAM parameters determines the stiffness. The stability of the milling process, which is associated with the chatter vibrations, significantly impacts the final surface formation.

The maximum surface roughness (Ra=1.862 µm) was obtained for sample 14. Sample 14 was deposited with *WFS* 2.9 m/min and *TS* 54 cm/min, resulting in *TWW* of 4.96 mm. Moreover, the interpass temperature was high, which resulted in high surface waviness obtained after deposition. The axial depth of cut was equal to 5 mm, and the total allowance was removed in one pass. Thick chips combined with low stiffness of the component and significant surface waviness led to the excitation of chatter vibrations and instability of the milling process, as shown in Figure 8-20. Sample 16 (Ra 1.694 µm) had a similar stiffness (*TWW* 5.72 mm) and surface waviness as sample 14. However, the number of passes in the radial direction was 5 instead of 1, leading to a smaller radial depth of cut per pass, smaller chip thickness, and lower cutting forces. As a result, the milling process was more stable, even though small chatter vibrations, as highlighted with a circle in Figure 8-20, still occurred in the profiling zone, causing surface roughness.

For sample 10 (Ra 1.545 µm), the milling process was stable, and no chatter vibrations occurred. Figure 8-20 shows that the amplitude of the forced oscillations was around 110 µm, one of the highest values within all the samples. Sample 10 is characterized by a *TWW* of 5.8 mm, like that of sample 14 and 16. It was produced with low interpass temperature (50°C) and low heat input that caused a lower flatness

deviation value (0.607 mm). A high number of milling passes (5 passes, a_e = 0.163 mm) and a low feed rate (0.05 mm/tooth) could lead to an unstable chip formation process resulting in an increase in plastic deformation and friction force on the back surface of the teeth. Unstable chip formation, together with high amplitudes of forced vibrations, may cause increased roughness.

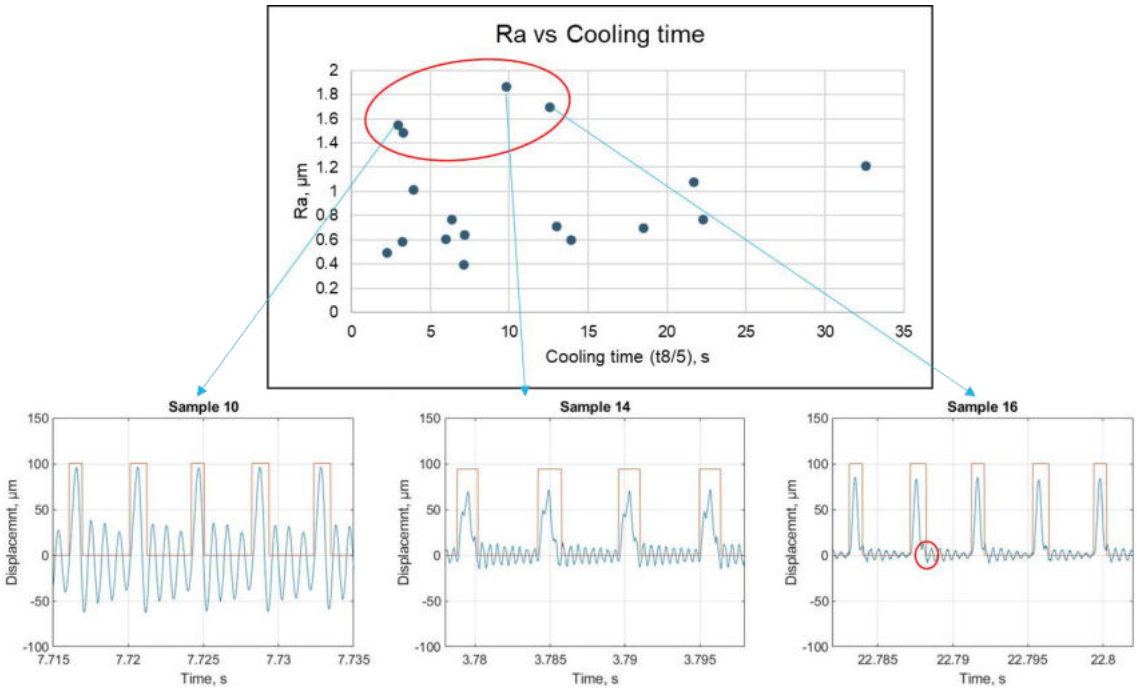

Figure 8-20: Time-domain displacement signals of WAAM samples with the highest surface roughness obtained after machining.

To predict chatter vibrations during milling, the existing methodology described in [8] was adapted for WAAM parts. For thin-walled components, the chatter vibration zone could be determined using Determining Ratio (**DR**):

$$DR = \frac{t_{cut}}{T_{nat}} \tag{2}$$

Where, t_{cut} – is a cutting time for one tooth of the mill, s; T_{nat} – period of one natural oscillation, s.

According to [8], chatter vibrations occur in the range of 7 > DR ≥ 1. Moreover, the highest amplitudes of the chatter vibrations were observed for the range 3 > DR ≥ 5. To predict the types of oscillations that will excite during milling, it is required to determine the natural frequency f_{nat} of the component and the cutting time for one tooth of the mill t_{cut}. The cutting time for one tooth of the mill for the square end mills is calculated from equation 2 provided in [9]:

$$t_{cut} = \frac{60}{\pi DS}\left[\frac{D}{2}\cdot \cos^{-1}\left(1-\frac{2a_e}{D}\right)+\frac{1}{2}F_z + \tan\omega \cdot a_p\right] \tag{2}$$

Where, t_{cut} is a cutting time for one tooth of the mill, s; D – diameter of the tools, mm; ω – flute helix angle, degrees; S – spindle speed, rpm; a_e – radial depth of cut, mm; a_p – axial depth of cut, mm; F_z – feed per tooth, mm/tooth.

Due to the significant waviness, the radial depth of cut varies for the WAAM samples. To overcome this problem, minimum, nominal, and maximum values were used to calculate the cutting time. The obtained

values were then compared to the duration of the contact signal. The comparison showed that the average experimental contact time for one tooth of the mill corresponds to the cutting time for one tooth calculated for the nominal radial depth of cut. The natural frequency f_{nat} of the samples was determined from the time-domain displacement signals obtained during the experiment using Fast Fourier Transformation Transform algorithm.

The obtained values of the DR were compared to the types of oscillations observed during milling. Figure 8-21 shows that only forced and free damped oscillations occur when DR is less than 1. When DR crosses the limit of 1, the low-amplitude chatter vibrations start to appear (e.g., sample 15). With an increase in DR, the amplitude of the chatter vibrations increases causing significant coarsening of the surface quality. During the current experiment, the maximum DR of 2.36 was reached. Thus, a further study of the dynamic behavior of the thin-walled parts for higher DR is required. Based on the obtained results, it can be concluded that the provided methodology allows to estimate the dynamic behavior of the milling process for the thin-walled WAAM parts.

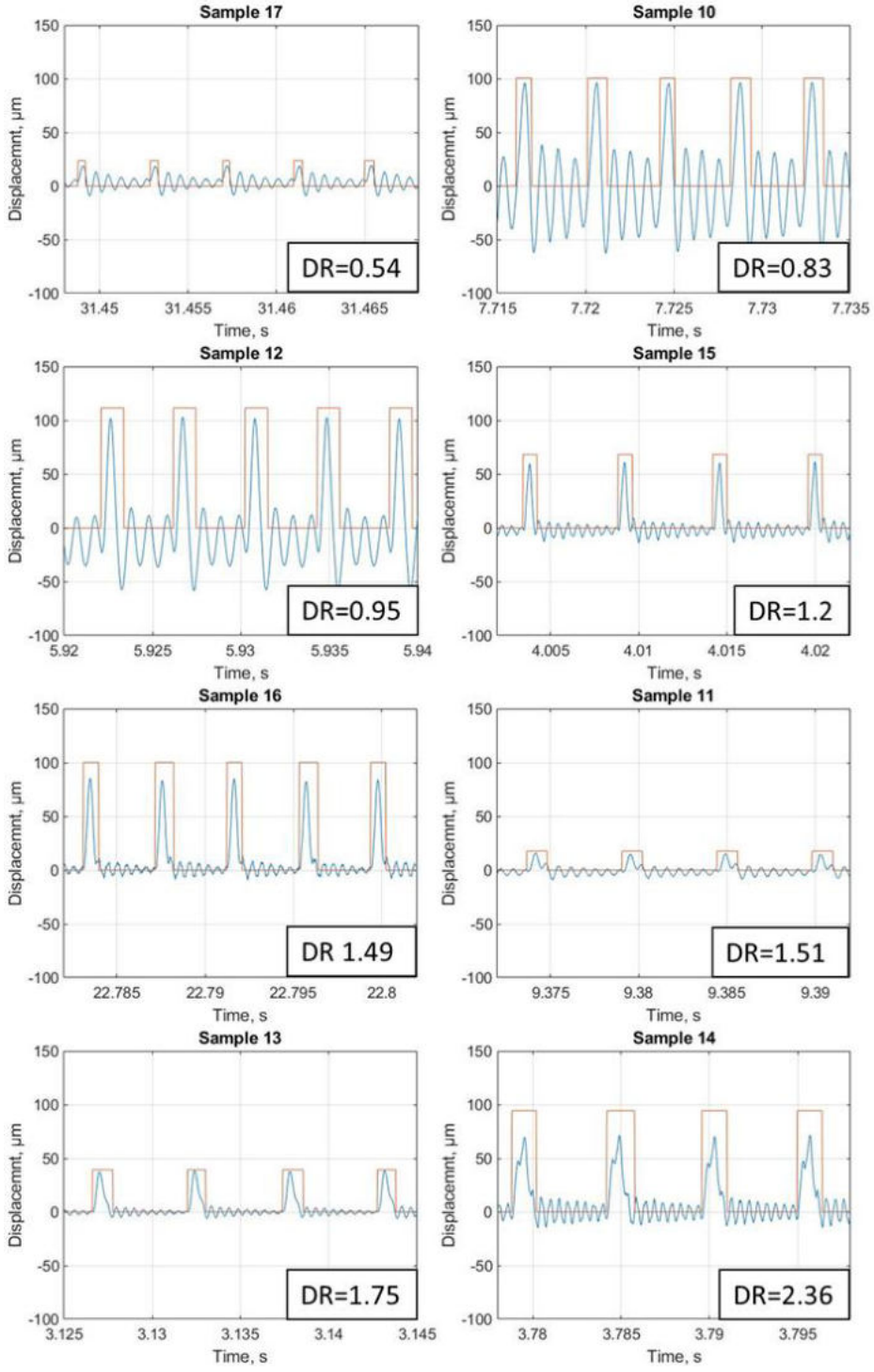

Figure 8-21: Time-domain displacement signals of WAAM samples during milling.

To avoid the chatter vibrations during milling of thin-walled WAAM parts, cutting parameters and/or geometry of the cutting tool might be adjusted. For example, Figure 8-22 shows the impact of the radial depth of cut on DR within the wide range of spindle speeds. With the reduction in a radial depth of cut, cutting time for one tooth of the mill and DR decrease leading to better stability. Increasing the spindle speed from 5570 rpm to around 8000 rpm also allows to avoid chatter vibrations for a_e 1.455 mm.

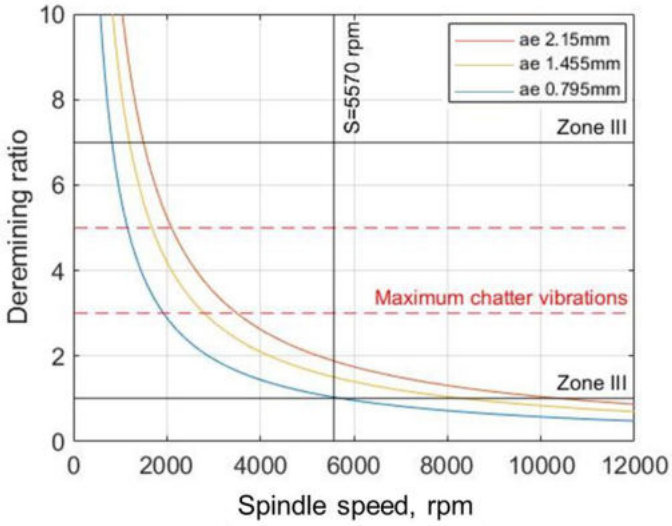

Figure 8-22: Prediction of the chatter vibrations zone.

Cutting parameters should be adjusted in a way leading to the reduction of cutting time for one tooth of the mill: (1) increase the spindle speed, (2) reduce the axial and radial depth of cut. Nevertheless, it is not recommended to significantly reduce the feed rate, as the bigger *Fz* values have a positive impact on damping of chatter vibrations. The diameter and geometry of the end mill might also be changed. Increasing the diameter of the tool and reduction in flute helix angle ω results in the reduction of cutting time for one tooth and DR. Besides the reduction of cutting time for one tooth, increasing the natural frequency of the thin-walled component leads to better process stability.

Summary

The major conclusions of the investigation are as follows:

i) The WAAM parameters, namely travel speed, wire feed speed, and interpass temperature, significantly impact as-deposited surface characteristics and the total wall width that further affects the milling process's kinematics and dynamics.

ii) The deposition of the WAAM components with shorter cooling time (i.e., low heat input and low interpass temperature) results in a hard and smooth as-deposited surface leading to a better chip formation, more uniform radial depth of cut, and thus better surface finish after machining.

iii) The surface roughness of the WAAM components can be expressed as a non-linear predictive function of welding and milling parameters. The wire feed speed, travel speed, interpass temperature, along with the cutting velocity, feed rate, and axial depth of cut, significantly affect the surface roughness.

iv) The milling parameters also have a significant impact on the kinematics and dynamics of machining. Sufficient allowance and feed per tooth should be provided to assure the stability of chip formation. From the dynamics point of view, WAAM walls deposited with lower cooling time result in lower component stiffness, which provokes chatter vibrations excitation during milling. The axial depth of cut significantly impacts the machining stability; thus, it should be limited to improve the final surface quality.

v) The existing methodology for the prediction of chatter vibrations during milling was adapted for the WAAM parts. The nominal radial depth of cut determined based on the analysis of the scanned WAAM component should be taken for calculations of the cutting time for one tooth when the allowance is removed in a single milling pass. The predicted dynamic behavior of the thin-walled parts was compared to the experimentally obtained time-domain displacement signals, showing the applicability of the methodology. The chatter vibration zone can be avoided by adjusting the cutting parameters or selecting other tool geometry: (1) reduce the axial depth of cut, radial depth of cut, flute helix angle, (2) increase the spindle speed, tool diameter.

8.2.5 Case study parts

Case study parts were provided by a few companies to develop and evaluate the ASM process chain or the part of the technology. GS Project design wanted to build a pedestrian bridge for Robotlan using WAAM technology. For this purpose, Thomas More designed the bridge and created the design for the WAAM process with further production of the bridge sections. After the evaluation, the process was approved, and GS Project design was capable of building the bridge. LCV company produced the TiGr5 part for a Belgium railway company using the WLAM process and wanted to implement the post-processing step. For this purpose, the part was scanned and further machined by Diametal with guidance from the research partners. The tool wear was monitored. As a result, no increased tool wear compared to the machining of the bulk material was observed. Finally, Sonaca provided the aerospace part to evaluate the ASM process chain as an alternative to the forging process for workpiece production. KU Leuven optimized the deposition strategy for WAAM with further prototype production from the low carbon steel. The energy and material efficiency of the ASM is being analyzed.

Besides the provided case studies from companies, other parts were produced to answer the critical questions raised by the user consortium. First, the feasibility and deposition path optimization was implemented for the parts with complex geometries that require either the variable slicing along the linear build direction or variable build directions along the specific curves. Three parts were produced: Duvel glass, heat exchanger and exhaust manifold with further knowledge transfer to the industrial partners. Second, the impact of the part production method (i.e., hybrid, when the substrate plate is pre-machined and further used as a part of the component) on the post-processing step and final part characteristics was evaluated based on the impeller. Third, the mechanical properties, internal and surface defects of the WAAM parts were of the big interest for the user consortium. Thus, the weld-neck flange for the pressure vessels application was produced with further detailed destructive and non-destructive material testing showing the potential of WAAM based ASM process chain to be used as an alternative method for part production.

Duvel glass (Thomas More)

In the first case, the shape is chosen for the contour of the dowel glass. This shape is rotationally symmetrical about the Z-axis of the glass. The challenge of this workpiece for the WAAM process is that the welding torch must always be held tangentially to the surface of the wall. This is necessary to obtain a good structure of the deposited welding layers.

This challenge ensures that the robot cell is equipped with a positioning table. By using the positioning table, the workpiece can be held at different angles if desired. This ensures that the welding torch is always in the ideal position (PA) to obtain an optimal weld pool.

After the workpiece had been drawn, it was possible to start programming the tool paths. Due to the knowledge already acquired of layer thicknesses and step heights, determining the right parameters for a desired wall thickness was no problem. The CAM software used for tool path programming is Siemens NX.

The tool paths are programmed per segment. Because Siemens NX uses a horizontal 2D slicer. Of these, only the vector of the slicer can be adjusted. A horizontal 2D slicer is not applicable for this case. As a result, a strategy is used that makes it possible to produce the workpiece. The current 2D slicer will always generate a tool path at a fixed height in the vector of the slicing.

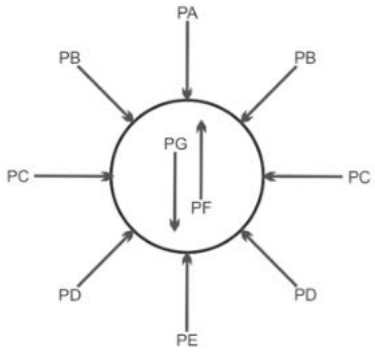

PA	Lassen onder de hand
PB	Staande hoeklas
PC	Horizontaal / Verticaal lassen
PD	Hoeklas boven het hoofd
PE	Lassen boven het hoofd
PF	Lassen naar boven
PG	Lassen naar beneden

Figure 8-23: Welding positions

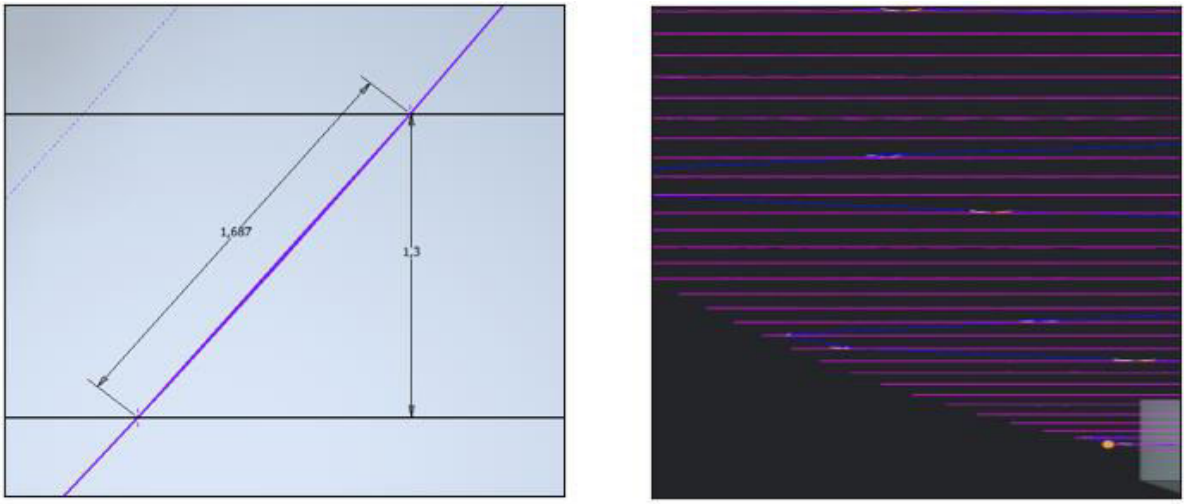

Figure 8-24: Step height

Generating a tool path at a fixed height relative to the previous path creates an error of up to 300% from the desired step height. In Figure 8-24, the desired step height is 1.3 mm, but because the slicer always slices a fixed height, the distance to the contour of the workpiece is 1.667 mm. The steeper the overhang, the greater the error between the desired step height and the actual one. The solution to this problem is to generate segments. The workpiece is divided into segments that always have the same overhang with respect to the X-axis. By working in this way, the horizontal slicer can always be set with

a different step height, so that the actual step height on the contour of the workpiece achieves the desired value.

The welding was done with a wire speed of 2m/min and a travel speed of 400mm/min. To maintain this travel speed, the rotational speed per segment was adjusted as a function of the average diameter of that segment. During the welding the temperature between the layers had always dropped to 120°C before depositing the next welding layer.

After the WAAM process, the workpiece was scanned with a GOM scanner. The GOM-inspect software offers the option of comparing a scan and the original CAD file. The scan results show that the workpiece is provided with sufficient oversize for finishing by means of a CNC-controlled lathe

	Layer	Layer thickness CAM (mm)
DUVEL_1	3_5	0,4
	6_9	0,5
	10_13	0,6
	14_17	0,7
	18_21	0,8
	22_26	0,9
	27_33	1
	34_43	1,1
	44_49	1,2
	...	...

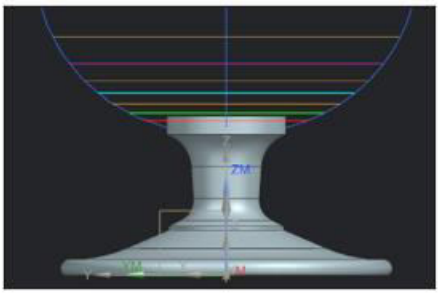

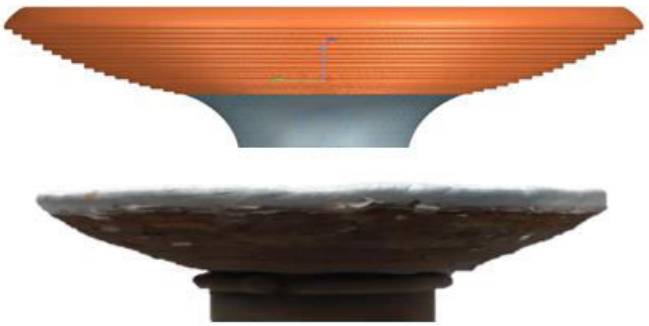

Figure 8-25: Slicing of Duvel glass

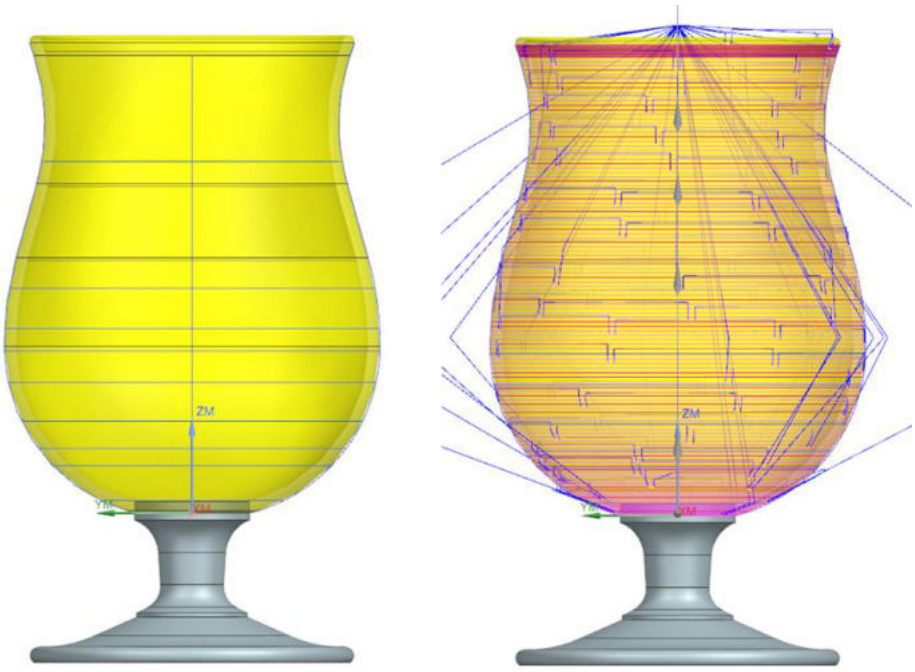

Figure 8-26: Deposition path for the Duvel glass

The turning of the outer contour was done with a CNC controlled lathe. As lathe tool, a round cutting plate with a diameter of 10mm was used. This ensured that the entire contour can be finished in 1 movement. The cutting speed was 24 m/min, feed speed 0.015 mm/rev and the speed was 93 rpm.

No irregularities occurred during post-processing. The material cut nicely in short chips. During the visual inspection after finishing, no irregularities in the deposited material could be detected. The homogeneity is the same over the entire piece.

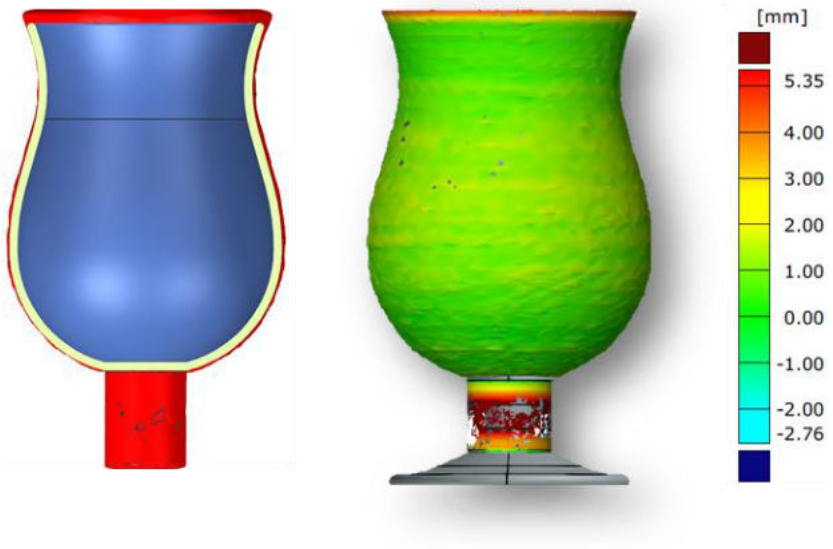

Figure 8-27: The result of Duvel glass scanning

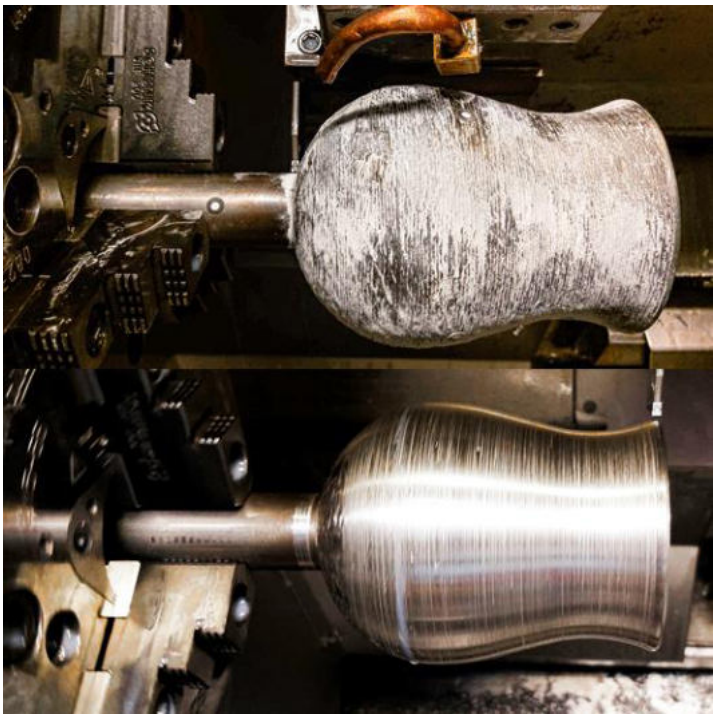

Figure 8-28: Post-processing of Duvel glass

Heat exchanger (Thomas More)

As a second case, it was decided to manufacture a heat exchanger. Such a heat exchanger can be used in many industries for cooling liquids or gases that are transported under high pressure. Several liquids can also flow through the workpiece, depending on the end purpose of the installation.

This case entails the following particulars. The workpiece has a 90° bend. Since the molten pool must be deposited in a PA position at all times, a positioning table must be used. In addition to the 90° bend, it must be ensured that the ribs fit together nicely. These ensure that the different liquids or gases remain separated from each other. Due to these particularities, we work on the basis of 2 sub cases. Separately, we first look at a way to create a 90° bend and ribs. The figure on the next page shows the heat exchanger. The yellow piece serves as a flange to mount this whole on a larger construction.

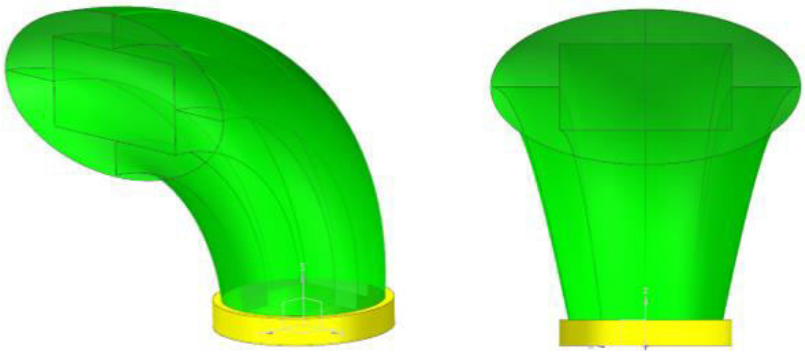

Figure 8-29: Heat exchanger

To slice a curve you can use the general function “slice while following the center curve”. However, this does not result in a good result, because the slicer only takes into account the curve along which the workpiece is shaped. This means that the step height entered in the slicer will ensure that the material build-up in the middle of the piece is exactly as expected. There is less material on the outside of the curve and on the inside there is a material build-up. Two solutions are relevant to this problem. The wire speed can be made to increase in speed at the outer radius and decrease at the inner radius. However, this results in a very complex control of the welding source. Solution two will ensure that the workpiece is completely segmented. Each segment contains 5° - 10° of the total curve. By always building up per segment, the whole can be designed in a stable manner.

Figure 8-30: Slicing segments

The figure above shows the problem of the standard slicer well. On the outer radius, the tool paths are further apart, in contrast to the inner radius. The effect of this is clearly visible in the figure. The stick-out length increases on the outer radius and will ensure that the weld pool is no longer protected from its impurities.

The figure on the next page shows 1 segment of a series of segments that make up the entire curve. It is clearly visible on this that more material is deposited on the outer radius.

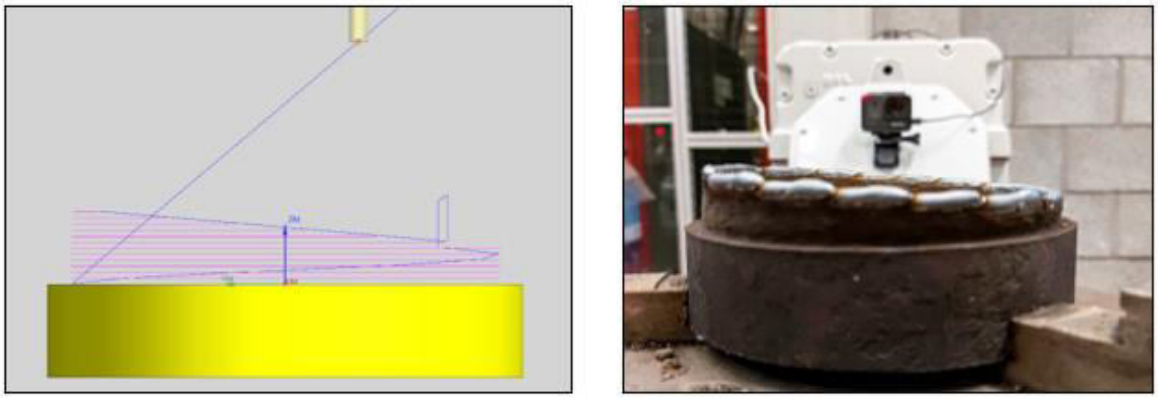

Figure 8-31: Successful build-up of segments

Ribs

To obtain a good adhesion between the outer and inner wall, the ribs must adhere nicely to both walls. It was already clear from previous experience that the start and stop point of the tool path has a major influence on successful bonding. The first test was therefore the welding of a rib against 1 central welding track. It was decided to perform this test with the same wire speed and lead speed from which the

original part is built. The test ribs were stopped in steps of 3-0mm before the center weld path and 0-3mm after the center weld path. This in intermediate steps of 0.5 mm.

This test has shown that the best result for starting and stopping a welding job is achieved by stopping the original wall at 1.5mm from the wall to be bonded. This results in a nice attachment and homogeneous crossing.

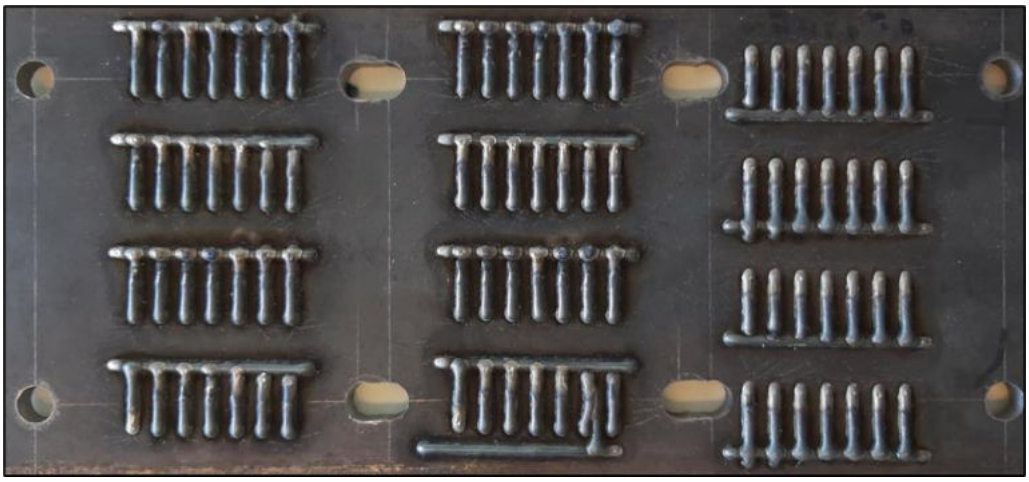

Figure 8-32: Deposited ribs

End result heat exchanger

To produce the heat exchanger, the 2 partial results of the 2 previous chapters were combined into 1 whole. The result is a successful heat exchanger that is ideally suited to industrial environments. The production time of the whole is 3 hours. Between the layers, the temperature is monitored with a thermocouple. The temperature of this must not exceed 120°C before depositing the next layer. After 10-15 layers, the workpiece is thermally stable, and the same cooling time can always be used on the basis of a fixed time span.

Figure 8-33: Result heat exchanger

Exhaust manifold (Thomas More)

Case 3 emphasizes the convergence of multiple components within 1 setup for WAAM. For this case, a simplified exhaust manifold was chosen. This exhaust manifold consists of 3 tubes that come together in 1 main tube. During this case, the already gathered information was used to create structures along a curve.

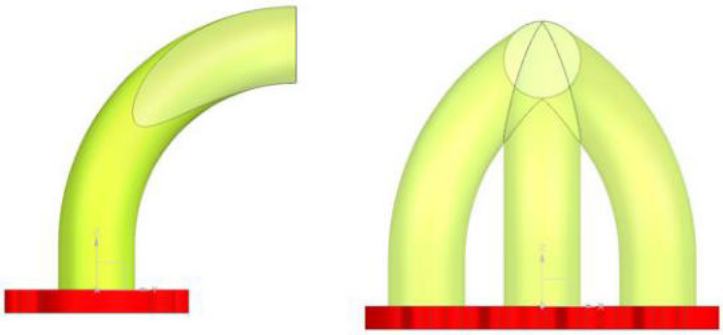

Figure 8-34: Exhaust manifold

As curves, the 3 centerlines of the tubes were chosen to generate the tool paths. The wire speed during welding is 2m/min and the lead speed of the robot is 400mm/min.

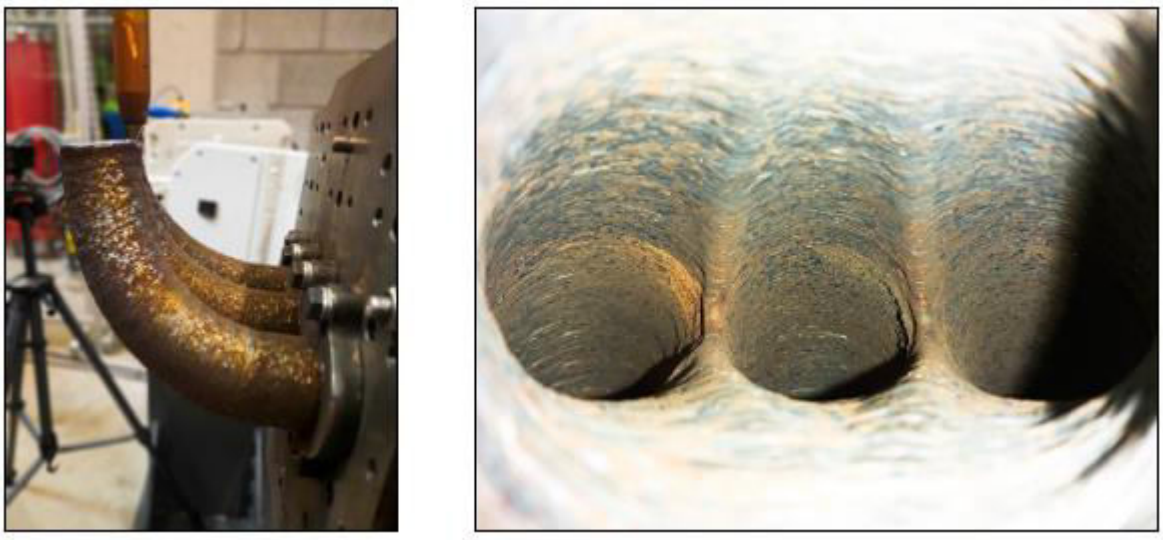

Figure 8-35: Result exhaust manifold

Impeller (Thomas More + KU Leuven)

As a last case an impeller was welded on. This impeller is constructed as a hybrid workpiece. The hub was completely turned off before welding. Afterwards, the welding layers were deposited. After welding, the piece was scanned. The scan ensured that the tool paths for finishing were precisely programmed.

This piece ensured that all axes of both the positioning table and the robot moved simultaneously with each other. This time the wire speed was 4 m/min and a feed speed of 400 mm/min. The piece could be constructed simultaneously, i.e., all sheets were deposited in 1 program.

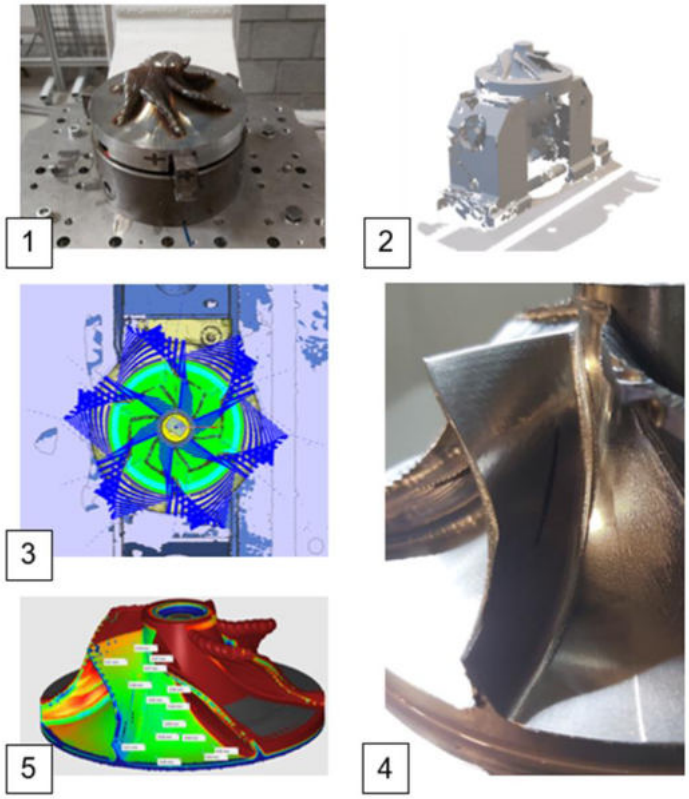

Figure 8-36: ASM process chain of impeller

LCV (Thomas More, LCV, Diametal)

LCV company produced the TiGr5 part for a Belgium railway company using the WLAM process and wanted to implement the post-processing step. For this purpose, the part was scanned and further machined by Diametal with guidance from the research partners. The tool wear was monitored. As a result, no increased tool wear was observed on the machining of the WAAM part, compared to the machining of the bulk material.

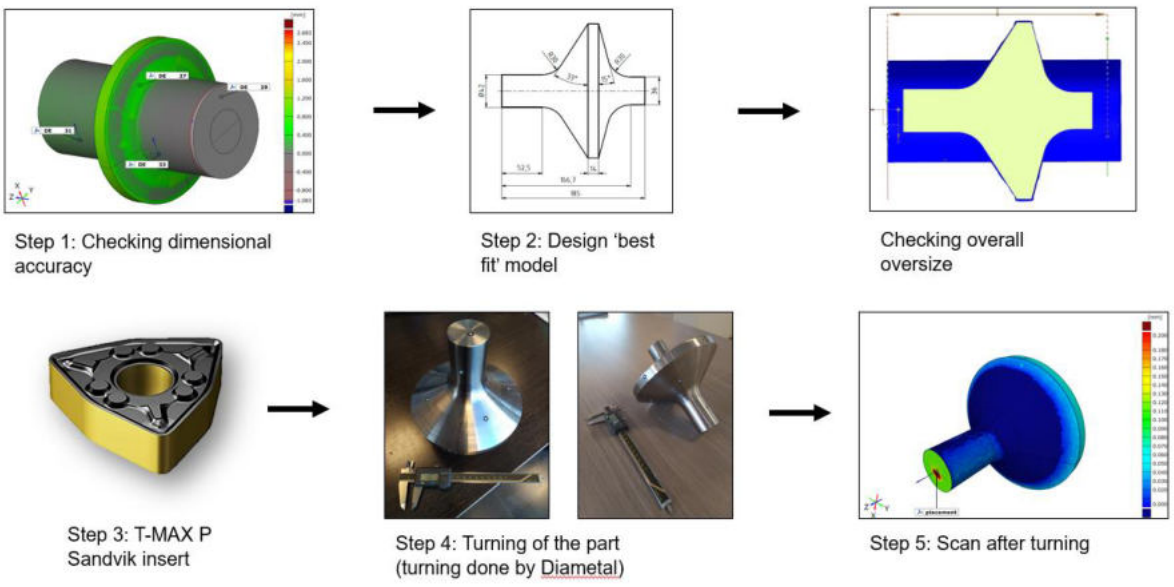

Figure 8-37: post-processing of part for railway company

Robotland bridge (Thomas More)

GS Project design wanted to build a pedestrian bridge for Robotlan using WAAM technology. For this purpose, Thomas More designed the bridge for WAAM with further production of the bridge sections from low carbon steel. After the evaluation, the process was approved, and the GS Project design was capable to start building the bridge.

- Goals:
  - Reduce distortion during welding
  - No wait time
  - Usage of sections
  - Minimize post-processing
- Specifications
  - Weight 1600kg
  - Width 1,5m
  - Bridge span 8m

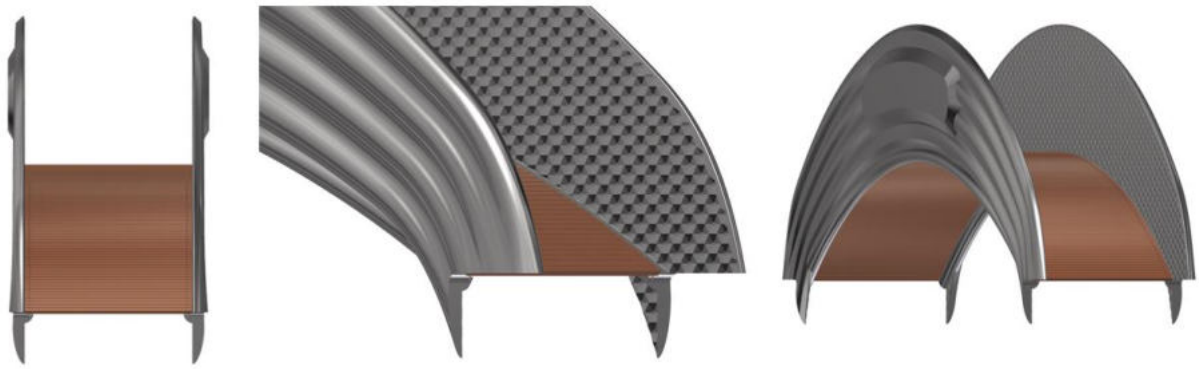

Figure 8-38: Design of the bridge

Result:

- Single contour sections
- Conform NBN 03-004
- Using T-bolts DIN 508 for mounting wooden walkway
- Special surface on the inside

The scaled part was printed with wire feed speed 2m/min and travel speed of the robot 400 mm/min.

Figure 8-39: Deposition of bridge prototype

Sonaca case (KU Leuven)

Sonaca provided an aerospace part to evaluate the ASM process chain as an alternative to the forging process for workpiece production. First, KU Leuven optimized deposition strategy for WAAM based on the simplified part that includes key features. Optimized strategies and part design were evaluated within the ASM process chain. Further, prototype was produced from low carbon steel.

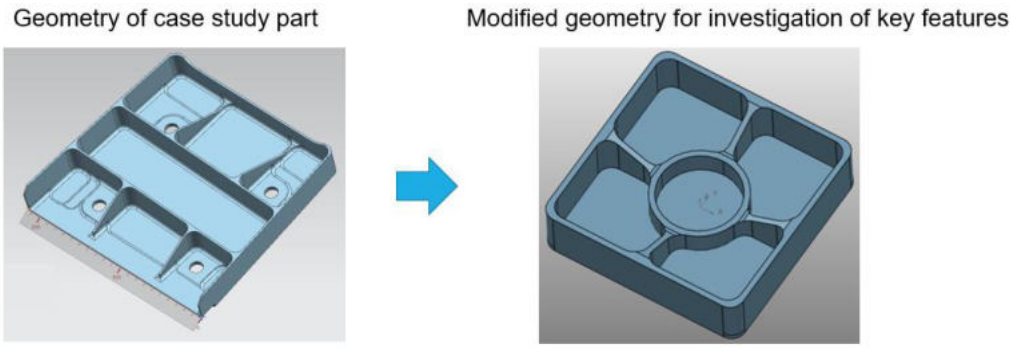

Figure 8-40: Geometry of the part for key features investigation

Investigation of deposition strategies

1) Initial strategy: Offset. Drive curve - MAT (medial axis).

Impact of deformations was considered during the design for WAAM stage. WAAM parameters were optimized as well. Reference dimensions after deposition met the requirement. Nevertheless, some problems were detected in the intersection points: (1) lack of material, (2) reduction of effective wall width.

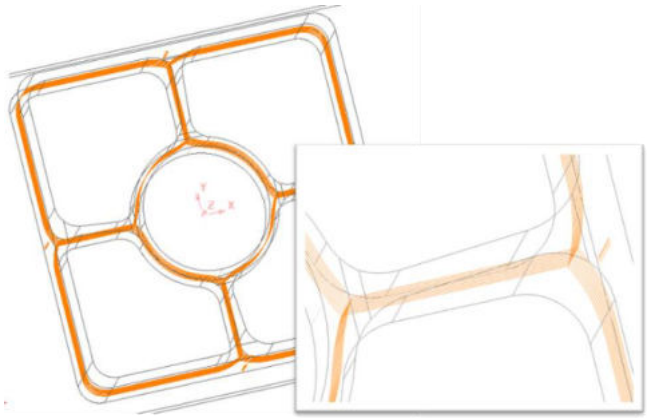

Figure 8-41: Offset strategy with MAT drive curve

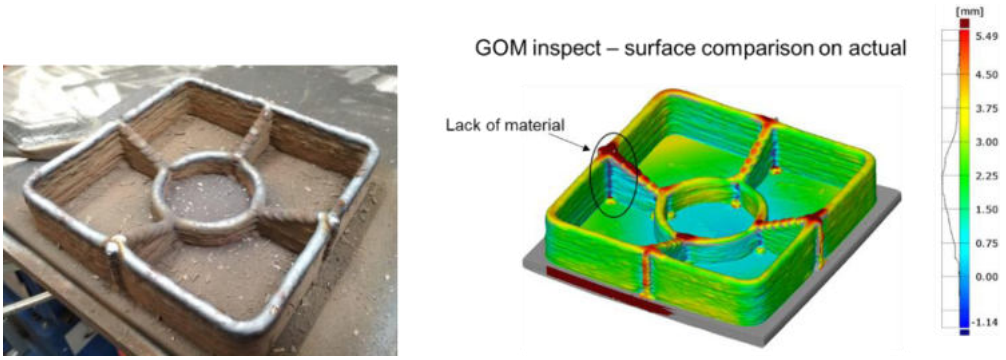

Figure 8-42: Resulting part with lack of material

2) Strategy: Offset. Drive curve – region perimeter.

WAAM workpiece was redesigned for the new strategy. WAAM parameters were adjusted respectively. The deposition strategy resulted in:

- Unstable deposition due to peak formation in intersection points
- Unacceptable quality (holes in the intersection points)
- Further optimization of the deposition strategy is required

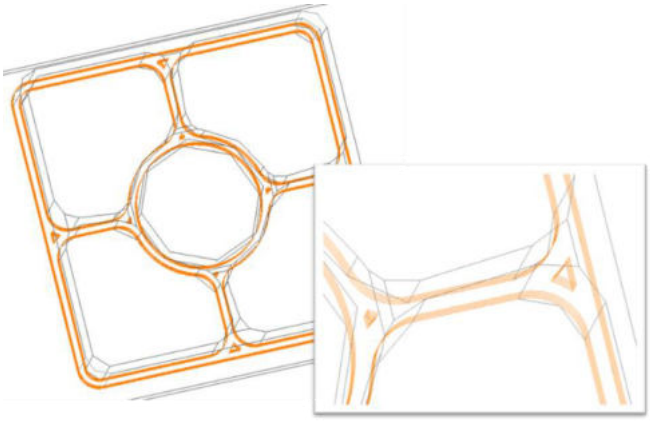

Figure 8-43: Offset strategy with region perimeter drive curve

Figure 8-44: Resulting part with unacceptable quality

3) Optimization of deposition strategy

After series of experiments, optimal deposition strategy was determined:

- Optimal S_o 1 = 0.825*w (where w – weld bead width) as it does not impact the base surface and provides proper overlapping
- Optimal S_o 2 = 0.738 w
- Optimal distance between the fillet passes and the tail was determined earlier and equal to 0.5 w + using of crater filling 0.5 s
- After every 4 layers, the fillet passes should be skipped

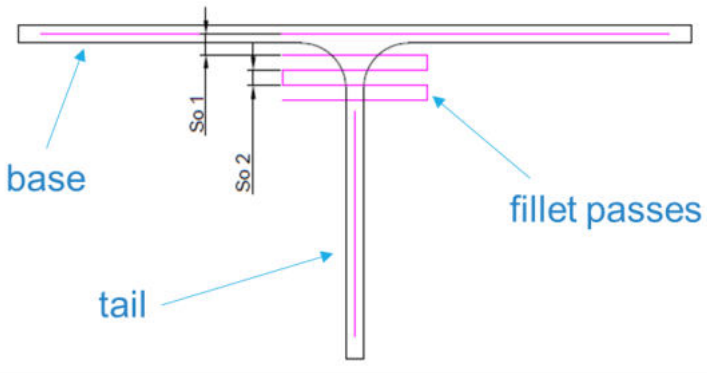

Figure 8-45: Schematic representation of the optimized deposition strategy for T-crossings

4) Optimized strategies and part design were evaluated within the ASM process chain

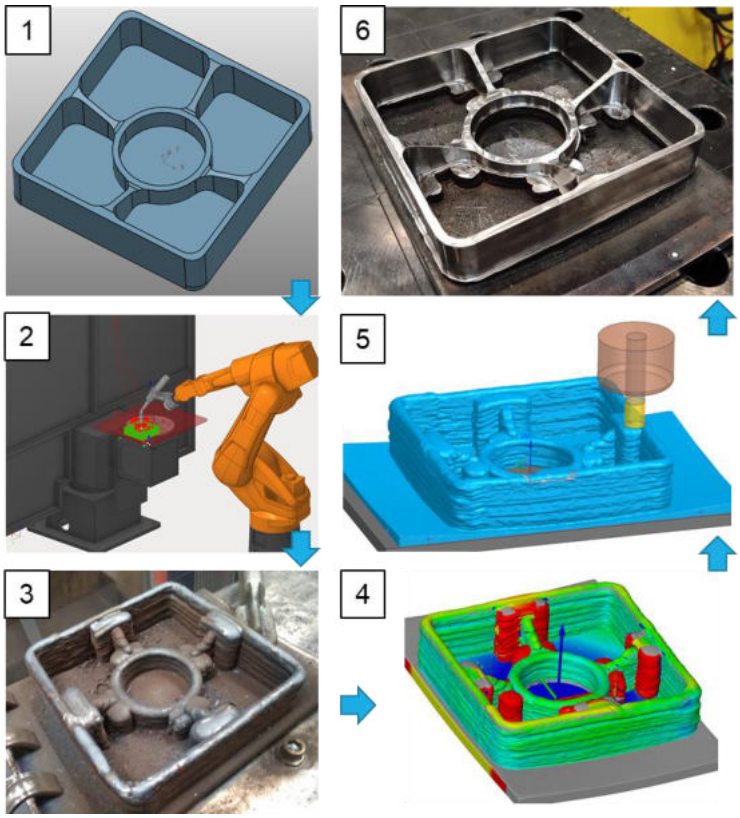

Figure 8-46: ASM process chain of the case study part

5) Prototype was produced from low carbon steel. Machining, energy and material efficiency analysis of the ASM are in process.

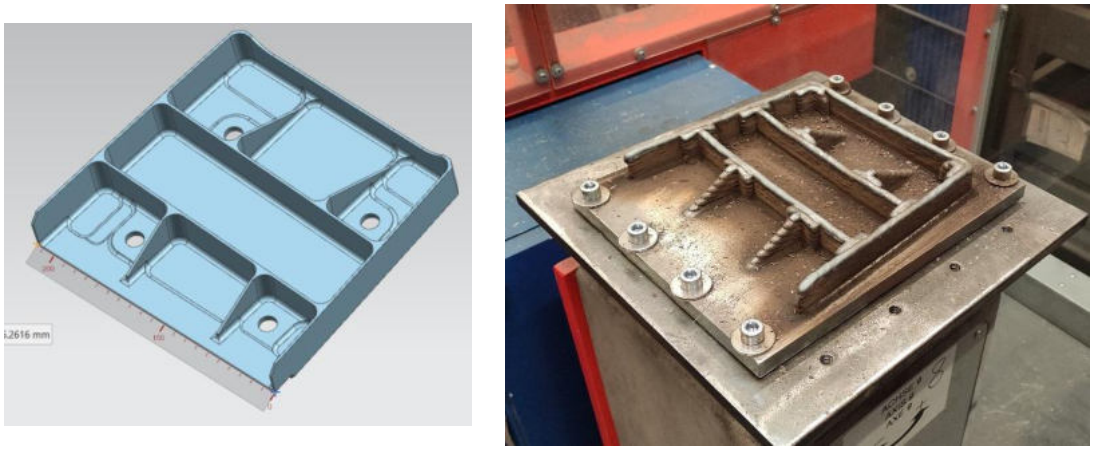

Figure 8-47: Prototype of the industrial part

Weld-neck flange for pressure vessels application (KU Leuven)

Two flanges (EN 1759-1 / 11 / B / DN 40 / Class 300 / SA105) were produced to evaluate the potential application of WAAM for pressure vessels. Flange 1 – without post weld heat treatment, and flange 2 – with stress relief post weld heat treatment as shown below. Overview of ASM process chain:

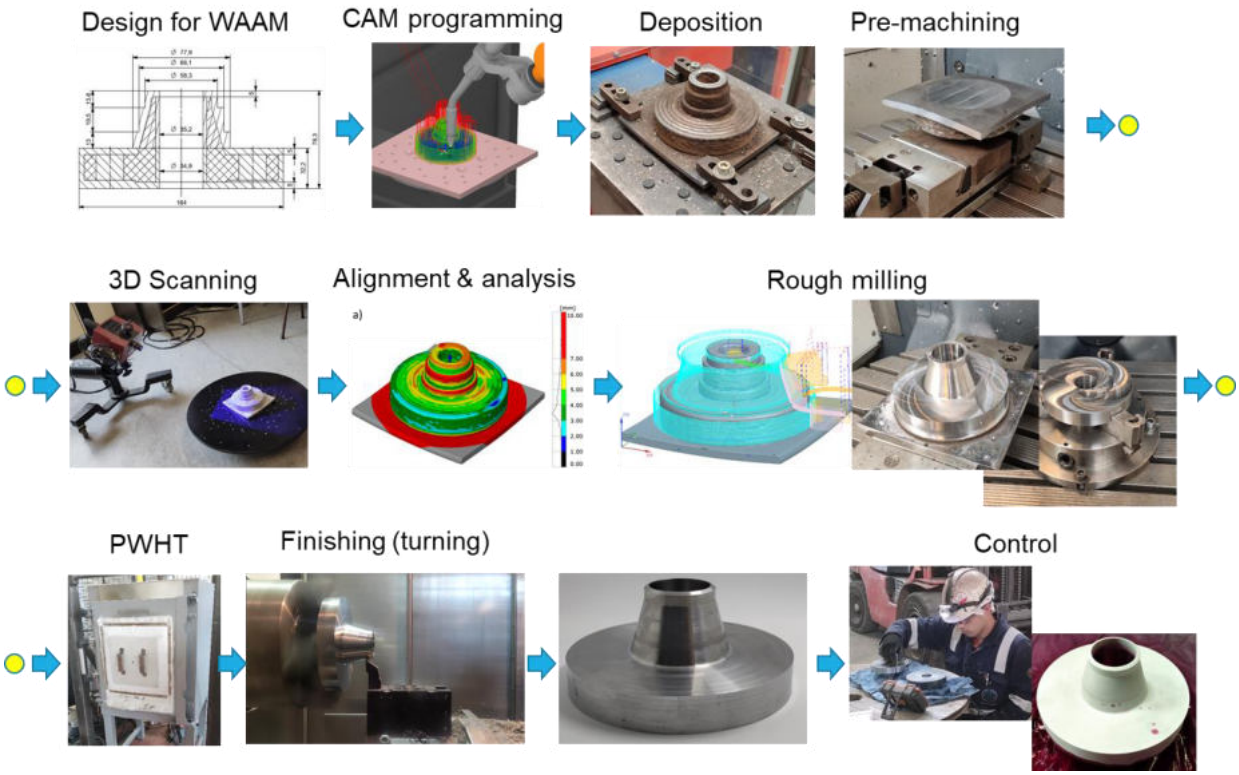

Figure 8-48: ASM process chain of the weld-neck flange

After post-processing, detailed destructive and non-destructive material testing was implemented. UT testing was performed by external certified company. No unacceptable defects were detected in the flanges. Liquid penetrant testing detected few unacceptable surface defects that may be repaired by local grinding and welding with further NDT according to EN 13445-4.

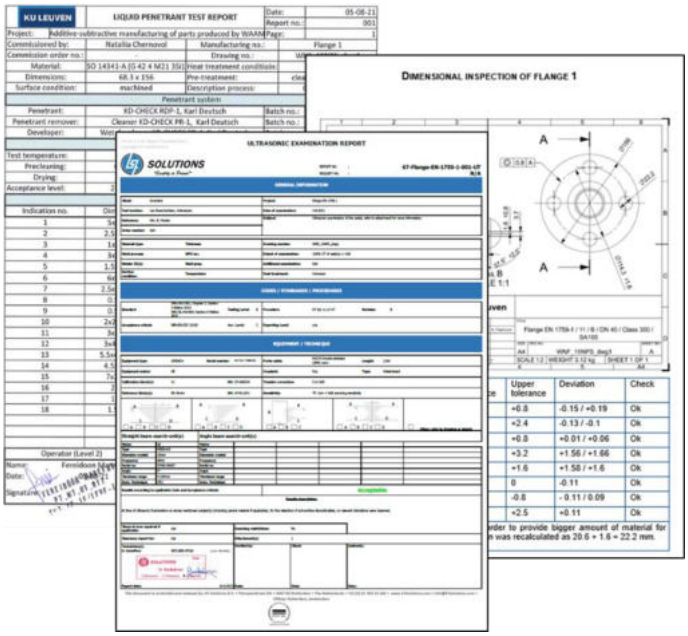

Figure 8-49: Test reports of the weld-neck flange

Macro-examination showed the build-up of beads and sound penetration.

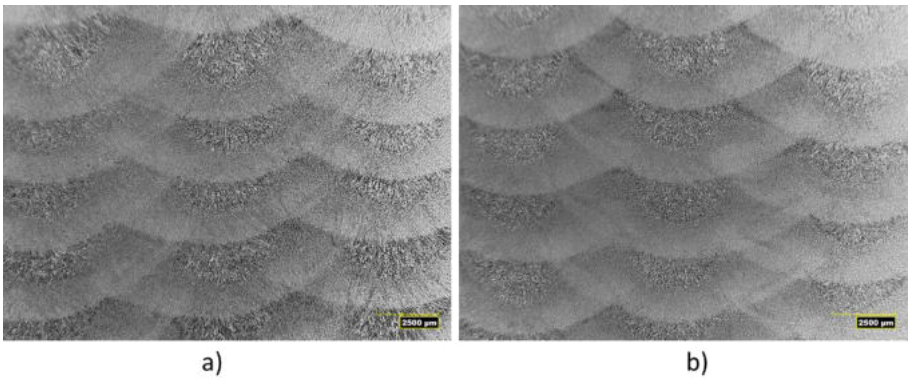

Figure 8-50: Macrostructure of (a) flange 1 and (b) flange 2.

The post weld heat treatment slightly impacts the yield strength and impact toughness of the material. The lower yield strength reduces by 6.9% and the upper yield strength reduces by 9.2%. Nevertheless, the properties of the WAAM material meet the requirements of ASTM A105 material. The average impact toughness increases after post weld heat treatment. Moreover, the toughness properties of the WAAM material go beyond the requirement set in EN 13445-2 (≥ 40.5 J).

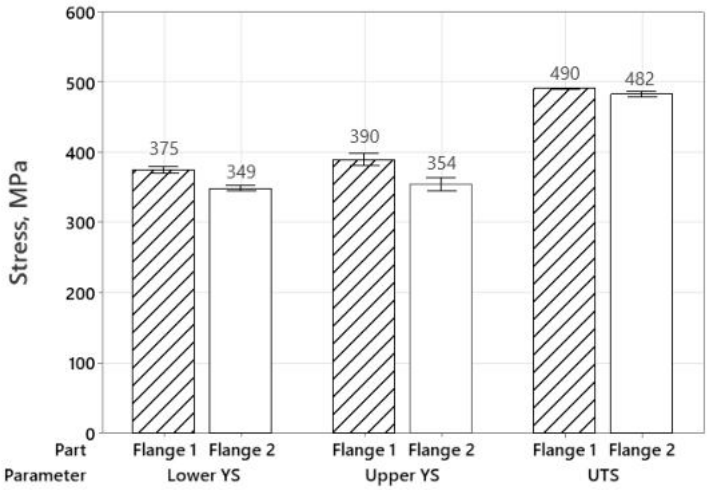

Figure 8-51: Lower Yield Strength (YS), Upper Yield Strength (YS) and Ultimate Tensile Strength (UTS) of flanges produced by WAAM..

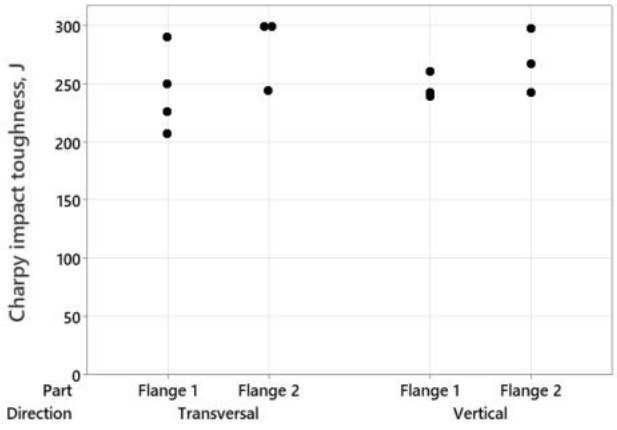

Figure 8-52: Charpy impact toughness of flanges produced by WAAM.

8.2.6 Dissemination activities

There were 3 companies where the WAAM process chain and part of the technology and know-how were integrated. Thomas More integrated the WAAM process into the GS Project design company. Virtual robot manufacturing environment where it is possible to slice, program and postprocess WAAM parts was created together with the welding parameters database. The output of the postprocessing is thus immediately usable on an KUKA robot that is equipped with a Fronius welding source. The second company was Oqton – developer of the cloud-based CAM software Factory OS for AM. Oqton partially integrated the knowledge of the optimal deposition strategies and slicing algorithms provided by KU Leuven into created WAAM module. Additionally, the AI was used for online process monitoring and control. The module was verified by the production of the industrial case study part. The third company was LCV. Based on the case study part that was implemented together with Thomas More, LCV considered the scanning step to be integrated within the wire and laser additive manufacturing based ASM to optimize the manufacturing process chain.

Three workshops were implemented for the target industrial companies. Due to the COVID-19 it was not possible to organize the workshops in person. That is why 3 webinars were filmed. The webinars contain a theoretical explanation together with a demonstration of the practical implementation of the certain process step. Webinars were shared with the users' group via a closed YouTube channel link. Due to the complex preparation and videos processing, it was only possible to deliver the workshops at the end of November 2021. The workshops can be accessed through the following links:

1) *Workshop 1* is devoted to Wire and Arc Additive Manufacturing:
   https://youtube.com/playlist?list=PLR65B4SgaCKBD36-fTKgan3p0yQCoqHki
2) *Workshop 2* is devoted to the intermediate processes. It covers such aspects as 3D scanning, CAD model fitting and alignment, preparation of the part for future programming of the machining step in CAM:
   https://youtu.be/mToCJ2-Fr4M
3) *Workshop 3* is devoted to the post-processing of the WAAM parts:
   https://youtu.be/V4PSYYdA6fk

Research results were presented at the CIRP conference ISEM 2020 (2 papers) and BIL|NIL Lassymposium. One paper was published in the CIRP JMST journal and 3 papers are currently in preparation. Furthermore, dissemination of the research results led to the collaboration of the researchers within KU Leuven.

- Chernovol, N., Lauwers, B., Van Rymenant, P. (2020). Development of low-cost production process for prototype components based on Wire and Arc Additive Manufacturing (WAAM). In: *Procedia CIRP*: *vol. 95*, (60-65). Presented at the 20th CIRP CONFERENCE ON ELECTRO PHYSICAL AND CHEMICAL MACHINING, Zurich, Switzerland. https://doi.org/10.1016/j.procir.2020.01.188
- Lauwers, B., Chernovol, N., Peeters, B., Van Camp, D., Van Riel, T., Qian, J. (2020). Hybrid Manufacturing based on the combination of Mechanical and Electro Physical–Chemical Processes. In: Procedia CIRP 95 (2020), (649-661). Presented at the 20th CIRP CONFERENCE ON ELECTRO PHYSICAL AND CHEMICAL MACHINING, Zurich. https://doi.org/10.1016/j.procir.2020.11.003
- Chernovol, N., Sharma, A., Tjahjowidodo, T., Lauwers, B., Van Rymenant, P. with Chernovol, N.

(corresp. author) (2021). Machinability of wire and arc additive manufactured components. *Cirp Journal Of Manufacturing Science And Technology*, *35* (C), 379-389. https://doi.org/10.1016/j.cirpj.2021.06.022

- Smismans, T., Chernovol, N., Lauwers, B., Van Rymenant, P., Hojjati Talemi, R. with Hojjati Talmei, R. (corresp. author) (2021). Influence of Post-Heat Treatments on Fatigue Response of Low-alloyed Carbon-Manganese Steel Material Manufactured by Direct Energy Deposition-Arc Technique. *Materials Letters*, Art.No. 130465 https://doi.org/10.1016/j.matlet.2021.130465

GMAW based WAAM and ASM process chain are included in multiple education courses in KU Leuven and Thomas More. 3 master theses in KU Leuven and 2 theses in Thomas More were written by the students. As the selection of master and bachelor thesis is based on a free choice/selection by the students, the proposed ASM related topics were not always selected. More master and bachelor theses on ASM are foreseen in future. A demonstration set-up including monitoring has been built and partially integrated into the GS Project Design company. A “holistic process planning approach” has already been finalized based on the experimental results and verified on the industrial case study parts.

8.3 Summary

The additive-subtractive process chain was investigated for parts produced by WAAM. Experiments were conducted to build the empirical models for bead geometry prediction for both conventional GMAW and CMT processes. Obtained models allow to select the optimal wire feed speed and travel speed of the robot to produce the part with a specific thickness. Comparison of the conventional and CMT processes showed that multiple factors determine the applicability and productivity of the GMAW process.

At the start of the project, the user group members found it important to understand how much material should be provided for the machining step to achieve the required dimensional and geometrical accuracy of the part. As a result, the allowance for machining was determined considering the WAAM process parameters and the effect of the thermal-induced deformations on the WAAM part performance:

- The WAAM process parameters significantly impact the effective wall width, as-deposited surface quality and corresponding minimum amount of stock material to be removed during post-processing step. It was shown that limiting the WFS to 4 m/min and keeping the TS in the range of 30 – 50 cm/min allows to reduce the minimum allowance to remove the wavy WAAM to 1 mm per side.
- The thermal induced deformations of the substrate plate during deposition leads to the reduction of the dimensions by 1.5 mm independently of HI and coarsening of the outer surfaces’ quality. After post-processing, the impact of the welding parameters on the geometrical quality of the surfaces was observed due to the redistribution of the residual stresses inside the components. Nevertheless, the reference dimensions do not differ significantly from as-deposited values (maximum difference 0.7%). The effective wall width is also affected by the substrate deformations, especially when the TS is high.

The issues related to the characteristics of the WAAM parts (significant waviness of the surfaces and deformations) raised the question about the optimal part positioning, alignment, and optimal cutting parameters for post-processing. A set of experiments were performed to investigate this and optimize the ASM process chain.

The WAAM process parameters, namely travel speed, wire feed speed, and interpass temperature, significantly impact as-deposited surface characteristics (i.e., flatness deviation and hardness) and the total wall width that further affects the milling process's kinematics and dynamics. The deposition of the WAAM components with shorter cooling time from 800°C to 500°C results in a hard and smooth as-deposited surface leading to a better chip formation, more uniform radial depth of cut, and thus better surface finish after machining. The milling parameters also have a significant impact on the kinematics and dynamics of machining. Sufficient allowance and feed per tooth should be provided to assure the good surface finish after machining. From the dynamics point of view, WAAM walls deposited with lower cooling time result in lower component stiffness, which provokes chatter vibrations excitation during milling. The axial depth of cut significantly impacts the machining stability; thus, it should be limited to improve the final surface quality.
The multi-sensor platforms were developed separately for the AM and post-processing steps to investigate the impact of different processes on the characteristics of the final part. For the WAAM step, the current, voltage, gas flow rate and temperature were monitored. It was shown that by current and voltage monitoring the stability of the WAAM process can be evaluated that allows to eliminate different material defects (e.g., pores) and enhance surface performance. Additionally, by controlling the interpass temperature, mechanical properties (hardness, tensile strength) and surface quality of the WAAM parts could be improved. The techniques used for monitoring the milling process include the use of dynamometers for force measurement, proximity sensors for vibrations monitoring. The contact between the workpiece and a tool was monitored to assess the analysis of the vibrations during the milling of the thin-walled part. The method to predict the chatter vibrations for the WAAM parts and adjust the cutting conditions to avoid them was proposed and experimentally verified.

The results obtained during the ASM process chain investigation were evaluated on the various industrial case study parts. The WAAM process chain and part of the technology and know-how were integrated into three companies. Workshops were implemented for the target industrial companies. The research results were disseminated to a variety of the target groups through the traditional dissemination channels (symposiums, international conferences, publications in international journals). GMAW based WAAM and ASM process chain are included in multiple education courses in KU Leuven and Thomas More.

8.4 Outlook

From the start of the project, collaboration with industrial partners from the user group was a key aspect for successful project implementation. During the regular meetings, companies provided relevant feedback, proposals and asked questions guiding further research and development. Few case study parts were produced in collaboration with industrial partners resulting in valuable output both for the companies and for the entire project. Moreover, the raised questions from the industry were answered based on the parts proposed by the research partners showing design rules for the WAAM part to achieve

dimensional accuracy and required surface quality, the impact of the WAAM process parameters on the material properties, different manufacturing approaches to produce parts with complex geometry (heat exchanger, exhaust manifold, impeller). Different parts configurations (i.e., symmetric and axisymmetric) were also investigated showing the significant impact of part geometry on deformations, machining allowance and optimal ASM process chain.

This approach showed not only the general interest from the industry in developing a WAAM-based production chain and the WAAM process in general, but also the main barriers for integration of the WAAM technology in the industry. One of the barriers is the generation of the optimal WAAM deposition strategies and optimization of slicing techniques. This brought wide interest from the CAM vendors and resulted in closer collaboration with such companies as Siemens NX, Cards PLM, CNC Solutions, Oqton. Another barrier is the standardization and certification of the WAAM parts. Although the material properties of the WAAM parts were investigated based on the industrial case study parts, further investigation for various functionally graded materials is required.

9 Process chain optimization - Results of the ETH

E. Öztürk

U. Hudomalj

L. Weiss

(inspire AG / ETH Zürich, Switzerland)

9.1 Introduction

9.1.1 Initial situation and background

Additive manufacturing (AM) is seen as having great potential in the further development of manufacturing technology, i.e. in the production of mechanical components made of metal. AM encompasses a variety of processes that create predetermined shapes by melting metal powder or wire, often using a laser. As a rule, AM cannot produce a finished component, but a blank, which then undergoes heat treatments and subtractive processes on machine tools, for example milling or grinding and/or surface treatments, which is collectively referred to as ASM. AM is economically interesting above all for components that are specially designed for additive processes and derive a particular benefit from them. For this reason, the share of AM in total manufacturing has so far been negligible.

9.1.2 Motivation of the project

As AM and ASM become more important, the question of how energy efficiency correlates with the associated process chain becomes relevant. In manufacturing, the issue of energy efficiency has been raised by the EU Ecodesign Directive (2005/32/EC, superseded by 2009/125/EC) namely in relation to machine tools. In addition to exemplary investigations of individual machine tools, which play the key role in manufacturing, there have been several unsuccessful attempts to build up databases with energy parameters for different manufacturing processes. The main difficulty is that reliable statements can only be made if an entire process chain is considered, but the number of different process chains is arbitrarily high. In the LCA of components, the manufacturing energy is usually neglected because it is considered minor compared to the grey energy in the material. Likewise, the energy demand in manufacturing is of little economic interest. Energy optimisation is particularly interesting if it improves the thermal stability of the process and/or reduces material consumption, thereby indirectly improving quality and/or saving costs. Since AM uses the material as needed through targeted mould design, there is a presumption that AM can contribute to energy-efficient manufacturing. At the same time, however, AM processes are thermal processes with high energy requirements. It is not clear a priori which aspects predominate.

9.1.3 Project goals

Ad-Proc-Add investigates the energy and material efficiency of ASM process chains. It shows which qualitative and which quantitative statements are possible, whether and how these can be generalised. Due to the large number of process chains investigated, there is an expectation that particularly interesting examples will be discovered in which AM leads to completely new, altogether more efficient process chains. By generalising the exemplarily obtained data, it is to be simulatively determined whether and how a stronger market penetration of ASM influences the energy demand in manufacturing.

When metal powder is used as a semi-finished product for AM, various losses occur which are known qualitatively and are being investigated quantitatively for the first time as part of the project. In the case of AM in powder bed – LPBF – only a small part of the powder is processed, while the largest part is recycled material. Therefore, the question of the reusability of the powder is of great importance in the quantification of material efficiency.

Another topic is the clamping technology for AM components, a previously neglected aspect of ASM process chains. Also on an exemplary basis, it is investigated which clamping methods are optimal for ASM and how these affect the energy and material efficiency of the process chains.

For the manufactured components, the benefit of AM or ASM mostly arises in their application, for example through weight savings. Using less material leads to lightweight construction and, in the case of "mobile objects", to lower energy requirements. The quantification of these effects in the life cycle of the component requires studies on a case-by-case basis. The project is limited to determining whether such effects are to be expected in the life cycle or not.

9.1.4 Context of the international consortium

A large number of manufacturing processes were carried out and analysed in the international consortium (see Figure 9-1). This work allowed a comprehensive understandingfor these processes, and revealed typical process chains. A large part of the analyses was devoted to quality aspects, since AM and some of the subtractive processes are recent processes that have not yet reached the level of conventional manufacturing in terms of quality assurance. For the assessment of the energy and material efficiency of ASM process chains, the industrial relevance of the cases considered was decisive. For this reason, it was only possible to rely in part on sample parts from the consortium, and industrially relevant sample parts were developed in collaboration with the partner companies of the Swiss User Committee (chapter 9.5).

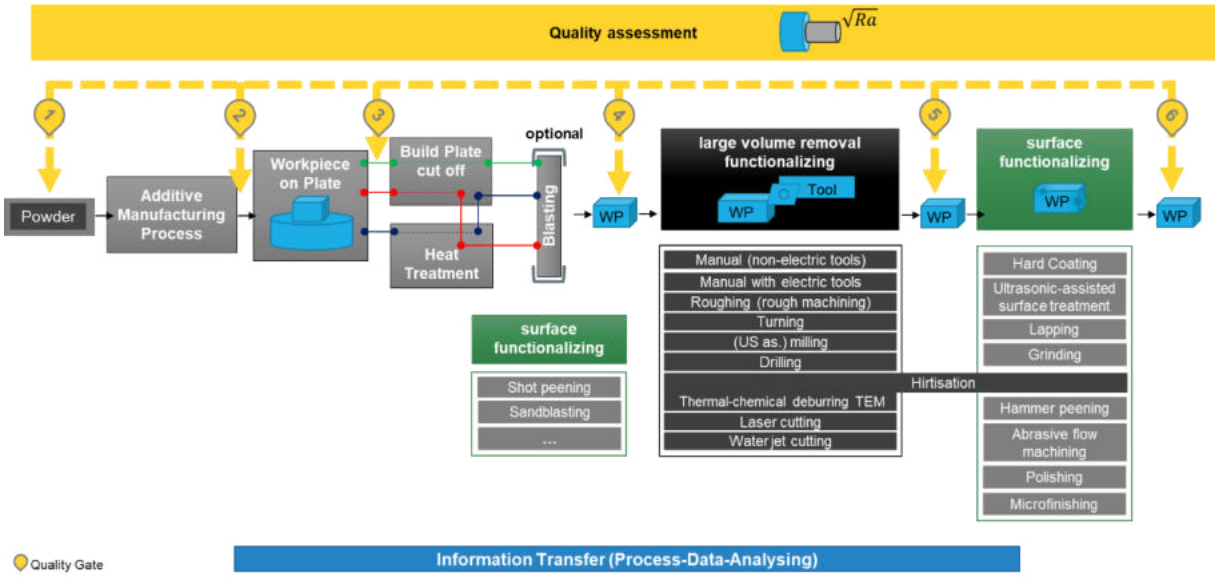

Figure 9-1: Process chains considered in the consortium.

The question of powder efficiency was a partial aspect of the powder quality analyses (chapter 9.3) provided by the Swiss partners within the consortium.

The clamping technology aspect (chapter 9.4) was mainly developed with expert knowledge, both from people within the international consortium and from UC Switzerland.

9.1.5 Interaction between design and manufacturing process

The design of a mechanical workpiece always takes into account several criteria and depends heavily on the context. The function of the workpiece is dictated by its function in the system, but usually leaves it open as to the exact form and whether the function is achieved with an integral design, or with a modular design, through several parts assembled together. In conventional manufacturing, a modular design can be very advantageous when assembled from simple parts made from standard semi-finished products. Additive processes claim that when producing small batch sizes, the cost per part does not increase (individuality for free), and that the complexity of the parts does not incur costs (see Figure 9-2).

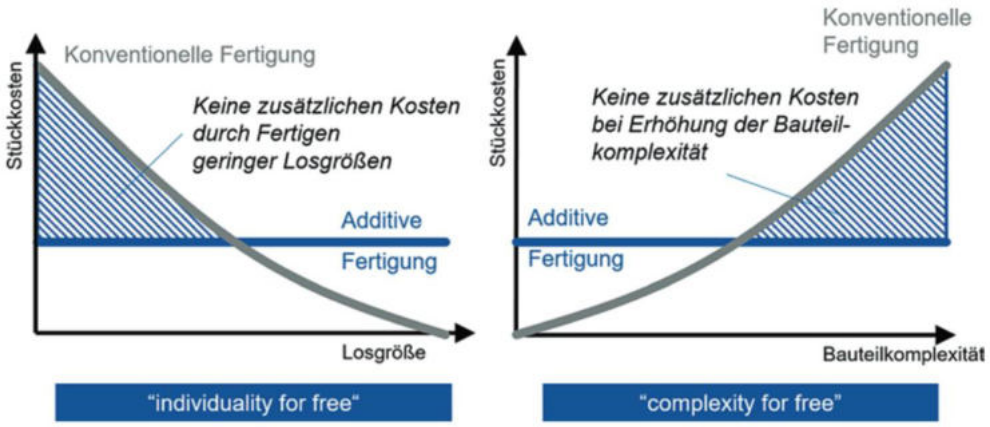

Figure 9-2: General advantages of AM with regard to lower initial costs and high workpiece complexity [1].

In this case, the design will tend to use this complexity for free in an integral design. This is not a priori a simplification. On the contrary, the use of the possibilities that AM opens up requires a more careful and elaborate development process. Different goals can be pursued and AM can support the development process as well as manufacturing in different ways, as illustrated in Figure 9-3 illustrated.

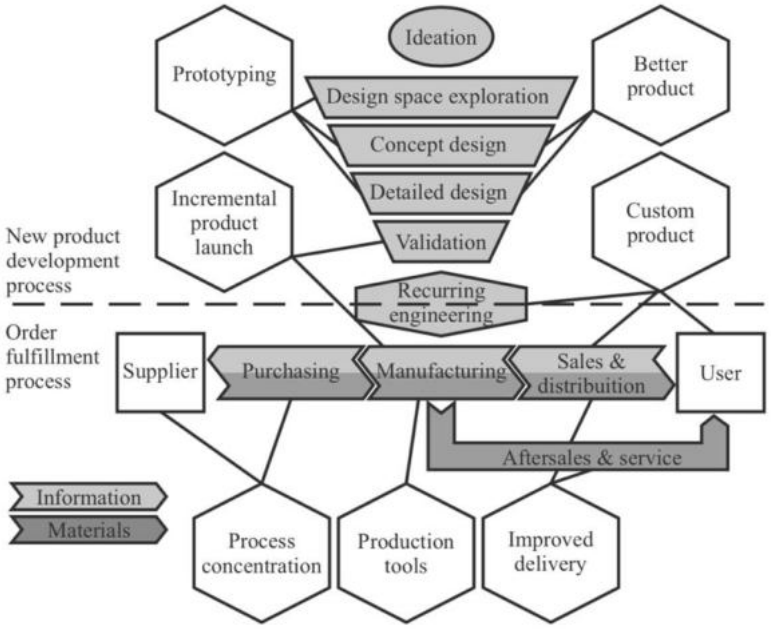

Figure 9-3: Added value of AM in product development and manufacturing [2].

- **Prototyping**: AM allows the rapid production of functional samples and prototypes, for example to check ergonomic aspects or a new function.
- **Incremental product launch**: The ability to produce single parts with high quality and no moulding costs allows incremental improvements in the early stages of product launch.
- **Better products**: The greater freedom of design fundamentally allows for better products, as more manufacturing compromises are necessary in the conventional development process.
- **Custom products**: The lower initial costs, especially for complex workpieces, allow customised products such as medical implants.

- The first three aspects are product-related, the last one is at the interface between product properties and manufacturing. Three further aspects are purely manufacturing-related:
- **Process Concentration**: AM as a Near Net Shape process promises shorter process chains
- **Production Tools**: By using AM, better and application-specific production tools can be provided with short lead times.
- **Improved Delivery**: The flexibility of AM increases delivery readiness.

These seven aspects form the framework for a qualitative assessment of the sample parts of this study.

9.2 Methodology

9.2.1 Research Question

How does AM influence the energy demand of manufacturing? - Does AM contribute to the energy transition, to the decarbonisation of the economy, or to developments such as electromobility? - What are the relevant energy aspects of an additive-subtractive process chain? - How will AM develop in the coming years in terms of energy demand? - Is AM a game changer? - Does AM increase the ratio of value creation to energy consumption? The study pursues two approaches in order to come closer to answering these questions: Firstly, the change of process chains due to AM is considered. Secondly, selected examples are used to show what effect these changes have on these components. Assuming that AM is only one part of a process chain that ultimately leads to a mechanical component, the study looks at how individual process chains are changed by AM and the impact on the energy side. Consequently, the focus is on the workpiece that is transformed from the raw material to the specified component, essentially using electrical energy and other resources that are mostly generated with electrical or primary energy.

9.2.2 Environmental assessment

All the studies carried out on the manufacturing process chain are based on the life cycle assessment method (DIN EN ISO 14040:2021 ff). First, the process chain and the machines and equipment involved were recorded, the inputs and outputs quantified and finally the impact estimated. For the ecology-oriented evaluation, it makes sense, after identifying the essential aspect(s), to focus on these issues and look for corresponding measures. In anticipation of the findings, the following fields of action or clusters for the classification of AM have proven to be promising:

More efficient planning / project planning: AM helps to improve the planning result, development runs faster (faster to market), the product achieves better quality, reduction of failures, more efficient, ergonomic, effective functions, manufacturability is a priori given, even if not necessarily cost-optimised.

More efficient production / manufacturing / production: AM enables a more efficient mannufacturing of a certain product (faster, better, cheaper) or the production of a product that cannot otherwise be produced in this way (direct benefit in the production of parts / products).

More efficient use: AM enables the production of parts for more efficient function, lower moving masses as well as longer service life (direct benefit in the use of these parts / products).

Since the study revolves around manufacturing, it is natural to take a closer look at the benefits of more efficient manufacturing. Typical benefits in manufacturing are:

- Use of more environmentally friendly materials
- Material savings: Less material required, needs-based and material-efficient
- Reduction of energy demand in manufacturing: Lower energy demand for manufacturing Reduce waste products, waste avoidance in production: Reduction of waste, rejects and thus also less material to recycle.
- Optimization of auxiliary materials: No or fewer auxiliary materials (such as cooling lubricants - elimination or reduction in cooling lubricant preparation as well as in recooling).
- Environmentally friendly transport logistics, shorter transport distances due to elimination of external process steps, less (and/or: less environmentally harmful) packaging material

Mechanical components are usually durable and in many cases they are either part of a mobile product (e.g. part of a vehicle), or an active product (e.g. an air compressor), or both (e.g. a jet engine). The life cycle inventory often applied to consumer goods, which essentially considers transport and material flows for provision and disposal, therefore falls short. In the case of active and/or mobile products, an environmentally oriented assessment must look more closely at the use phase, as explained in Figure 9-4.

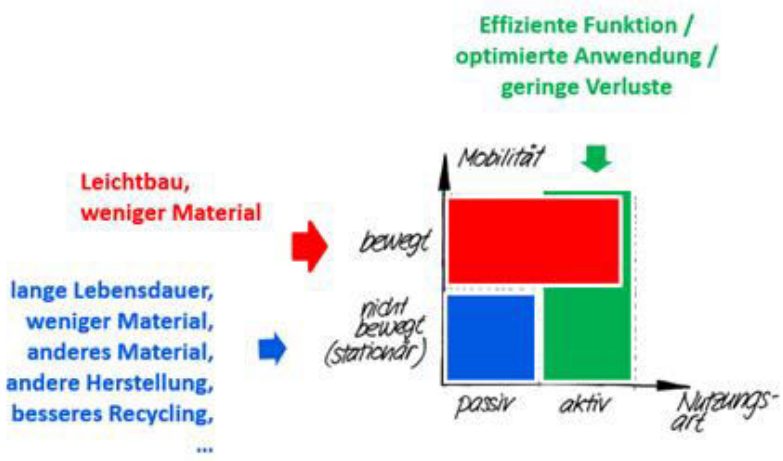

Figure 9-4: Portfolio for the life cycle assessment in relation to the type of product (Image: Rainer Züst).

9.2.3 State of the art

If we also look at the existing life cycle inventories for metals (ferrous and non-ferrous metals) and for the various processing methods (primary shaping, forming, surfacing and ablation processes), it becomes apparent that these are often only available in isolated cases and therefore make detailed ecological optimisation difficult or even impossible.

Statements on the life cycle assessment of process chains with AM have become more numerous in recent years [3], usually with a focus on AM as a new element. Obviously, the energy requirement for primary moulding with AM is higher than for conventional processes [4]. This is a factor of 10 to 100 in comparison with injection moulding for plastics or machining in metal processing.

Since there is agreement that AM is comparatively energy-intensive, there is also interest in proving the benefits of the new technologies over the life cycle, at least for selected workpieces. However, these calculations struggle with the uncertainties mentioned at the beginning regarding system boundaries and eco-factors. The two aspects are also interdependent: Factors that are difficult to determine tend to be omitted, even if they would be highly relevant, which decisively increases the uncertainty of the statement. In addition, especially in the case of workpieces that are used in active and/or mobile applications, design details can cause major differences in the use phase.

In manufacturing, specific energy is a popular indicator. In subtractive machining, mostly by cutting, this value represents the energy required to remove a volume. This value varies by one to two orders of magnitude depending on the machining task for the same process, for example milling [5]. The reason for this is that in this process it makes a big difference whether large volumes of material are removed by roughing or whether exact dimensions and demanding surface qualities are achieved by finishing. Attempts to collect and make available indicator values on a broad basis [6] have so far also failed because of this uncertainty and difficulty.

Initially, the demand-dependent use of materials was assumed to be typical for AM and was cited as an advantage. However, critical considerations have led to the assessment that material efficiency is generally overestimated and deserves critical consideration. [7] therefore proposes an extended analysis. The relatively low material efficiency leads to the conclusion that AM processes must be seen and further developed in the context of the circular economy [8].

Few studies have so far looked at the benefit aspect of AM. A meta-study identified [9] the three most important of the 20 benefits examined were flexibility in production, shorter development times for new products and local availability. While the findings are partly consistent with [2], they are likely to be strongly influenced by the assessment of AM with plastics and therefore give too little importance to aspects such as increased design freedom.

9.2.4 Material cycles

The material cycle within a process step takes on a special position, particularly in the case of casting: A part of the cycle material always runs along, e.g. from the sprues. In the case of LPBF, the powder is a recycled material; this cycle was explicitly investigated in this study. With LMD, direct reuse of the powder is not possible; it must be considered as scrap material. These material cycles in the process are directly added to the process step and are therefore relatively easy to handle.

9.2.5 Benefits of the first, second and third kind

The first kind of benefit relates to the optimised production of the part, and its consideration was the original aim of this study. However, as will be shown in the results, it falls short, or rather, it misses the essential ecological aspects.

The shape and other part properties are mostly aimed at the application, at the use phase of the parts, especially when they are active and/or mobile. This is called benefit of the second kind. As will be shown, most applications of AM aim at this. In the case of active and/or mobile components, this second kind of benefit is usually much higher than the (additional) effort required for manufacturing.

In addition, a third-party benefit can arise for another value chain that is influenced by the component. An illustrative example is a railway composition that is built lighter to reduce energy demand. This requirement may make production somewhat more costly - a harm rather than a benefit of the first kind, as it were - but this is more than compensated for by the lower energy requirement in operation, the benefit of the second kind. This is a requirement for the use phase of the train, and benefits the train's operating company. In addition, however, the lower weight will also cause less wear and tear on the rails and track, which is a third kind of benefit. The rail network may be maintained by a third company. This company derives a benefit without participating in the effort. If track fares are differentiated according to vehicle weight, this benefit is passed on to the train operator.

The leverage effect of this third-party benefit can be very great, as examples [10, 11] show. Statements can only be made by taking a close look at the individual case. Furthermore, it is not always possible to claim or pass on this third-party benefit, as in the example given.

9.3 Powder efficiency

9.3.1 Introduction

An advantage of AM that is often mentioned is the demand dependent consumption of material. While subtractive manufacturing sometimes involves machining 90% or more of the material, AM only builds up the necessary shape as a *near net shape,* which suggests a much lower material loss. Nevertheless, AM also causes material losses, for the LPBF process for three reasons.

Firstly, LPBF works with a **powder cycle** because only a small part of the powder is melted with each build-up process. The majority of the powder is collected, sieved and reused after the process is complete. Screening mainly removes spatters, i.e. material that was melted but did not remain in the component but splashed to the side. Furthermore, the cycle is not perfect, for example, some of the powder sticks to the surface of the component and is therefore lost. This is referred to below as handling loss.

Secondly, almost all workpieces require **reworking** for certain functional areas, during which material is removed. The material loss caused by the reworking depends on the component, therefore it cannot be determined in a generic consideration of the process. In chapter 9.5 this proportion is shown for various sample parts.

Thirdly, LPFB with metal powder needs so-called **support structures** (see Figure 9-**5)**, creating a thermal bridge to the base plate. Overhanging, concave structures could only be built with restrictions. These support structures are process-dependent and also component-dependent. They are also quantified in chapter 9.5 for various sample parts.

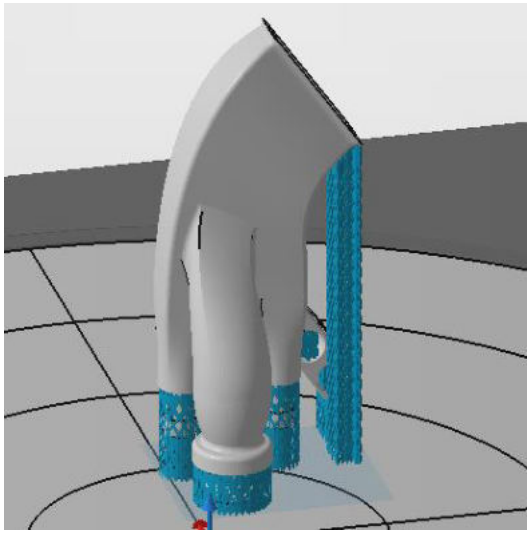

Figure 9-5: Support structures (blue) of a workpiece in the LPBF process (Image: inspire icams, Netfabb 3D Software).

The following experiment was dedicated to the first of these three aspects. In addition to quantifying the aforementioned losses in the cycle, there is also the question of whether the reuse of the powder affects the component quality. If this were the case, reuse would have to be limited, which would result in a systematic loss of material. The question is justified insofar as in AM with plastic powder a strong degeneration of the material properties actually occurs. One estimated that only about half of the powder can be processed and the other half has to be disposed of after a few cycles due to changed powder properties. There are also reservations about the multiple reuse of the powder when processing titanium.

Therefore, an attempt was made to experimentally answer the powder efficiency using the example of LPBF with aluminium (AlSi10Mg). To answer this question, the two sub-questions were adressed:

- How often can the powder be reused?
- How much powder is lost with each cycle?

9.3.2 Material and methods

The experimental procedure is shown in Figure 9-6. The experiment was dond in such a way that a total of 1.095 kg aluminium powder (AlSi10Mg, from the manufacturer Carpenter Additive) was processed, over several cycles, until only a residual amount of 0.107 kg powder remained. First, three different types of test parts were produced with fresh powder in three separate processes. The material properties of these test parts were determined. Then, the residual powder from these three tests was combined, sieved, and four consecutive AM cycles were performed, with the spatter in the powder sieved out after each cycle. The powder properties were also determined after each cycle. The experiment was stopped when the residual powder was not large enough for further AM cycles.

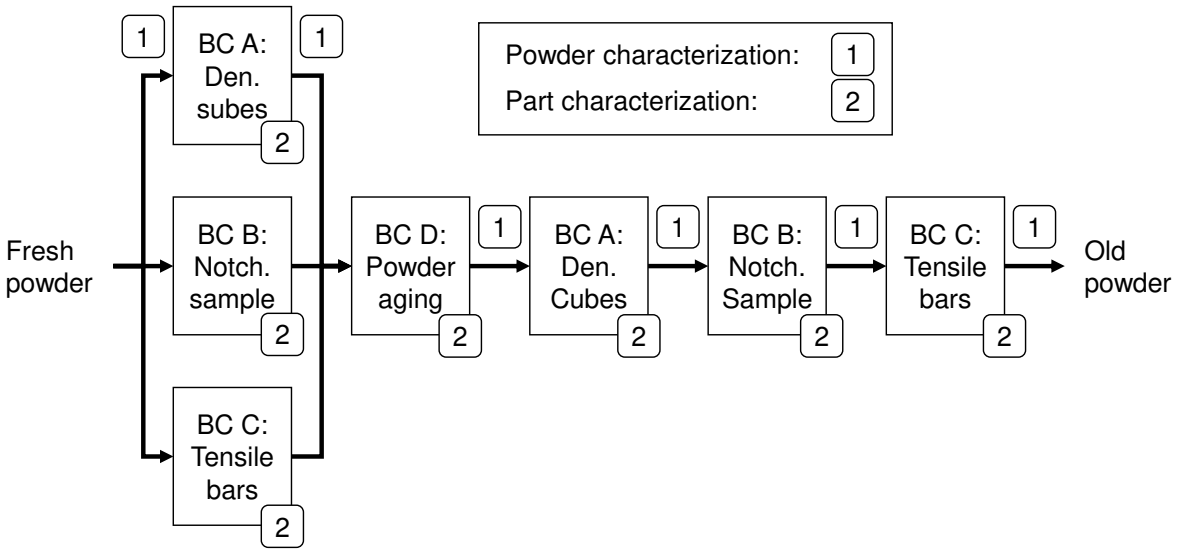

Figure 9-6: Powder flow and build cycles (BC) of the experiment.

In industrial practice, the missing amount of powder is constantly replaced by fresh powder, so that the powder is always a mixture of fresh and used powder, and no clear statement can be made about the influence of ageing on the component quality, nor about the losses that occur. In the experiment, the same powder went through a maximum of 5 cycles. Statistically, this is more than is likely to occur in practice, as will be shown in the following.

To characterise powder and parts, the following powder and part properties were measured along each step of the experiment:

- Particle size distribution (PSD)
- Bulk density, tap density and Hausner ratio
- Flowability with the Revolution Powder Analyzer
- Form factors
- Resulting final tensile strength
- Notched impact strength
- Chemical composition of the parts

9.3.3 Results

How often can the powder be reused? - The results show only a very slight change in the powder properties. The particle size distribution remains almost the same with a possible loss of fine particles, the shape factors remain unchanged and the flowability improves. The change in chemical composition of the finished parts was measured and an increased amount of impurities was found in parts made from old powder. However, no deterioration was observed in the mechanical properties of the parts. The reusability demonstrated here for aluminium is therefore not a limitation: The powder is melted in the component before it has degenerated through too many cycles. There is no systematic loss due to powder that can no longer be reused.

How much powder is lost with each cycle? - The experiment provides a basis for a model calculation for the powder efficiency of LPBF, in relation to three influencing variables:

Load factor

- Handling losses
- Splash losses

The lower the **load factor**, the higher the average number of cycles a powder grain remains in the circuit until it is processed, i.e. melted in the component. In practice, a load factor of 7% to 12%, simplified 10%, can be assumed. This means that 90% of the volume is filled with powder, from which the spatter is subsequently sieved out and which remains in the circuit. A high load factor is aimed at in any case for economic reasons, and thus the powder losses decrease because the powder runs through fewer cycles, fewer handling losses occur, and because the spatter losses decrease. Since the load factor has a great influence, the values are varied in the above range.

The **handling losses** related to the total amount of powder strongly depend on the degree of industrialisation. In the experiment conducted, they were relatively high at 4% in the first three experiments due to the manual handling, and even higher in the subsequent experiments with a smaller total amount of powder. In industrial practice, when the workpieces are cleaned in closed vessels, they should be below 3%; 1% is assumed for the model calculation.

The share of **spatter** can be influenced by process parameters, but cannot be minimised unilaterally without compromising other optimisation variables. In addition, it depends on the material; in the present case it is relatively high for aluminium and lower for steel. With a better load factor, the spatter losses decrease because the probability increases that spatter is located in a place that is subsequently melted. Maximising the load factor depends on the shape of the components and the logistics. These two aspects cannot be quantified in a generic statement, but are determined by specific circumstances. Spatter losses become quantifiable during sieving. In relation to the non-melted powder minus the handling losses, they amount to between 3% and 10% of the remaining powder. Since the spatter losses have a high influence on the powder efficiency, the values are varied over this range.

With these assumptions, a model calculation can be made which shows that the powder efficiency is in the range of about 75%. With the above assumptions, the highest value is 87%, the lowest 58% (Figure 9-7). This means that about 1/3 of the mass must be added to the raw part as powder loss. A powder efficiency of 80% should be achievable under good conditions, but it can also be below 60% if two or three of the influencing factors mentioned are unfavourable.

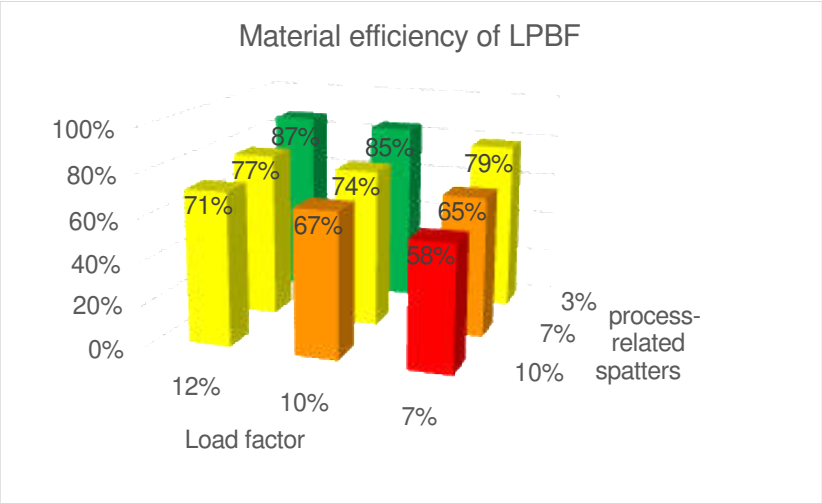

Figure 9-7: Powder efficiency with LPBF assuming a powder handling loss of 1%. The highest value is 87% with high occupancy and low spatter, green are values above 80%, yellow are values above 70%, orange are values above 60% and red is the lowest value, 58%, with low occupancy and a high spatter percentage.

According to this model calculation, the powder loss is therefore around 25%. This result was challenged by various members of UC Switzerland. According to them, powder losses should amount to 3% to 10%. However, it can be assumed that the statement refers to the recognisable powder loss, and that is the spatters that get visible during sieving. This is the range that was assumed for the model calculation. The powder loss during handling is not quantifiable for the user, because this powder gets outside the system boundary. The difference in the estimate may therefore be due to a different way of looking at things. When recording the data for the sample parts, the information on powder losses varied greatly, from negligibly small to 15% of the remaining powder quantity. The latter corresponds to a powder efficiency of 65%, which, according to the model calculation, is in the lower, but quite possible range. Assumptions above 90%, on the other hand, are unrealistic even under optimal conditions.

For the medium case with 10% volume load factor, 7% spatters and 1% handling losses, the overall balance for the powder mass is as follows (Figure 9-8):

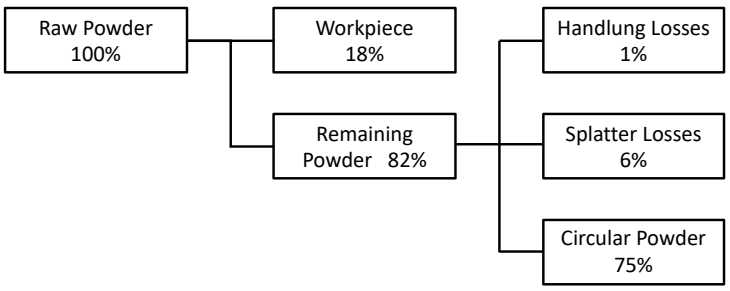

Figure 9-8 Material balance for LPBF with average assumptions related to weight. The powder efficiency is calculated as follows: Workpiece / (workpiece + spatter loss + handling loss), with these assumptions with unrounded initial values 73.5%.

An increase in powder efficiency requires minimal losses in powder handling, a high load factor, which is aimed for anyway for economic reasons, and low spatter losses. The latter can hardly be improved if the parameters are already optimal. Therefore, handling losses remain the most important factor. A

complete elimination of handling losses from 1% to zero would increase the powder efficiency in the model calculation (Figure 9-7) by 2.6 percentage points.

9.4 Clamping technology

9.4.1 Motivation

In general, parts have to be machined after AM shaping and rigidly clamped for this purpose. The best known conventional clamping devices are vises for cubic machining such as drilling or milling, if necessary with different geometries of the clamping jaws for polygonal or round parts. In lathes, three-jaw chucks are used for larger diameter parts, and collets for smaller diameter parts. Parts in the complex integral design group, which are highly interesting applications for AM, often also have complex shapes that rule out conventional clamping devices. Figure 9-9 shows the clamping of two topology-optimised parts in conventional fixtures with auxiliary devices.

With AM, the question arises whether the inherently high design freedom of AM is restricted when clamping for finishing.

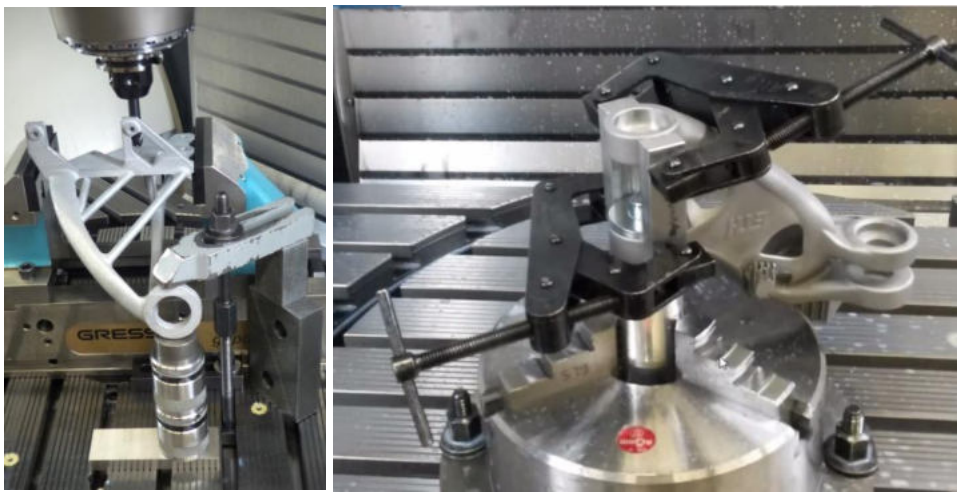

Figure 9-9: Conventional clamping of AM parts for machining [12]

9.4.2 Method

Four alternative clamping systems were contrasted with the conventional vice and their suitability was evaluated in relation to various criteria in a panel of experts. The first alternative was modular building platforms according to Figure 9-10 which can be incorporated directly into the zero-point clamping system for the finishing operation.

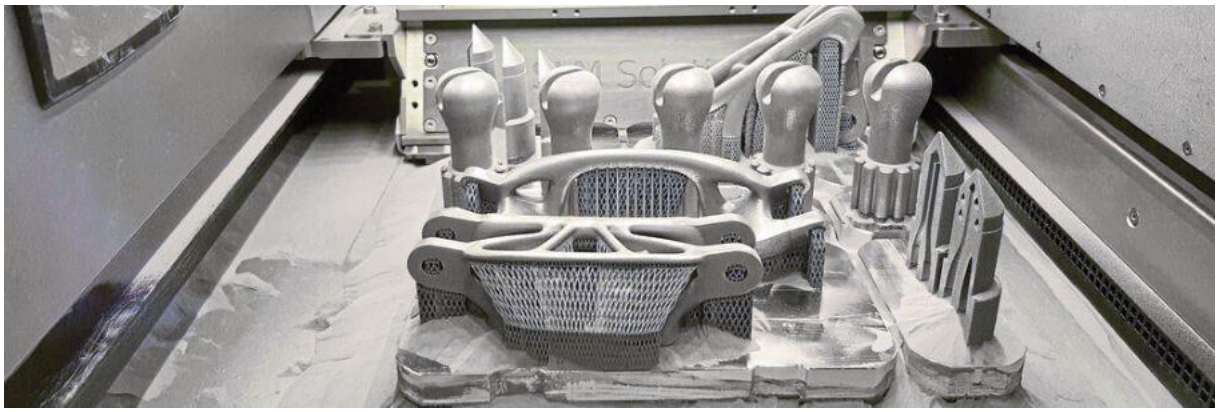

Figure 9-10: Filled modular build-up platform for powder bed AM after partial removal of the unconsolidated powder. The support structures are clearly visible on the components at the front left (photo Lehmann, CH-3552 Bärau).

The second alternative was a matrix clamping system as shown in Figure 9-11. This is a vice whose clamping jaws can be flexibly adapted to the workpiece by means of pins.

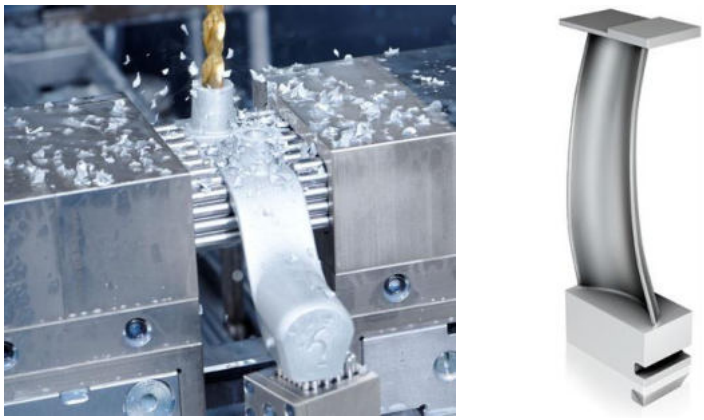

Figure 9-11: Matrix clamping system (left) as it is suitable for a turbine blade (right).

The third alternative was a system where the clamping is done on specially mounted bolts with ball ends that can be sheared off after machining by a manual operation. This system was developed by Gressel (CH 8355-Aadorf) and is currently undergoing industrial testing.

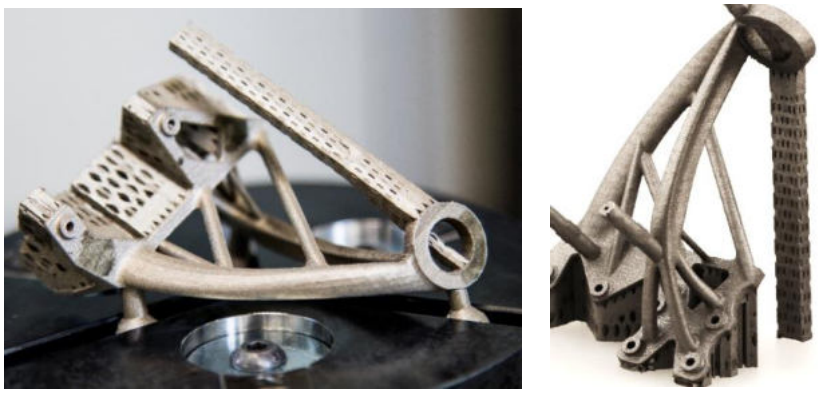

Figure 9-12: Bolt-It system for clamping on bolts specially attached to the workpiece for this purpose, with screwable ball ends (left) or bolts without form fit (right).

The fourth alternative was based on metal sheets clamped over the build platform in the powder bed, and then reclamped for machining in the machine, as shown in Figure 9-13.

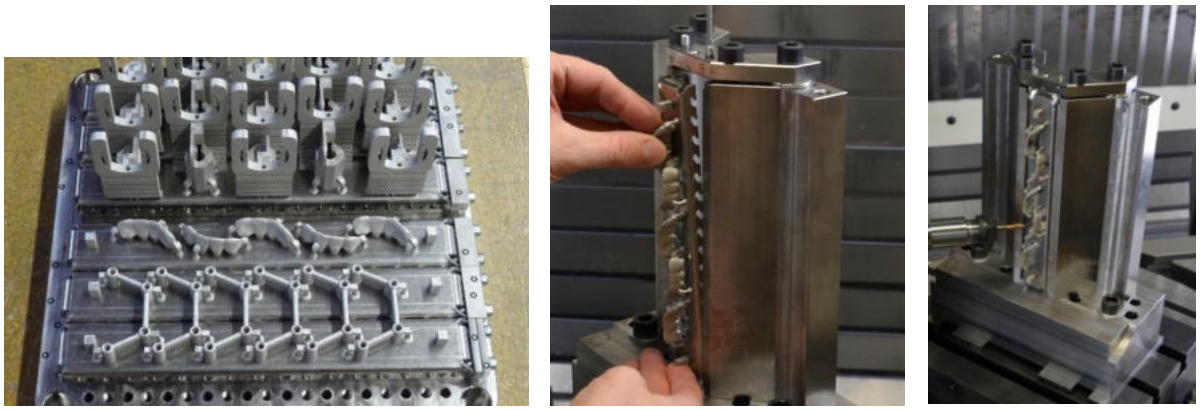

Figure 9-13: AM platform covered with metal sheets that are reclamped for finishing.

9.4.3 Result

The evaluation matrix in Figure 9-14 shows at a glance that each of the clamping systems has several strengths and also weaknesses. It is noteworthy that the seemingly universal matrix clamping system (middle column) is only sufficient in terms of isolated aspects according to this assessment, and is therefore likely to be used in niches. In individual cases, however, it is not the general suitability that is decisive, but whether the specific part can be clamped. A single aspect can be decisive for this.

Criteria	Selection of relevant quality factor	Level of Relevance	Zero-Point Clamping System	Parallel Clamping Jaw	Form Adapting Clamping Jaw	Bolt Clamping System	Sheet Metal Clamping System
Part Characteristics	Fragile thin walled AM parts	4	+	--	≈	+	+
	Free form shaped AM parts	4	++	-	+	++	++
	Round shaped AM parts	3	++	++	-	++	++
	Right angle shaped AM parts	3	++	++	-	++	++
	Recommended for small volume AM parts (<20 mm)	3	++	+	-	≈	++
	Recommended for medium volume AM parts (20-100 mm)	3	++	++	++	++	+
	Recommended for large volume AM parts (>100 mm)	2	++	++	+	≈	--
	Massive AM part	3	++	++	≈	≈	--
Design	High machining accessibility	5	+	≈	--	++	++
	Design freedom	4	-	-	-	++	+
	Customization	4	-	+	+	++	++
	Top/and bottom accessibility	2	-	≈	≈	+	++
	Side accessibly	2	≈	+	≈	++	≈
Process	Good surface quality	4	+	++	+	+	+
	High stiffness	4	+	++	≈	+	+
	Potential for mass customization	4	-	-	--	++	++
	Potential for series production of standardized parts	4	+	++	+	≈	≈
	Position detection necessary	3	+	+	+	+	≈
	Degree of automation	3	++	+	+	+	+
	Low clamping pre-process effort	2	++	-	-	+	+
	Low part-induced calming forces	1	++	--	--	++	++
	No customized tooling	1	++	≈	++	++	++
	Low support removal effort	1	--	-	-	++	++
Environment	Low additional interface build height	2	++	≈	≈	--	++
	Low material consumption	2	+	+	++	≈	≈

++ ≙ entirely sufficient, + ≙ partially sufficient, ≈ ≙ depending on the application, - ≙ limited sufficient, -- ≙ not sufficient at all

Figure 9-14: Evaluation matrix of the expert workshop on clamping systems.

The conclusion from the assessment is that the choice of clamping system depends on the part shape, the necessary finishing and aspects such as the number of pieces and the available equipment. This is also the case with conventionally produced parts. In contrast to this, however, it can be assumed that the freedom of design for AM will be exploited to a greater extent and that clamping technology will

experience a boost in innovation as a result of these new applications. The variety and upcoming developments in clamping technology lead to the conclusion that clamping for post-processing can be a challenge, but does not represent a major restriction of component design freedom.

The resource aspect of clamping technology cannot be assessed in general. In machining, i.e. purely subtractive production, only what has to be removed is removed. The design is advantageously aimed at leaving material that can serve as a clamping surface without additional effort. In contrast, AM builds up only what is necessary in the sense of *near net shape.* If additional surfaces have to be built up for clamping, this represents an additional expense only for clamping. This asymmetry of the resource input has a negative effect on AM with regard to clamping. For LPBF, the height is relevant because it determines the number of layers. If it has to be increased because of the clamping, process time and resource demand increase. This is a disadvantage of bolt clamping, for example. On the other hand, the resulting clearance of the workpiece by the *Bolt-It* System offers much better machining possibilities than machining on the building platform or the sheet metal solution.

The clamping technique for finishing depends mainly on the shape of the component and the necessary machining operations, just as it does in conventional manufacturing. It must be selected individually for the workpiece from a number of possibilities. Compared to a conventional casting, there is the additional complication that support structures often have to be removed, and that they are located between the component and the building platform. In these cases, the building platform, which would be very suitable for clamping, cannot be used.

9.5 Sample parts

9.5.1 Motivation

A series of sample parts with industrial relevance (Table 9-1) is intended to provide a basis for an exploratory assessment of additive-subtractive process chains. The examples were provided by members of the Swiss User Committee, some by the international consortium partners:

	Designation	Process	Material	Application
a	Nozzle ring	LPBF	Stainless steel	Component in a turbo compressor
b	Cooling lubricant nozzle	LPBF	Stainless steel	Component for a machine tool
c	Mould with cavity	LPBF	Tool steel	Component of an injection mould
d	Lightweight component	LPBF	Aluminium	Part of a measuring instrument (without image release)
e	Medical part	LPBF	Titanium	Use in the area of the spine
f	Turbocharger	LPBF	Nickel-chromium alloy	Use in a Formula 1 engine
g	IMR demo part	LPBF	Al-Si alloy	Sample part

h	RENA benchmark part	LPBF	Steel	Sample part
i	Test Cube	WAAM	Welding steel	Sample part
j	Flange	WAAM	Welding steel	Sample part
k	Impeller	WAAM	Welding steel	Sample part
l	Turbine blade repair	LMD	Stainless steel	Turbine
m	Aviation component	Milling	Aluminium	Reference part for machining, aircraft structural component

Table 9-1: Sample parts.

Parts a) to f) show a wide range of industrially relevant applications of AM. g) and h) are sample parts used to investigate innovative process chains in powder bed manufacturing. i) to k) are also sample parts created using the WAAM process, which is significantly more efficient than LPFB. l) illustrates the efficiency of a repair, as opposed to procuring a new cast blank and machining it. m) is a reference part illustrating the state of the art in subtractive machining.

Figure 9-15: Pattern pieces, from large to small from left to right.

The broad selection of parts in terms of shape, size, material, and other aspects is intended to open up the possibility of recognising individual particularities and, if necessary, systematic phenomena. The latter would be a basis for a resource simulation based on macro indicators, such as material, weight, volume, number of features, surface area, etc. The macro indicators material, weight, construction volume, partly surface, and on the resource side the process energy, as well as the grey energy of material and auxiliary materials were effectively recorded.

9.5.2 Methodological notes

The description of the parts is based on the principle of grey energy, i.e. the accumulated energy required to produce the part. It is also reported as specific grey energy in MJ/kg. It should be taken into account that the specific grey energy changes not only when energy is added, but also when the part weight changes because the accumulated energy input is related to a different remaining mass.

For LPBF, a maximum load factor for the specific part is assumed. Due to the long process time of AM, this assumption has a strong effect on the process time per part and on the energy supplied. For further process steps, this assumption is also made, provided that the batch size corresponds to that of the AM process.

Electrical energy is converted into primary energy by weighting with a factor of 3 in order to be comparable with the values for grey energy for the other resources.

For all thermal treatments, an average value is applied, as it results from the operating balance of a hardening shop. This hardening shop is a service provider for a large number of manufacturing companies, with part sizes ranging from a few millimetres to several metres, and 12 different types of thermal treatments. The average value is 25 MJ/kg in primary energy, and is applied regardless of the duration and type of thermal treatment. Figure 9-16 shows an example of process documentation.

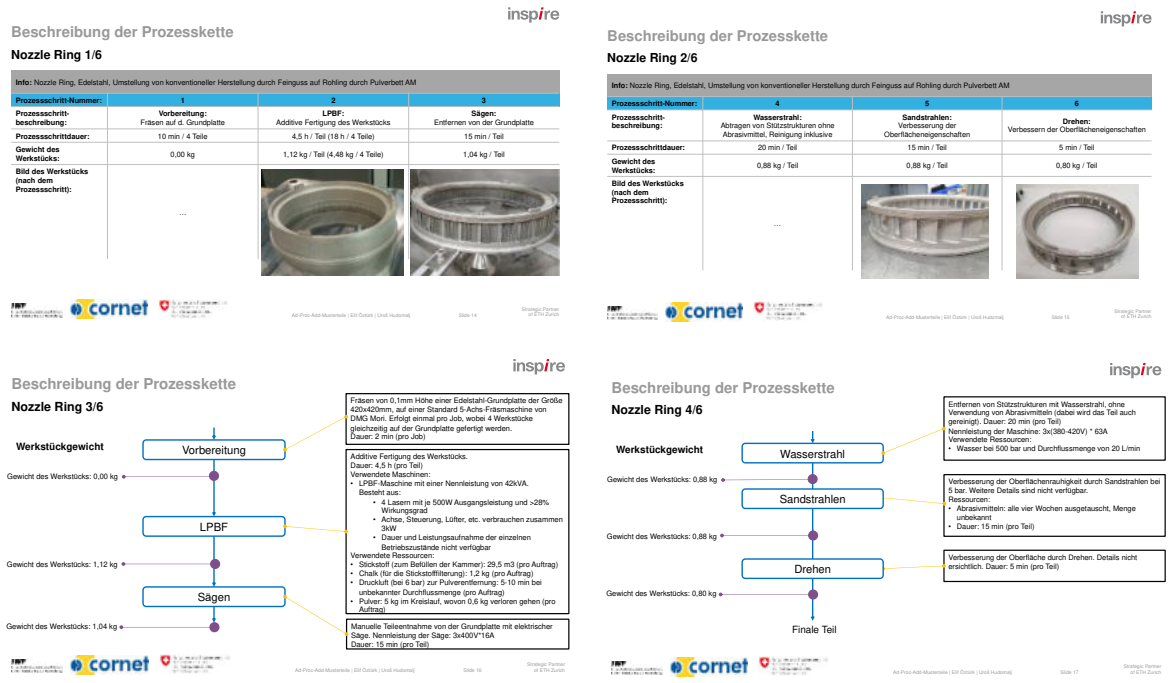

Figure 9-16: Example of process documentation.

With a qualitative assessment, according to the framework (Table), attempts to assess the motivation for and added value of AM. With the metric

- 0 neutral
- \+ partially/conditionally advantageous
- ++ clearly advantageous
- ? not assessable

The seven aspects are rated by the authors. For clarity, the ratings are highlighted with different shades of grey.

	Assess-ment	Comment
Prototyping		Benefit from the rapid production of prototypes

Incremental product launch		Step-by-step improvements in the product launch
Better Products		Better product, mostly: benefit of 2nd and/or 3rd kind
Custom Products		Customised product
Process Concentration		Short process chain
Production Tools[6]		Expenses for means of production
Improved Delivery		Readiness for delivery

Table 9-2: Evaluation criteria for the benefits of process chains with AM.

9.5.3 Example: Noozle ring

Stainless steel, specific grey energy 1'011 MJ/kg.

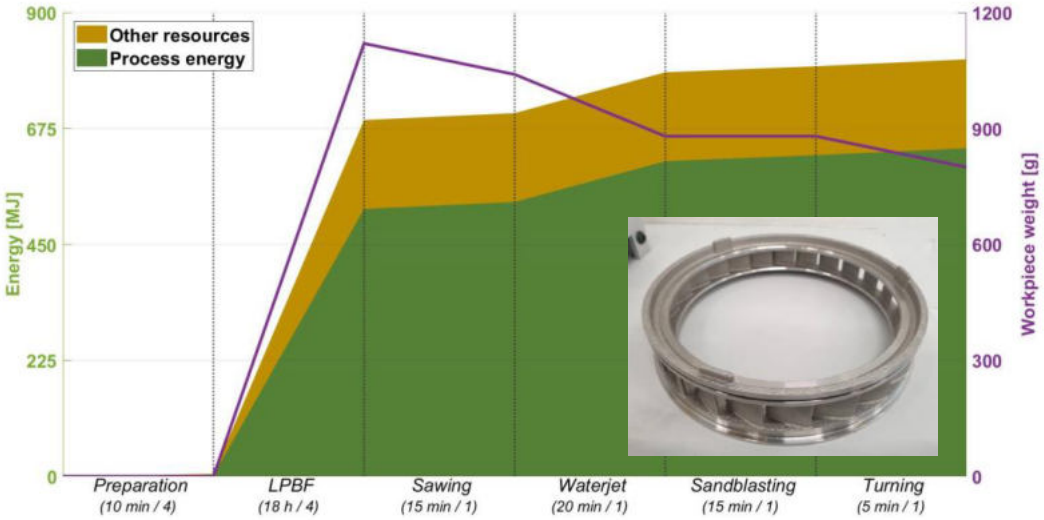

Figure 9-17: Accumulation of grey energy by process energy, other resources, especially material, and development of the workpiece weight over the manufacturing cycle.

[6] The source 2. Fontana, F., C. Klahn, and M. Meboldt, *Value-driven clustering of industrial additive manufacturing applications.* Journal of Manufacturing Technology Management, 2019. **30**(2): p. 366-390. understands this to mean only the benefits for manufacturing production resources using AM. In a slight variation of this approach, the effort required for the means of production in general was evaluated here, for example the elimination of a mould.

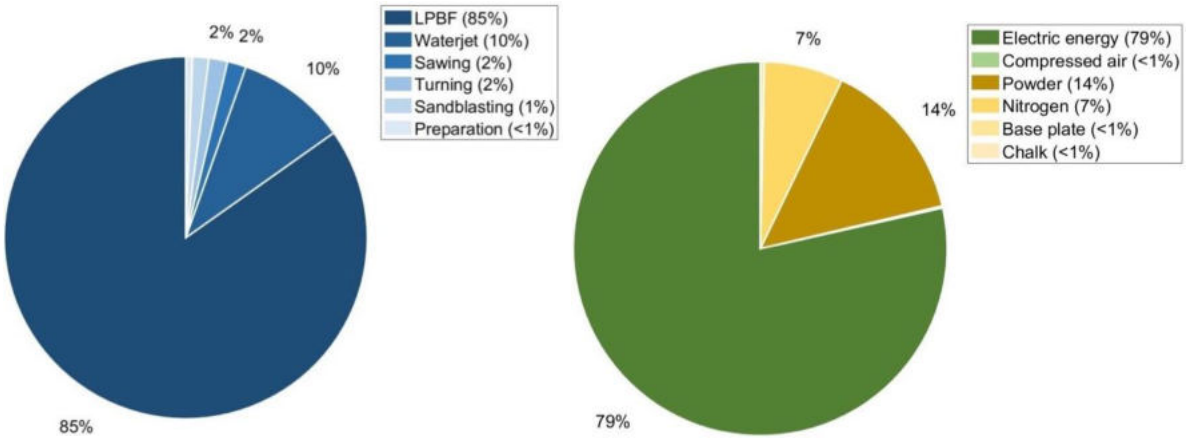

Figure 9-18: Left: grey energy per process step in descending order of importance, right: according to resources used.

Comment: The part can also be produced conventionally by fine casting. The logistical advantage of a short lead time justifies the additional expense for AM. The critical process is the removal of the support structures. In this case it is carried out with an innovative process using water jets.

	Assess-ment	Comment
Prototyping	+	First time right design by means of engineering
Incremental product launch	0	First time right design by means of engineering
Better Products	0	Alternative fine casting produces the same shape
Custom Products	+	Variety easily possible
Process Concentration	+	In-house production, but support structure removal
Production Tools	++	No mould necessary
Improved Delivery	++	Main motivation: Spare parts for customised machinery

Table 9-3: Evaluation criteria for the benefits of process chains with AM.

9.5.4 Example: Medical part

Titanium, specific grey energy 3'397 MJ/kg.

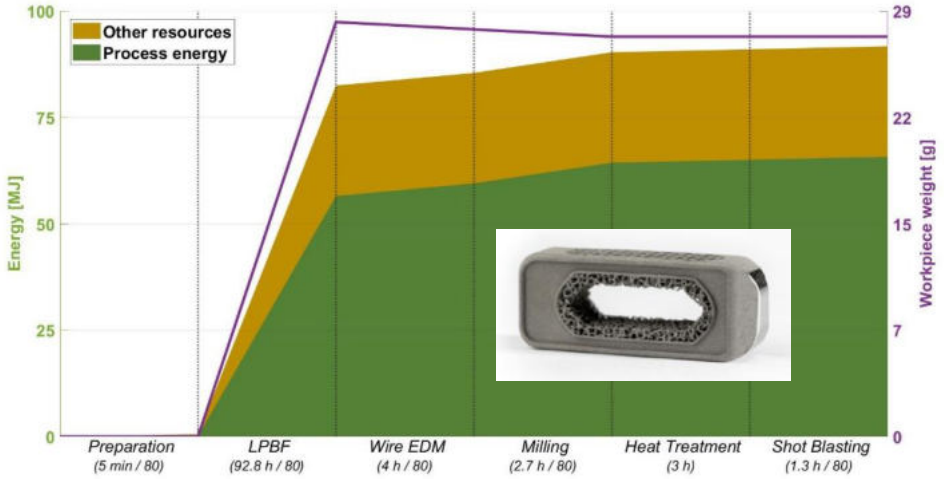

Figure 9-19: Accumulation of grey energy by process energy, other resources, especially material, and development of the workpiece weight over the manufacturing cycle.

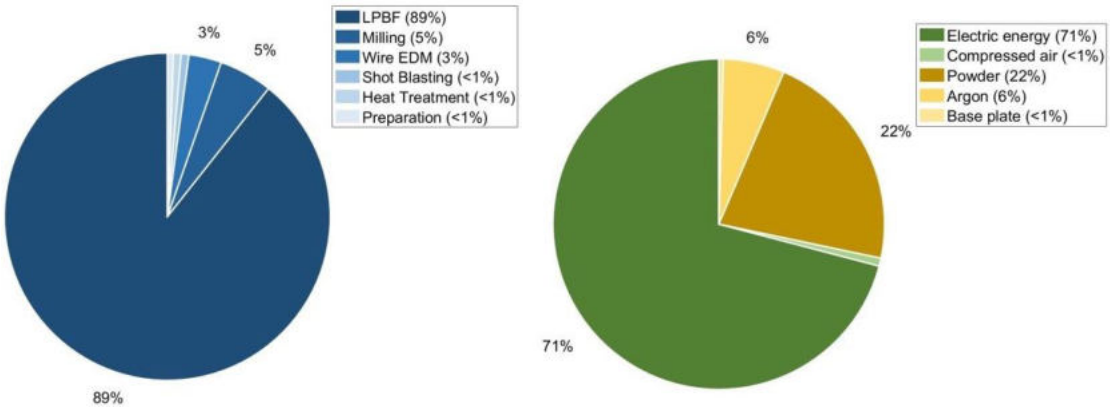

Figure 9-20: Left: grey energy per process step in descending order of importance, right: according to resources used.

Note: The part is small and light, and can be made in large numbers in one batch and only with AM.

	Assess-ment	Comment
Prototyping	+	Practical trials necessary
Incremental product launch	+	Iterations based on practical experience
Better Products	++	Not feasible without AM with these properties
Custom Products	++	Application-specific design
Process Concentration	?	No assessment as otherwise not feasible
Production Tools	++	No mould necessary
Improved Delivery	?	No assessment as otherwise not feasible

Table 9-4: Evaluation criteria for the benefits of process chains with AM.

9.5.5 Example: Flange

Steel, specific grey energy 348 MJ/kg.

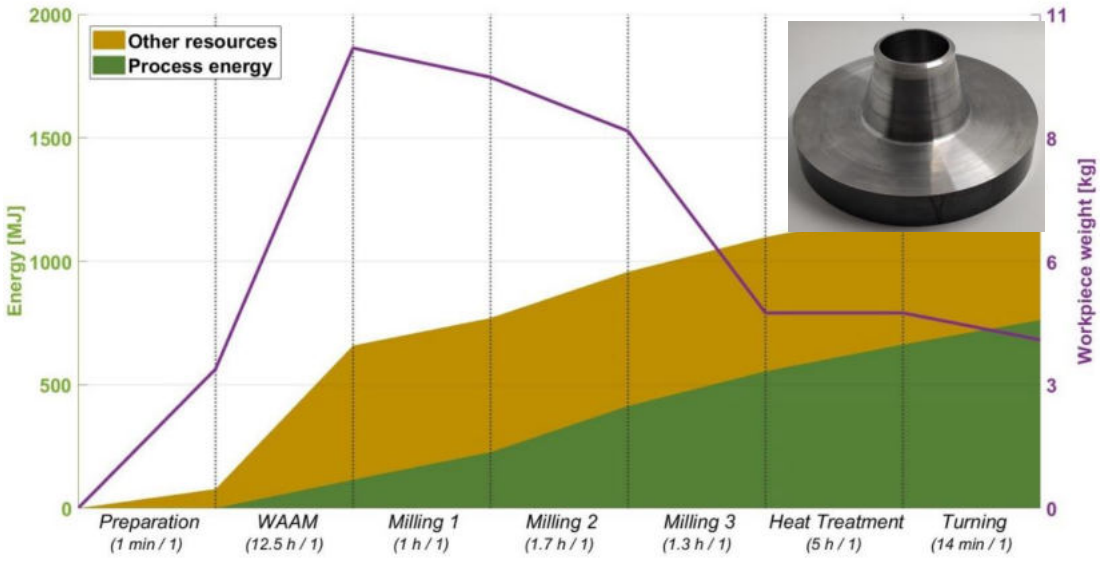

Figure 9-21: Accumulation of grey energy by process energy, other resources, especially material, and development of the workpiece weight over the manufacturing cycle.

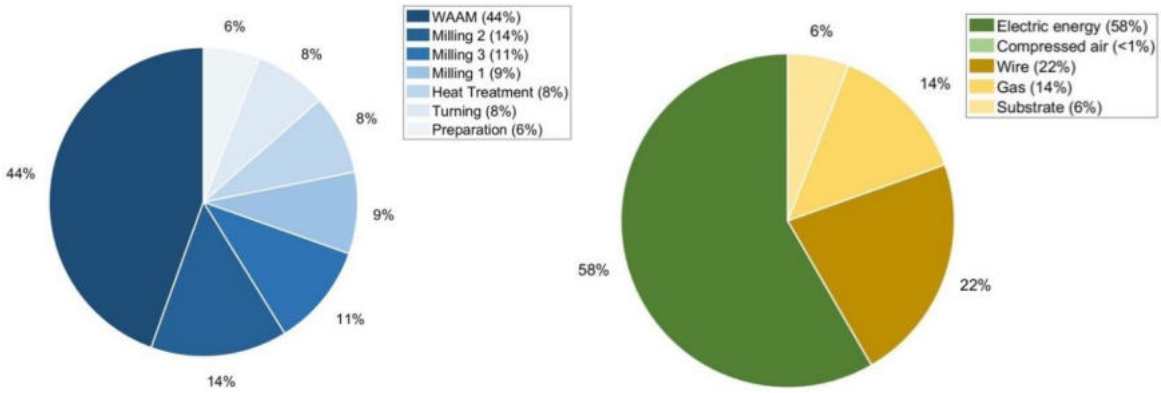

Figure 9-22: Left: grey energy per process step in descending order of importance, right: according to resources used.

The motivation for using AM in this case is the reduction of raw material. Conventionally, such a flange is turned from solid material, with a significantly higher machining volume. This eliminates WAAM and the subsequent three milling operations in the process chain, possibly also heat treatment. In their place is a roughing process, with a resource input of 5 MJ and a grey energy of 300 MJ for the additional raw steel. This is less than a third of the resource input with WAAM of around 1'100 MJ. The example shows the tremendous increases in performance in conventional machining, especially in roughing, which greatly reduce the resource input for removing large volumes of material. In fine machining, the process energy is comparatively high, and it is precisely this machining that cannot be avoided with AM.

	Assess-ment	Comment
Prototyping	0	Hardly necessary for a part of this low complexity
Incremental product launch	0	Iterations also possible with conventional production
Better Products	0	Can be produced conventionally without any problems
Custom Products	0	Conventionally possible without problems
Process Concentration	0	Conventional production is easier
Production Tools	0	Conventional production is easier
Improved Delivery	0	Conventional complete manufacturing is leaner

Table 9-5: Evaluation criteria for the benefits of process chains with AM.

9.5.6 Example: Turbine blade repair

Stainless steel, specific grey energy 65 MJ/kg (based on total weight, excluding grey energy in the part before repair, because it is re-used).

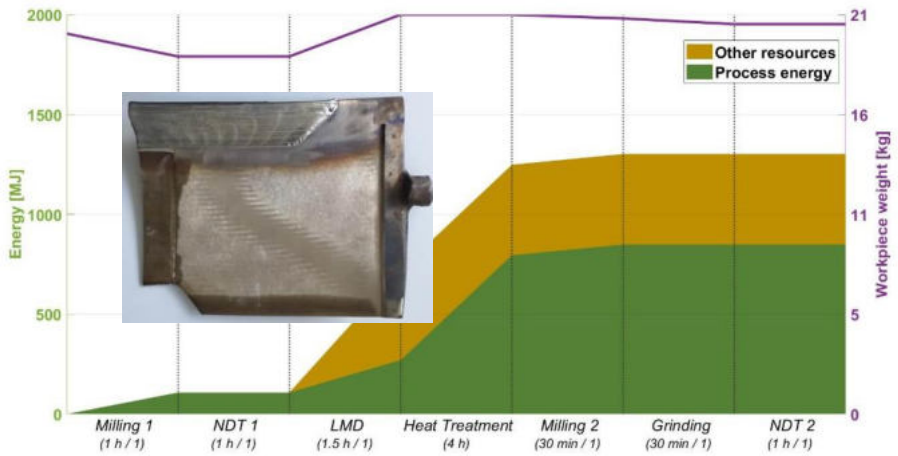

Figure 9-23: Accumulation of grey energy by process energy, other resources, especially material, and development of the workpiece weight over the manufacturing cycle. The workpiece weight includes the entire blade.

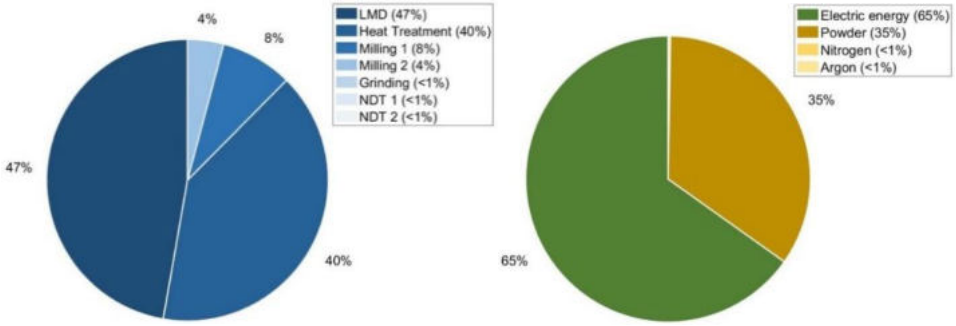

Figure 9-24: Left: grey energy per process step in descending order of importance, right: according to resources used.

Comment: The grey energy related to the total weight shows the great leverage of the repair process. In the case of heat treatment, the advantage is not present because it affects the whole workpiece.

	Assessment	Comment
Prototyping	0	Optimised blade geometry by engineering tools
Incremental product launch	0	Repair case
Better Products	++	Applied material layer can have improved properties
Custom Products	++	Single part
Process Concentration	++	Significant simplification of the process chain
Production Tools	++	Production of a new blank requires a casting mould
Improved Delivery	++	Shorter process chain, no blank necessary

Table 9-6: Evaluation criteria for the benefits of process chains with AM.

9.5.7 Reference example: Aviation component

Aluminium, specific grey energy 1'240 MJ/kg.

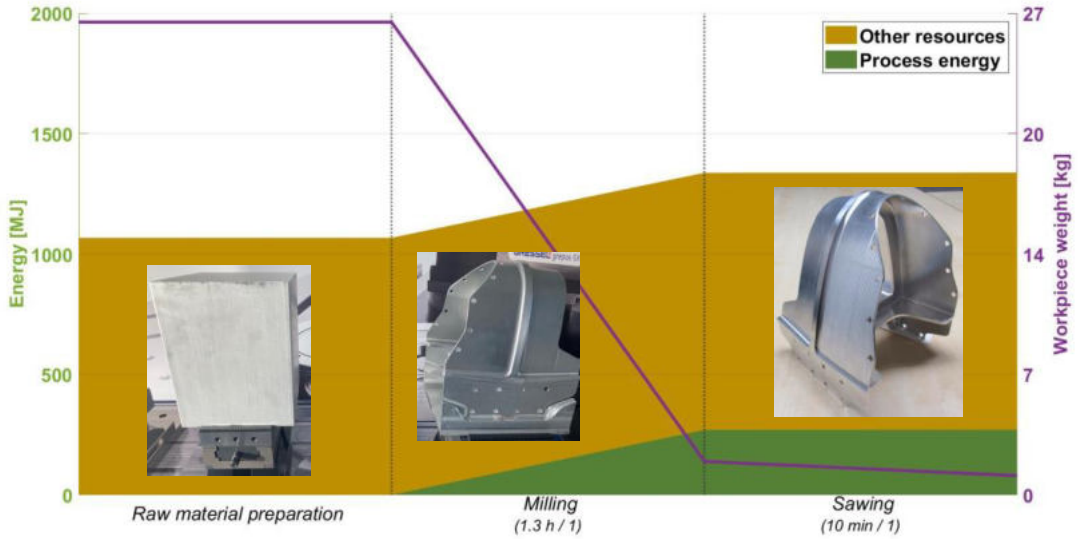

Figure 9-25: Accumulation of grey energy by process energy, other resources, especially material, and development of the workpiece weight over the manufacturing cycle.

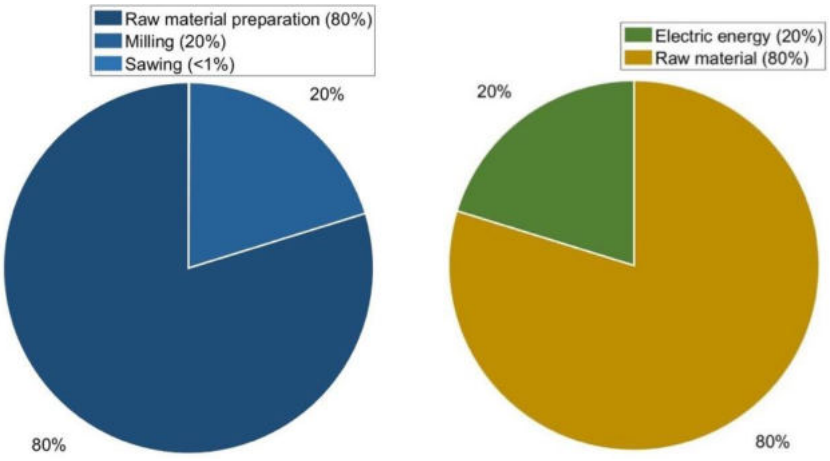

Figure 9-26: Left: grey energy per process step in descending order of importance, right: according to resources used.

Comment: The part serves as a reference for a machining process with very high material loss, and thus a very unfavourable case for purely subtractive machining. Only 4% of the raw material remains on the workpiece. 3% of the material loss is accounted for by the clamping loss, i.e. the lowest part of the raw material that is used for clamping and is cut off at the end, and 93% accumulates in the form of chips that are recycled. The logistical advantage of complete production in one clamping and minimal post-processing for cutting off the clamping area is obvious. The disadvantage is the high grey energy of the raw material, which, however, comes largely from recycling, since the chips can be returned and melted down at the end of the process, when sorted by type of alloy. This aspect becomes very important when there is a high proportion of machining, because the recycling of aluminium under good conditions, i.e. from a clean mono-fraction, causes low energy consumption.

9.6 Discussion

A total of twelve sample parts plus one reference part (conventional production) were analysed and evaluated:

- 8 of which relate to LPBF applications; the energy demand of the LPBF process compared to the whole process chain varies between 57% and 97%, and the specific energy demand per kilogram of finished part is 900 to approx. 7'600 MJ/kg, i.e. a difference of almost one order of magnitude.
- 3 Examples concern WAAM, with a specific energy requirement of approx. 350 and 860 MJ/kg, i.e. a difference of a factor of 2.5.
- 1 Example concerns LMD, with a specific energy demand of only 65 MJ/kg - this involves the repair of a turbine blade weighing approx. 20 kg with a relatively low AM share.
- 1 Example concerns a reference part from the aviation industry with a very large proportion of machining volume (93%); the specific energy requirement here is 1'240 MJ/kg.

A look at the consolidated qualitative assessment shows a mixed picture (Table 9-7). Obviously, better product properties, partly the customised design, the shorter process chain and the associated better delivery readiness speak in favour of AM. The production of prototypes and advantages in the incremental product introduction are rated as less important. This certainly has to do with the fact that product development today is almost universally carried out with 3D CAD systems, namely with the aim of completely preventing[7] prototypes.

						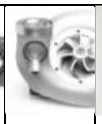					
Prototyping	+	++	+	0	+	+	+	+	0	0	0
Incremental product launch	0	+	+	0	+	+	+	+	0	0	0
Better Products	0	++	++	++	++	++	+	++	0	+	++
Custom Products	+	++	++	0	++	+	++	++	0	+	++
Process Concentration	+	++	++	+	?	++	++	++	0	+	++
Production Tools	++	++	++	0	++	+	0	+	0	0	++
Improved Delivery	++	++	++	+	?	++	++	++	0	+	++

Table 9-7: Qualitative assessment of the benefits of AM.

[7] This assessment is likely to be completely different for workpieces made of plastic, because functional samples are more important in the development of plastic products. In addition, in the case of plastic injection moulding, the production of a mould is associated with very high expenditure, so that the prior production of prototypes is of interest.

Figure 9-27 shows an evaluation of the weight of the sample parts and the corresponding energy supply per kg of workpiece. The blue dots refer to LPBF, the red dots show WAAM and LMD (dot on the far right), the black dot is the reference part from aviation (1'240 MJ/kg).

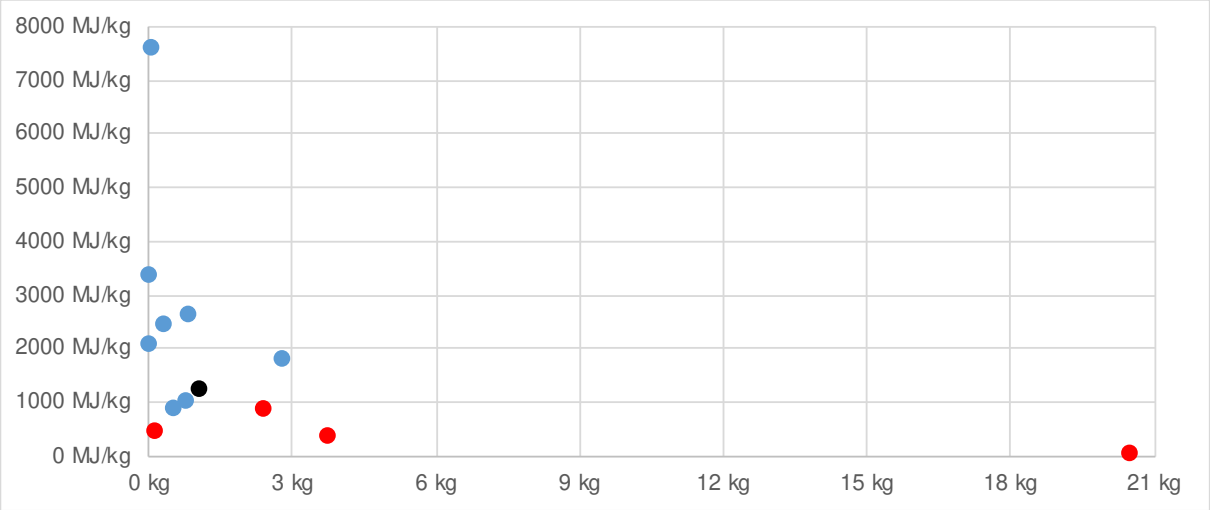

Figure 9-27: Distribution of component weight and specific grey energy; WAAM and the repair case with LMD (far right) are marked in red, the reference case is marked in black.

The high specific energy supply for AM processes is striking: The specific grey energy is very high in all cases, compared to solid material, where only materials such as aluminum and titanium exceed 100 MJ/kg. Even though a certain amount of machining always occurs in conventional production, such high values for the specific grey energy only result in exceptional cases, such as the reference case of an aviation part (1'240 MJ/kg). The energy supplied for the production of typical semi-finished products such as plates or rods made of metallic materials is one to two orders of magnitude lower than production by AM.

This goes along with the tendency to use AM to produce only small parts with high energy input. The repair case with LMD is an exception, and it confirms this assessment. Never would such a large part be fully built up in AM. In a hybrid approach, AM is of interest, when the largest part of the workpiece is provided with other processes, and AM is only used to manufacture a special feature, in the cited case the selective repair. In contrast, for very small parts with high added value, the specific energy is of little relevance because the absolute energy requirement is low.

Advancing AM into applications for large workpieces is difficult to imagine with the current state of the art. The low productivity of LPBF in the range of 6-20 cm^3 per hour and laser source (0.015 to 0.150 kg/h depending on the material) is very modest. WAAM has a higher productivity with build-up rates of 0.5 to 2 kg/h, but even with this the build-up of larger volumes is not very attractive. The development of these processes will do little to change this, because considered in isolation, powder or wire are semi-finished products, comparable to conventional semi-finished products such as sheet metal, rods or rolled profiles. The effort required to produce a workpiece with powder or wire by AM is much higher than when using a conventional semi-finished product or a casting, especially for large workpieces. It is essential whether AM achieves sufficient added value in the sense of the applied qualitative evaluation grid.

A further insight is provided by the comparison of specific grey energy and specific process energy, which is logically always lower because it is contained in the grey energy (Figure 9-28).

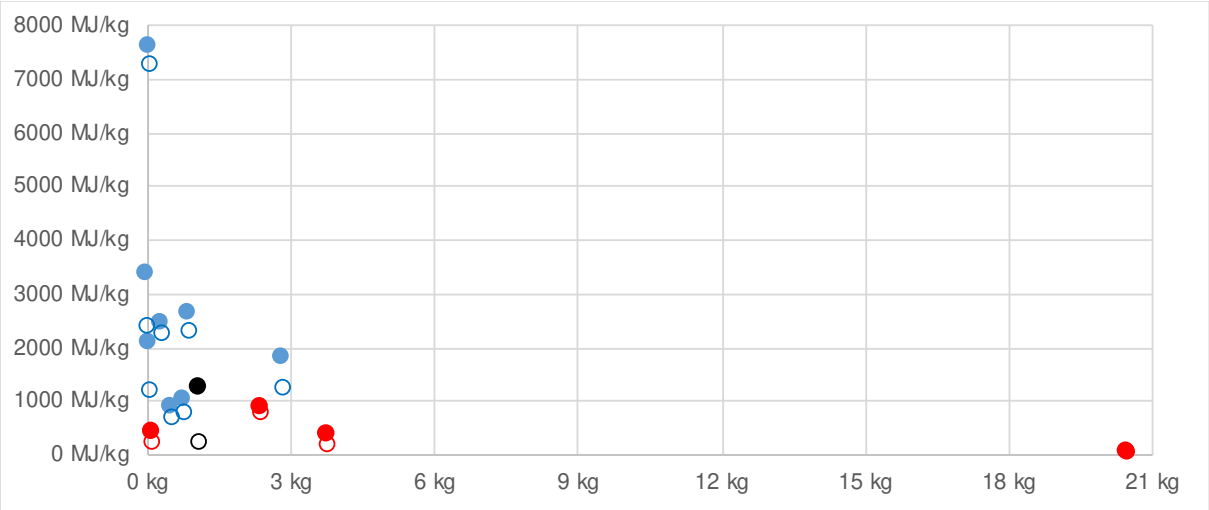

Figure 9-28: Distribution of component weight, specific grey energy and specific process energy (empty dots) WAAM and the repair case with LMD (far right) are marked in red, the reference case is marked in black.

The clear difference for the reference part is particularly striking. It shows that the energy demand is mostly caused by material loss. The low specific process energy (empty circle) also reflects the productivity gains in machining. It further confirms the widespread practice of primarily calculating the grey energy of the material in the ecological or energetic assessment of metallic parts, and of using no or flat-rate values for common machining processes, for example "Machining, drilling, turning of metal: 20 MJ/kg". For AM, such a rough assessment should be avoided, as the specific energy is much higher and strongly depending of the part.

9.6.1 Assessment of energy and resource requirements

The specific grey energy is not systematic, at least when assessed on the basis of the parts examined. This statement also applies within the same AM processes and excluding the repair case, which is obviously out of the ordinary in terms of weight at 20 kg for the part to be repaired. A general energy assessment based on macro indicators such as mass, volume, surface area or dimensions in individual dimensions leads to statements with errors of one or more orders of magnitude and is therefore useless.

For a given process chain, it is quite possible to calculate the energy supply without measuring it in each individual case. Essential input variables are the average power supply level of the production equipment and the production time per part. However, it is difficult to make a general quantitative statement on the development of the energy demand for manufacturing due to the increasing use of AM. Obviously, AM leads to a significantly higher energy demand than machining a part from solid material. This is not surprising because conventional semi-finished products are produced in energetically optimized, large-scale processes. Even if a large part of the bulk material is machined during production, the resource input is lower than with AM. However, AM can be used to produce parts that could not be manufactured conventionally and that may lead to high energy savings in their application. The 2nd and 3rd order benefits can have a strong leverage effect that dwarfs the manufacturing of the part. On the energy side

and for the case of Switzerland, it should be noted that in machining, the majority of energy in the form of grey energy is imported with the raw material, while the electricity is produced nationally.

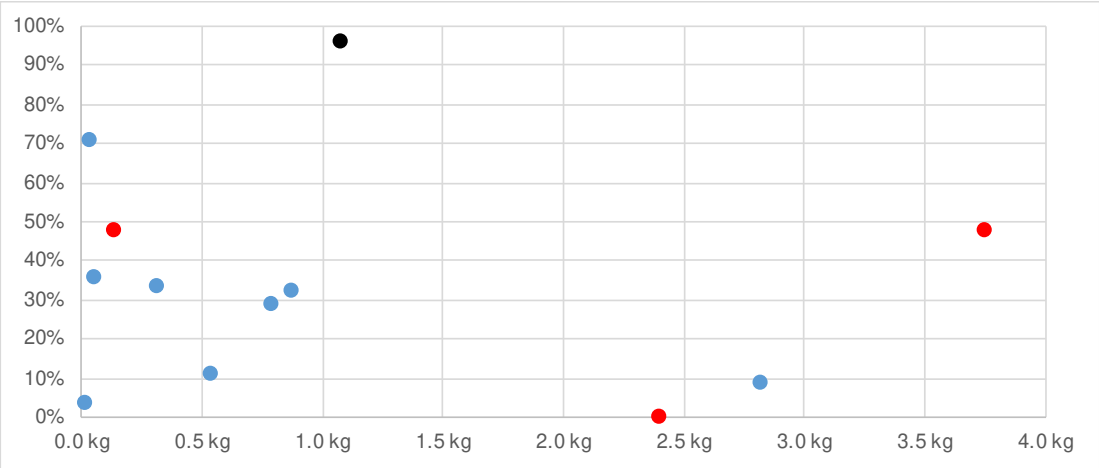

Figure 9-29: Share of material removed by machining. Marked in red are the parts with WAAM, marked in black is the reference case.

Based on the sample parts, it must be assumed that AM does not significantly improve material efficiency in manufacturing. There are a few cases of *near net shape*, with a material loss in post-processing of less than 10%. In most cases, the share of machining is considerable, and in the case of the support structures caused solely by AM as a process (Figure 9-29). This process-related disadvantage could trigger increased efforts to remedy it and could be eliminated with future, more advanced AM such as binder jetting[8]. However, material efficiency will hardly be a valid argument in favor of AM, because it comes at the price of high energy demand for the production of the semi-finished product, i.e. the powder, when powder is used.

A special feature of AM is the surface of the raw part produced, both the ratio of surface area to mass and the quality of the surface. If we look at the sample parts with the greatest specific energy demand, we notice that they are filigree parts, i.e. large surface areas compared to the volume; these are typically

- lightweight small parts that are advantageous in mobile applications (hand-held devices, car, airplane, etc.);
- Parts with hidden functional surfaces that cannot be produced conventionally and that create superior product properties;
- Parts with a function-related high surface area per weight and volume, e.g. in the medical sector, catalytic converters, etc.

LPBF produces rough surfaces comparable to some casting processes. The sample parts show that surface finishing is not absolutely necessary, at least not by machining, just as with castings. On the contrary, a rough surface can create desirable turbulence in a fluid channel, for example, or improve biocompatibility in medical applications. In most cases, surface finishing will only be partially necessary for workpieces manufactured using AM, otherwise other manufacturing strategies will be chosen. The

[8] en.wikipedia.org/wiki/Binder_Jetting

case is different for WAAM, where extensive downstream machining of most surfaces must be assumed. This post-processing will partly trigger innovations. Overall, however, the industry is so diverse and well positioned in machining that post-processing per se is unlikely to trigger developments.

9.6.2 Benefit assessment

The evaluation of motivation and added value of the sample parts (Table 9-8) shows that mostly *better product*, i.e. the production of a superior product, is an important aspect, which indicates benefits of a second or third kind in the application. In some cases, advantages in manufacturing, i.e. benefits of the first kind, can also be identified. In this context, not only the resource input was evaluated, but also aspects such as logistics and demand-controlled manufacturing. These aspects do have an impact on the LCA however, beyond the system boundary considered in the study.

	Benefit			
Sample part	1. kind	2. kind	3. kind	Comment
Nozzle ring	+	+	+	Mostly: better availability of spare parts
Cooling lubricant nozzle	+	++	+	Further optimisation possible
Mould with cavity	++	++	+	Conventional manufacturing with extra effort
Lightweight component	+	++	++	More precise measuring instrument, therefore better use of resources in the application
Medical part	++	++	?	Hardly feasible conventionally, advantageous in the application
Turbocharger	+	++	++	Additional effort, but better performance, impact on (higher) engine efficiency
IMR demo part	+	?	?	Functionality conventionally complex to produce, no industrial application
RENA benchmark part	+	?	?	No industrial application, no evaluation
Test cube	+	?	?	No industrial application, no evaluation
Flange	0	?	?	No industrial application, no evaluation
Impeller	+	?	?	No industrial application, no evaluation
Turbine blade repair	++	++	+	Less effort, longer service life, thus less production downtime or the turbine
Aviation component	?	?	?	No rating

Table 9-8: Assessment of the benefits of the 1st, 2nd and 3rd kind.A quantitative evaluation is not possible for two reasons: On the one hand, because of the sample selection being broad but not representative, and on the other hand, because of the fact that above all the second and third kind benefits would have to be assessed in individual studies, taking into account the life cycle of the component.

9.6.3 Conclusion and outlook

AM is a group of processes that are becoming increasingly common in the manufacturing of smaller components and can add value in niche applications. It can be assumed that further development will reduce certain disadvantages of today's AM processes. This may pave the way out of the niche to suitable application areas. The study was focused on the manufacturing process, and therefore primarily on a possible 1st kind benefit. The grey energy assessment shows that AM leads to high energy demand in manufacturing, with a high dispersion of the specific energy input.

The exemplary study approach, the investigation of components in a wide variety of applications, has revealed a great diversity of process chains. The motivation for using AM in the sample parts from industrial applications lies primarily in the creation of superior products. Logistical advantages, cost and time savings in manufacturing occur, but are unlikely to justify the use of AM. Better products can produce energy savings in application, especially as components in active systems, that are several orders of magnitude greater than the energy to produce them. This scale effect is the most interesting aspect of AM and deserves closer consideration in the future. However, a quantification of the benefits of the 2nd and 3rd kind is only possible in individual case studies. At best, applications can be clustered and these clusters can be evaluated in a statically relevant number in order to quantify the benefits per cluster.

The energy required for manufacturing with AM is very high. In addition to the energy required to produce the semi-finished product, the powder or wire, there is also the process energy for remelting in the AM process. This leads to a specific energy input [MJ/kg] that is one to two orders of magnitude higher than that for the large-scale industrial production of semi-finished products such as sheet metal, bars, profiles, cast and forged blanks as used in conventional machining. Together with the low productivity, this limits the use of AM to small parts, or in the case of larger parts, to feature production. Not all AM processes are suitable for the latter.

AM produces a blank that requires reworking in every case. Part of this reworking is directly caused by process disadvantages of AM, for example the removal of the support structures, and part by demands that AM cannot meet, such as fine surfaces. This reworking is mainly done by known machining processes. In selected cases, innovative niche processes are used for reworking.

Basically, AM aims to require only the material needed for the ideal shape, i.e. to produce a blank with a *near net shape.* In some cases, this is achieved with a material loss of less than 10% during rework. In other cases, the material losses are comparable to those of conventional machining of semi-finished products, cast or forged blanks, i. e. 30% and more. In the case of LPBF and other powder-based processes, material losses through the powder cycle must also be taken into account, which are by no means negligible. In relation to the raw part, they are about one third in the powder bed, and higher in powder application processes such as LMD. Material efficiency is not an argument for the use of AM, firstly because it is not better than in machining, and secondly because it comes at the price of an energy-intensive process.

With AM, components can be produced that conventionally can only be manufactured with long process chains, assembled from several parts, or cannot be produced at all. This does not mean that manufacturing with AM is easy. Even if the process chains are shorter with AM, this does not mean that a benefit of the first kind - i.e. in manufacturing - can be achieved, on the contrary. The big challenge for industry is to exploit the component design possibilities gained by AM to produce superior products with 2nd and/or 3rd kind benefits in application. Future studies should therefore focus more on the quantitative evaluation of these applications, because this is the only way to justify a higher resource demand of AM in manufacturing.

10 Summary and conclusions of the AdProcAdd project

Within the Ad-Proc-Add project remarkable research results were achieved by the partners.

Systematic and detailed investigation of the interactions within ASM process chains and their effects on the resulting component properties were carried out. With those investigations, process improvements regarding tool life, stability, quality and productivity were achieved. The assessment of various combined ASM chains considers the geometry, distortions and accuracy of produced parts, their surface topography and porosity. Further on, correlations of AM parameters and workpiece properties to enable to configure and control the AM step with respect to targeted part characteristics, were identified. Intermediate processes in order to consider their influence on the parts' properties for the layout and control of ASM chains were analyzed. And, first interdependencies of "functionalizing processes" were identified to enable and adjust the workpiece properties by a sophisticated process implementation. This was done to reveal and quantify interrelations between the different process steps in order to enable the targeted set up, application and adaptation of combined ASM chains so that pre-defined workpiece properties can be achieved directly.

The results of the Ad-Proc-Add project could only be achieved by the intensive collaboration of the involved partners and associated industrial companies. All partners are sincerely grateful for the funding of this project!

11 Appendix

11.1 Bibliography

11.1.1 Bibliography (chapter 3)

[1] Das P, Chandran R, Samant R, Anand S (2015) Optimum Part Build Orientation in Additive Manufacturing for Minimizing Part Errors and Support Structures. Procedia Manufacturing 1:343–54.

[2] Pereira S, Vaz AIF, Vicente LN (2018) On the optimal object orientation in additive manufacturing. Int J Adv Manuf Technol 98(5-8):1685–94.

[3] Yasa E, Poyraz O, Solakoglu EU, Akbulut G, Oren S (2016) A Study on the Stair Stepping Effect in Direct Metal Laser Sintering of a Nickel-based Superalloy. Procedia CIRP 45:175–8.

[4] Townsend A, Senin N, Blunt L, Leach RK, Taylor JS (2016) Surface texture metrology for metal additive manufacturing: a review. Precision Engineering 46:34–47.

[5] Muthaiah VS, Indrakumar S, Suwas S, Chatterjee K (2022) Surface engineering of additively manufactured titanium alloys for enhanced clinical performance of biomedical implants: A review of recent developments. Bioprinting 25:e00180.

[6] Huynh L, Rotella J, Sangid MD (2016) Fatigue behavior of IN718 microtrusses produced via additive manufacturing. Materials & Design 105:278–89.

[7] Scholtes B, (Ed.) (1991) Eigenspannungen in mechanisch randschichtverformten Werkstoffzuständen: Ursachen, Ermittlung und Bewertung. Zugl.: Karlsruhe, Univ., Habil.-Schr., 1990. DGM-Informationsges. Verl., Oberursel.

[8] Schulze V (2006) Modern mechanical surface treatment: States, stability, effects. Wiley-VCH, Weinheim.

[9] Di Angelo L, Di Stefano P, Marzola A (2017) Surface quality prediction in FDM additive manufacturing. Int J Adv Manuf Technol 93(9-12):3655–62.

[10] Černašėjus O., Škamat J., Markovicˇ V., Visniakov N., Indrisiunas S., 2019, Surface Laser Processing of Additive Manufactured 1.2709 Steel Parts: Preliminary Study, Advances in Materials Science and Engineering, 2019, 1–9.

[11] Spierings A.B., Herres N., Levy G., 2011, Influence of the Particle Size Distribution on Surface Quality and Mechanical Properties in AM Steel Parts, Rapid Prototyping Journal, 17/3, 195–202.

[12] Cabanettes F., Joubert A., Chardon G., et al., 2018, Topography of as built surfaces generated in metal additive manufacturing: A multi scale analysis from form to roughness, Precision Engineering, 52, 249–265.

[13] Lalehpour A., Barari A., 2018, A More Accurate Analytical Formulation of Surface Roughness in Layer Based Additive Manufacturing to Enhance the Product's Precision, Int. J. Adv. Manuf., Technol., 96/9–12, 3793– 3804.

[14] M.F. Zaeh, M. Ott, Investigations on heat regulation of additive manufacturing processes for metal structures, CIRP Annals, Volume 60, Issue 1, 2011, Pages 259-262, ISSN 0007-8506, https://doi.org/10.1016/j.cirp.2011.03.109.

[15] Kruth J.-P.; Badrossamay, M.; Yasa, E. et al.: Part and material properties in selective laser melting of metals; 16th International Symposium on Electromachining; 2010.

[16] Branner, G.: Modellierung transienter Effekte in der Struktursimulation von Schichtbauverfahren. Herbert Utz Verlag, München 2011.

[17] Doll, R., Partes, K., Vollertsen, F., 2009, Friction Measurements on Graded Metal Matrix Composites Generated by Selective Laser Melting, Lasers in Manufacturing (LIM09) eds.: A. Ostendorf, T. Graf, D. Petring, A. Otto, F. Vollertsen, AT-Fachverlag, Stuttgart, 189-194.

[18] Alkahari, M. R., Furumoto, T., Ueda, T., Aziz, M. S. A., and Hosokawa, A., 2012, "Monitoring of Laser Consolidation Process of Metal Powder With High Speed Video Camera," Phys. Procedia, 39, pp. 760 766.

[19] Vasinonta, A., Beuth, J., 2007, Process Maps for Predicting Residual Stress and Melt Pool Size in the Laser-Based Fabrication of Thin-Walled Structures, Manufacturing Science and Engineering, 129:9.

[20] Brinksmeier, E. & Levy, G. & Meyer, Daniel & Spierings, Adriaan. (2010). Surface integrity of selective-laser-melted components. Cirp Annals-manufacturing Technology - CIRP ANN-MANUF TECHNOL. 59. 601-606. 10.1016/j.cirp.2010.03.131.

[21] Tapia, Gustavo & Elwany, Alaa. (2014). A Review on Process Monitoring and Control in Metal-Based Additive Manufacturing. Journal of Manufacturing Science and Engineering. 136. 060801. 10.1115/1.4028540.

[22] Spierings A, Herres N, Levy G (2011) Influence of the particle size distribution on surface quality and mechanical properties in AM steel parts. Rapid Prototyping Journal - RAPID PROTOTYPING J. 17. 195-202. 10.1108/13552541111124770.

[23] Möhring, H.-C.; Stehle, T.; Maucher, C.; Becker, D.; Braun, S.: Structural and thermo-mechanical FEM simulation of the fused layer modelling (FLM) process to predict the shape accuracy of manufactured parts. Journal of Machine Engineering (2019) 19(1):114-127.

11.1.2 Bibliography (chapter 4)

[4-1] Bundesministerium für Wirtschaft und Energie (BMWi): Nationale Industriestrategie 2030. PDF-Broschure, Berlin, 2019. Zugriff am 20.11.2021: https://www.bmwi.de/Redaktion/DE/Publikationen/Industrie/nationale-industriestrategie-2030.html.

[4-2] Strategy&: Globales Marktvolumen von 3D-Druck-Verfahren in ausgewahlten Branchen im Jahr 2015 und eine Prognose fur 2030 (in Milliarden Euro), Veroffentlichungsdatum Januar 2018. Zugriff am 15.11.2021: https://de.statista.com/statistik/daten/studie/802439/umfrage/globales-marktvolumen-von-3d-druck-verfahren-in-ausgewaehlten-branchen/.

[4-3] Bourell, D.; Kruth, J.P.; Leu, M.; Levy, G.; Rosen, D.; Beese, A.M.; Clare, A.: Materials for additive manufacturing. CIRP Annals - Manufacturing Technology 66 (2017) 2, S. 659–681. DOI: https://doi.org/10.1016/j.cirp.2017.05.009.

[4-4] Tofail, S.A.M.; Koumoulos, E.P.; Bandyopadhyay, A.; Bose, S.; O'Donoghue, L.; Charitidis, C.: Additive manufacturing: scientific and technological challenges, market uptake and opportunities. Materials Today, 21 (2018) 1, S. 22-37. DOI: https://doi.org/10.1016/j.mattod.2017.07.001.

[4-5] Maucher, C., Moehring, H.-C., Tilger, M., Biermann, D. Mastering of the additive-subtractive process chain, Proceedings of the Metal Additive Manufacturing Conference 2020; Virtual Conference, September 30 - October 2, (2020) S. 211–222.

[4-6] Goeke, S.: Oberflächenstrukturierung tribologisch beanspruchter Funktionsflächen durch Microfinishen Dissertation, Technische Universität Dortmund, Vulkan Verlag, Essen, 2016, ISBN 978-3-8027-8790-4. DOI: http://dx.doi.org/10.17877/DE290R-17770.

[4-7] Hashimoto, F.; Yamaguchi, H.; Krajnik, P.; Wegener, K.; Chaudhari, R.; Hoffmeister, H.W.; Kuster, F. Abrasive fine-finishing technology. CIRP Annals - Manufacturing Technology, 65 (2016) 2, S. 597–620. DOI: https://doi.org/10.1016/j.cirp.2016.06.003.

[4-8] Schumann, S.: Mehrskalige Modellierung und Simulation des Hochleistungs-Innenrundschälschleifens Dissertation, Technische Universität Dortmund, Vulkan Verlag, Essen, 2019, ISBN: 978-3-8027-8914-4. DOI: http://dx.doi.org/10.17877/DE290R-20295.

11.1.3 Bibliography (chapter 6 and 7)

[1] F. Caiazzo, V. Alfieri, and G. Casalino, 'On the Relevance of Volumetric Energy Density in the Investigation of Inconel 718 Laser Powder Bed Fusion', *Materials*, vol. 13, no. 3, Art. no. 3, Jan. 2020, doi: 10.3390/ma13030538.

[2] J. Metelkova, Y. Kinds, K. Kempen, C. de Formanoir, A. Witvrouw, and B. Van Hooreweder, 'On the influence of laser defocusing in Selective Laser Melting of 316L', *Additive Manufacturing*, vol. 23, pp. 161–169, Oct. 2018, doi: 10.1016/j.addma.2018.08.006.

[3] M.- Prießnitz, *In-situ Überwachung eines selektiven Laserschmelz-Prozesses*. Wien, 2020.

[4] 'm4p type13-x technical datasheet'. m4p material solutions GmbH Austria, Aug. 2020.

[5] L. Yang *et al.*, 'Design for Additive Manufacturing', in *Additive Manufacturing of Metals: The Technology, Materials, Design and Production*, L. Yang, K. Hsu, B. Baughman, D. Godfrey, F. Medina, M. Menon, and S. Wiener, Eds. Cham: Springer International Publishing, 2017, pp. 81–160. doi: 10.1007/978-3-319-55128-9_5.

[6] F. Trevisan *et al.*, 'On the Selective Laser Melting (SLM) of the AlSi10Mg Alloy: Process, Microstructure, and Mechanical Properties', *Materials*, vol. 10, no. 1, Art. no. 1, Jan. 2017, doi: 10.3390/ma10010076.

[7] D. Nikolaev, I. H. Yavuz, L. R. Enzenberger, and L. R. Enzenberger, 'Porosity distribution in sub-skin boundary area of the powderbed additively manufactured parts'. Zenodo, Jan. 18, 2022. doi: 10.5281/ZENODO.5872357.

[8] D. Nikolaev and M. Prießnitz, 'Vibration assisted drilling (VAD) application to the manufactured maraging steel X3NiCoMoTi18-9-5 (1.2709) and aluminium AlSi10Mg (EN AC-43000) parts'. Zenodo, Jan. 13, 2022. doi: 10.5281/ZENODO.5845462.

11.1.4 Bibliography (chapter 8)

[1] S. W. Williams, F. Martina, A. C. Addison, J. Ding, G. Pardal, and P.Colegrove, "Wire + Arc Additive Manufacturing," Materials Science and Technology, vol. 32, no. 7, pp. 641–647, 2016, doi: https://doi.org/10.1179/1743284715Y.0000000073.

[2] D. Ding, Z. Pan, D. Cuiuri, and H. Li, "Wire-feed additive manufacturing of metal components: technologies, developments and future interests," International Journal of Advanced Manufacturing Technology, vol. 81, no. 1–4, pp. 465–481, 2015, doi: https://doi.org/10.1007/s00170-015-7077-3.

[3] Klocke, F., & Kuchle, A. (2009). Manufacturing processes (Vol. 2, pp. p-433). Berlin: Springer.

[4] Hassan, A.M., Hayajneh, M.T., 2001, Statistical Analysis of the Effects of Machining Parameters and Workpiece Hardness on the Surface Finish of Machined Medium Carbon Steel. Journal of Materials Engineering and Performance, 10/3: 282–289. http://dx.doi.org/10.1361/105994901770344999.

[5] Rodrigues, A.R., Matsumoto, H., Yamakami, W.J., Paulo, R.G.D.R., De Assis, C.L.F., 2010, Effects of Milling Condition on the Surface Integrity of Hot Forged Steel. The Journal of the Brazilian Society of Mechanical Sciences and Engineering, 32/ 1: 37–43. http://dx.doi.org/10.1590/S1678-58782010000100006.

[6] Xiong, J., Li, Y., Li, R., Yin, Z., 2018, Influences of Process Parameters on Surface Roughness of Multi-Layer Single-Pass Thin-Walled Parts in GMAW-Based Additive Manufacturing. Journal of Materials Processing Technology, 252/September: 128–136. http://dx.doi.org/10.1016/j.jmatprotec.2017.09.020.

[7] Schmitz, T.L., Smith, K.S., 2009, Machining Dynamics.Springer US, Boston, MA.

[8] S. I. Dyadya, Y. M. Vnukov, O. B. Kozlova, V. O. Logominov, and N. M. Chernovol, Автоколебания при фрезеровании тонкостенных элементов деталей [Chatter at milling of thin-walled components]. Zaporizhzhia: ZNTU, 2017.

[9] Y. M. Vnukov, S. I. Dyadya, O. B. Kozlova, and N. M. Chernovol, "Анализ условий контактирования зубьев концевой цилиндрической фрезы с деталью [Analysis of conditions for contacting tooth end mills with cylindrical piece]," Journal of Engineering Sciences, vol. 1, no. 4, pp. A1–A7, 2014, [Online]. Available: http://essuir.sumdu.edu.ua/handle/123456789/44334.

11.1.5 Bibliography (chapter 9)

[1] Lachmayer, R., R.B. Lippert, and S. Kaierle, Additive series manufacturing: success factors and fields of action for application. 2018.

[2] Fontana, F., C. Klahn, and M. Meboldt, Value-driven clustering of industrial additive manufacturing applications. Journal of Manufacturing Technology Management, 2019. 30(2): p. 366-390.

[3] Agrawal, R. and V. S, State of art review on sustainable additive manufacturing. Rapid prototyping journal, 2019. 25(6): p. 1045-1060.

[4] Kellens, K., et al, Environmental Impact of Additive Manufacturing Processes: Does AM Contribute to a More Sustainable Way of Part Manufacturing? Procedia CIRP, 2017 61: p. 582-587.

[5] Gutowski, T., J.B. Dahmus, and A. Thiriez, Electrical Energy Requirements for Manufacturing Processes, in 13th CIRP International Conference of Life Cycle Engineering. 2006, CIRP: Lueven.

[6] Kellens, K., et al., Methodology for systematic analysis and improvement of manufacturing unit process life-cycle inventory (UPLCI)-CO2PE! initiative (cooperative effort on process emissions in manufacturing). Part 1: Methodology description. The International Journal of Life Cycle Assessment, 2012. 17(1): p. 69-78.

[7] Ma, K., et al, Environmental Sustainability of Laser Metal Deposition: The Role of Feedstock Powder and Feedstock Utilization Factor. Procedia Manufacturing, 2017 7: p. 198-204.

[8] Colorado, H.A., E.I.G. Velásquez, and S.N. Monteiro, Sustainability of additive manufacturing: the circular economy of materials and environmental perspectives. Journal of Materials Research and Technology, 2020. 9(4): p. 8221-8234.

[9] Agrawal, R. and S. Vinodh, Application of total interpretive structural modelling (TISM) for analysis of factors influencing sustainable additive manufacturing: a case study. RAPID PROTOTYPING JOURNAL, 2019. 25(7): p. 1198-1223.

[10] Klahn, C. and F. Fontana, Impact and assessment of design on higher order benefits, in Impact and assessment of design on higher order benefits F. Moreira da Silva, Editor. 2017, CRC Press: London.

[11] Weber, M. and R. Züst, New MAG process chain for crankshaft production - Faster, cheaper, more environmentally friendly, in Umweltperspektiven Sonderausgabe. 2013, galledia verlag ag: Flawil. p. 3.

[12] Leutenecker-Twelsiek, B., Additive manufacturing in industrial series production: component identification and design. 2019, ETH Zurich.

11.2 List of figures

11.3 List of tables

11.4 List of abbreviations

AM	Additive manufacturing
D	Diamond
DOE	Design of experiments
LPBF	Laser Powder Bed Fusion
MF	Microfinishing
PBF-LB/M	Powder bed fusion of metal with laser beam
SEM	Scanning electron microscopy
WAAM	Wire arc additive manufacturing
WAJM	Wet abrasive jet machining